Fabrication, Testing and Modelling of Palladium Membranes for Fuel Cell Applications

Robin Jonathan Lloyd

University College

Thesis for the degree of D.Phil.

Department of Engineering Science

University of Oxford

Trinity Term 2004

Confidentiality

The examiners are bound by the terms of the confidentiality agreement between Oxford University and Johnson Matthey Plc. Under the obligation to non-disclosure, they agree not to make or keep any copies of this report or to discuss its contents with any third parties. A copy of the final thesis is deposited in the Bodleian Library, but is only accessible to those granted permission by both the Oxford University Department of Engineering Science and Johnson Matthey Plc.

Fabrication, Testing and Modelling of Palladium Membranes for Fuel Cell Applications

Robin Jonathan Lloyd, University College, D.Phil. Thesis, Trinity Term 2004

Department of Engineering Science, University of Oxford

Abstract

Increasing carbon emissions and insecurities in oil supply have led to heightened interest in hydrogen powered fuel cells. Preferably, the cell runs on hydrogen gas, though due to the sensitivity of the catalytic components in the fuel cell to carbon monoxide, the hydrogen must be extremely pure (typically <50 ppm CO). Due to a lack of hydrogen infrastructure, it is envisaged that a medium term solution will be the reforming of more conventional fuels such as gasoline. The gas mixture produced however, contains impurities such as CO, CO_2 and CH_4. Purification may be achieved using palladium membranes, which allow selective permeation of hydrogen. This thesis describes the research carried out in conjunction with Johnson Matthey on thin (typically 7.5 μm) palladium/silver alloy membranes supported on both ceramic and stainless steel porous tubular substrates. Extensive experimental flow testing has been performed to assess the effect of temperature, feed composition, including wet feeds, and membrane thickness on the hydrogen purification properties. An existing Fortran based model was validated and revised to accurately account for the effects of operating conditions such as temperature and carbon monoxide concentration. This work provided excellent correlation between experimental and simulated results. The validated and improved model was incorporated in the design of a hydrogen refuelling station in Aspen Plus and the palladium membrane requirements assessed to supply 650 fuel cell vehicles per day. The system incorporated a steam reformer, membrane clean-up module, water trap and high pressure compressor for hydrogen storage at 1000 bara. Operating conditions such as system pressure, fuel feed and steam to carbon ratio were investigated and adjusted to optimise the overall system efficiency. An efficiency of 52% was achieved with a steam to carbon ratio of SCR = 2.5. A membrane requirement of 6000 standard tubes was found to provide a 90% hydrogen recovery efficiency.

Contents

Nomenclature

Å	-	angstrom (= 1.0×10^{-10} m)
Ag	-	silver
$AgNO_3$	-	silver nitrate
atm	-	atmosphere (= 1.01325 bara)
ATR	-	autothermal reforming
bara	-	absolute pressure
barg	-	gauge pressure
°C	-	temperature in degrees centigrade
C	-	carbon
Co	-	cobalt
CO	-	carbon monoxide
CO_2	-	carbon dioxide
CH_4	-	methane
CH_3OH	-	methanol
Cu	-	copper
ΔH	-	enthalpy change of reaction
e^-	-	electron
exp	-	exponential
Fe	-	iron
ft	-	length in feet (= 0.3048 m)
g	-	weight in grammes
h	-	hour
H^+	-	hydrogen ion
H_2	-	hydrogen
$H_2O_{(l)}$	-	water in liquid state
$H_2O_{(g)}$	-	water in gaseous state
K	-	temperature in Kelvin
kW_e	-	electric power in kilo watts
kW_{th}	-	thermal power in kilo watts
kg	-	weight in kilograms
m	-	length in metres
m^3	-	volume in cubic metres
mol	-	1 mole = 6.022×10^{23} particles (Avogadro number)
mm	-	length in millimetres
Mn	-	manganese
MW	-	power in megawatts
MJ/*l*	-	power density in megajoules per litre
MJ/kg	-	power density in megajoules per kilogram
µm	-	length in micrometres (= 1×10^{-6} m)
N_2	-	nitrogen
Ni	-	nickel
Pd	-	palladium
$PdCl_2$	-	palladium chloride
ppm	-	concentration in parts per million
psi	-	pressure in pounds per square inch (1 psi = 0.06895 bar)

Pt	-	platinum
R	-	universal gas constant (= 8.314 J/mol K)
Re	-	Reynolds number
Ru	-	ruthenium
sccm	-	standard cubic centimetres per minute at 0 °C and 1 atmosphere
scf	-	standard cubic feet
SCR	-	steam to carbon ratio
slm	-	standard litres per minute at 0 °C and 1 atmosphere
$SnCl_2$	-	tin chloride
wt. %	-	weight percentage
Zr	-	zirconium

Other symbols, terms and chemical formulae are introduced as they appear.

Acknowledgements

There are many people who have willingly given their time, advice and encouragement during this work. Special thanks goes to Mike Petch, Julia Rowe and James Sun at Johnson Matthey, for all the supervision, support and resources made available to me. I wish to thank all my friends and colleagues at Johnson Matthey and in particular Hugh Hamilton, Kate Lloyd, David Wails and Peter Walker for helping to make my time here extremely enjoyable. I also wish to thank Richard Stone at the University of Oxford who has been a dedicated and patient supervisor. I also wish to thank my friends in Oxford and elsewhere and particularly Mackenzie Bartlett, Mikel Duke and Lucy Tuner as well as my family who have all kept me going.

1 Fuel Cells and the Hydrogen Economy

1.1 Introduction

The fuel cell, predominantly employing hydrogen as a fuel, has often been portrayed as the answer to the problem of ever increasing carbon dioxide emissions. In reality, the fuel cell can improve on the efficiency of the Internal Combustion Engine (ICE), but still the question as to what fuel to use remains. Hydrogen gas is not a primary energy source and it must either be produced by electrolysis, or by reforming conventional fuels. The latter method is, in the shorter term, seen as the most viable alternative for reasons of power density and practicality though produces an impure hydrogen gas mixture. These issues are discussed later in this chapter. This report is concerned with the clean-up systems employed after the reforming process to purify this hydrogen. This report addresses the use of palladium membranes, which permit selective diffusion of hydrogen gas. This work assesses the fabrication and testing of palladium membranes and describes the development of a model to simulate the membranes in practical applications.

1.2 Background

In 1990, 20 billion tonnes of carbon dioxide were emitted worldwide. In order to achieve stabilisation of the climate, a 50% reduction in CO_2 emissions is required by 2050 (Müller-Hellmann, 2000). However this limit will be increasingly difficult to attain if we rely on the conventional internal combustion engine. Vehicles currently only account for about one quarter of all CO_2 emitted (Müller-Hellmann, 2000) and thus solutions are needed for stationary as well as mobile applications. Higher efficiencies do not in themselves solve emission problems or the exhaustion of natural resources. Thus both alternative energy sources to fossil fuels as well as efficient conversion of fuel are required.

A more urgent requirement for alternative power sources has recently emerged after the deregulation of electricity providers, especially in the USA and more recently in the UK. This has resulted in a number of blackouts and highlighted how dependent society, industry and therefore the economy are on centralised electricity production.

One solution to this would be the installation of a fuel cell power plant in every home. This would most likely be in the form of a combined heat and power plant that could provide both heating and electricity to the home and any excess electricity could then fed back into the network. This is termed decentralised power generation. A renewable hydrogen economy would also provide a solution to the more recent increased insecurity of Middle East oil supply and this has resulted in increased interest in fuel cell technology especially in the United States where President George W. Bush has proposed $1.7 billion to develop hydrogen powered fuel cells (CNN, 2004).

The fuel cell has presented itself as a viable alternative to the conventional internal combustion engine. The conversion of the fuel is electrochemical rather than thermal and efficiencies in the order of 50% are achievable using natural gas. The localised pollution is minimal with most fuel cells producing just water and heat. Automotive manufacturers such as BMW have developed conventional internal combustion engines running with hydrogen (Hollis, 2003), though pollutants in the form of NO_x emissions are still produced. Proposals to sequester CO_2 in depleted oil reservoirs and aid oil recovery are not a proven and reliable way to reduce CO_2 and the recovery of all CO_2 emissions would be impossible by this method (Wilkinson, 2003). If the hydrogen production can be carried out efficiently, through the use of renewable sources, then there would be an overall reduction in CO_2 emissions.

1.3 The Fuel Cell

A basic diagram of a hydrogen-powered fuel cell is shown below in Figure 1.1. The structure consists of two electrodes, an anode fed with fuel and the cathode with oxidant. In the example of a solid polymer fuel cell (SPFC), these are hydrogen and oxygen respectively. The electrodes are mounted either side of a conducting electrolyte that allows the mobile ions to pass through. An external circuit connected between the electrodes allows the electrons to flow from the anode to the cathode through a load, thereby producing electrical power. In the case of a SPFC the electrolyte is a proton exchange membrane (PEM) that allows protons (H^+ ions) to pass from anode to cathode.

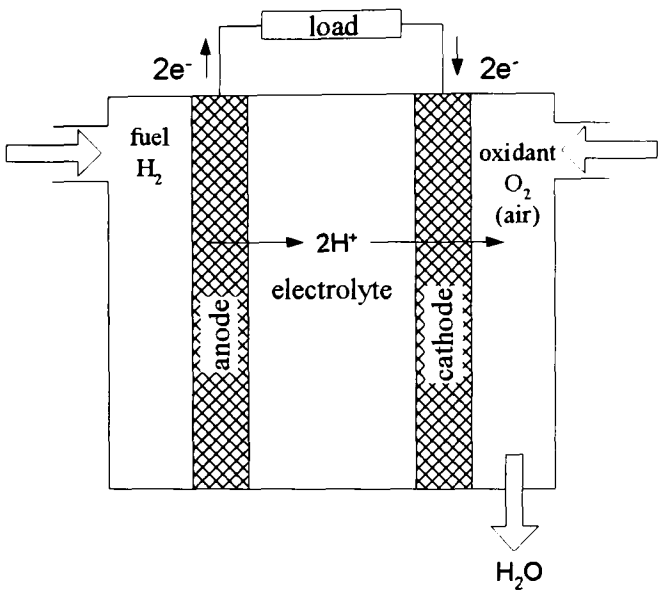

Figure 1.1: *Simple schematic of a solid polymer fuel cell.*

The electrochemical reactions for the above fuel cell are as follows:

$$\text{Anode: } 2H_2 \rightarrow 4H^+ + 4e^-$$

$$\text{Cathode: } O_2 + 4H^+ + 4e^- \rightarrow 2H_2O$$

The open circuit voltage of such a cell is only in the order of 0.7 volt (Larminie and Dicks, 2000) so that in order to produce a useful voltage, many cells are assembled together (~250) to form what is termed a stack.

1.4 History

The fuel cell was invented by Sir William Grove in 1839 as a "gaseous battery". He was able to produce electricity by exploiting the electrochemical properties of oxygen and hydrogen. In the experimental set-up, two platinum electrodes were halfway submerged into a beaker of aqueous sulphuric acid, and a tube was inverted over each of the electrodes, one containing hydrogen gas, the other oxygen. When the tubes were lowered, the gases displaced the electrolyte, leaving only a thin layer of the acid solution on the electrode; a galvanometer deflected to indicate a flow of electrons between the two electrodes. After the initial deflection the current decreased in magnitude, but the reaction rate could be restored by renewing the electrolyte layer. Because of this coating layer, Grove realised that the reaction was dependent on the "surface of action" (Grove, 1839), an area of contact between the gas reactant and a layer of liquid electrolyte thin enough to allow the gas to diffuse to the solid electrode. With platinised electrodes to increase the surface of action, and with 26 batteries in

series, Grove was able to achieve his goal of electrolysing water by the products of electrolysis – hydrogen and oxygen (Grove, 1842).

In 1932, Francis T. Bacon was inspired to produce the first alkali fuel cell using nickel electrodes and aqueous potassium hydroxide as the electrolyte. In 1959 he demonstrated a 40-cell stack producing 5 kW (Bacon, 1969).

In the 1960s, NASA looked for a portable power source for space missions and rejected batteries and nuclear power in favour of fuel cells. Fuel cells were attractive due to their mechanically stable operation, high power density, efficiency and reliability. The water produced in the cell could also be used as drinking water for the crew and for humidifying the cabin. In the Gemini Space Programme (1962-1965) a 1 kW_e fuel cell was developed by the General Electric Company using a solid polymer membrane as the electrolyte. The system operated at the low temperatures of 21 °C and the reactant gases were humidified before reaching the membrane because the conductivity of the polystyrene sulphonic acid membrane was dependent on water content. The fuel cell reaction also produced water and this accumulated in the pores of the electrode, flooding them and decreasing the efficiency of the cell. The electrodes were made water-proof by using polytetrafluoroethylene (PTFE), but the difficulty of water management in the system led to the selection of alternative fuel cell technology for the later space programmes (Warshay and Prokopius, 1990). The Apollo moon landing programme and the Orbiter programme used alkaline fuel cells, which are outlined in Section 1.5.4.

1.5 The Five Main Fuel Cell Technologies

There are currently 5 different fuel cell technologies competing for the markets of the future. It is likely that fuel cells represent a more viable replacement for stationary applications rather than mobile applications in the shorter term. This is in part due to the poor cycling durability of such systems and the currently inferior hydrogen infrastructure. The five fuel cell types are as follows: solid oxide fuel cell (SOFC), molten carbonate fuel cell (MCFC), phosphoric acid fuel cell (PAFC), alkaline fuel cell (AFC), solid polymer fuel cell (SPFC) and direct methanol fuel cell (DMFC). The five technologies are summarised in Figure 1.2 shown overleaf.

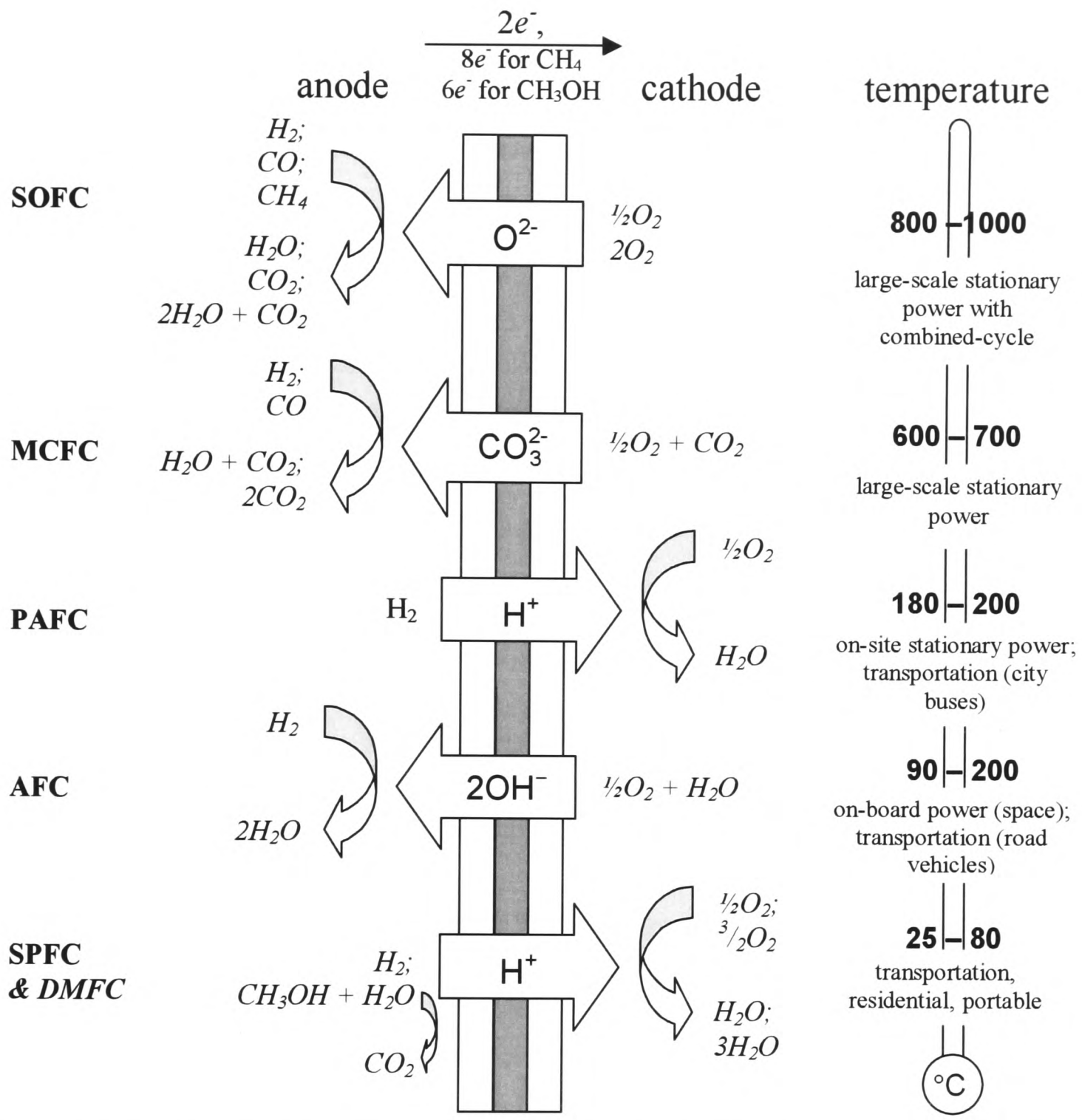

Figure 1.2: *A cross-sectional view of a fuel cell showing types of cell, migrating ions and operating temperatures. At the square end of both the curved and straight arrows are the reactants and at the pointed end are the products of the electrochemical reaction* (Chen, 1999).

1.5.1 Solid Oxide Fuel Cells

A solid oxide fuel cell (SOFC) uses an ion-conducting ceramic as the electrolyte and is completely solid state. It is thus simpler than other forms of fuel cell with only two phases i.e. gas and solid. It may operate with either carbon monoxide or hydrogen. The electrolyte is comprised of zirconia (ZrO_2), which conducts oxygen ions at high temperature. The zirconia is held in the cubic phase by yttria (Y_2O_3). The oxygen ion flows through the electrolyte by moving between interstitial sites. Normal operating temperatures lie between 800 °C and 1000 °C. The anode is often made of a zirconia cermet, a mixture of ceramic and metal. The metal is usually nickel, due to its high electronic conductivity yet stability under chemically reducing conditions. The cathodes of the SOFC are either produced from electrically conducting oxides, or mixed ceramics with ion-conducting and electrically conducting properties, of which strontium-doped lanthanum manganite is one example.

The electrode reactions are as follows:

Anode: $H_2 + O^{2-} \rightarrow H_2O + 2e^-$

Cathode: $\frac{1}{2}O_2 + 2e^- \rightarrow O^{2-}$

SOFC units of up to 2 MW have been developed and marketed by Siemens Westinghouse, consisting of some 10,000 individual cells (Larminie and Dicks, 2000).

1.5.2 Molten Carbonate Fuel Cell

The molten carbonate fuel cell (MCFC) uses a mixture of a molten alkali metal carbonates as the electrolyte retained in a porous ceramic matrix, commonly carbonates of lithium (Li_2CO_3) and potassium (K_2CO_3) in lithium aluminate ($LiAlO_2$). The ceramic material provides increased stability during temperature cycling. The operating temperatures of the cell vary according to the melting temperature of the electrolyte. Generally operating temperatures of 600 - 700 °C form a highly conductive molten salt.

The mobile ion in the MCFC is the carbonate ion (CO_3^{2-}), which passes from the cathode (e.g. porous nickel oxide material doped with lithium) to the anode (e.g. strontium titanate ceramic particles). The electrode reactions are as follows:

$$\text{Cathode: } \tfrac{1}{2}O_2 + CO_2 + 2e^- \rightarrow CO_3^{2-}$$

$$\text{Anode: } H_2 + CO_3^{2-} \rightarrow H_2O + CO_2 + 2e^-$$

The SOFC and MCFC operate at temperatures greater than 500 °C enabling fuel to be used without a separate external reformer. Hydrocarbons such as natural gas (methane, CH_4) can be utilised as in the following reaction:

$$CH_4 + 2O_2 \rightarrow CO_2 + 2H_2O + \text{Heat}$$

Electrical energy is also produced when carbon monoxide oxidises to form carbon dioxide. The reaction is as follows:

$$\text{SOFC case: } CO + O^{2-} \rightarrow CO_2 + 2e^-$$

$$\text{MCFC case: } CO + CO_3^{2-} \rightarrow 2CO_2 + 2e^-$$

In addition to producing the fuel for the cell, these reactions also generate high grade heat that can be used to heat the fuel cell. If the heat is incorporated into a combined heat and power system (CHP) then up to 70% thermal efficiency (Stone and Ball, 2004) can be achieved.

1.5.3 Phosphoric Acid Fuel Cell

Phosphoric acid fuel cells (PAFC) operate on an acid electrolyte (phosphoric acid, H_3PO_4) held in a matrix of silicon carbide powder with a PTFE binder across which the H^+ ion can migrate. The relatively low operating temperatures (in the region 180-220 °C) require that the electrodes be made of a catalyst such as platinum, so as to increase the rate of reaction. An alloy of platinum and ruthenium can be employed as the anode, but this electrode is very sensitive to carbon monoxide adsorption, which then blocks the adsorption of hydrogen in the catalyst. Carbon monoxide is

unfortunately a by-product of natural gas reformation. Clean-up of the carbon monoxide is discussed in more detail in Chapter 2.

The electrode reactions are as follows:

$$\text{Anode: } H_2 \rightarrow 2H^+ + 2e^-$$

$$\text{Cathode: } \tfrac{1}{2}O_2 + 2H^+ + 2e^- \rightarrow H_2O$$

Water in the form of steam is a by-product of the fuel cell, which can be used in the reformation of natural gas to produce the hydrogen fuel. This is discussed in Section 1.6.3.

1.5.4 Alkali Fuel Cells

The alkali fuel cell (AFC) had its debut in the NASA Apollo moon-landing programme (1968-1972), where the high power density and by-product of water were exploited. An electrolyte of aqueous potassium hydroxide (KOH) requires the use of pure hydrogen, otherwise KOH reacts with carbon dioxide to form potassium carbonate in the following reaction:

$$2KOH + CO_2 \rightarrow K_2CO_3 + H_2O$$

Platinum electrodes are employed due to the relatively low operating temperatures (50-200 °C). The mobile ion is the hydroxyl ion (OH^-) and the half-cell reactions are as follows:

$$\text{Anode: } 2H_2 + 4OH^- \rightarrow 4H_2O + 4e^-$$

$$\text{Cathode: } O_2 + 2H_2O + 4e^- \rightarrow 4OH^-$$

1.5.5 Solid Polymer Fuel Cell

The solid polymer fuel cell (SPFC) is also known as a proton exchange membrane fuel cell (PEM) due to the mobile ion being a proton, an H^+ ion. The solid polymer currently used is usually a perfluorinated sulphonic acid membrane that conducts protons. The electrodes are porous carbon/graphite, which enable the gases to diffuse to the membrane surface. The operating temperature of a PEM is in the order of 80 °C and to increase the electrode reactions a platinum-based catalyst is employed on the electrodes. Platinum is also the only catalyst that can withstand the corrosive environment at the cathode. The catalyst particles are supported on particles of carbon black to increase the dispersion and therefore the surface area for the electrochemical reactions. The half-cell reactions are as follows:

$$\text{Anode: } H_2 \rightarrow 2H^+ + 2e^-$$

$$\text{Cathode: } \tfrac{1}{2}O_2 + 2H^+ + 2e^- \rightarrow H_2O$$

PEM cells have the greatest potential for automotive applications due to their low operating temperature, which can be reached quickly from ambient conditions (Murray *et al.*, 1986). The high power density of the cell also makes it attractive due to vehicle volume and mass restrictions. Ballard Power Systems of Canada is the leading supplier of SPFCs and in partnership with Daimler Chrysler is developing a fuel cell power unit for a Mercedes A-Class, which was due for commercial introduction in 2004, though changes in zero emission vehicle (ZEV) legislation in California would suggest 2005 at the earliest. Power densities in the order of 1000 W/l and 700 W/kg have been achieved using fuel cells operating on hydrogen and air under practical vehicle operating conditions (Wilinson and Steck, 1997).

The electrodes of the solid polymer fuel cell are porous to allow the reactant gases, which are distributed on the electrode by the flow field plates, to diffuse to the catalyst and the proton exchange membrane. The flow field plates also collect the current from the electrodes. When a stack of many individual cells is assembled, the cells are arranged back-to-back. Bipolar plates are used to enable this back-to-back stacking, with gas passages on each side of the flow field plates connecting to an

anode on one side and a cathode on the other. These cells are termed the membrane electrode assembly (MEA), an example of which is shown in Figure 1.3.

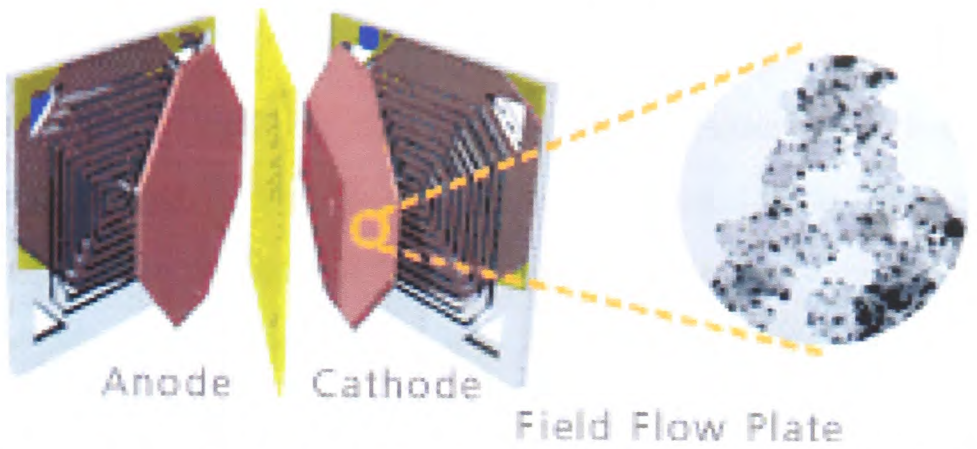

Figure 1.3: *A membrane electrode assembly, showing field flow plates, anode, cathode and the polymer membrane* (Johnson Matthey, 2002).

1.5.6 Direct Methanol Fuel Cell

The direct methanol fuel cell (DMFC) is similar to the solid polymer fuel cell, sharing components such as substrates and the solid polymer electrolyte. The methanol is diluted with water in the ratio 3:97% wt. The methanol mixture is fed in either liquid or vapour form and is oxidised on the anode catalyst and the protons migrate to the cathode. Methanol diffuses through the membrane dissociating into six protons and electrons and reacts with water to form carbon dioxide in the oxidation reaction as shown in the following half cell equations:

Anode: $CH_3OH + H_2O \rightarrow CO_2 + 6H^+ + 6e^-$

Cathode: $\frac{3}{2}O_2 + 6H^+ + 6e^- \rightarrow 3H_2O$

Advantages of the DMFC are that there is no need for a fuel reformer as methanol is used directly and without the reformer the power density for the volume and size can be considered less in spite of a lower power density in the cell itself. The catalyst requirements however make the system expensive.

1.6 Sources of Hydrogen for Solid Polymer Fuel Cells

As previously mentioned, hydrogen is the fuel of choice for most fuel cell applications. The main problem however is that hydrogen is not a primary energy carrier. Storing the hydrogen and the problem of the low calorific density of hydrogen

by mass compared with gasoline is another issue, which is discussed in Section 1.6.6 of this report.

1.6.1 Electrolysis

Hydrogen can be produced by electrolysing water. However, although in theory this is reversible, in practice it is only about 80% efficient. Using electricity to produce the hydrogen also raises the issue of emissions when the electricity has been created from fossil fuels. Norwegian studies (Kloed, 2001) use renewable hydroelectric power to produce the electricity required for electrolysis; these resources are not available in every country.

Fuel reforming offers a more practical way to produce hydrogen for the fuel cell and there are three main methods currently employed: Partial Oxidation (POX), Steam Reforming (SR), and Autothermal Reforming (AR), each of which will now be discussed.

1.6.2 Partial Oxidation

Partial oxidation involves the reaction of the fuel with oxygen (air) below the stoichiometric amount in the following reaction:

$$C_xH_y + \frac{x}{2}O_2 \Leftrightarrow xCO + \frac{y}{2}H_2$$

Carbon (soot) deposits on reformer surfaces can be prevented and carbon monoxide production reduced by the addition of a small amount of steam as follows:

$$CO + H_2O_{(g)} \Leftrightarrow CO_2 + H_2 \Rightarrow CO, CO_2, H_2, H_2O$$

The reaction does waste a lot of the heat from the fuel if it is not efficiently recovered. However, the primary advantages are that it is exothermic and therefore self-sustaining, and it can also be used for a variety of different fuels because catalysts are not required.

1.6.3 Steam Reforming

Steam reforming is widely used in the petrochemical industry. It is an endothermic reaction where a vaporised hydrocarbon is reacted with steam over a catalyst to produce carbon monoxide and hydrogen gas. Often catalysts of nickel on an alumina support are used with temperatures in the region 700 °C to 1100 °C. The reaction proceeds as follows:

$$C_xH_y + xH_2O \Leftrightarrow xCO + (y/2 + x)H_2 \Rightarrow CO, CO_2, H_2, H_2O$$

Simultaneously the water-gas shift reaction takes place whereby the hydrogen in the water (steam) is converted to hydrogen gas as follows:

$$CO + H_2O_{(g)} \Leftrightarrow CO_2 + H_2$$

Steam reforming reactors in industry are generally tubular in form, consisting of a furnace containing several tubes filled with catalysts through which the reactants pass. Heat is supplied to the reaction from a flame external to the tubes. Tubular reformers are not easily miniaturised and are thus not so adaptable for small PEM systems. However one such example is the HotSpot™ reformer (Edwards *et al.*, 1998) developed by Johnson Matthey Plc, which is capable of handling a variety of different fuels.

1.6.4 Autothermal Reforming

Autothermal reforming is a combination of steam reforming and partial oxidation, enabling the heat produced by the exothermic reaction of the fuel and oxygen to be utilised for the endothermic reaction of the fuel and steam. The reaction is as follows:

$$C_xH_y + zH_2O + (x - z/2)O_2 \Leftrightarrow xCO_2 + (z + y/2)H_2 \Rightarrow CO, CO_2, H_2, H_2O$$

In the case of methane the change in enthalpy for the above reaction is zero when z is equal to 1.115. The primary benefits of autothermal reforming are:

1) the high thermal efficiency from combining the reactions,
2) the compactness, as no separate combustion stream is required as with a steam reformer,
3) the rapid start up and load following, which is also due to combining the reactions.

The disadvantage of autothermal reforming is the lower hydrogen yield, only 42- 48% (dry) hydrogen content in the output gas stream which compares with 75-80% in steam reforming. The low yield is due to the dilution of the output gas by the uptake of nitrogen.

Because of the rapid start-up, autothermal reformation is attractive for automotive applications while steam reformation suits stationary systems because of the higher thermodynamic efficiency.

1.6.5 Fuels Suitable for Reformation

Methanol (CH_3OH) had been the fuel favoured for on-board reformers because of a reformation temperature of 300 °C compared with 750 °C for gasoline. Methanol does not contain sulphur, which can lead to poisoning of the catalyst. However, the handling of methanol requires special measures to avoid its toxic effect on the human body. In case of possible leakage, because of its solubility, it cannot be separated from water systems. There is also currently no infrastructure for methanol distribution.

Natural gas consists primarily of methane gas (~95%) and is used both in power plants for electricity distribution and also in the home for central heating. It is also used in the chemical industry for the production of hydrogen and methanol. There already exists a natural gas distribution network and its handling is relatively safe. It therefore presents itself as an attractive fuel for fuel cell applications. Natural gas does however contain sulphur compounds, which must be removed to avoid poisoning of the fuel cell catalyst.

Gasoline and diesel, including biodiesel, have a high calorific density and have well established and accepted storage solutions and supply networks. This would aid their use as a medium term solution towards providing a hydrogen infrastructure. Reforming temperatures are in the region of 750 °C. These fuels contain sulphur

compounds, which can poison reforming catalysts, and other additives to improve internal combustion engine performance. Legislation to reduce the sulphur content of fuels is coming into force.

Domestic heating oil can also be used and again there is already a supply infrastructure. The oil however, contains compounds incorporating sulphur that must be removed before use in the fuel cell. The reformation of domestic heating oil does produce a large amount of carbon compounds in the form of soot. High temperatures are required (~750 °C) and suitable methods of producing a homogeneous air and fuel mixture are required. One such method of achieving this mixture is the use of cool flames (Lucka and Köhne, 1999).

1.6.6 Biological Hydrogen Production

Steam reforming processes account for around 90% of hydrogen production (Das and Veziroglu, 2001). There are a number of biological methods of hydrogen production using biomass, which are mostly operated at ambient temperatures and pressures and therefore are less energy intensive than the conventional reforming processes. They can also make use of waste material. Biological processes include the biophotolysis of water using algae and cyanobacteria, the photodecomposition of organic compounds by photosynthetic bacteria, and the fermentative hydrogen production from organic compounds. The gases produced contain hydrogen in the range 60-90% and some impurities.

1.7 Hydrogen Storage and Infrastructure

There are two schools of thought as to how the hydrogen will be supplied to the fuel cell in automotive applications. Some believe that a renewable hydrogen infrastructure will exist whereby hydrogen will be available at the roadside filling stations much like gasoline is today. There is also the option that the hydrogen will be generated locally at the filling station or transported to it by reforming other fuels. It has been estimated with the latter option, that for the equivalent amount of energy, hydrogen will require 13 times the volume of gasoline (Dempsey, 2001). Therefore in practical terms of the number of trucks, hydrogen distribution from a central reformation plant poses a problem. On the other hand, on-board reformation has its

supporters and, in the short term before a hydrogen infrastructure has been developed, could be the most practical solution.

Hydrogen can be stored either as a liquid (at –253 °C), under high pressure as a gas (250 bar and higher) or adsorbed into a material. The three options are outlined below:

1.7.1 Cryogenic Hydrogen

Liquid storage needs to minimise the boil-off loss, which is typically about 1% per day, and have a means of handling this safely. The liquid density is only 71 kg/m^3, and with a net calorific value of 120 MJ/kg, the energy density is 8.5 MJ/*l*. Ignoring the mass and volume of the storage system, this is about a factor 4 lower than any hydrocarbon. The volume of the tank is typically double the volume of the liquid, and its mass might be 4-5 times the mass of the hydrogen, so the energy storage density is typically about 24 MJ/kg or 4.25 MJ/*l*. A significant amount of energy is also needed to liquefy hydrogen (about 16% of its calorific value in a thermodynamically reversible process), so the overall 'well to wheel' efficiency of a liquid hydrogen fuelled system is inherently poor (Stone and Ball, 2004).

1.7.2 Pressurised Hydrogen

At 250 bar, hydrogen has a density of about 22.5 kg/m^3, and by the time the volume and mass of the tank are considered, the energy storage density is typically about 4 MJ/kg or 1.7 MJ/*l*. This is lower than for liquid hydrogen, but the work for reversible isothermal compression to 250 bar is only about 6% of its calorific value, which is much lower than the energy required for liquefaction. Furthermore, the irreversibilities associated with liquefaction are likely to be much greater than for gas compression.

1.7.3 Activated Carbon and Reversible Metal Hydrides

The final option is to make use of a material that adsorbs hydrogen. The simplest approach is to use active charcoal to adsorb hydrogen. For a given temperature and pressure, the mass of hydrogen per litre is greater than for the compressed gas, despite the volume occupied by the carbon. A litre of activated carbon at 150 K and a pressure of 56 bar can store 14 g of hydrogen. Related to this is the use of carbon nano-fibres that are claimed to store up to 3 times their own mass of hydrogen, but

tests have been limited to samples of a few grams, so clearly more work is needed (Stone and Ball, 2004).

A well established technique for storing hydrogen is the use of metal hydrides, such as titanium iron hydride ($TiFeH_2$). There is a reversible reaction, controlled by pressure in which:

$$TiFeH_2 \Leftrightarrow TiFe + H_2$$

Hydrogen is adsorbed when the system pressure is raised, and released when the pressure is reduced. When hydrogen is adsorbed the reaction is exothermic, so it is necessary to cool the system. Conversely, when hydrogen is released, heat is adsorbed, so it is necessary to heat the hydride store. This provides a useful safety feature, since if there was a sudden loss of pressure the rate of hydrogen release is governed by the heat supply. This is a very efficient way to store hydrogen, with 1 kg stored in 9.8 litres (a greater 'density' than with liquid hydrogen), but the system is very heavy, with only about 1.9% hydrogen by mass.

1.8 Conclusions

This chapter has introduced the main issues surrounding fuel cell technology and highlighted the increasing need for an economy that is not reliant on oil to ensure both the protection of the environment and security and reliability of power sources. In the long term, hydrogen will be generated through renewable means. However, until that time, reforming of conventional fuels will provide a medium term solution. Reforming has been shown to produce a non-pure hydrogen gas mixture and gas purification techniques are now explored in Chapter 2.

2 Gas Clean-Up Systems

2.1 Gas Clean-Up Systems

Although the reforming processes described in the previous chapter are suitable for the production of hydrogen gas, the product gases contain a variety of constituents, which can be harmful to certain elements in the fuel cell system. A typical reformate (also known as synthesis gas or syngas) composition is: 43% H_2, 15% CO_2, 21% H_2O, 3.3% CO, and 17.4% N_2. The presence of other gases lowers the partial pressure of the hydrogen at the anode, and this combined with the presence of CO can result in about a 10% reduction in the power output of the SPFC (Larminie and Dicks, 2000). It follows therefore that a fuel cell which is not operating on pure hydrogen needs to be supplied with significantly more hydrogen than is actually utilised. The gas mixture will flow through the channels in the bi-polar plate and the partial pressure of the hydrogen will fall along the length of the channel as it is used up. This would lead to a reduction in the voltage generated. A surplus of hydrogen reduces this 'dilution' loss though does mean that some of the hydrogen is in effect 'wasted'.

If the cathode is being supplied with air as opposed to pure oxygen, then it needs to be supplied with excess oxygen to reduce the 'dilution' losses. The only penalty with supplying excess air to the system is the need for compression when the cell is operating above ambient pressure. Some of this compression work can be recovered by reaction of the exit gases from the anode and cathode, raising their temperature, and then expanding in an expander (e.g. a turbine).

The main problem with using a reformate, which does not consist solely of hydrogen, is the fact that carbon monoxide is preferentially adsorbed onto the surface of the catalyst on the electrodes, and this degrades the performance of the fuel cell as shown by Figure 2.1. This degradation, also called poisoning, occurs on the anode as CO blocks access to the hydrogen oxidation sites, decreasing the area for the chemisorption of hydrogen. The anode is required to operate at a higher polarisation to compensate for the reduced number of catalyst sites. This increases the reaction rate at the other sites, but leads to a reduction in the cell voltage.

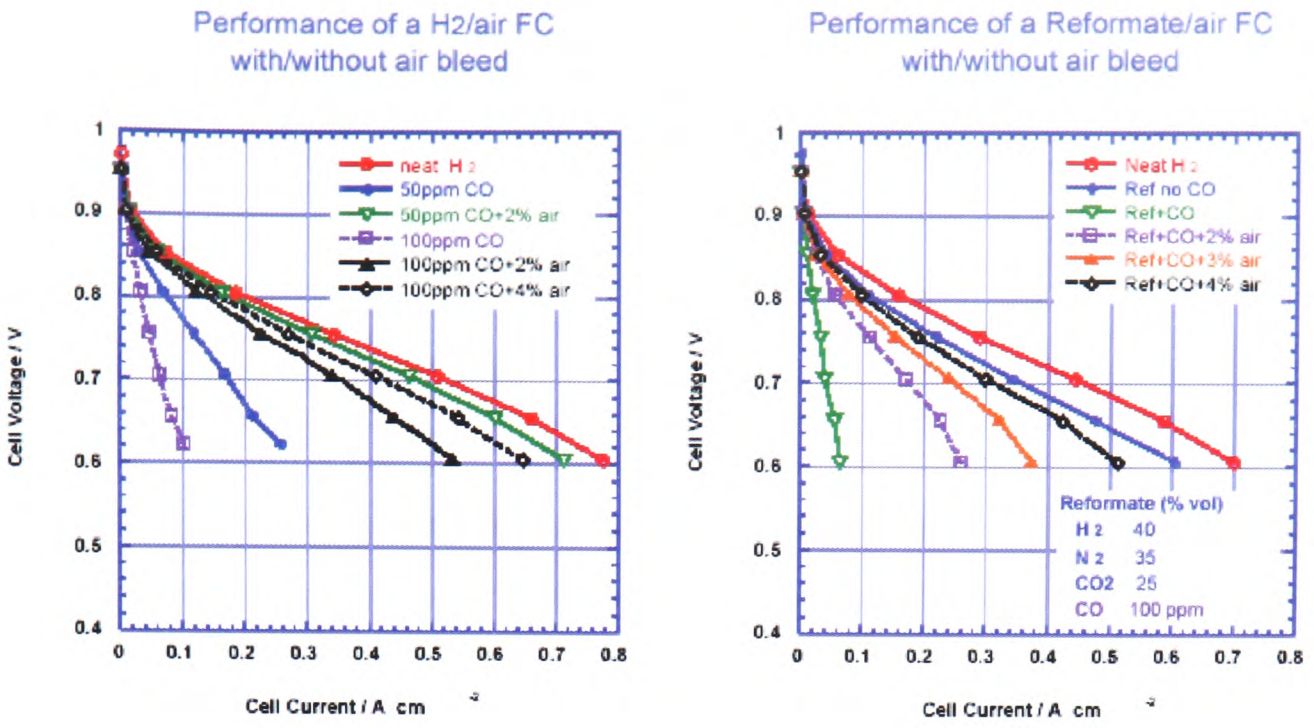

Figure 2.1: *Effect of CO level on PEM fuel cell performance using 0.2 mg Ru-Pt/cm^2 anode and 0.2 mg Pt/cm^2 cathode. Temperature = 80 °C* (Uribe *et al.*, 2002).

The performance of a cell operating with a reformate containing CO and CO_2 as well as hydrogen will depend on the reformate tolerance of the anode which can be improved by the incorporation of ruthenium. If the anode has complete reformate tolerance to CO and CO_2, then it will perform as though the fuel were diluted by an inert gas in the same volume fraction as occupied by the CO and CO_2.

Carbon monoxide concentrations of less than 50 ppm (Stone and Ball, 2004) are usually required to prevent the poisoning of the catalyst and resulting performance deterioration. More tolerant catalysts are being developed. The equilibrium level of the carbon monoxide is shown in the following shift reaction:

$$CO + H_2O_{(g)} \Leftrightarrow CO_2 + H_2$$

As temperature decreases the equilibrium shifts to the right so CO is reduced and the level of hydrogen increases. However, operating at a lower temperature reduces the rate of reaction to such an extent that even the use of a catalyst to help achieve equilibrium would not reduce the carbon monoxide to a low enough level.

CO_2 was thought to have no effect of the performance of the fuel cell. However at high concentrations (~20% CO_2), performance reductions are present beyond its dilution effects thought due to CO_2 being reduced to CO on the anode in the following reaction:

$$CO_2 + H_2 \Leftrightarrow CO + H_2O$$

The CO tolerance of the cell can be improved by a number of methods. These include the use of different catalysts such as the alloying of the catalysts with noble metals and base metals. The cell can also be operated at higher temperatures or selective oxidation of CO at the anode can be carried out using an oxygen or air bleed added to the fuel stream. However, the oxidation of CO to CO_2 is exothermic and this may cause problems with the catalyst durability.

It is thus preferable to clean the reformate before it reaches the fuel cell to avoid poisoning the anode and reducing the cell performance. The four main methods of CO clean-up are: methanation, selective oxidation, pressure swing adsorption, and hydrogen purification membranes. The water-gas shift reaction can also be included as a clean-up stage, which was discussed in Section 1.6.3. The four other types will now be discussed further as well as an overview of gas separation processes.

2.1.1 Methanation

The conversion of carbon monoxide to methane (methanation) is an exothermic process and can reduce the CO concentration from 0.3%, from a low pressure shift reaction, to less than 10 ppm (Lloyd, 1996). Reaction temperatures in the order of 200-350 °C are used, and if CO levels are high, a steep rise in temperature can be caused. The reaction however uses three moles of hydrogen in the reaction, which reduces the overall efficiency of the reformer:

$$CO + 3H_2 \rightarrow CH_4 + H_2O \qquad \Delta H = -206.2\ \text{kJ/mol}$$

Carbon dioxide is also converted in the reaction and so additional hydrogen is used if there are high levels of CO_2 in the reformate:

$$CO_2 + 4H_2 \rightarrow CH_4 + 2H_2O \qquad \Delta H = -164.9\,\text{kJ/mol}$$

Industrially, CO_2 is removed from the gas stream using a scrubber such as potassium hydroxide, KOH, (Ledjeff-Hey *et al.*, 1999), however this would add complexity to an onboard reformer.

2.1.2 Selective or Preferential Oxidation

Carbon monoxide, in the presence of hydrogen, can be selectively oxidised by oxygen on a noble metal catalyst with only minor losses in H_2 content. This selectivity is attributed to the CO coverage on the catalyst that blocks the adsorption, and therefore oxidation of H_2. As the selectivity is very temperature sensitive, a selective-oxidation clean-up system uses several stages rather than one single catalyst. This means that at each stage, the temperature of the reactor could be set depending on the amount of CO that enters the stage. The CO concentration is attenuated through each stage, though as CO levels become very low, the amount of hydrogen oxidised increases because the number of catalyst sites occupied by CO decreases. For a stream of 1% or 10,000 ppm CO, a selective oxidation stage can reduce this to 5 ppm.

2.1.3 Cryogenic Purification

Cryogenic purification technology occurs through the difference in boiling temperatures (relative volatility) of the feed components (Whysall and Picioccio, 1999). Hydrogen has a high relative volatility compared with hydrocarbons and the process condenses the required feed impurities by cooling the feed stream against the warming product. Water must be removed from the stream which could freeze the system. Hydrogen is removed from the two phase stream in a separator. A purity up to 98% may be achieved.

2.1.4 Metal Getters

Metal getters consisting of zirconium alloys such as those with aluminium, iron or vanadium in porous pellet form, have been used for gas purification for over 30 years (JMGPT, 2004). Zirconium alloys are very reactive and form irreversible chemisorbed oxides, nitrides and carbides with the gas impurities such as CO, CO_2 and N_2. Hydrogen is dissociatively chemisorbed and dissolved into the bulk of the getter. Outlet purities of the order parts per trillion (ppt) are possible. Getters are

generally used to remove impurities from rare earth gases such as argon, helium, krypton and xenon as well as hydrogen for use in high sensitivity applications such as analytical equipment.

2.1.5 Pressure Swing Adsorption

Pressure swing adsorption (PSA) makes use of adsorbent materials to which gas molecules physically bind dependent on the partial pressure and operating temperature (Wiessner, 1988). Due to different adsorption forces between different gas components and the adsorbent material, separation can be achieved. More effort is required to separate components which have similar adsorption forces and in fact hydrogen and helium cannot be separated by adsorption. There are a number of consecutive steps in the PSA process:

1. Raw gas flows into a vessel filled with one or more layers of adsorbent material at the highest operating pressure of the system.
2. The adsorbable components of the raw gas are adsorbed, whilst a purified gas leaves the vessel.
3. The adsorbent material becomes saturated and then the raw gas is fed to another adsorbent-containing vessel.
4. The saturated adsorbent-containing vessel is depressurised adiabatically i.e. 'swings' the vessel to low pressure, and if done concurrently this step may be utilised to pressurise a subsequent repressurisation in a process called pressure equalisation.
5. The depressurised adsorbent vessel is purged at low pressure to remove the adsorbed impurities.
6. The adsorbent-containing vessel is returned to high pressure.
7. The process starts again.

The PSA process is a short-term cyclic process. Several vessels are combined to ensure a continuous flow of raw gas into and pure gas out of the system. The more pressure equalisation steps, the better the efficiency of the unit, but the more complex the flow switching control. Flow fluctuations of less than $\pm 3\%$ can be achieved. Hydrogen purities of >99.9% (Wiessner, 1988) may be achieved. PSA is however best suited to large scale applications.

2.1.6 Desulphurisation

The removal of sulphurous compounds, which are present in natural gas or petroleum, is essential to avoid poisoning of the reforming or fuel cell catalysts that can have a sulphur tolerance of less than 0.1 ppm (Larminie and Dicks, 2000). Hydrogen gas can be used to convert the sulphur containing compounds over a nickel-molybdenum oxide or cobalt-molybdenum oxide catalyst to form hydrogen sulphide via hydrogenolysis reactions at temperatures in the region of 300-400 °C. The hydrogen sulphide is then adsorbed onto a bed of zinc oxide to form zinc sulphide. The use of hydrogen is this way does mean that it cannot then be used in the fuel cell.

2.2 Membrane Classification and Overview

A membrane may be described as an interphase, which separates two phases and restricts the transport of various chemical species in a rather specific manner (Strathman, 1981). Any material which can be formed sufficiently thin and remain stable can be used as a membrane including metals, glasses, ceramics and polymers. Membranes may be homogeneous or heterogeneous, symmetric or asymmetric and dense or porous. Membranes with pore sizes of greater than 5000 nm are used to filter particulates. Microfiltration membranes, having pore sizes in the range 100-5000 nm can be used to remove suspended particles such as blood cells. Ultrafiltration membranes with pores in the range 2-100 nm can be used to remove large molecules such as albumin. Finally, nanofiltration membranes, with pores less than 10 Å, can separate small molecules such as dissociated acids and sugar.

2.3 Porous Membranes

The separation of a gas through a porous membrane may involve a number of transport mechanisms depending on the nature of the membrane. A schematic of the transport mechanisms involved is shown in Figure 2.2 and is described below.

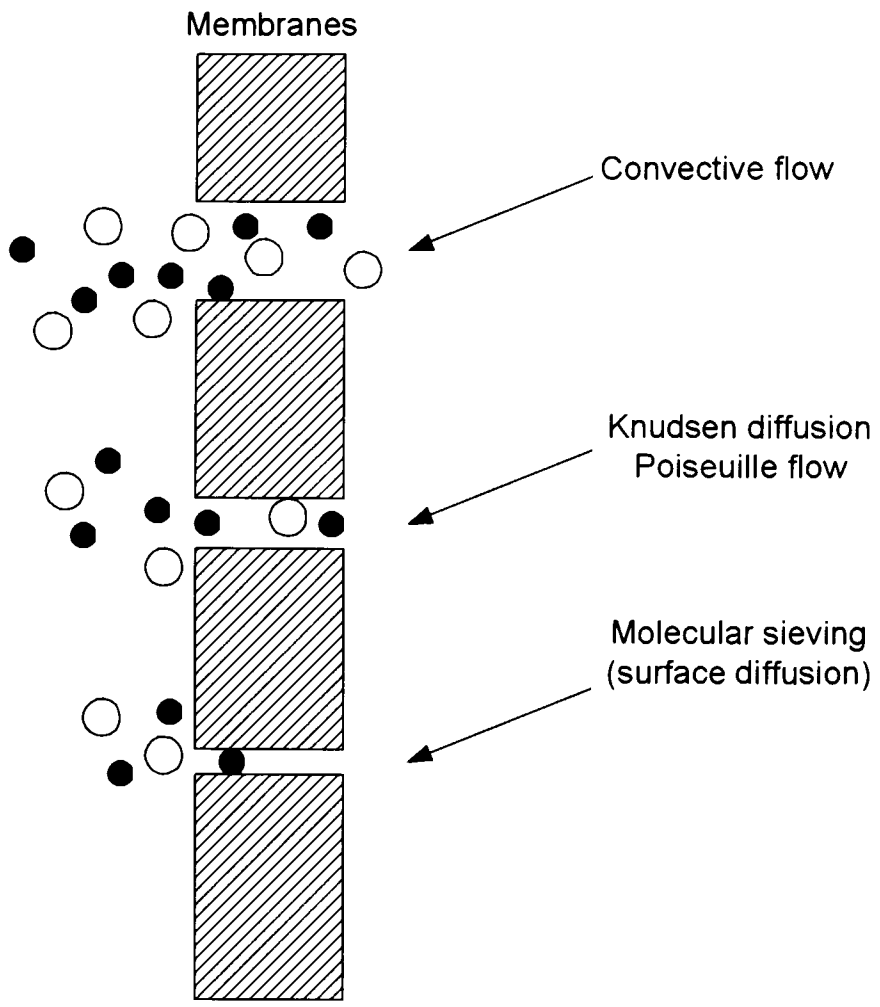

Figure 2.2: *'Schematic representation of mechanisms for permeation of gases through membranes.'* (Pandey and Chauhan, 2001).

2.3.1 Knudsen Diffusion and Poiseuille Flow

The proportion of Knudsen to Poiseuille flow is determined by the ratio of the pore radius in the porous membrane, r, to the mean free path, λ, of the gas molecules. The mean free path, λ, is given by the following expression (Pandey and Chauhan, 2001):

$$\lambda = \frac{3\eta}{2P}\frac{(\pi RT)^{1/2}}{2M}$$

where: η is the gas viscosity

R is the universal gas constant

T is the absolute temperature

M is the molecular weight

P is the pressure.

If $\lambda/r << 1$ then viscous or Poiseuille flow predominates and the gas flux, G_{vis} , through the pores is described as follows (Pandey and Chauhan, 2001):

$$G_{vis} = \frac{r\,(P_1 - P_2)}{16 L \eta R T}$$

where: r is the pore radius

P_1 is the partial pressure of the gas on the feed side

P_2 is the partial pressure of the permeate side

L is the pore length,

η is the gas viscosity

G_{vis} is the viscous molar gas flow rate

T is the temperature

R is the universal gas constant.

In the case of Knudsen flow, $r/\lambda << 1$, there are more collisions with the pore walls than with the other gas molecules. At every collision with the pore walls, the gas molecules become momentarily adsorbed and reflected in a random direction. Due to there being fewer collisions between molecules than with the pore walls, each molecule will move independently of the others. The separation is achieved through differences in the molecular weight of the species. The gas flux in this case is given by the following expression (Pandey and Chauhan, 2001):

$$G_{mol} = \frac{8r(P_1 - P_2)}{3L(2\pi \mathrm{MRT})^{1/2}}$$

where: G_{mol} is the molar gas flow rate

r is the pore radius

P_1 is the partial pressure of the gas on the feed side

P_2 is the partial pressure of the permeate side

L is the pore length

M is the molar mass

R is the universal gas constant

T is the absolute temperature.

In the case of Knudsen flow the selectivity ratio or separation factor for a binary gas mixture may be estimated from the square root of the ratio of the molar masses. Knudsen diffusion is observed with membranes having pore sizes less than 50 nm. In homogeneous porous media with a pore radius larger than 1.5 nm, combined Knudsen and Poiseuille diffusion occurs (Uhlhorn *et al.*, 1989).

2.3.2 Microporous Membranes

Microporous membranes are those which act as molecular sieves and require the pore diameters to be in between those of the gas molecules to be separated. With pore diameters less than 0.5 nm, separation factors of at least 10 are achievable and the development of zeolite membranes with very narrow pore size distribution is increasing (De Lange *et al.*, 1994). If the pore diameters of the membrane lie between the diameter of the smaller and larger gas molecules then only the smaller molecule may pass. Practically the membrane will consist of pores with a range of sizes, and the gas permeability is influenced by a combination of transport mechanisms. Microporous membranes exhibit activated gas transport as given by the following expression:

$$J = J_0 \exp\left(\frac{-E_{act}}{RT}\right)$$

where: E_{act} is the apparent activation energy

J is the flux

T is the temperature

R is the universal gas constant

J_0 is the pre-exponential factor

In mesoporous materials (regularly arranged, uniform pores 5-50 nm), the gas transport mechanisms are controlled by Knudsen, Poiseuille and activated diffusion which decrease as a function of temperature. Also, as the pore size decreases, the membrane porosity also decreases, resulting in a lower gas flow through the membrane. A balance must therefore be reached between the pore size and the permeability.

Silica based microporous membranes are being developed (Duke, 2002 ; Duke 2003) for fuel cell applications, but have low permeation (200×10^{-8} compared with 467×10^{-8} mol. $Pa^{-1}.m^{-2}.s^{-1}$ for a thin Pd/Ag membrane) and require numerous and highly controlled sol gel applications.

2.4 Non-porous Membranes

These membranes provide high selectivity but the rates of transport are usually low. The main types are described below.

2.4.1 Dense Polymeric Membranes

The transport through polymeric membranes is of a solution-diffusion type (Pandey and Chauhan, 2001). In this mechanism, the permeants dissolve in the membrane material and diffuse through the membrane down a concentration gradient. There are three main steps:

1. Adsorption at the upstream boundary
2. Activated diffusion (solubility) through the membrane
3. Desorption or evaporation at the downstream boundary

These membranes are low cost and may be spun into asymmetric fibres or spiral wound modules. Purity of up to 98% can be achieved. The main problems include the loss in performance stability at high temperature and pressure, and the retention of highly absorptive components.

2.4.2 Hydrogen Diffusion Through Palladium Membranes

Palladium, with an atomic number of 46 and atomic weight of 106.42, is a member of the platinum group metals (PGM) (Weast, 1989), and is found in deposits in Russia, South and North America and Australia. It is a steel-white metal, does not tarnish with air, and is the least dense and lowest melting (melting point = 1554 °C) of the PGMs. Palladium is alloyed with gold to form white gold for jewellery and can be used as a catalyst for hydrogenation and dehydrogenation reactions. At room temperature, palladium can adsorb up to 600 times its own volume of hydrogen as discovered by Sir Thomas Graham in 1866 (Grashoff *et al.*, 1983). Palladium in the form of a

membrane allows only the diffusion of hydrogen gas. For the application of reformate purification they are particularly suited due to their potentially infinite selectivity. A pure hydrogen feed for the fuel cell of 99.9999% purity may be achieved (Grashoff *et al.*, 1983). The chemisorption of carbon monoxide onto palladium is high at low temperatures and a concentration of 2.6% CO in the reformate may hinder the permeability of the hydrogen through the membrane. The CO that adsorbs onto the palladium membrane can be oxidised by a small air bleed and exits as CO_2 with the rest of the exhaust gases. However a minimum operating temperature of 350 °C and a pressure of 30 bar for a 100 µm-thick unsupported palladium/silver membrane (77/23 atomic ratio) will ensure a low coverage of CO and a sufficient rate of H_2 permeance ($8.7\ m^3/h/bar^{0.5}$).

The transport of hydrogen through the membrane is a 5-step process as shown in Figure 2.2:

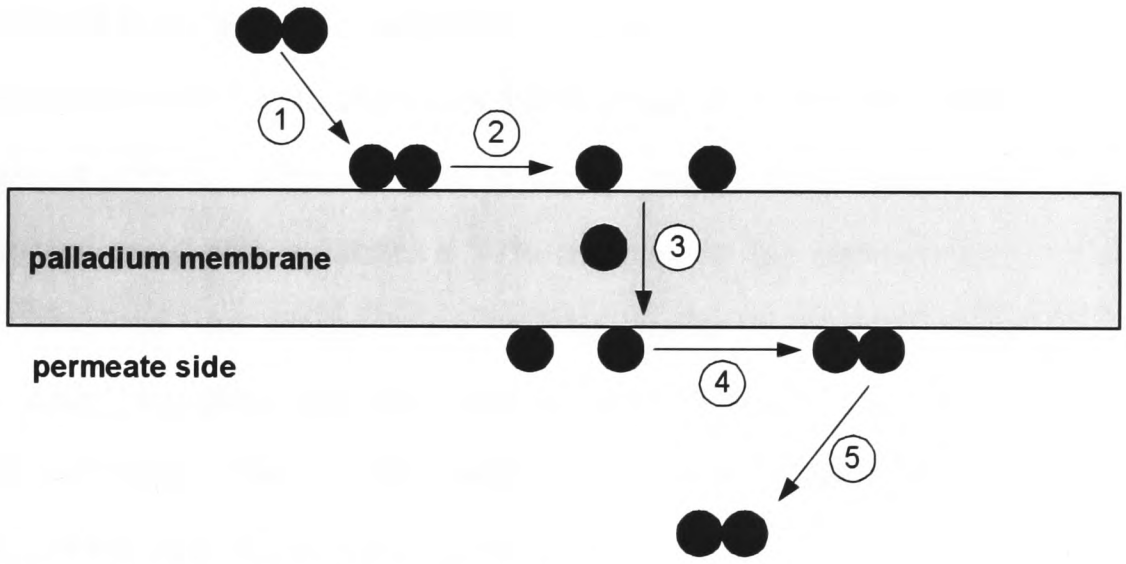

1. **Adsorption** on the membrane surface.
2. **Dissociation** of molecules into hydrogen atoms on the catalytically active palladium surface.
3. **Diffusion** through the membrane and emergence on the permeate side.
4. **Reassociation** to form hydrogen molecules.
5. **Desorption** of the hydrogen molecules from the surface.

Figure 2.3: *Diffusion of hydrogen through palladium* (Athayde, 1994).

The palladium membrane is a polycrystalline film with a fine grain structure. The palladium is thought to form a hydride during the diffusion process (Koros and

Mahajan, 2000; Glasstone, 1950). The grain boundaries form pathways for the diffusion of other gases and thus limit the selectivity of the membrane.

The high price of palladium ($248 per troy ounce as at 24/05/04 (FT, 2004)) leads to thinner membranes in the order of 1-5 μm. However at such a thickness, the membrane needs to be mechanically supported, typically using a porous ceramic substrate to withstand the pressure differentials across it. This produces what is termed an asymmetric membrane. Thermal cycling in a non-inert atmosphere results in delamination of the membrane from the substrate, due to the different thermal expansion coefficients of palladium and the substrate and the retention of hydrogen in the membrane causing hydrogen embrittlement. Alloys of palladium with copper (Roa and Way, 2002; 2003; 2004) and silver (Burch, 1969) can improve the mechanical properties of the membrane.

The adsorption of hydrogen into palladium produces two immiscible phases which are face-centred-cubic in structure and designated α and β. Only the α-phase exists above a temperature of 300 °C, whereas both α and β phases exist below this temperature. The formation of the β-phase causes a 10% increase in the metal volume (Tovbin and Votyakov, 1999) and thus temperature cycling results in repeated phase changes that disrupt the grain structure and can lead to embrittlement and dislocations, which rupture the membrane. Due to the instability of pure thin palladium membranes, alloys of palladium and silver have been produced which reduce the miscibility gap and produce an α-phase, which is stable at room temperature (Hunter, 1963). However in practice, thermal cycling should be carried out in an inert atmosphere to avoid any undue strain on the membrane. Also, any unalloyed islands of palladium will undergo α/β transition and pull the membrane apart.

Palladium membrane reactors can also be used to improve the efficiency of chemical reactions such as the water gas shift reaction (Uemiya *et al.*, 1990), by the rapid removal of hydrogen from the system and thus shift the thermodynamic equilibrium to the product side.

2.5 Hydrogen Fuel Cell System

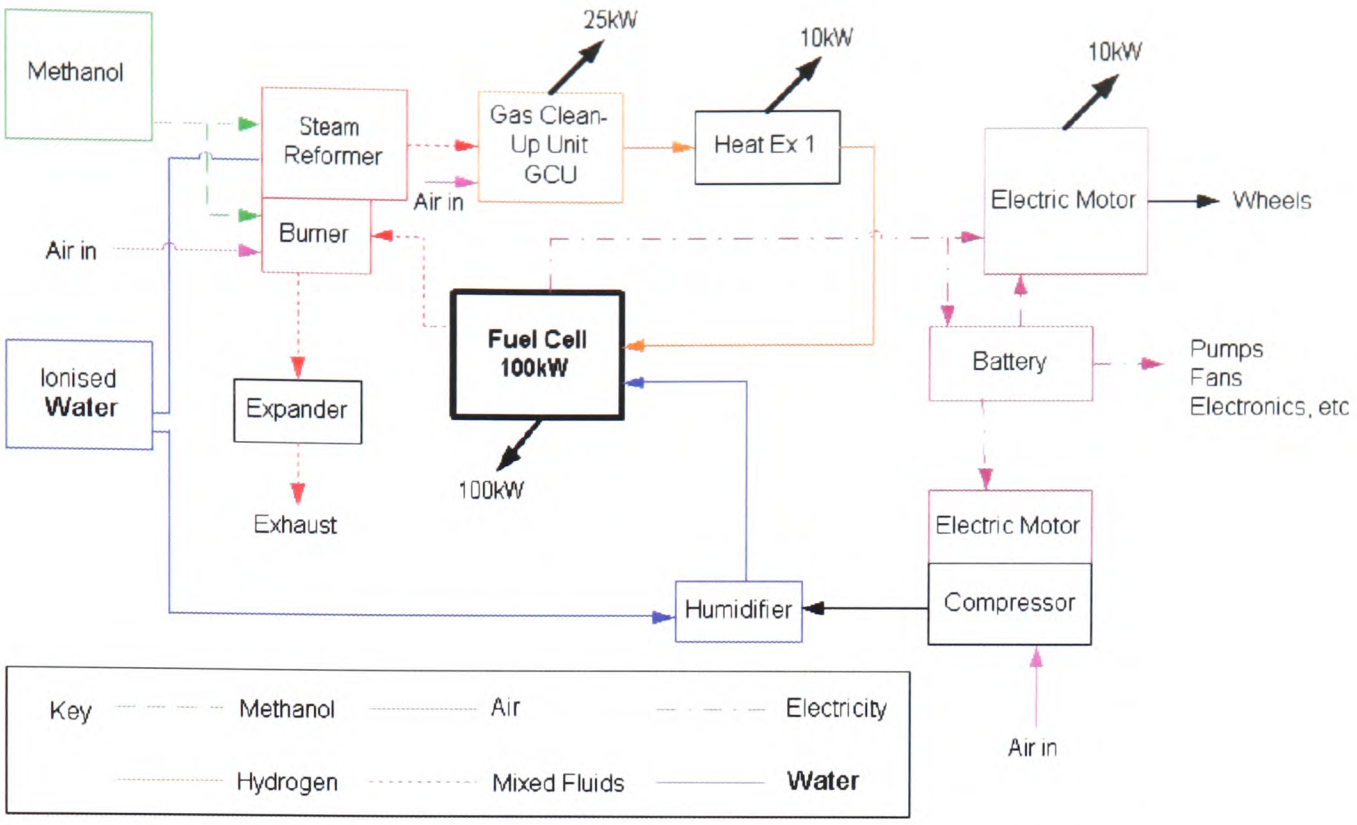

Figure 2.4: *100 kW PEM Fuel Cell system showing steam reformer and gas clean-up unit* (Ricardo, 2000).

In Figure 2.4, a fuel cell system is presented and shows how components may be connected. The steam reformer reacts the methanol to produce a mixture of mostly hydrogen, carbon dioxide, water vapour and carbon monoxide. To prevent poisoning of the platinum catalyst within the fuel cell, the carbon monoxide has to be selectively oxidised within the gas clean-up unit (GCU). The GCU needs to be cooled to control the selective oxidation, and then further cooling is needed since the fuel cell (e.g. solid polymer) is likely to operate at 80 °C. This heat is likely to be used for pre-heating the reactants to the steam reformer, and the air after it is compressed, but before it is humidified. The fuel cell is shown with an electrical output of 100 kW, and an equal quantity of heat to be rejected; a further 10 kW_e is dissipated from the electric motor and its control system. It must be remembered that the fuel cell is likely to be operating at 3 bara, so in addition to compressing the air, it is necessary to pump the methanol and water (prior to evaporation) to this pressure.

The anode and cathode off-gases leave the fuel cell and enter a catalytic burner where any un-reacted hydrogen from the anode is reacted, so that the exhaust stream consists of carbon dioxide, nitrogen, water vapour and oxygen. Since this is hot and

at a high pressure, it can be expanded in a turbine to produce work. The exhaust gases are then likely to be cooled, so that water can be condensed to eliminate the need for storing (and replenishing) large quantities of water that might freeze.

2.6 Conclusions

A number of gas clean-up approaches have been discussed in this chapter to remove impurities such as carbon monoxide, which can adversely affect the performance of the fuel cell. Pressure swing adsorption and palladium membranes both provide means to produce high purity hydrogen. As a refiner of platinum group metals, Johnson Matthey's interest is in the use of palladium membranes. This work looks in particular at thin supported membranes, and their fabrication is described in the following chapter.

3 Palladium Membrane Fabrication

As highlighted in Chapter 2, unsupported palladium membranes, known as drawn tubes, can have a thickness of some 100 μm which has high cost implications and limits the flux of hydrogen. Supported membranes therefore offer a solution to both the cost and the low hydrogen flux; the choice of the support material or substrate is discussed below. A photograph of a range of Johnson Matthey membrane tubes is shown in Figure 3.1.

Figure 3.1: *A selection of Johnson Matthey membranes. The large tubes are 200 mm in length and 25 mm in diameter. The white tubes (right) are the bare sol-gelled tubes. The silvery tubes have a Pd/Ag membrane. The small tube has a Pd/Cu membrane* (Johnson Matthey, 2001).

3.1 Substrate Choice

In choosing a suitable substrate on which to lay a membrane a number of factors should be taken into consideration:

- Surface finish - needs to be smooth enough to support a thin membrane though allow the membrane to key into the surface to avoid delamination.

- Porosity of the substrate - must be such to allow hydrogen to permeate; the resistance to flux through the substrate can be the dominant factor in the membrane/substrate unit.
- Sealing – how the membrane is sealed into a unit should also be considered, as even small leaks in the membrane will reduce the effectiveness of the membrane.

3.1.1 Ceramic Substrates

Before commencement of the project, a number of substrates had been examined to find a suitable one to support a thin membrane. The chosen substrate is a porous ceramic tube, open at one end and closed at the other, being easier to seal than flat plates (Knapton, 1973). The tube is a slip cast alumino-silicate comprising 76% alumina with an apparent porosity of 42.5%. The surface pore size measured by a scanning electron microscope (SEM) was in the region 1-2 μm with a median pore size throughout the substrate of 0.6 μm. The tubes are 200 mm in length, 25 mm in outer diameter and have a wall thickness of 2-3 mm. There is some variation in the geometry of the tubes and the surface does contain some pores much greater than the 1-2 μm size. These must be removed by a suitable surface preparation technique. The pore size is however important as to the thinness of the membrane which can be produced. Small pores may hinder the effective anchoring of the membrane to the supporting substrate and result in a membrane that easily delaminates. However the smaller the pores, the thinner the membrane can be to cover the surface adequately. During thermal cycling, the different expansion coefficients of the membrane and its support become important for the durability of the membrane. It was deemed necessary to apply a sol-gel layer to the surface of the ceramic substrate to reduce the pore size from the micron to the nanometre range. Sol-gels and their application are discussed in Section 3.1.5.

3.1.2 Thick-Walled Stainless Steel Substrates

Stainless steel is seen as a preferred long term alternative to ceramic substrates due to its similar expansion coefficient compared with palladium and ease of sealing in a system (Mardilovich *et al.*, 1998; Ma *et al.*, 2003). The thick-walled tubes that have been used are supplied in lengths of 2.5 ft, which then have to be cut to size. The tubes have an external diameter of 1 inch (25.4 mm) and a wall thickness of 4 mm.

They are produced of 316L stainless steel by a sintering technique, which results in an average pore size of 3 μm at a grade of 0.5 μm (95% rejection) (Mott, 2002). Due to changing project priorities, only preliminary work has been performed on stainless steel substrates. This work is summarised in Section 3.4.1.

3.1.3 Thin-Walled Stainless Steel Substrates

The thin-walled tubes have an external diameter of ½" (11.8 mm) and were supplied in lengths of 200mm for use in the test apparatus. These tubes are made of sintered 316L stainless steel. The nominal wall thickness of the tubes was 0.46 mm. The internal surface of the tubes has a 10 μm zirconia (ZrO_2) layer and comprises particles of 200 nm diameter with a pore size of 1 μm (Pall, 2004). The tubes have a 2 μm absolute liquid removal rating. The thin-walled substrates were supplied with welded stainless steel end flanges which not only served to provide a good sealing point, but also prevented these relatively weak tubes being crushed. A further batch of tubes was supplied with a thicker zirconia layer, though optical microscopy analysis found the variation to be between 5.5 μm and 13 μm.

3.1.4 Surface Treatment of Ceramic Substrates

The surface of the tubes has a slightly ridged surface due to their manufacturing procedure. The tubes have to be sanded with a range of silicon carbide papers up to a 1000 grade paper using a wet sanding technique. After the surface has been sanded, the tubes are fired to remove any residual organics and ensure that they are thoroughly dry.

3.1.5 Sol-Gel Application

A sol-gel is a colloidal suspension of solid particles in a solution in which the dispersed phase is so small (~1-1000 nm) that gravitational forces are negligible. The use of sols for coating the ceramic tubes has concentrated on alumina sols, as this is similar to the substrate material. A solution is produced consisting of the sol mixed with PVA to produce a controlled rheology sol that will adhere to the tubular geometry until the substrate is fired. The sol must be free from bubbles and other particulates, which may prevent the sol forming a smooth consistent surface layer on the substrate. The ceramic tube is dipped at a set rate using an electronic speed controlled dipping unit into the sol-gel mixture and removed slowly to ensure that the

layer produced is as even as possible with a thickness in the order of 5μm. Capillary action draws the water into the pores of the ceramic and leaves the hydrated alumina as a gel on the surface of the substrate. After withdrawing and allowing to dry at room temperature the sol-gel is calcined by heating at 1 °C/min to 1250 °C and holding for 1 hour. The calcination cycle must be at a slow enough rate to prevent the undue straining of the sol-gel layer and its subsequent delamination from the substrate (Bosco *et al.*, 1998). The calcination cycle produces a porous ceramic with a body with pores in the micron range and a surface layer consisting mainly of crystalline α – aluminium oxide as determined by X-Ray diffraction (XRD) analysis (Jobson, 2002), that has a smooth surface appearance and smaller pores and make it ideal for the application of a palladium membrane.

3.2 Palladium Deposition

The deposition of palladium onto the substrate material may be carried out in a number of ways. These include, spray pyrolysis (Li *et al.*, 1993), rolling (Tosti *et al.*, 2002), metal-organic vapour deposition, (Jun and Lee, 2000), magnetron sputtering (Jayaraman and Lin, 1995) and electroless plating (Collins and Way, 1993). It is the electroless procedure though which has been successfully applied here, and this is described below.

3.2.1 Electroless Plating

Electroless plating occurs in the absence of an external current and so the reductant in the solution supplies the electrons to reduce the metal ion. It is a selective deposition of metal from aqueous solutions, by a heterogeneously catalysed reduction on a metallic substrate. The film thickness of the plate can be built up with successive plating batches or the addition of more metal to the electroless plating baths. The process is autocatalytic as the metal is itself a catalyst for the reduction process.

The reaction that occurs is a heterogeneously catalysed transfer of electrons across an interface from a reducing agent R to metal ions M^{n+}. Two partial reactions make up the overall reaction and occur simultaneously on the substrate between which there is a flow of electrons. These reactions are as follows:

- Anionic oxidation of the reducing agent $R_{red} \rightarrow R_{ox} + ne^-$

- Cathodic reduction of the metal ions $M^{n+} + ne^- \rightarrow M$

where R_{red} and R_{ox} are the reduced and the oxidised forms of the reducing agent.

For the reaction to proceed, the standard reversible reduction potential of the reducing agent must be more negative than that for the metal/metal ion system to be reduced. Rewriting the two partial reactions as reductions, with standard reversible reduction potentials E_c and E_a gives:

$$M^{n+} + ne^- \rightarrow M \qquad [1] \qquad E_c$$

$$R_{ox} + ne^- \rightarrow R_{red} \qquad [2] \qquad E_a$$

Combining [1] and [2] gives the overall reaction for the electroless plating as:

$$M^{n+} + R_{red} \rightarrow M + R_{ox} \qquad E_{reaction} = E_c - E_a$$

Thermodynamically for the reaction to proceed $E_{reaction}$ must be positive.

Electroless plating requires the selective reduction of the metal at the surface of the substrate. Non-catalytic surfaces such as a glassy sol-gel layer need to be sensitised and activated in order to form nucleation sites. These sites catalyse the reducing agent and allow the metal film to grow.

3.2.2 Sensitising

The surface of the substrate is sensitised by the adsorption of a reducing agent, often $SnCl_2$, by immersion of the substrate in a sensitising solution. Following rinsing and drying the sensitiser remains on the surface of the substrate.

3.2.3 Activation

The activating solution is a solution of readily reducible salt, typically $PdCl_2$, which is reduced by the sensitising solution when the substrate is immersed. Fine catalytic seeds are formed on the substrate surface in the order of 1-100 nm. A simplified mechanism of the formation of the palladium seeds is as follows:

$$Sn^{2+} + Pd^{2+} \rightarrow Sn^{4+} + Pd_{(metal)}$$

3.2.4 Reducing Agent

It is important that the metal to be plated catalyses the oxidation reaction of the chosen reducing agent at a fast enough rate for plating to be practicable. All reducing agents used in electroless plating contain hydrogen atoms and a simplified mechanism for the oxidation reaction of the reducing agent, R, is as follows:

- Dehydrogenation of the reducing agent $RH \rightarrow R + H$

- Charge transfer across the surface $R + OH^- \rightarrow ROH + e^-$

Generally electroless plating operates in the alkaline regime as can be seen by the presence of the OH^- ions. Hydrogen adsorbed at the surface can also recombine to form H_2 gas, which is often evolved during plating.

3.2.5 Meta-Stable Bath

The plating bath is meta-stable in the sense that no reduction of the metal ions occurs after the reducing agent has been added until the catalytically active substrate is immersed in the solution. There are a number of interdependent factors which contribute to a stable plating bath. Due to their interdependency it is difficult to isolate the exact effect of each factor. However the following is known:

Complexing Agents: These act to stabilise the metal ions as complexes, buffer the pH, control the plating rate and change the reduction potential of the metal ion. Complexing agents need to be able to prevent spontaneous bath decomposition.

Reducing Agents: The metal/reducing agent combination needs to be chosen carefully to ensure autocatalytic metal deposition. The pH is usually alkaline and the concentration of the reducing agent is low to ensure controlled deposition.

pH: Plating rates increase with higher pH although there is usually an optimum window in which to work. Both the reducing agent and the stability of the metal ion complexes are affected by the pH.

Temperature: The plating rate increases as the plating bath temperature is increased, but can also affect the bath stability and cause premature bath decomposition.

Other Factors: The absolute and relative concentrations of reagents greatly affect the stability of the electroless bath. It is also important to ensure that all plating vessels are clean as any debris may act as a seed and cause the bath to decompose. The volume of the bath to the plating surface must also be taken into account to ensure an even plate.

3.3 Johnson Matthey Palladium Plating Procedure

The method successfully used by Johnson Matthey for plating ceramic substrates is a proprietary procedure and will not be detailed here. The method produces a palladium membrane with a thickness of order 5 μm and active area of 138 cm^2. It is possible to get a qualitative prediction of the membrane quality simply by inspecting the surface. A shiny surface tends to indicate low palladium deposition and imperfections and non-uniform coloration are usually quite self-evident. The surface of a good membrane tends to be a matt grey colour. A 2 μm silver plate is then electrolessly deposited onto the palladium.

3.3.1 Reduction and Analysis

The sample is heated in a reducing atmosphere to form a homogeneous alloy by mass diffusion. The membranes currently being produced have an alloy composition of Pd-23%Ag being the optimum composition to prevent lattice distortion but maintain hydrogen diffusion (Grashoff, *et al.*, 1983; Lewis, 1967). EPMA (Electron Probe Microanalysis) is used to analyse cross sections of the membrane and determine the palladium/silver distribution through the thickness of the film. The film thickness can be measured to a reasonable degree of accuracy (± 0.1 μm) using an optical

microscope. The flow testing and durability characteristics of the membrane are performed using purpose built test stands, the details of which are described in Chapter 5. A scanning electron micrograph of a 7 μm Pd/Ag membrane is shown in Figure 3.2. The pores in the substrate are clearly visible. The sol-gel layer can be seen to smooth out the majority of the surface imperfections in the ceramic substrate. The palladium/silver layer can be seen as an even, coherent coat over the surface of the sol-gel layer.

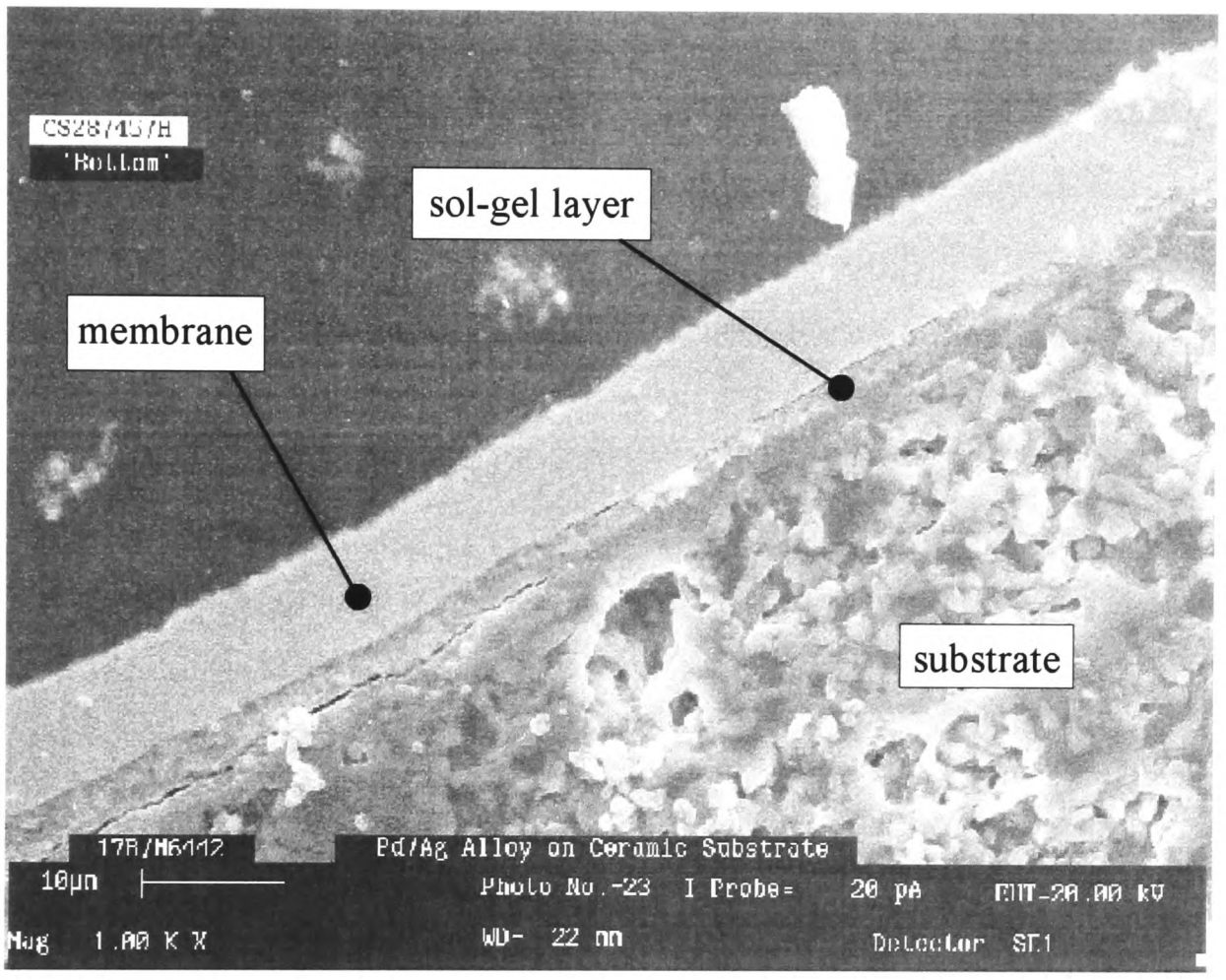

Figure 3.2: *SEM image of a 7 μm Pd/Ag membrane on a ceramic substrate. The sol-gel layer is also clearly visible* (Johnson Matthey, 2001).

3.3.2 Improvements in Plating Procedure

Over the course of the project, significant successes were had in improving the quality of the plating procedure. These techniques included alternative sol-gel recipes, application techniques, drying cycles and improving the plating bath cleanliness. The improvements led to nitrogen leaks commonly less than 2 sccm (440 °C, 3 barg pressure drop).

3.4 Stainless Steel

As mentioned in Section 3.1.2 only preliminary work was carried out on stainless steel substrates using both the thick-walled and thin-walled substrates. This work is summarised below.

3.4.1 Thick-Walled Stainless Steel Substrate Surface Preparation

The surface of the thick-walled stainless steel tubing is relatively rough and in order to be able to lay a thin palladium membrane on the surface it is necessary to smooth and clean the surface. An optical microscope image of the surface can be seen in Figure 3.3, which clearly shows the rough undulating surface of the substrate. The holes in the surface make the production of a thin membrane very difficult. Several forms of surface modifications have been tried which included mechanical as well as chemical techniques in an attempt to reduce this roughness.

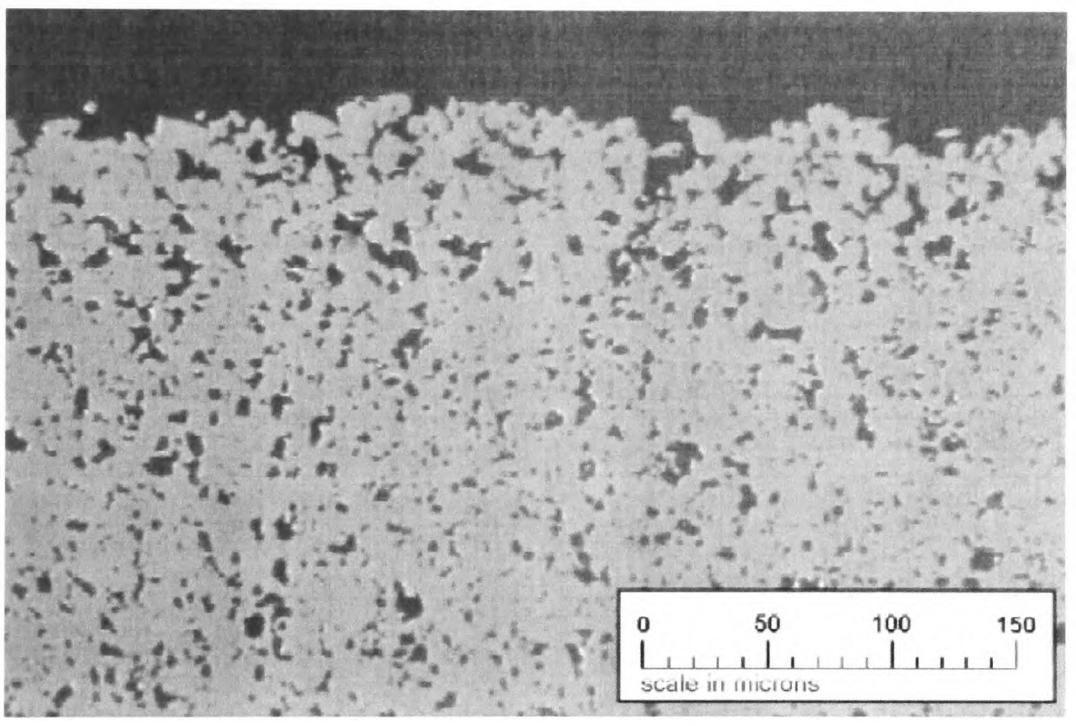

Figure 3.3: *An as received thick-walled stainless steel tube clearly showing the undulating and incoherent outer surface as shown using an optical microscope. The porous structure of the substrate is also visible.*

3.4.2 Mechanical Surface Preparation

Mechanical surface preparation offers a visibly shinier and thus smoother surface, which also serves to remove any small imperfections in the surface that would be difficult to plate. So far two techniques have been attempted which are as follows:

3.4.2.1 Rolling

A rolling device was developed at Johnson Matthey that consists of two rollers. One of these rollers is on a spindle on a fixed arm while the other is on a hinged arm so it can follow the contours of the surface of the tube as it rotates. A spring keeps the two rollers on the surface with the aim to flatten the surface. The rolling device is fixed to a turning machine so the roller moves along the central axis of the rotating tube. It has been possible to produce a surface that appears quite shiny though it has been noticed that some parts are left untouched by the roller. This is due to the stainless steel tube not being round and the rollers too large to be able to follow all the contours. The results of this technique can be seen in Figure 3.4. The surface appears flat, though a number of small surface imperfections remain.

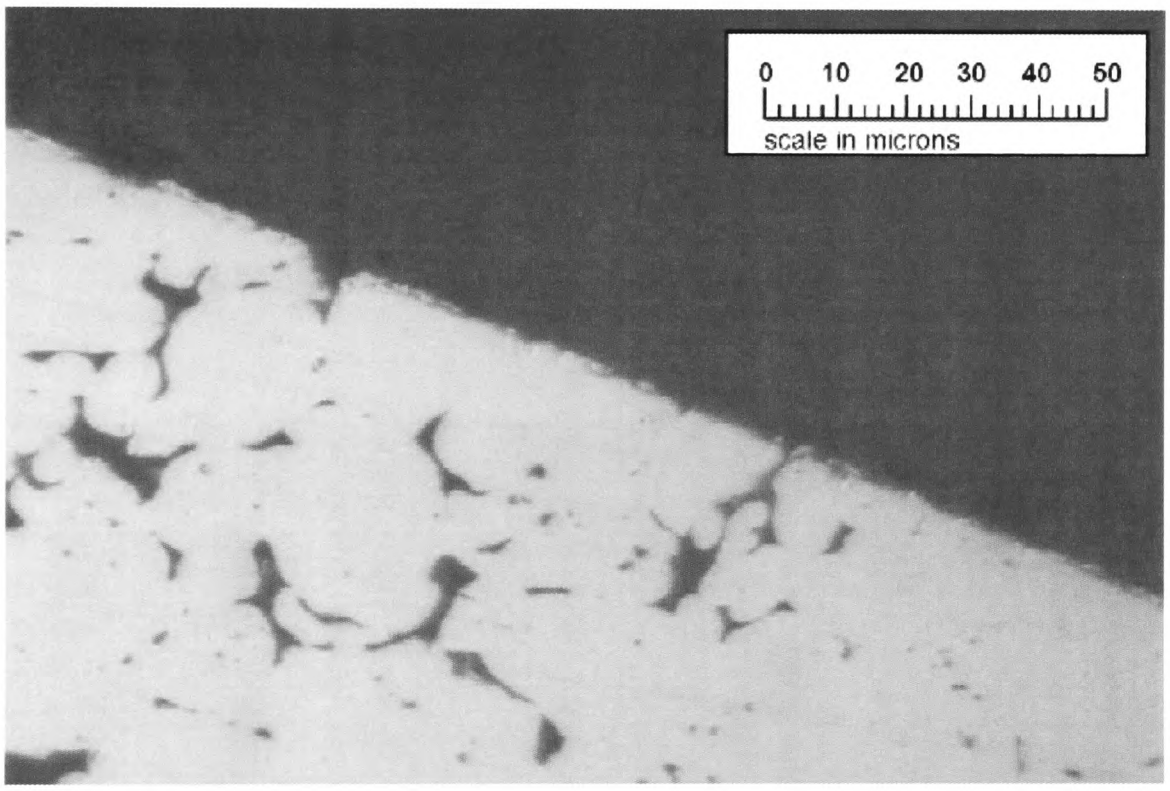

Figure 3.4: *An optical microscope image (x50 optic) of the surface of a stainless steel tube, which has been rolled using a 'high' load setting.*

3.4.2.2 Bead Blasting

Bead blasting, akin to that by Jemaa *et al.*, 1996, has also produced some promising effects. High-grade 100 μm glass blasting particles have been used at pressures ranging from 0.7 to 3.5 barg. The surface appears visibly shinier and analysis under an optical microscope shows a smoother surface finish. It is difficult however, due to the manual nature of the bead blasting apparatus, to ensure an entirely even finish. The

effects of bead blasting at 0.7 and 3.5 barg can be seen in Figure 3.5 and Figure 3.6 respectively. At higher pressure the surface of the substrate is clearly more compacted.

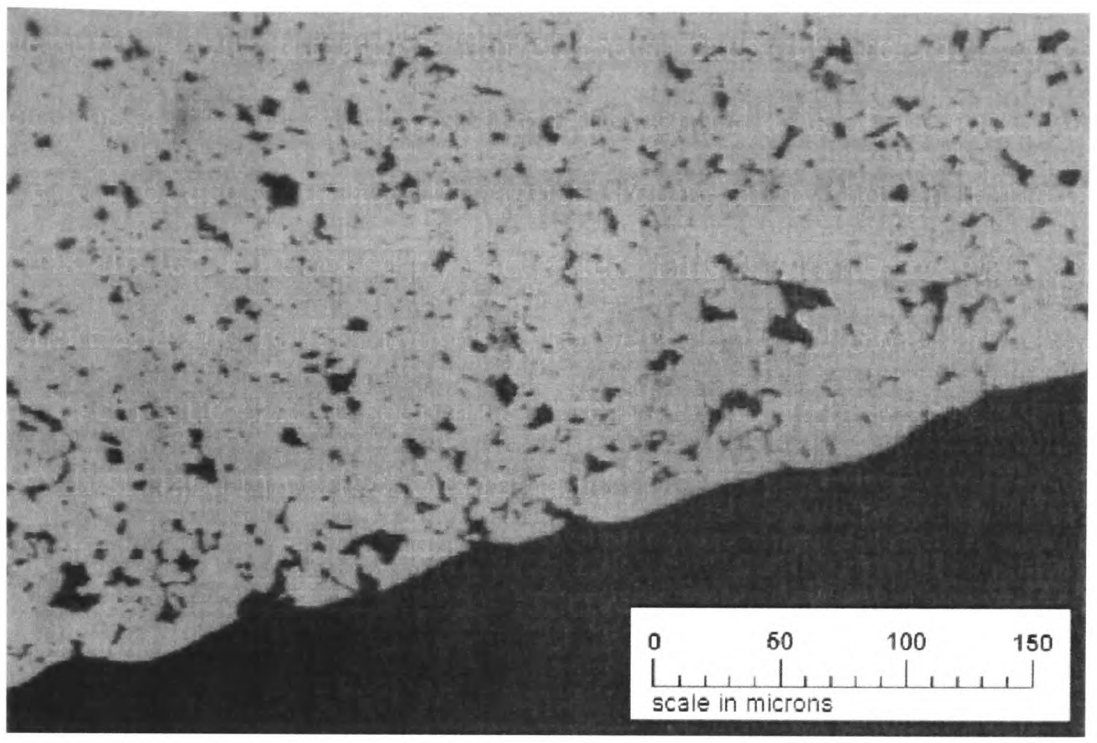

Figure 3.5: *Optical microscope image (x20 optic) of the surface of a stainless steel substrate bead blasted at 0.7 barg (10 psig).*

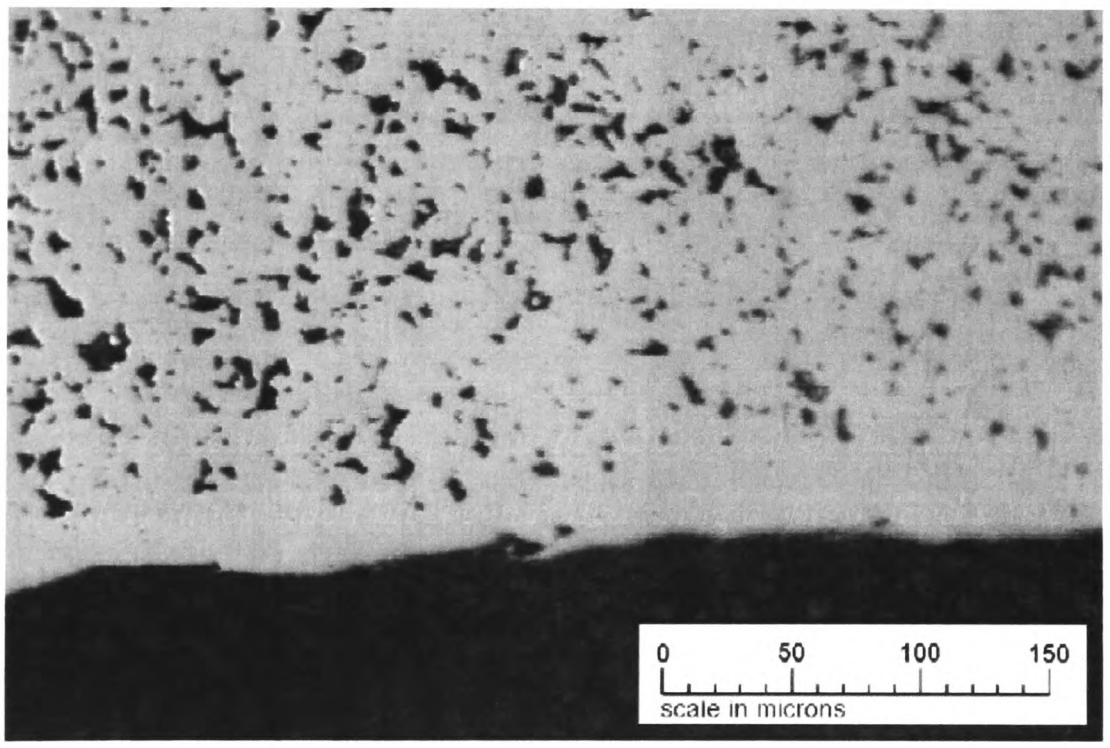

Figure 3.6: *Optical microscope image (x20 optic) of the surface of a stainless steel substrate bead blasted at 3.5 barg (50 psig).*

3.4.3 Electro-polishing

Some preliminary work was done to investigate the effectiveness of etching and electro-polishing the surface of the stainless steel substrate. However the pore size of the substrate is quite large and any chemical treatment tends to affect the whole structure and not just the surface. This can result in surface imperfections actually being exaggerated. The effect of electro-polishing can be seen in Figure 3.7 and should be compared with the as received substrate shown in Figure 3.3.

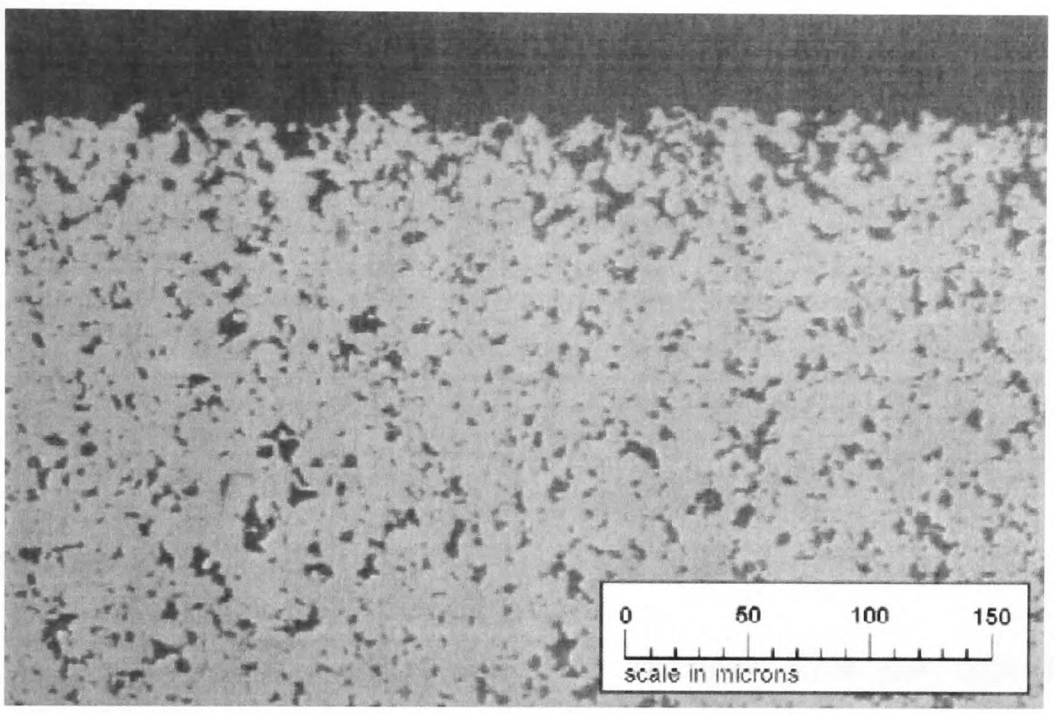

Figure 3.7: *Optical microscope image of an electro-polished stainless steel substrate.*

3.4.4 Barrier Layer formation

Due to the large pore size of the stainless steel substrate it was thought necessary to produce a barrier layer to produce both a smooth surface as well as ensuring the membrane will only be developed on the outer surface of the substrate. Palladium tends to diffuse with time and a sample, which was heated to 500 °C for 1 week, showed between 0.5 – 1 μm depth of diffusion of the palladium into the surface of the stainless steel. A barrier layer was considered in order to prevent this. Sol-gels as well as other alumina layers were tried with varying successes, but tended to 'mud crack' on calcination or disintegrate during subsequent plating procedures. Different heat treatments were also performed to investigate how the formation of an oxide layer would help prevent the diffusion of the palladium, but increased temperature led to a

reduction in the permeability of the substrate as shown in Figure 3.8. Firing temperatures above 500 °C led to increasing deterioration in substrate permeability. At a temperature of 800 °C, no nitrogen flow was possible.

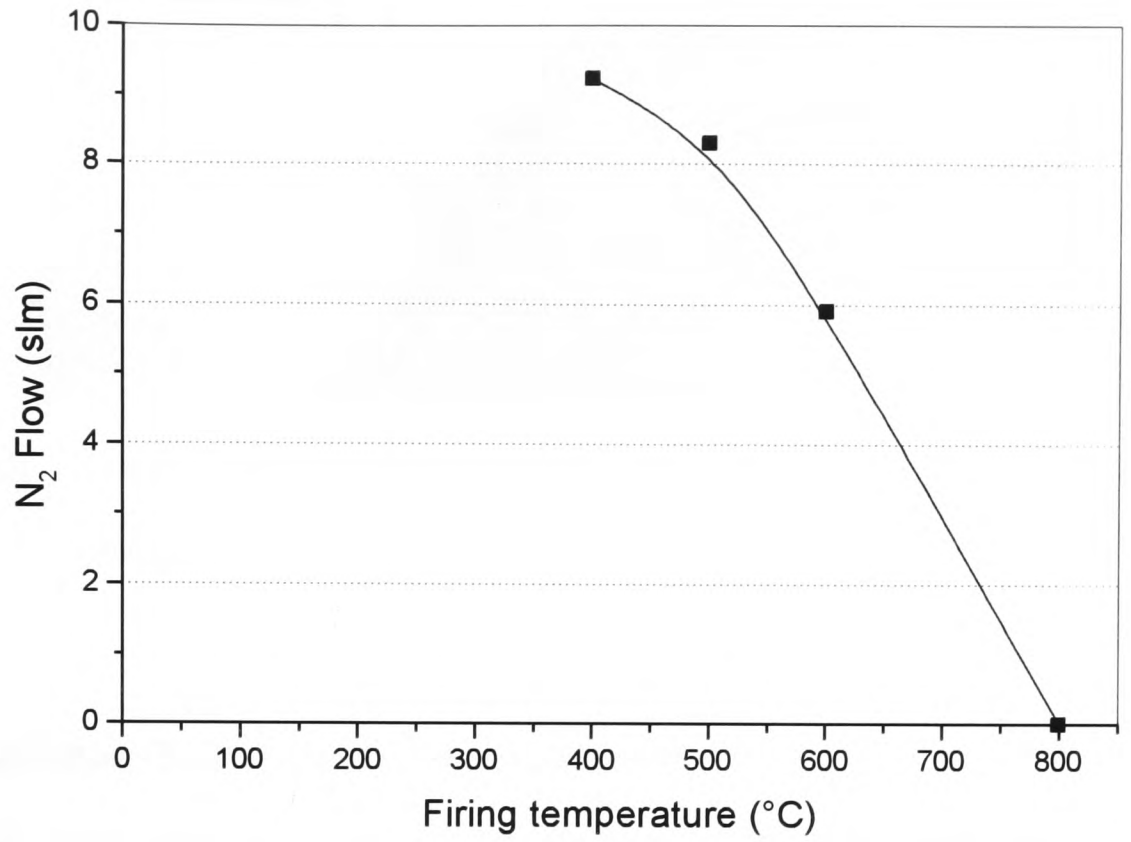

Figure 3.8: *Effect of firing temperature on nitrogen flow through thick walled stainless steel substrate with 1 barg pressure drop at 440 °C.*

Although these surface preparation techniques produce a substrate with finer surface pores and thus a more suitable surface for palladium deposition, care must be taken to avoid total closing of the surface pore structure especially in the case of the mechanical surface preparation.

3.4.5 Thin-Walled Stainless Steel Substrates

The thin-walled stainless steel substrates have a zirconia layer on the inner surface to provide both a smoother surface on which to plate and a barrier to prevent diffusion of the palladium into the substrate. The as-received thin-walled stainless steel substrate can be seen in Figure 3.9. The substrate is clearly visible, though the zirconia layer is less distinct due to the difference in surface reflection (it is the layer adjacent to the light steel with an even grey colouration). The boundary with the sample mount resin is highlighted by the addition of the white line.

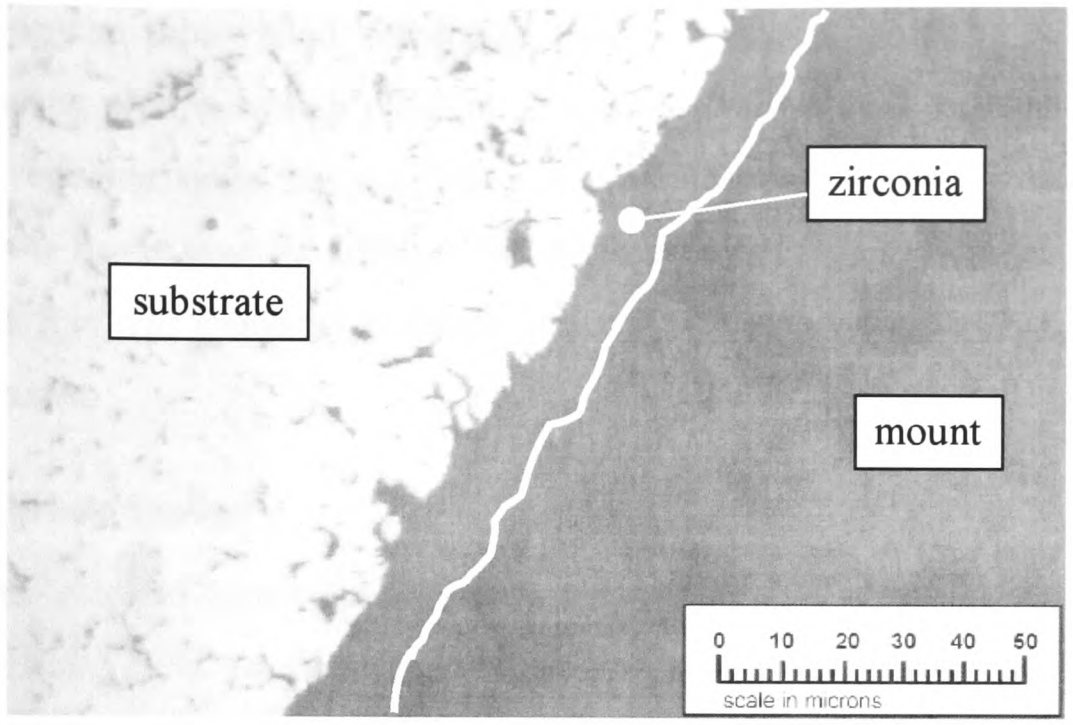

Figure 3.9: *Thin-walled stainless steel substrate with a thin (approx 10 μm) zirconia layer on the inner surface.*

3.4.6 Palladium Deposition on Stainless Steel

The initial treatment for any of the stainless steel substrates was the use of isopropanol in an ultrasound bath to remove any greasy residues that may be present after the manufacturing process. Without this degreasing process, finger print marks were sometimes observed on plating.

The thick-walled substrates were generally plated on the outer surface, but in the case of the thin-walled substrates, plating took place on the inner zirconia layer surface. In order to be selective as to which surface was exposed to the plating solutions, heat shrink wrap was used either on the outside of the tube in the case of the thin-walled substrate and rubber bungs for the thick-walled substrate to mask the substrate.

The conventional sensitising and activation procedures were initially used on the substrates, but one of the problems encountered was the corrosion of the steel due to the use of acidic solutions. Alternative methods were employed including coating the surface with a colloidal palladium solution to activate the surface. This novel plating process had the additional benefit of hindering the formation of the membrane within the zirconia layer. This result is discussed in Chapter 4.

When plating the thin-walled substrates, there tending to be little mixing of the solutions during plating, which resulted in a greater tendency for the plating bath to crash if the reducing agent was supplied in a similar manner to the ceramic substrates. This led to a more gradual addition of the agent and frequent forced mixing of solution and this was found to go some way to prevent premature decomposition of the plating bath.

3.5 Membrane Sealing

As discussed later in Chapter 5, the sealing arrangement of the ceramic membranes in the test chambers relies on a soft graphite seal which eases with repeated temperature cycling as the thermal expansion of the alumina tube ($7x10^{-6}$ $°C^{-1}$) is significantly less than that for the stainless steel chamber ($17x10^{-6}$ $°C^{-1}$). The sealing has been found to be adequate for test purposes, but a real system would demand a more reliable 'hard' seal. One method investigated was the use of a Kovar collar. Kovar (53% Fe, 29% Ni, 17% Co, <1%Mn), having a similar thermal expansion coefficient to the substrate ($5x10^{-6}$ $°C^{-1}$), was considered a suitable material for the application. The ceramic substrate was initially machined down to provide a smooth and perfectly round surface so that the collar would sit flush with the membrane surface. Kovar collars were then brazed onto the open end of the ceramic substrate using a proprietary technique by a third party supplier, though the principles of active brazing are presented in the work by Zhang *et al.*, 2001. After the brazing process, the ceramic substrate surface was found to be light grey in appearance and it was thought that the tubes were contaminated. This was confirmed by flow testing showing a 25% reduction in nitrogen flow from 1.83 slm to 1.35 slm using a 1 bara vacuum. Other areas of concern with this sealing technique were the seamless plating of a membrane around the closed end of the tube which would now be exposed. Also of concern was the collar to membrane interface and how this would be bridged. Thermal cycling of an alumina/Kovar joint is described in the work by Qiao *et al.*, 2002 and suggests that the temperature cycles actually reduce residual joint stress and increase the shear strength.

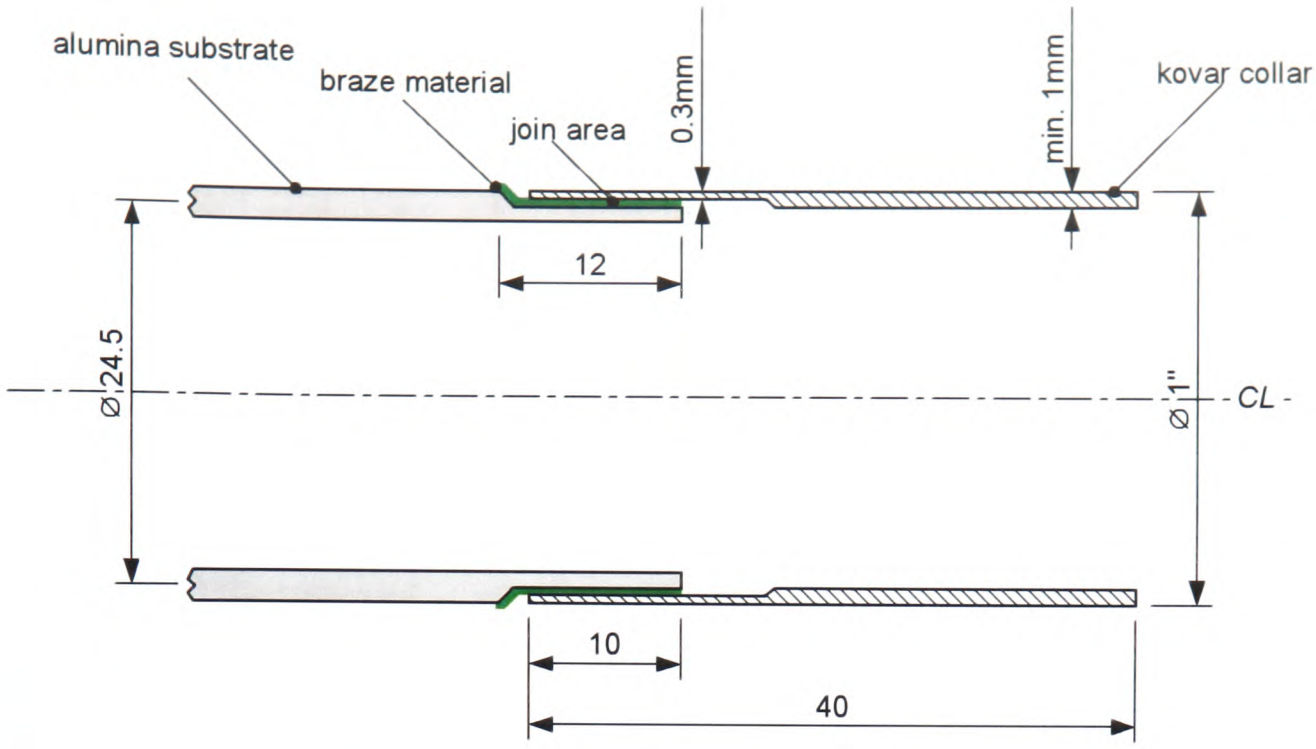

Figure 3.10: *Cross section of Kovar collar arrangement.*

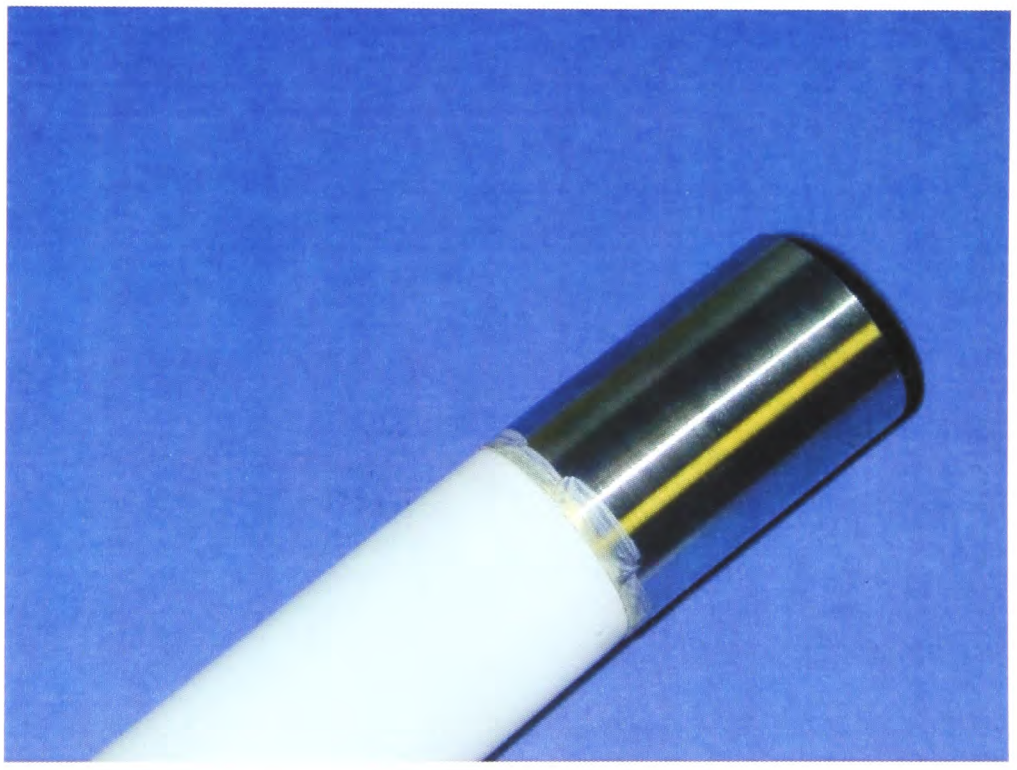

Figure 3.11: *Photograph of Kovar collar brazed onto ceramic substrate.*

In order to seal the Kovar collar into a chamber, attempts were made to use a standard stainless steel compression fitting, however it was found that the thermal expansion mismatch now between the stainless steel and the Kovar collar was a problem. Using Kovar ferrules in the fitting did not improve this and the manufacture of compression fitting entirely from Kovar was deemed too expensive. All of these issues as well as the high cost of Kovar and the brazing procedure even before a leak-free membrane had been applied, resulted in this sealing arrangement being abandoned.

3.6 Conclusions

Ceramic substrates have been successfully plated with a palladium silver alloy membrane. Improvements in the plating procedure have resulted in reduced leaks in the membrane on subsequent flow testing. The standard plating procedure produces a 7.5 μm Pd/Ag membrane. Testing of thicker and thinner membranes is discussed in Chapter 6. It can be said though that without improvements in the surface quality of the substrate, thinner membranes are more prone to cracks. Thicker membranes on the other hand show reduced hydrogen flux suggesting that at the current stage of development, the standard thickness is the optimum. Stainless steel substrate materials have been investigated and look promising in the long-term, though are not at a sufficient stage of development for application in this work.

4 Membrane Microscopy Analysis

4.1 Optical Microscopy Analysis

Membranes were sectioned using diamond cutting wheels and hot mounted in epoxy mounting resin using a Struers Predopress. The samples were then polished using increasingly fine grades of silicon carbide paper up to a grade of 2400 on a Struers RotoPol-22 rotary polisher. A final polishing step was performed with a Buehler Minimet polisher using 6 μm and 1 μm polishing particles. Images were taken with an Olympus BH-2 microscope using Global Lab Image v2.0 image analysis software for the greyscale images and Syncroscopy AcQuis image analysis software in the case of the colour images.

4.2 Electron Microscopy Analysis

Optical microscopy analysis is a suitable method for determining the thickness of the membranes. However such analysis only provides limited details as to the extent to which the palladium and silver have alloyed. A standard membrane tube was examined by scanning electron microscopy (SEM) and electron probe microanalysis (EPMA) to determine the membrane alloy composition across a section of the membrane tube. A section of membrane was taken at both ends of the tube as well as a section towards the centre of the tube in order to give an indication of any variation along the length of the membrane tube. The first images give some indication of the coherence of the membrane over the surface of the tube and whether any cracks or delaminations exist. In Figure 4.1, a section of a membrane tube is shown which has been taken from the top of the tube, i.e. near to the open end. The membrane is visible in the middle of the image as the light grey stripe running vertically from top to bottom. To the left of the image the porous ceramic substrate is visible and to the right of the image, the sample mounting resin can be seen. It is not clear from these images, but the slightly darker grey stripe to the left of the membrane is the area where the membrane is mechanically keyed into the substrate.

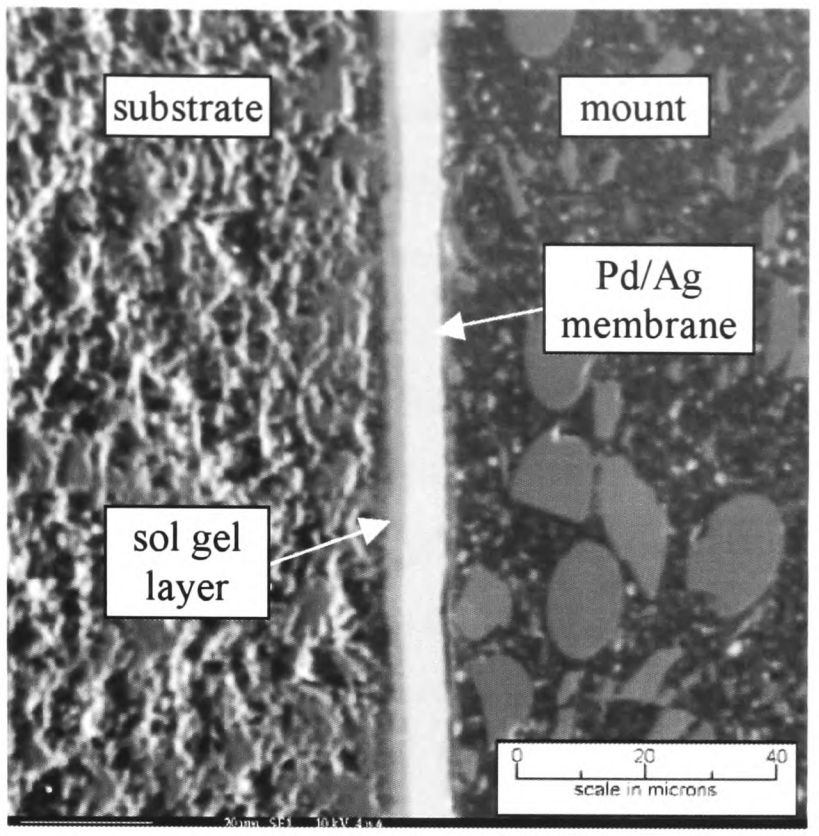

Figure 4.1: *Cross section at open end of standard 7.5 μm Pd/Ag membrane using SEM.*

A smaller scale image of a membrane section from the open end of the tube is shown in Figure 4.2. The membrane is of a consistent thickness around this segment of the tube and appears to be well adhered to the surface.

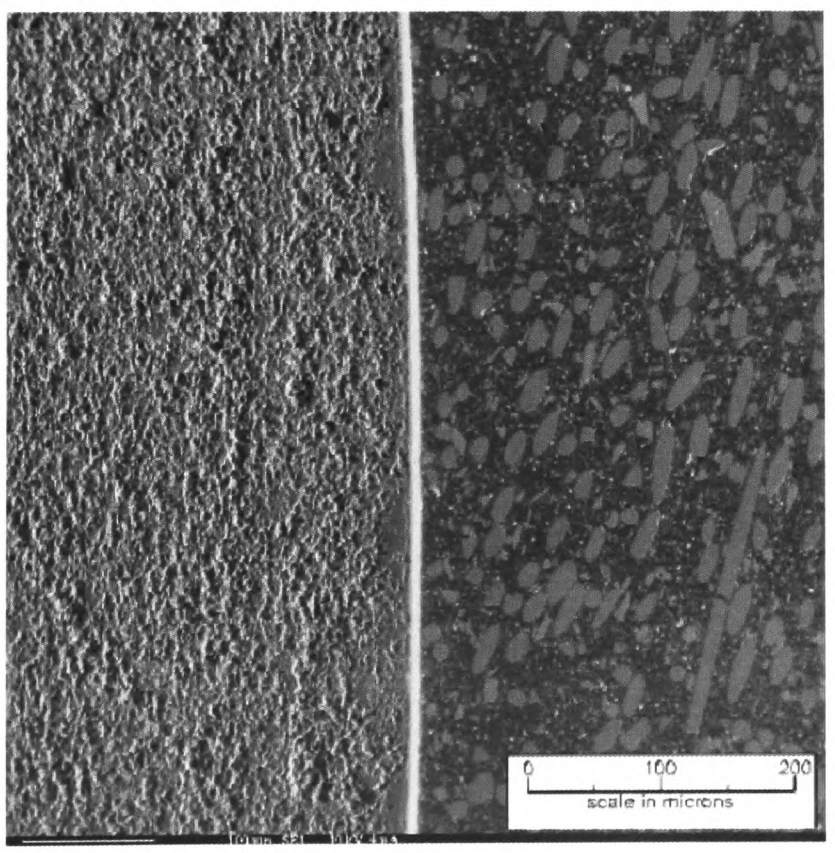

Figure 4.2: *Cross section at open end of standard 7.5 μm Pd/Ag membrane using SEM – small scale.*

Sections of the standard Pd/Ag membrane were analysed at the central section of the tube as shown in Figure 4.3. There are some loose particles that appear in the image, but as far as the membrane itself is concerned the section is similar to that from the top of the tube. The substrate however does exhibit a feature, which is often found to be present in the ceramic substrate, where there is an area of increased density in the substrate. This shows up as the smooth dark grey area to the left of the membrane which is labelled in Figure 4.3. The presence of areas of different substrate density was also observed during the membrane plating activating procedures. After drying the activated tube, patches would appear which would be slightly lighter in colouration. It is thought these denser areas form due to the slip cast method of manufacturing the tubes. These areas being indicative of the mould entry flow points. The patches do not seem to have a significantly adverse effect on the metal deposition process though the quality of the substrate in terms of consistency is an issue that could be examined in further work.

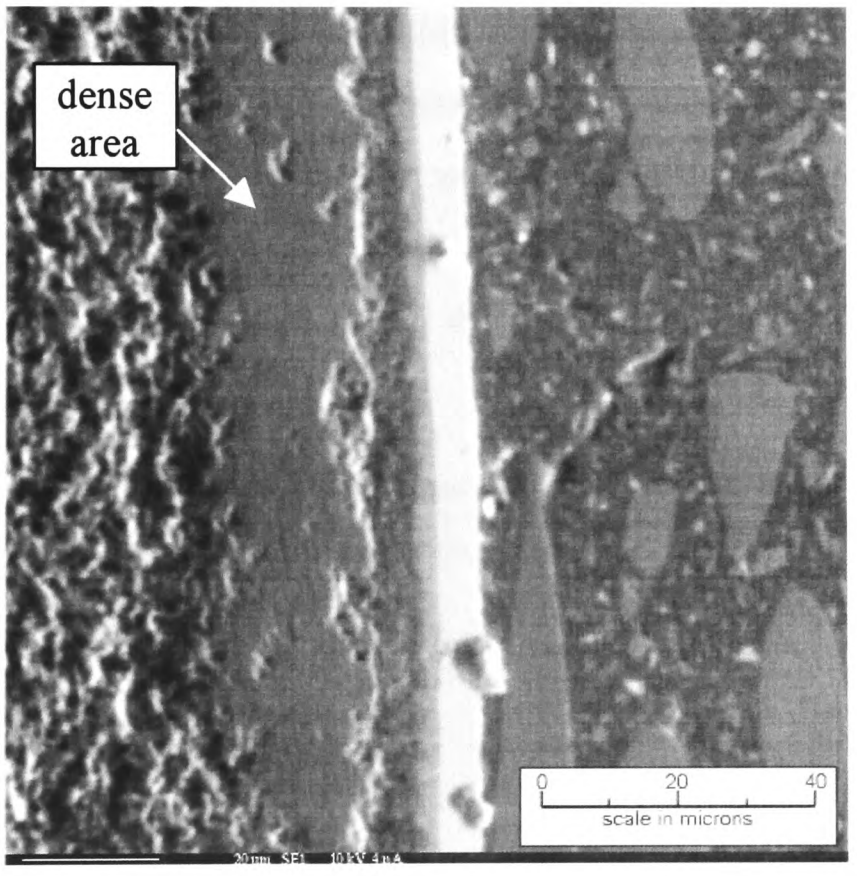

Figure 4.3: *Cross section at middle of standard 7.5 μm Pd/Ag membrane using SEM.*

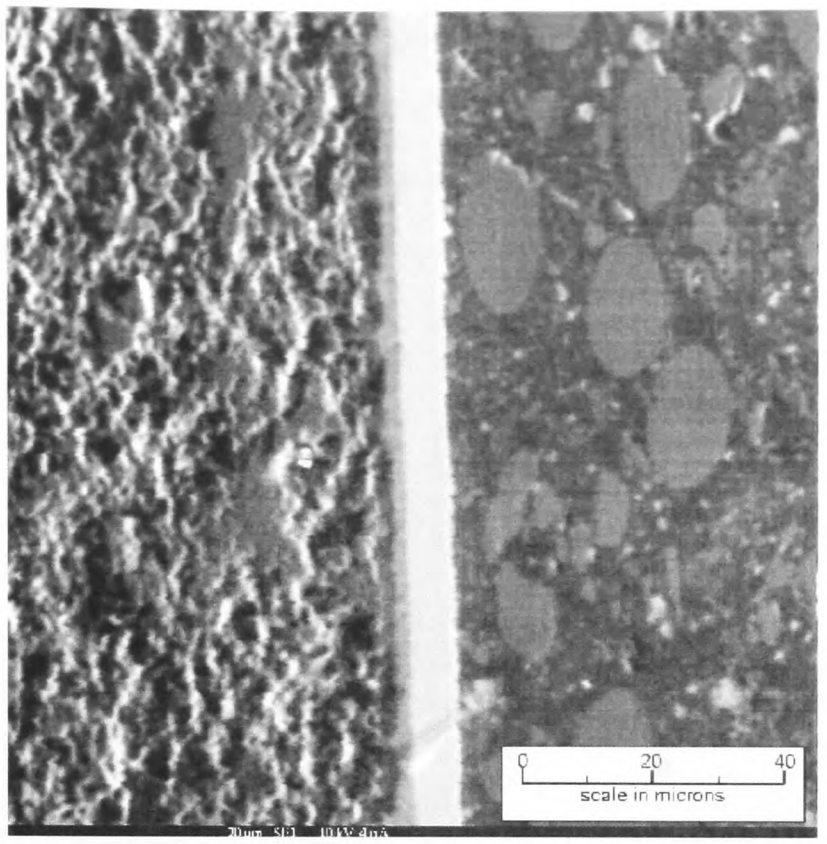

Figure 4.4: *Cross section at closed end of standard 7.5 μm Pd/Ag membrane using SEM.*

Optical Analysis of the membrane provides a quick assessment of the quality of a membrane in terms of its consistency and thickness. All of these techniques though do require the membrane to be sectioned and thus the membrane destroyed. The thickness can be estimated by considering the mass gain (~1 g) of the bare substrate (~85 g), using a mass balance accurate to 2 decimal places, after each plating stage as follows:

$$\text{membrane thickness} = \frac{\text{mass change}}{\text{density} \times \text{substrate surface area}} = \frac{\Delta m}{\rho \times (\pi r^2 + 2\pi r l)}$$

where: r is the external tube radius

l is the coated tube length

Δm is the mass gain after the plating step

ρ is the metal density (ρ_{Ag} = 10490 kg/m^3, ρ_{Pd} = 12023 kg/m^3)

Comparison of the thickness determined by this mass difference as well as by optical means has shown that if the sample is sufficiently free of residual water through

drying at 80 °C whilst connected to a vacuum pump, then an accuracy of around ± 0.2 μm between the values has been found. It is essential to be able to determine the thickness of the membrane without damaging the membrane. The variation in membrane thickness around the circumference of the substrate has been measured to be up to ±1 μm.

The image shown in Figure 4.5 shows a section through a Pd/Ag membrane. The bright white band running diagonally across the image is the membrane, with the area to the right being the porous support material. This particular image is interesting because it shows a crack in the sol gel layer. This crack must have been present before metal plating commenced as the crack has been filled. Although the membrane is coherent it is not possible to quantify whether this area is more susceptible to failure upon operation of the membrane in hydrogen. Also visible in this image are the faint strands of metal that act as the mechanical keys into the sol gel layer surface.

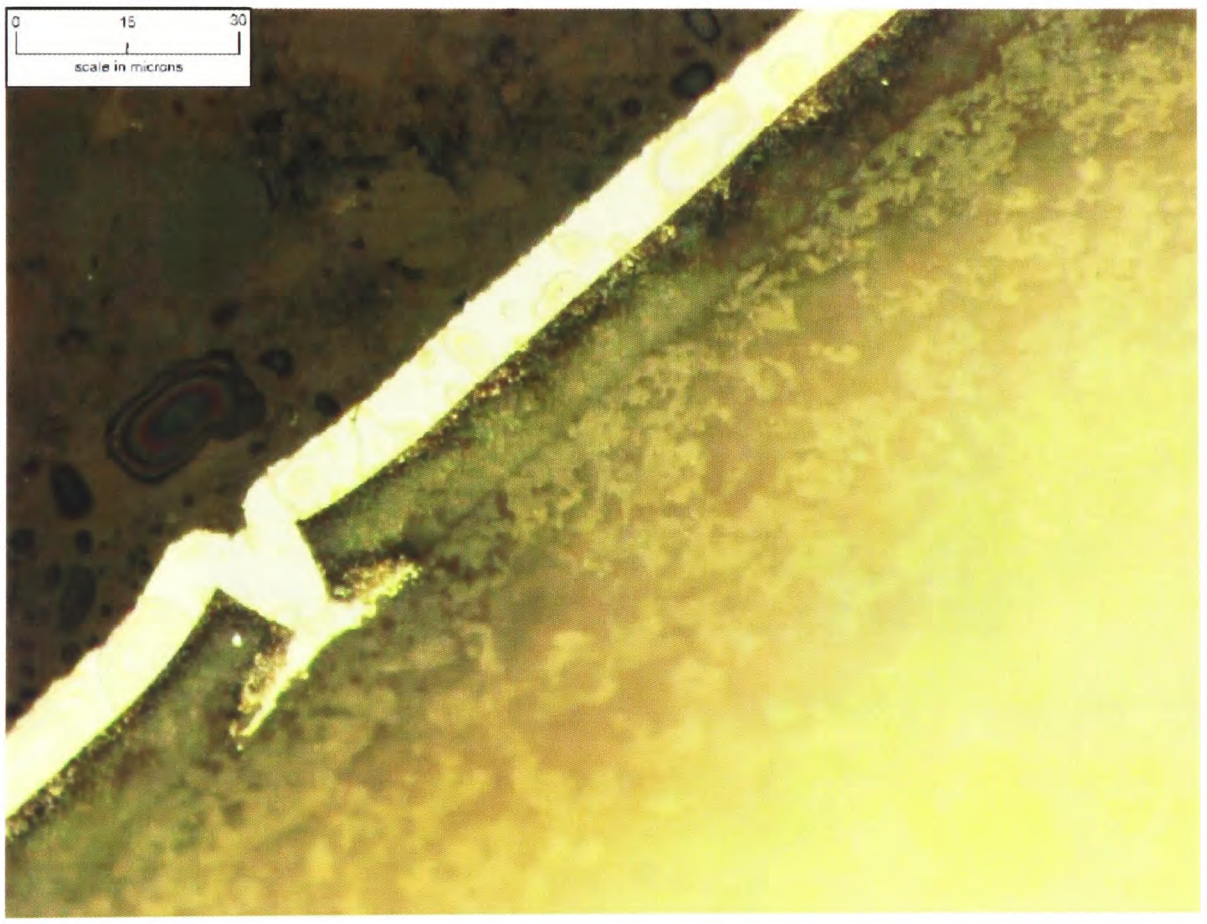

Figure 4.5: *Optical microscopy image of a Pd/Ag membrane on porous support.*

4.3 Alloy Composition Analysis

Elemental mapping of a section from the open end of a standard tube indicates the concentration of each metal on the surface of the cross section. Elemental mapping

images of palladium and silver are shown in Figure 4.6 and Figure 4.7 respectively. Both images show a relatively even distribution of palladium and silver within the membrane. Also visible are the slightly lower concentrations, indicated by the more blue areas to the left of the image, where the membrane adheres to the sol gel layer.

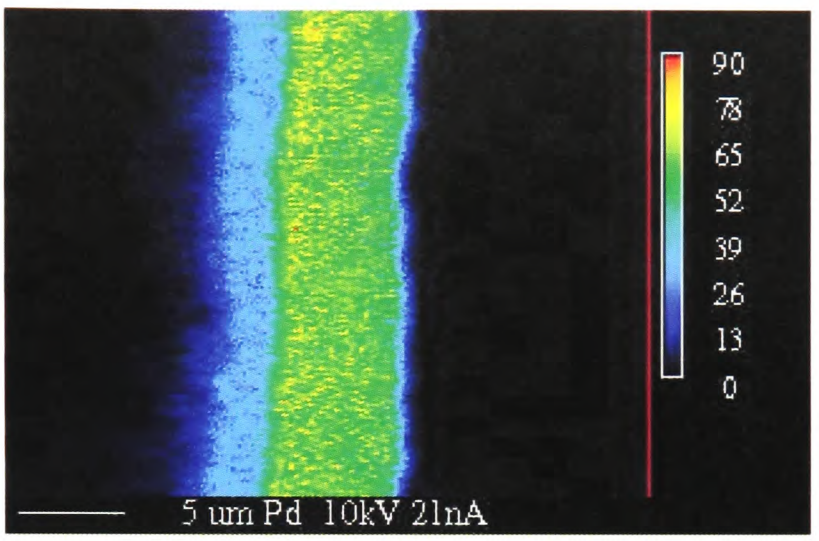

Figure 4.6: *Elemental map showing Pd concentration at open end section of standard 7.5 μm Pd/Ag membrane.*

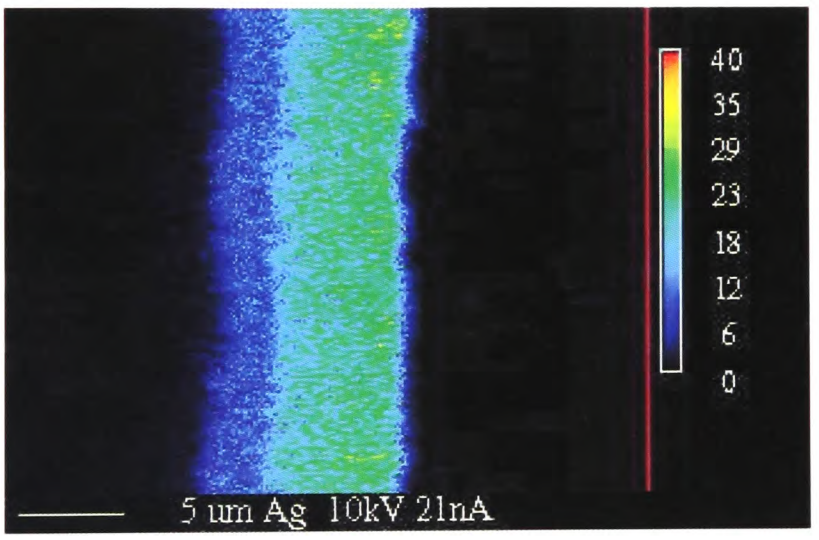

Figure 4.7: *Elemental map showing Ag concentration at open end section of standard 7.5 μm Pd/Ag membrane.*

It is possible to quantitatively measure the variation in elemental weight across the membrane thickness. This enables the variation in alloy composition to be determined. Analysis of this type is shown in Figure 4.8. The start point for the analysis (on the substrate side) is not well defined, though the outer edge of the membrane is evident by the sudden fall off to the right of the plot. From this outer edge to the inner edge there is a reasonably steady plateau for both the palladium and

the silver. The silver does however tend to slightly decrease in comparison. The alloy composition is of the order 70% palladium with the silver providing the remaining 30%. At around the 7 to 7.5 μm point from the outer membrane surface (4.5 – 5 μm on the scale), there is a visible decrease in both the palladium and silver elemental weight percentage. This is the area which was shown by the blue area in Figure 4.6 and Figure 4.7 where the membrane is connected to the sol gel layer of the substrate. The further into the substrate, the more the amount of palladium and silver decrease until at a distance of 12 μm from the outer edge of the membrane or around 4 μm from the start of the sol gel layer, the elemental weight percentage is negligible.

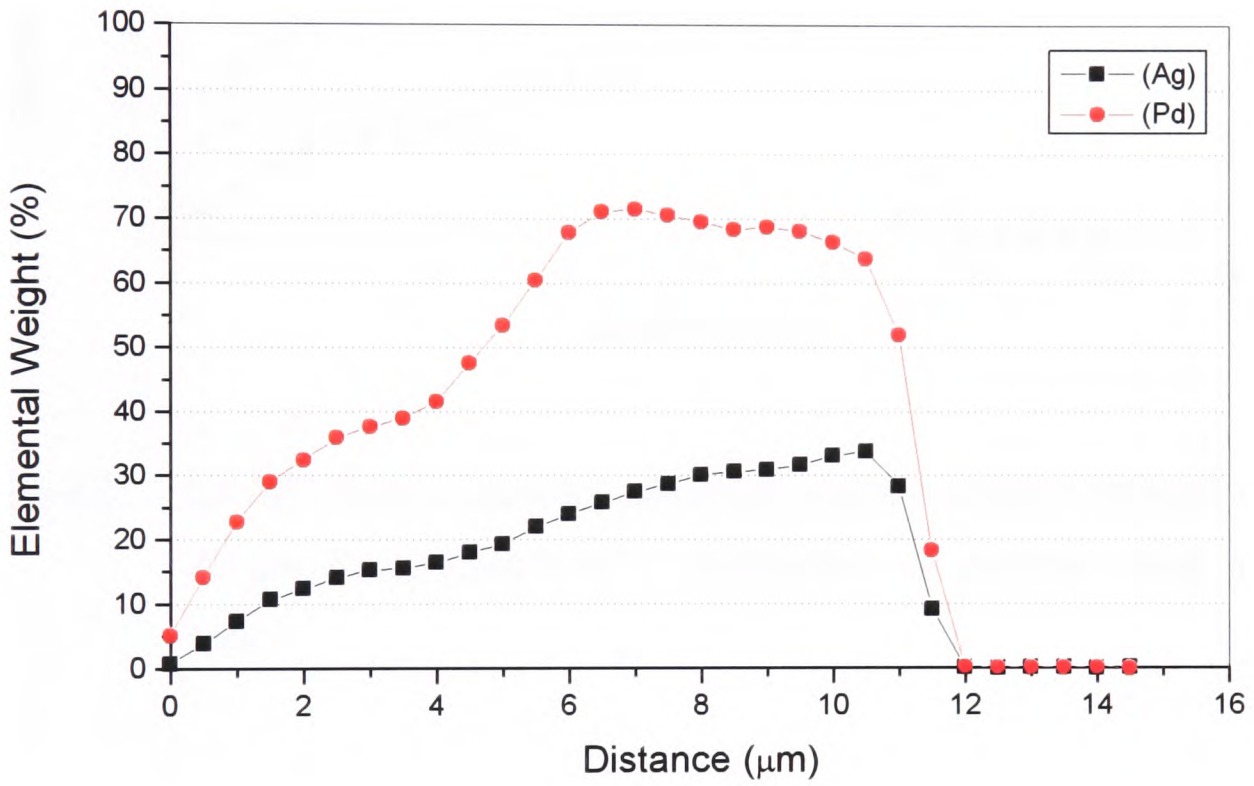

Figure 4.8: *EPMA analysis showing elemental weight variation through open end section of standard 7.5 μm Pd/Ag membrane.*

The composition analysis was repeated along the length of the tube at both the middle and the bottom of the tube and these results were plotted with those from the top of the tube to provide an indication of the variation in composition along the length of the tube. These results are to be seen in Figure 4.9. There is a similar trend to the results already discussed for the top of the tube. The main membrane section at each point along the length of the tube is again 7.5 μm. The decrease in elemental weight percentage observed further into the sol gel layer and substrate is not so marked as with the section at the open end of the tube. The slight shift in the plots is due to the

start point of the EPMA analysis not being at exactly the same point. The alloy composition is similar to the open end section of membrane, though there is a slight increase in silver weight percentage in the middle section.

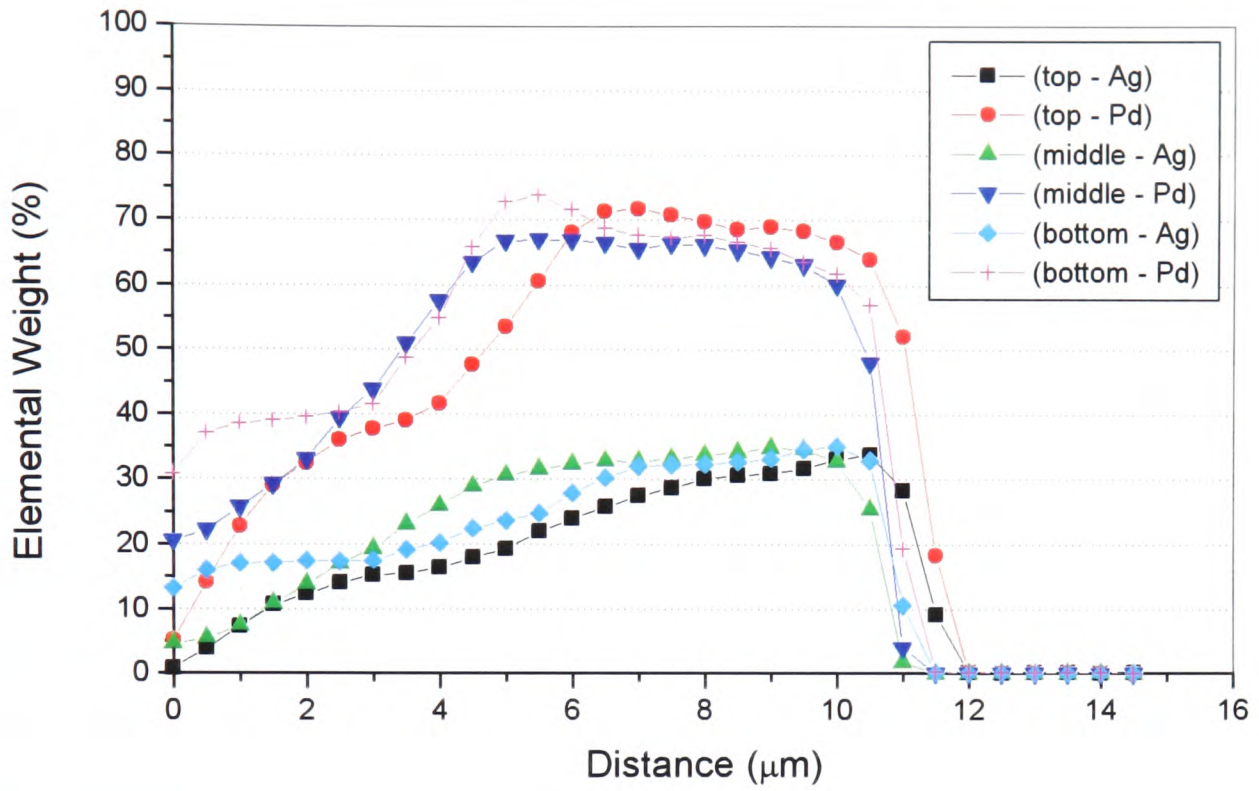

Figure 4.9: *EPMA analysis showing elemental weight variation through standard 7.5 μm Pd/Ag membrane – comparison of sections along length of tube.*

Ideally, the membrane would be more discrete and not seep so far into the substrate material. However it is this interaction with the sol gel layer that provides the mechanical support for the membrane and helps to prevent delaminations.

EPMA analysis of a number of 'standard' palladium tubes has shown a similar variation in alloy composition through the membrane. However the silver crash plating procedure does not produce an entirely consistent deposition and thus there is some variation between membrane tubes. There is no observable trend in the variation in alloy composition along the length of the membrane tube though any variation is put down to variation in the substrate material (as shown in Figure 4.3) or its finishing which can lead to variation in the quality of the sol gel application. For lab scale fabrication this variation, though undesirable, is to be expected.

The quality of the ceramic substrate material is one of the major factors in the eventual quality of the palladium membrane tubes. Several alternative suppliers were sought and some evaluation samples were provided, but changing project priorities meant these alternatives were not investigated further.

4.4 Stainless Steel Substrates

A number of optical microscope images of plating procedures on stainless steel substrates can be seen below. Palladium plating on an as-received thick-walled stainless steel substrate can be seen in Figure 4.10. Although the membrane appears to be coherent over the surface of the substrate, there is quite a significant variation in the membrane thickness from around 3 μm to around 10 μm. This is due to the undulating surface, which hinders the flow of plating solution over the substrate surface and also has a tendency to trap evolved hydrogen during the plating procedure. There is also a section where the membrane is in effect bridging a large surface pore in the membrane and this point may well be susceptible to failure during high pressure testing. The layered appearance to the membrane (slightly lighter in appearance than the substrate) is thought due to the stepwise addition of the reducing agent during plating.

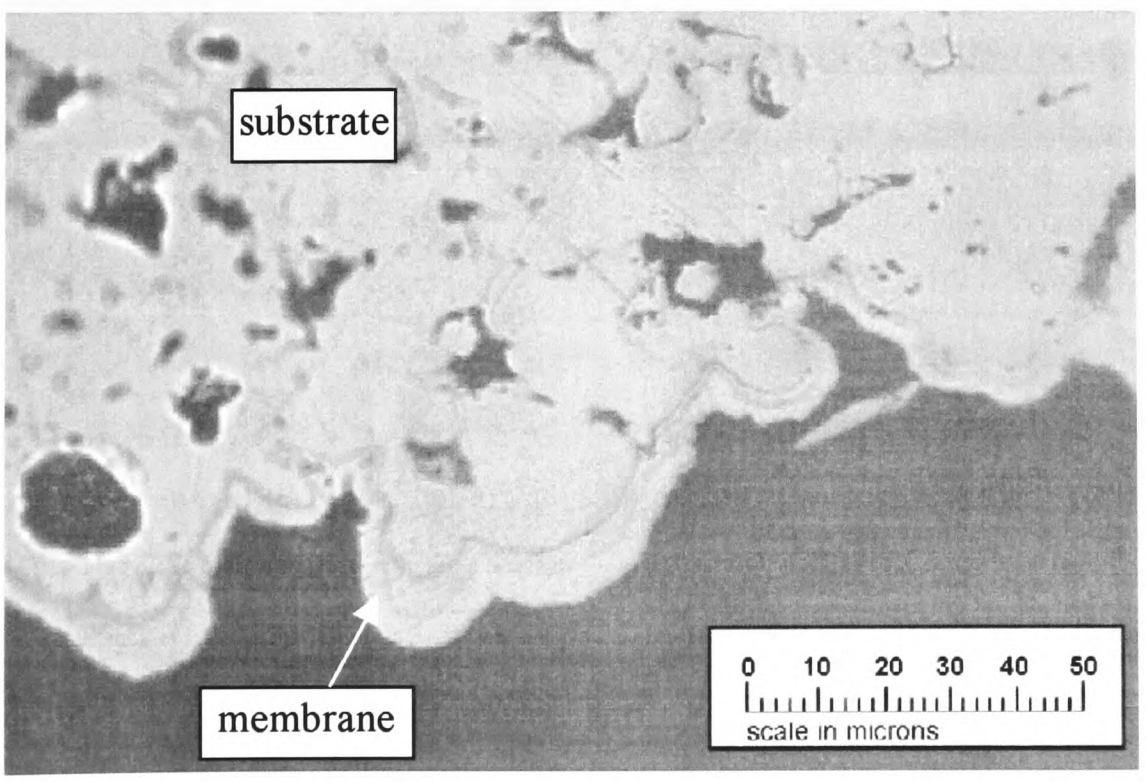

Figure 4.10: *An optical microscope image (x50 optic) of a stainless steel substrate fired at 550 °C with a sol gel layer and 20 hour Pd plate.*

The first hurdle to overcome has been the surface finish though bead blasting has proved a reasonably effective method as discussed in Chapter 3. The results of an attempt to plate a thick-walled porous stainless steel substrate, which has undergone a bead blasting treatment, can be seen in Figure 4.11. The much smoother surface has resulted in a palladium membrane of much more consistent thickness. There do not appear to be any inconsistencies in the surface, though again there is still a slight line visible in the membrane, which is thought to be due to the stepwise addition of the reducing agent.

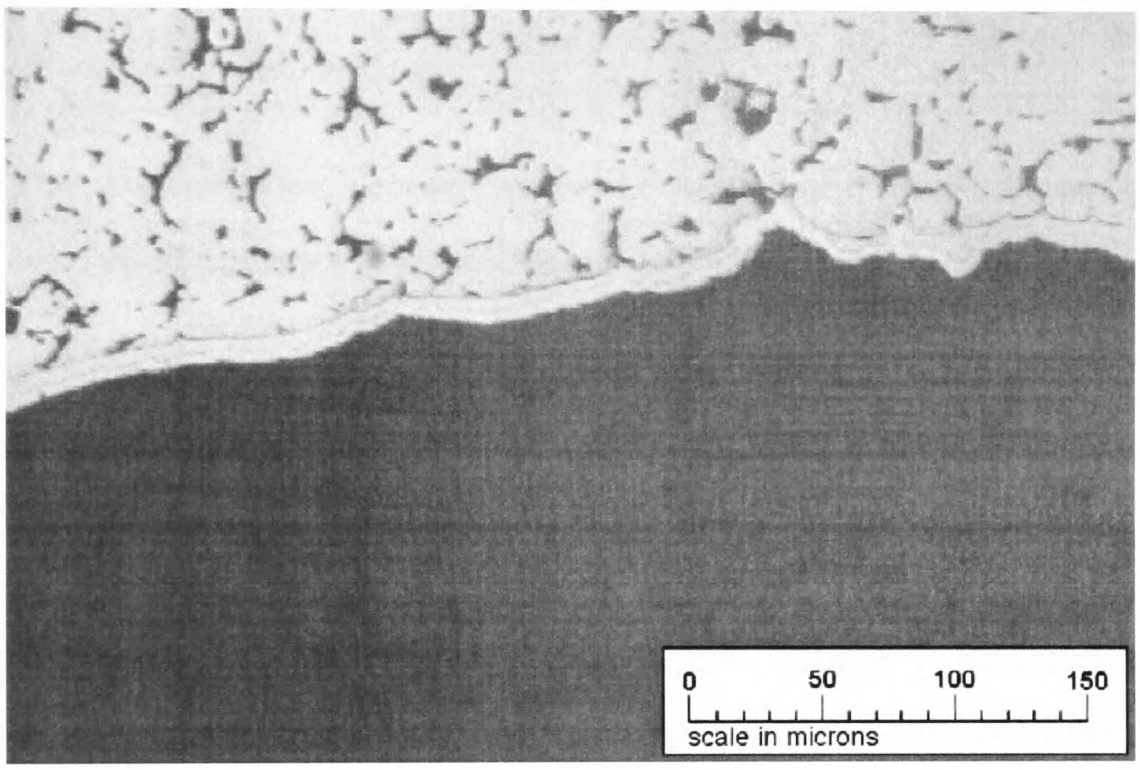

Figure 4.11: *An optical microscope image (x20 optic) of a stainless steel substrate that has been bead blasted at 0.7 barg, given a 500 °C heat treatment and a 20 hour Pd plate.*

Bead blasting provides one solution to the undulating surface finish of the thick-walled stainless steel substrate. However, due to the manual application of the bead blasting technique it is difficult to apply in a consistent manner over the full surface of the substrate. Another solution was to use the inner surface of the stainless steel substrate, as this appeared smoother than the outer surface through the manufacturing process. A thick-walled stainless steel substrate with a 20 μm Pd membrane on the inner surface can be seen in Figure 4.12. The surface of the substrate is noticeably flatter than in the case of the bead blasted tube. However there are still some large pores that the membrane must fill. If a thinner membrane was sought then these deep pores may become a location of weakness in the membrane.

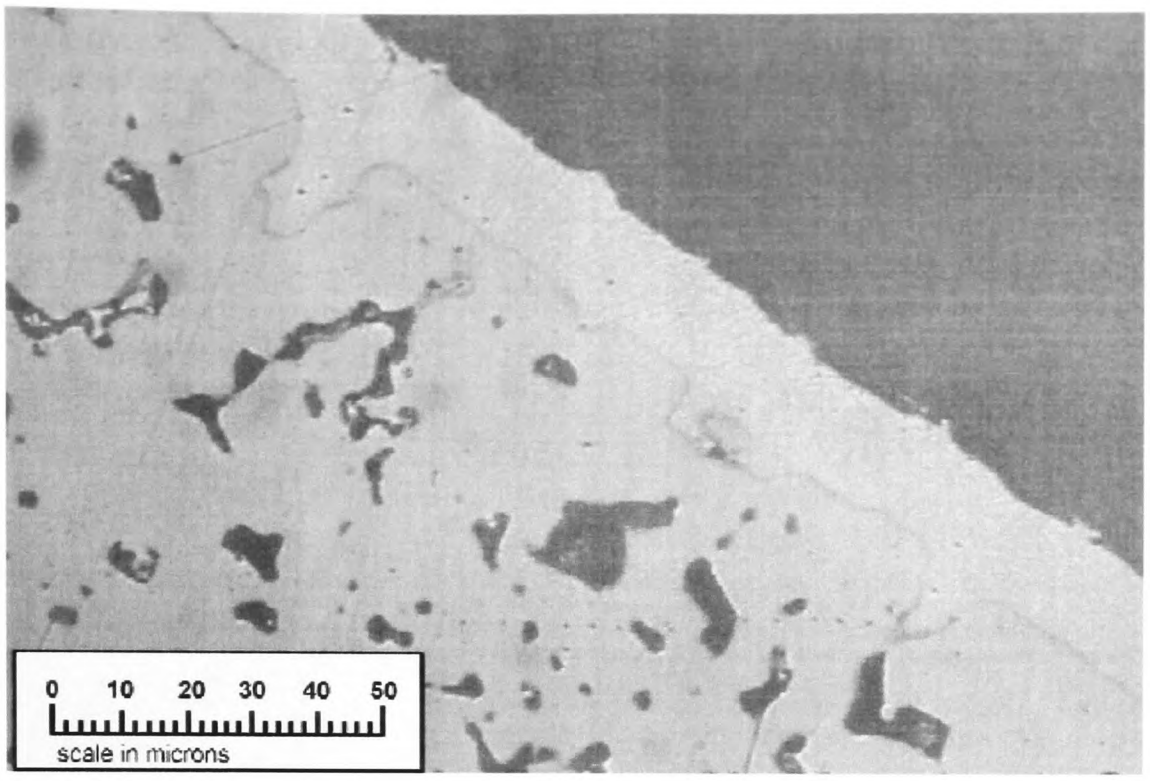

Figure 4.12: *Thick-walled porous stainless steel tube with 20μm palladium membrane on inner surface.*

The other variety of substrate tested was a thin-walled stainless steel substrate with a zirconia layer on the inner surface of the tube. This extra layer served not only as a barrier layer, but also as a smooth level layer on which to plate. The presence of this layer required a novel plating method as discussed in Chapter 3. Although initial leak tests suggested a coherent and leak free membrane, optical analysis of the surface as shown in Figure 4.13 reveals that the membrane has formed well within the zirconia layer and so the use of the zirconia as a barrier layer has not been effective in terms of preventing diffusion of palladium, but has covered the surface imperfections in the substrate. It was also noted that the internal surface of the tube after plating was not as shiny as with the conventional ceramic substrate materials, which also suggests that the membrane is not a distinct layer on the surface of the substrate. Subsequent flow testing of the membrane found that there was negligible flow through the membrane as the effective membrane thickness is much thicker due to palladium deposition actually within the porous zirconia layer.

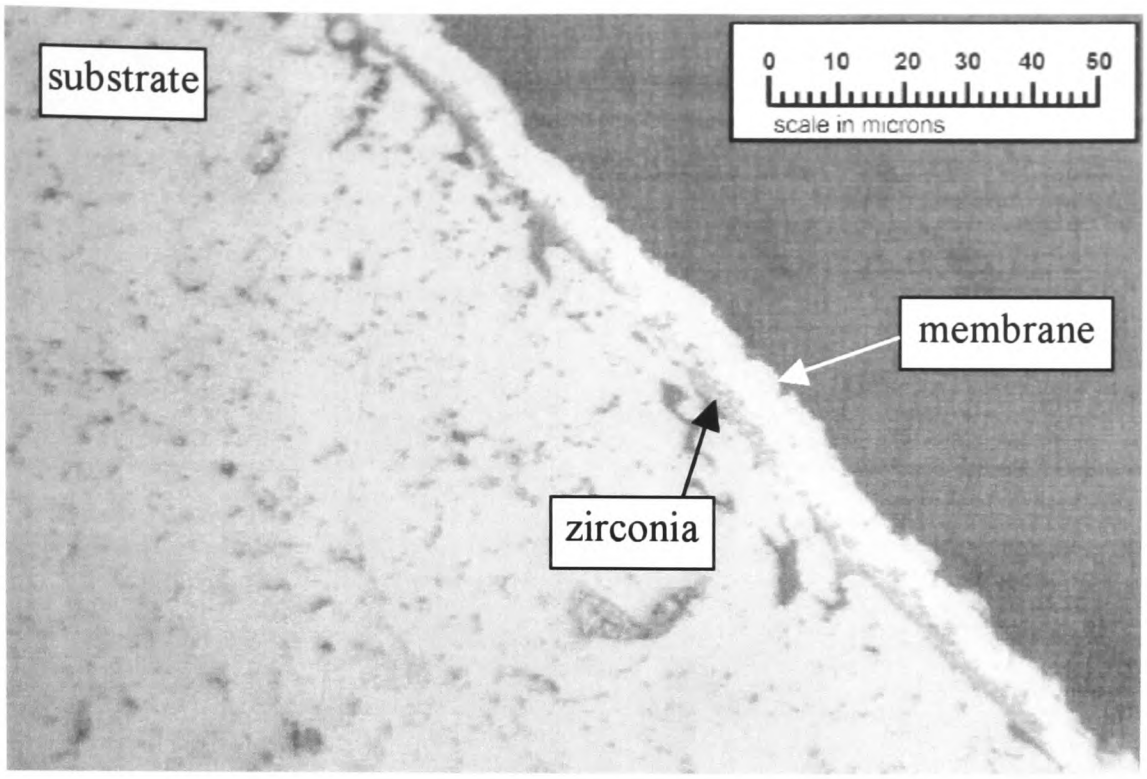

Figure 4.13: *Thin-walled porous stainless steel with a thin, 10 μm zirconia coating and 20 hour Pd plate*

Thin-walled stainless steel substrates with a thicker zirconia barrier layer were sourced and again a palladium layer was deposited upon the surface. The results of this can be seen in Figure 4.14. The large gap which can be seen is actually where the zirconia layer has been polished away during preparation of the sample with a diamond polisher. Where the membrane is visible it can still be seen that the membrane has permeated the zirconia layer and the problems that were associated with the thinner zirconia layer are still present. The fact that the zirconia layer has been polished away may also go some way to explaining the fragility of the membranes in such substrates, where the palladium membrane pulls the zirconia surface away from the substrate. Another point of potential weakness with the thin-walled stainless steel substrates was at the point where the end flanges had been attached to the substrate tube where the zirconia layer finished. If palladium were to be plated on these non-porous stainless steel sections, the membrane would not have any anchorage to the surface and would be prone to delamination on flow testing.

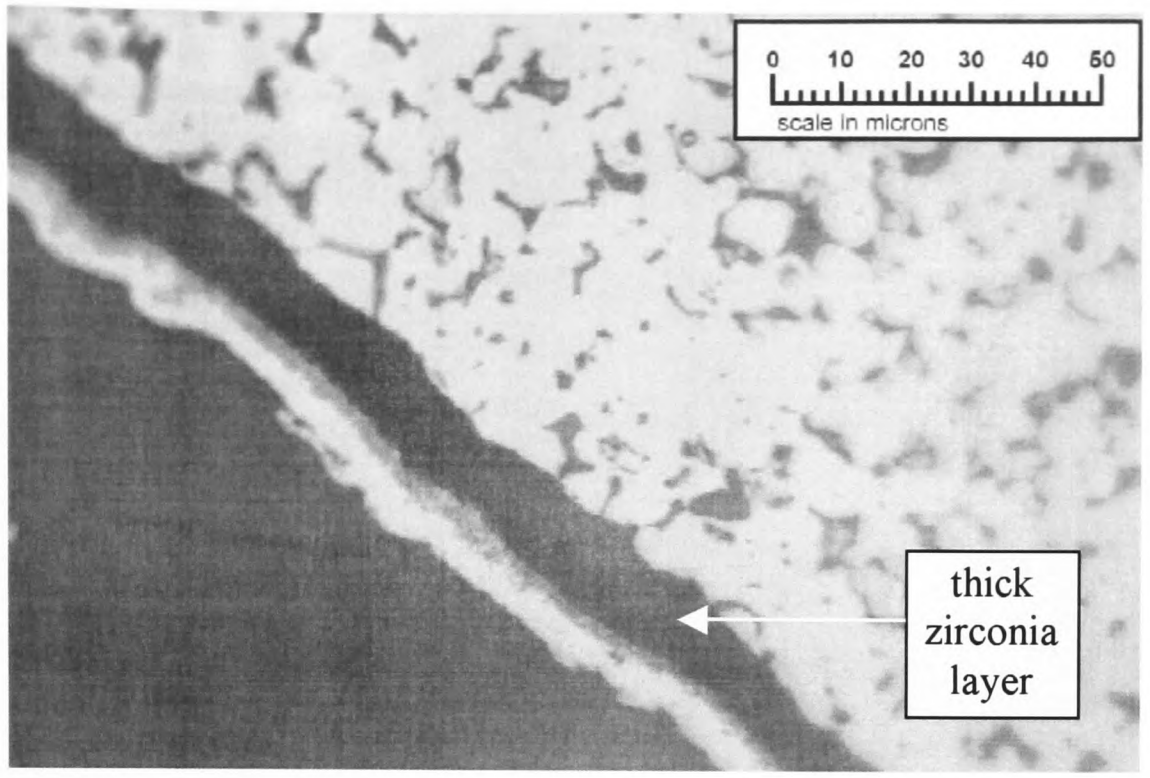

Figure 4.14: *Thin-walled porous stainless steel with thick, 13 μm zirconia coating and 20 hour Pd plate.*

Another phenomenon observed with stainless steel substrates was that of Kirkendall voiding. This is where voids appear in the membrane layer due to different rates of diffusion of the alloy species. Silver diffuses into palladium 10 times faster than palladium into silver. This results in a build up of vacancies in the silver that coalesce to form voids (Bassler *et al.*, 2002). This can be seen in Figure 4.15. Reducing the firing temperature for alloying can help prevent this effect. It was also observed using EPMA that without a barrier layer, not only did the palladium membrane layer begin to diffuse into the substrate layer (0.5-1 μm after 1 week at 500 °C), but components of the stainless steel also began to diffuse into the palladium membrane layer. It was thought that with continued operation of the membrane at temperature, the diffusion of species into the membrane layer would continue and increasingly affect the composition of the membrane and consequently the hydrogen diffusion properties as well as the membrane strength.

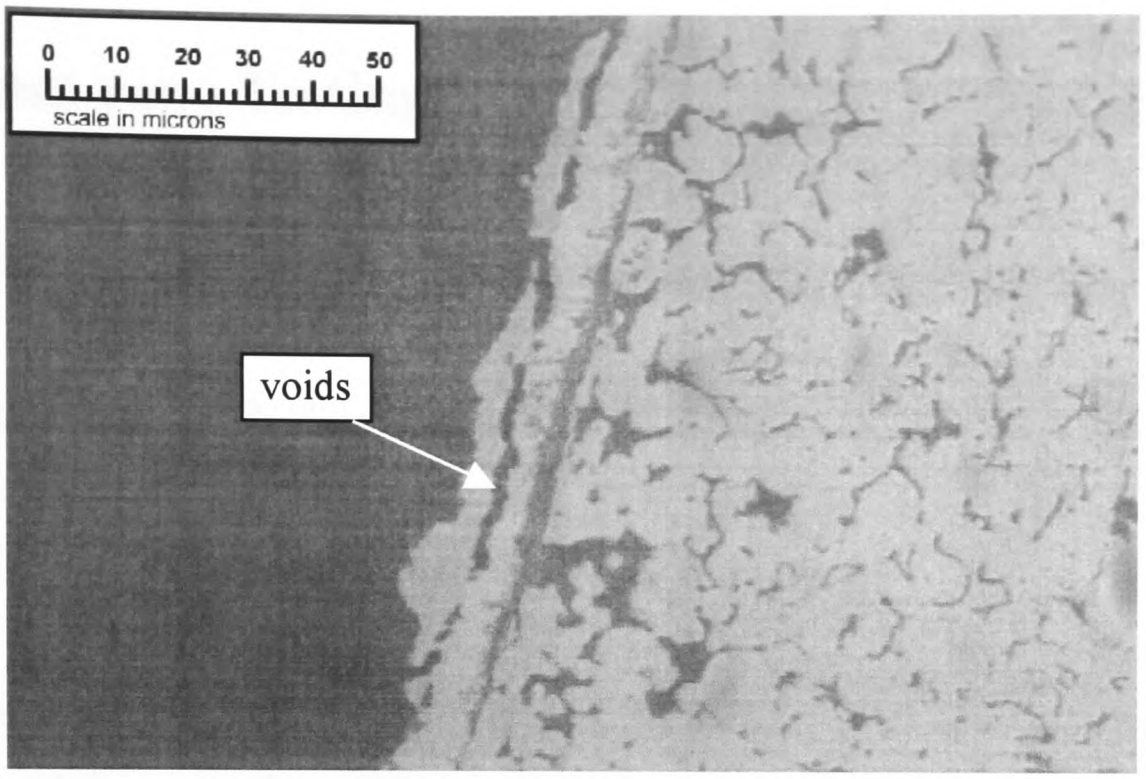

Figure 4.15: *Kirkendall voiding on thin-walled stainless steel tube with a palladium and silver coat.*

4.5 Conclusions

The microscopy analysis has shown the membranes deposited on porous ceramic substrates to be well adhered and consistent in both thickness as well as alloy composition along the membrane length. Stainless steel substrates have shown an inconsistent membrane coverage due to problems associated with poor surface finish. Some success was had with barrier layers on the stainless steel substrates, though the flow testing of such substrates highlighted durability problems as discussed in Chapter 6.

5 Membrane Testing

Three test stands were available for evaluating the membrane performance:

- Flow Test Stand, consisting of four membrane pressure chambers, which is run manually and allows the collection of steady state performance data over a wide range of flow rates, temperatures and pressures.

- Steam Test Stand, consisting of one membrane chamber, which again is run manually, but has a steam generator in order to be able to perform membrane tests with a wet reformate mixture.

- Durability Test Stand, which automatically cycles the membranes over a range of temperatures and feed compositions, 24 hours a day, to determine their longevity.

5.1 Flow Test Stand

The flow test stand consists of four 316 stainless steel pressure chambers (see Figure 5.1), each of which can hold one membrane. The chambers have an external diameter of 48 mm, and internal diameter of 28 mm and overall length of 229 mm. The pressure chambers are tested to 58.5 barg and designed to operate at up to 25 barg. They are resistant to corrosive attack. Up to four membranes can be loaded into the test stand, but each chamber can be isolated for testing an individual membrane. The gas streams into and out of the membrane pressure chamber are labelled in Figure 5.1 and are conventionally referred to as follows:

Feed:	The gas inlet stream into the chamber.
Permeate:	The gas which passes through the membrane.
Retentate/Bleed:	All the remaining species, not passing through the membrane.
Sweep/Purge:	Usually an inert gas used to flush the membrane of other species.

All the connecting gas lines in the flow test stand (Figure 5.4) have been made using ¼ inch Swagelok pipe work and fittings. Swagelok flow check valves in the feed lines and exhaust lines prevent backflow through the system. Flash back arresters at the main gas supply valves prevent ignition of the supply lines.

The membrane is sealed in the chamber with graphite o-ring seals at either end of the tube. These graphite seals have an outer diameter of 28 mm, and an inner diameter of 25 mm and a thickness of 10 mm. On the inner side of the graphite seal a stainless steel o-ring is used. In addition, on the outer facing side of the graphite o-rings, a copper o-ring is positioned to ensure a good seal with the M36 threaded end sealing nut. The chamber has a 1 kW thermostatically controlled heating element coiled around it and is operated at about 70% power. This enables an operating temperature of up to 500 °C to be maintained, although testing is normally performed at 440 °C. The chamber heaters are controlled using Cal 3200 controllers. K-Type thermocouples, used for the control of the chamber heating elements, are situated in the centre of the membrane chambers. Thermocouples are also situated in the feed and retentate streams.

Supply lines to the test stand include air, hydrogen, synthetic reformate and nitrogen. These are fed through one of two Aera (FC-7710CU) mass flow controllers, MFCs, depending on the range of flow and gas being used. An Aera mass flow controller calibrated with hydrogen is used for both pure hydrogen feeds as well as hydrogen mixtures. These digital MFCs are accurate to 1% of the set-point down to 25% of the flow range and accurate to 0.25% of full scale below 25% of the flow range. Repeatability is 0.2% of full-scale. The zero drift is less than 0.5% of full scale over a one year period (Aera, 2004). The feed pipeline is preheated by intercoiling it with the heater element around the main chamber to bring the flow to temperature before being fed into the chamber. A purge gas may also be fed to the permeate side of the membrane, if required. A Bellofram 2-150 psig pressure valve on the downside of the chamber (the bleed/retentate stream) serves to regulate the chamber pressure on the membrane surface. The permeate from the membrane is fed through one of two Aera gas flow meters, (Aera FM-390 100sccm, Aera FM-391 30slm) again depending on the flow, and both the retentate and the permeate gases then flow into the exhaust line. The permeate and retentate streams can be analysed using two Maihak S710 infrared

gas analysers to determine their compositions. One of the Maihak analysers provides ppm level analysis of CO and CO_2. The second Maihak provides vol % analysis of H_2, CO and CO_2. The gas analysers are calibrated using the appropriate span gases. All the flow meters/controllers in the test stand are Aera thermal mass flow meters giving digital display readings and controlled using an Aera ROD4 control box. The chambers are also well insulated with Thermoblanket glass wool to prevent heat loss.

Permeate and retentate flows are cooled through air-cooled coils. A schematic diagram of the flow test stand is shown in Figure 5.4.

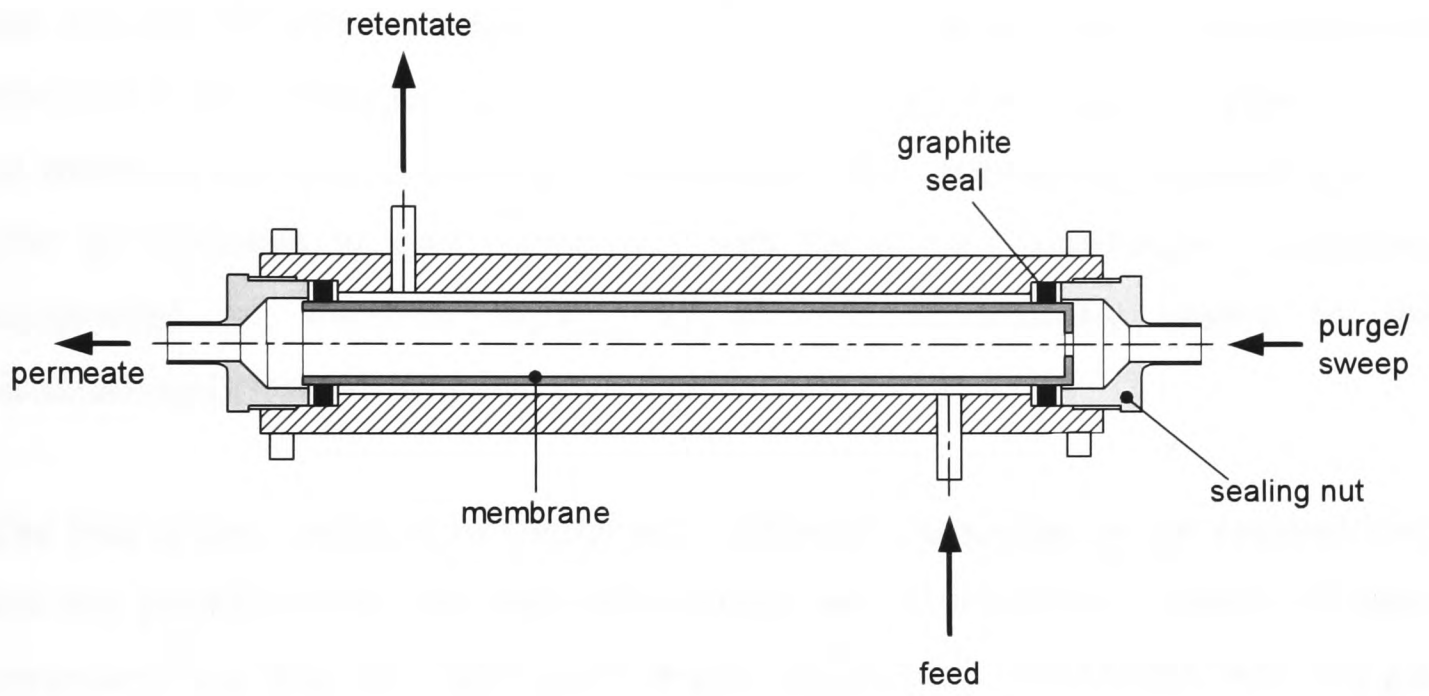

Figure 5.1: *A cross section of the membrane test chamber.*

5.1.1 Membrane Flow Testing Procedure

Before testing can commence, the seals around the membrane in the chamber are tested by performing a cold leak test. This involves flowing nitrogen to the chamber at 3 barg. If the membrane is of good quality, no nitrogen should pass through the membrane and any flow which is recorded is attributed to the leak past the graphite seals. In practise a 7.5 μm membrane is deemed to be of satisfactory quality if it passes no more than 10 sccm of nitrogen with a 3 barg pressure drop at an operating temperature of 440 °C. The seal-retaining nuts are then tightened to ensure the graphite seals are sufficiently well seated on the membrane surface, giving an active length of 172 mm, and ensuring that there is no further change in the measured leak.

The membrane chamber is then heated to 440 °C whilst flowing nitrogen gas. When the test temperature has been attained, a hot leak test is performed in a similar fashion to a cold leak test, and the seals tightened further as required. This takes account of any thermal expansion that may have occurred during the heating of the chamber. Any remaining leak is assumed to be gas passing through defects in the membrane. Care must be taken to avoid over-tightening the graphite seals as this can result in cracking of the substrate material.

Once the membrane is at the required temperature, it is usual for an air treatment to be carried out. This involves flowing around 1.5 slm of air at 3 barg over the membrane and this has the effect of removing any organic surface deposits. Improvements of around 0.5 slm in the pure hydrogen flow test at 3 barg can be expected after such an air treatment has been carried out. It is imperative that the chamber is purged with N_2 after air treatment to avoid mixing air with H_2 at high temperature. Interlocked compressed air actuators ensure that air and H_2/reformate cannot be fed simultaneously into the chamber.

The feed is then switched to hydrogen or reformate depending on the required test, and the permeate flow rate and compositions are recorded for a variety of input parameters e.g. feed flow rate, pressure and composition. The Maihak infra red gas analysing equipment is used to determine the CO and CO_2 composition of the retentate and permeate streams and the H_2 permeate flow rate is measured on the Aera thermal conductivity mass flow meter.

After test completion, the chamber is allowed to cool in nitrogen to prevent adsorption of hydrogen into the membrane. The standard composition of the synthetic reformate used in testing is as follows: CO 10%, CO_2 12%, H_2 40%, and N_2 38%. This is the typical dry output of a gasoline autothermal reformer (ATR). Other compositions can be supplied to the chamber either from stand-alone cylinders or by mixing the available feed gases using mass flow controllers.

5.1.2 Membrane Performance Characteristics

There are a number of parameters that may be used to express the performance of a membrane. The first of these is the permselectivity which a non-dimensional value

and is the ratio of hydrogen flux to that of non-hydrogen species flowing through the membrane. In theory a perfect palladium membrane should possess infinite permselectivity, but unless a perfect membrane has been fabricated, cracks and other imperfections in the membrane will permit the diffusion of non-hydrogen species. In the case of palladium membranes the permselectivity will describe the quality of the membrane and thus its ability to purify hydrogen. The non-hydrogen species typically used was nitrogen and the permselectivity, F_α, for a pressure drop of 3 barg and at a temperature of 440 °C for pure gases is given by the following expression:

$$F_\alpha = \frac{J_{H_2}}{J_{N_2}}$$

where: J_{H_2} and J_{N_2} are the fluxes of hydrogen and nitrogen respectively

The separation factor, α, is used for multi-component gas mixtures such as synthetic reformate and is expressed by the following:

$$\alpha_{1/2} = \frac{C_{p,1}}{C_{r,1}} \cdot \frac{C_{r,2}}{C_{p,2}}$$

where: C is concentration

r is permeate

p is permeate

Subscripts 1 and 2 are species 1 and 2 e.g. H_2 and CO

The other measurement is the hydrogen permeance, ρ, of the membrane, which can be expressed in a number of different ways. The Johnson Matthey preferred expression of permeance is as follows:

$$\rho = \frac{J_{H_2}}{D_{tube} \times \pi \times l_{active} \times (P_2^n - P_1^n)}$$

where: J_{H_2} is the hydrogen flux at the operating temperature, e.g. 440 °C

D_{tube} is the membrane tube diameter

l_{active} is the active membrane tube length (i.e. exposed to hydrogen)

P_2 and P_1 are the feed and permeate pressures respectively

n is the pressure exponential, which according to Sievert's law is n = 0.5, (see Chapter 6)

This produces a value of permeance in $m^3/m^2.hr.atm^{0.5}$. Figures in the literature may be expressed as a molar permeance. A value of specific permeance may be obtained by multiplying the permeance, ρ, by the membrane thickness in microns, to obtain a figure for a membrane, which allows comparison with membranes fabricated by different means.

The quality of a membrane in terms of leakage of non-hydrogen species could be estimated without full flow testing of the membrane at temperature by the use of a vacuum permeability system. This involved applying a 1 bara vacuum to the membrane tube using a soft silicone rubber seal and measuring the flow of air being pulled through the membrane. It was found experimentally that the hot leak test with nitrogen was approximately four times the cold vacuum leak test. The nitrogen permeance was calculated using the same expression used for calculating hydrogen permeance, but using a pressure exponential of n = 1.5 (Collins and Way, 1993).

In the membrane test results described in Chapter 6, the membrane performance is described in terms of volumetric flow rates which are readings from the mass flow meters and expressed in either standard litres per minute (slm) and standard cubic centimetres per minute (sccm) where standard indicates a pressure of 1 atmosphere and a temperature of 0 °C. As this work uses just one surface geometry, flow rate is sufficient for comparison.

5.2 Steam Test Stand

The steam test stand operates in exactly the same way as the flow test stand described above, but in addition to the gas supply lines, it is also served by a ultra high purity water reservoir. Water is dosed using an FMI QG150 Q0SSY 1/8" stainless steel piston reciprocating displacement pump, calibrated at the chamber operating pressure. The water is then fed into a steam generator (see Figure 5.2) consisting of two 750 W

cartridge heaters positioned at the ends of a large U-bend section of 1 inch diameter pipe work. The steam generator is well insulated and the length of pipe work, from the steam generator to the outlet of the chamber, is kept to a minimum to reduce further heat loss. By ensuring the temperature of the gas/steam mixture is above the saturated vapour temperature at that pressure, it can be assumed that the water has been fully vaporised. The feed gases also pass through the steam generator in order to produce a homogeneous gas and steam mixture before entering the test chamber.

The water pump must be calibrated at the chamber pressure as it has been found that the flow decreases as the pressure is increased. The pump is also limited to the pumping pressure against which it will continue to operate, which in the case of the Q0SSY pump head is 6.9 barg.

The stable gas and steam exit temperature attained after the steam generator is around 300 °C. The stream is heated further as it is coiled around the membrane chamber to the standard test temperature of 440 °C. The steam generator has a large volume which helps to buffer the flow and pressure fluctuations as the water is pumped and vaporised. Initial tests with a compact small volume steam generator resulted in significant fluctuations in the flow and pressure, highlighted by noise on the mass flow meters. The schematic of the steam generator in Figure 5.2, shows the layout of the thermostatically controlled heaters and the gas/water inlet lines. Flow check valves are used in all lines into the steam generator in order to prevent steam returning up the inlet lines and damaging the mass flow meters.

Both the permeate and the retentate streams are cooled using plate heat exchangers to condense the water out of the gas streams. Armstrong 11 LD liquid drainers then remove the water from the gas stream in order to prevent damage to the mass flow meters. A Drierite anhydrous $CaSO_4$ moisture trap ensures the feed to the gas analysers is thoroughly dried. A schematic of the steam test rig is shown in Figure 5.4.

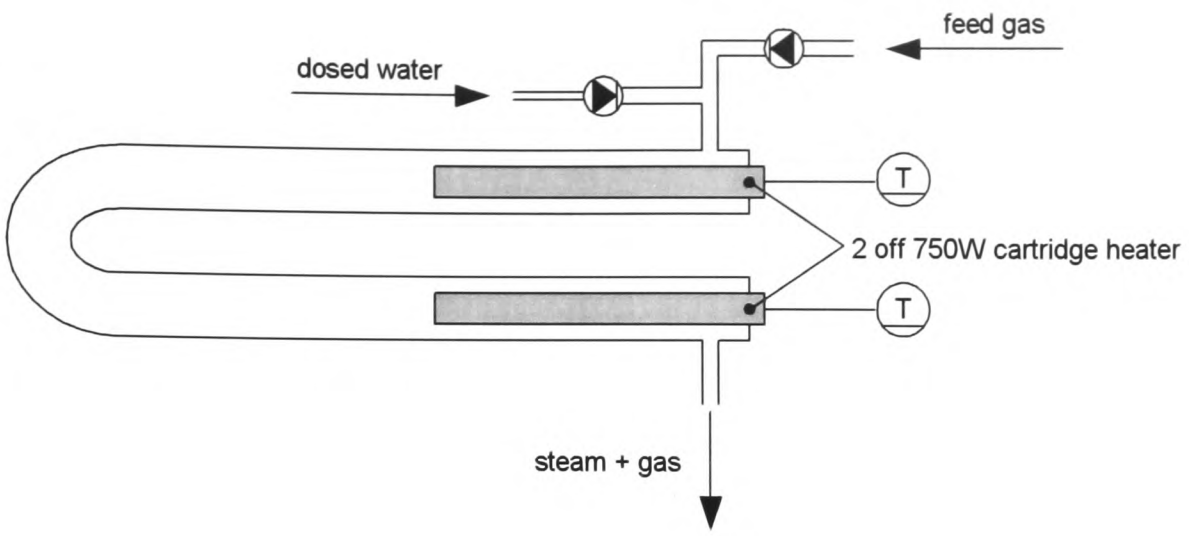

Figure 5.2: *Steam generator schematic.*

5.2.1 Steam Dosing

The typical wet and dry compositions of the product gas from a gasoline ATR with a steam to carbon ration SCR = 2 are as follows:

Wet Reformate Composition:	**Dry Reformate Composition:**
H_2 = 28.8%	H_2 = 40%
N_2 = 27.36%	N_2 = 38%
CO_2 = 8.64%	CO_2 = 12%
CO = 7.2%	CO = 10%
H_2O = 28%	

Dry reformate mixture is supplied to the laboratory in cylinders. In order to produce the wet mixture, steam was added to the dry mixture. If the membrane test pressure was to remain constant with the introduction of steam, the partial pressure of the other species would fall in the ratios of their volume % indicated above (i.e. with a 3 barg (= 4 bara) chamber pressure, the partial pressure of H_2 would fall from 1.6 bara to 1.152 bara). Because the flux of H_2 through the membrane is proportional to the H_2 partial pressure, it is important to ensure that the H_2 partial pressure drop as well as the CO concentration remain constant over the membrane tests. In order to achieve this the chamber test pressure was increased to 4.55 barg.

As mentioned in Section 5.2, the dosing pump has to be calibrated at the operating pressure of the membrane which was 4.55 barg so as to compare with dry reformate tests at 3 barg. A calibration curve was produced showing a linear relationship between pump stroke angle setting and the flow rate, and this can be seen in Figure 5.3.

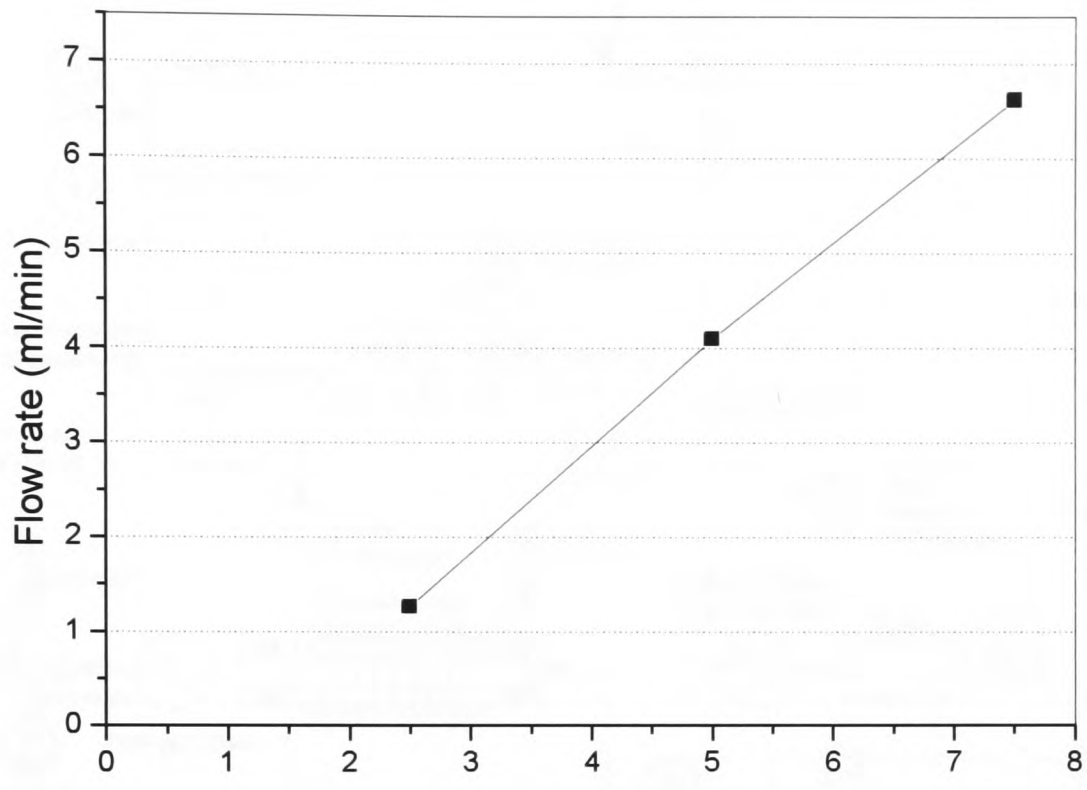

Figure 5.3: *Pump calibration curve showing flow rate as a function of the arbitrary pump setting with a downstream pressure of 4.55 barg.*

If it is assumed that the constituent gases of the reformate mixture are ideal gases then with, for example, a set flow rate of 15 slm, the molar flow rate is the volumetric flow rate divided by the molar volume of an ideal gas at standard conditions e.g. 22.41 m^3/kmol and is equal to 0.6696 mol/min. The dry gases constitute 72% of the wet stream with steam making up the remaining 28%. Thus, the molar flow rate of steam required is 0.2604 mol/min. The molar weight of H_2O is 18 g/mol, which means that 4.68 ml/min of water must be pumped into the steam generator to be vaporized into steam. By interpolating from steam tables (Rogers and Mayhew, 1996), the saturation temperature at 4.55 barg is T_s= 156 °C. Maintaining the steam generator outlet temperatures above this temperature should ensure that all the water is vaporised.

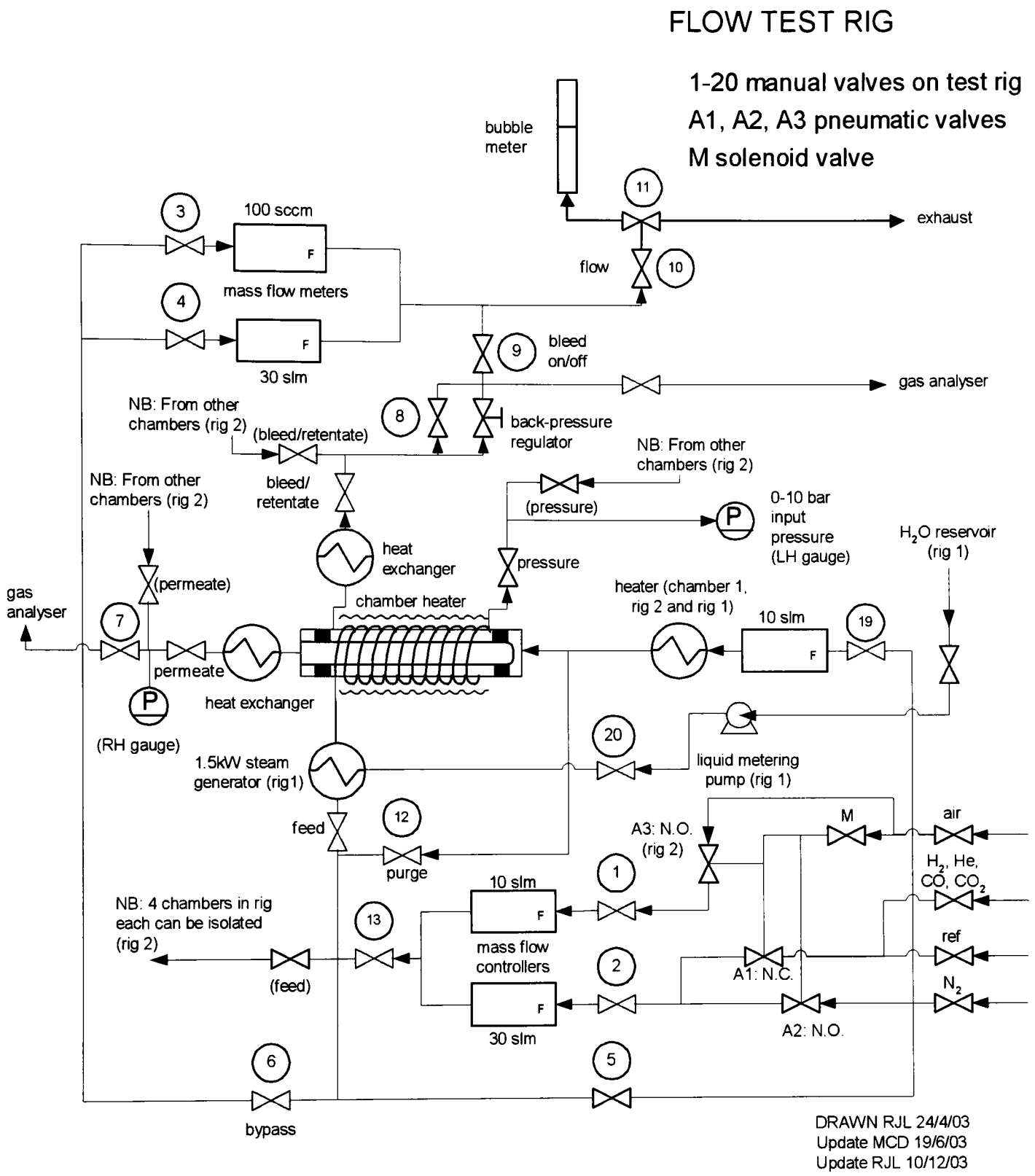

Figure 5.4: *Schematic of the flow test and steam test stand apparatus.*

5.3 Durability Test Stand

The durability test stand consists of one thermally insulated chamber into which the membrane is inserted. The configuration is very similar to the flow test stand, but an automated test programme can be run and the data logged using LAB-View software. Multiple cycles of a single test programme are run 24 hours a day until a membrane fails. A typical single cycle programme is as follows:

- cold N_2 leak test
- heat to 440 °C in N_2
- N_2 hot leak test
- H_2 flow test at 3, 5, 7, 10, 15 slm
- N_2 hot leak test
- cool in N_2

Warming and cooling of the membrane in nitrogen significantly increases the durability of the membrane, as this prevents the retention of hydrogen in the palladium lattice that causes a significant volumetric expansion. The resulting strain when the membrane substrate cools to ambient conditions (to which the expanded membrane is mechanically keyed) can be enough to cause the membrane to delaminate from the ceramic substrate. An example of a typical durability test is shown in Figure 5.5. With time it can be seen that the N_2 leak increases from 20 to 80 sccm with peaks around 40, 60 and 85 temperature cycles. Tightening the membrane seals at these points, as indicated in the figure, results is a marked reduction in the leak. However with continued cycling the membrane itself begins to fail as shown by increases in both the N_2 leak and the H_2 permeate. The membrane finally ruptures after 90 cycles as the membrane delaminates from the ceramic substrate.

Some work was carried out into improving the membrane sealing to reduce the effect of temperature cycling on the performance of the graphite seals. This work is described in Chapter 6.

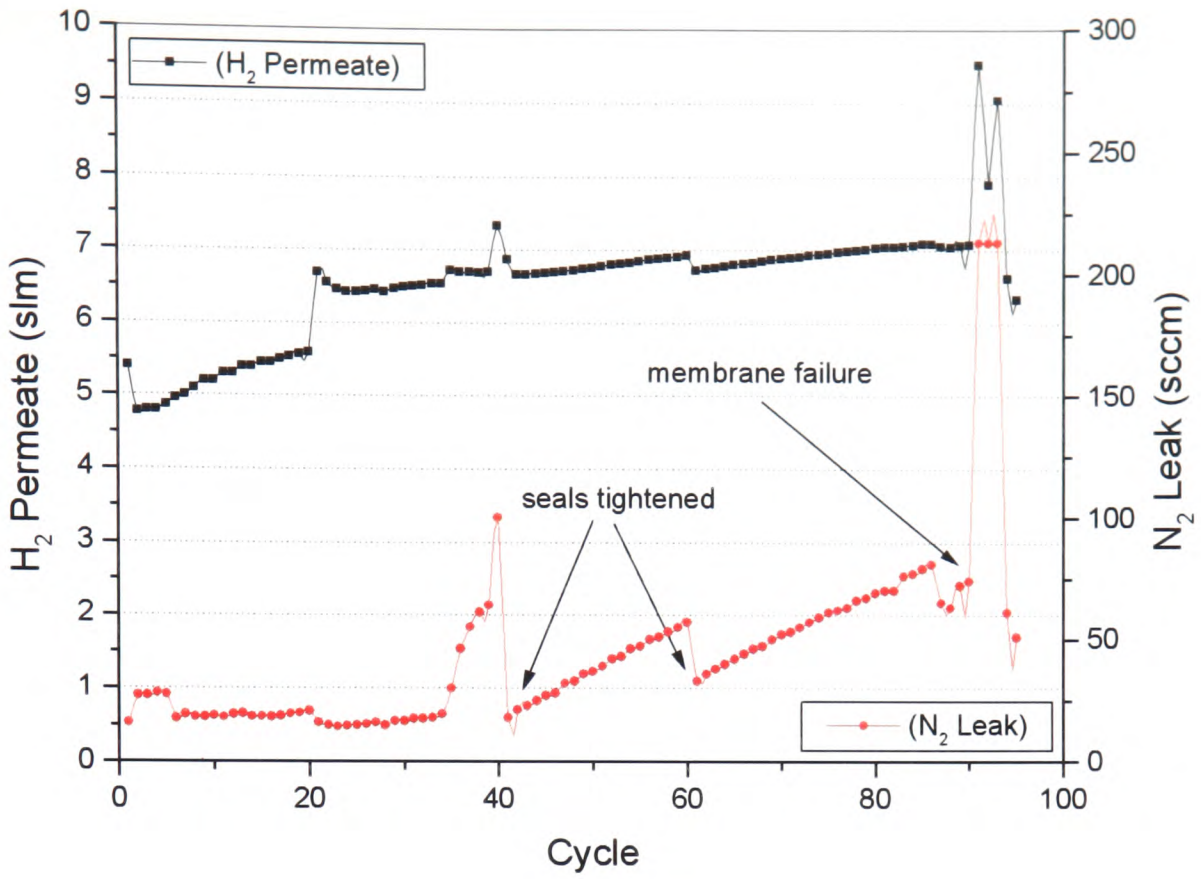

Figure 5.5: *Durability test of a Pd/Ag membrane by cycling in hydrogen and nitrogen between 50 °C and at 400 °C with a chamber pressure of 3 barg* (Walker, 2001).

5.4 Conclusions

The flow test stands provide comprehensive performance evaluation of the supported Pd/Ag membranes. Significant work was undertaken to enable flow testing with wet reformate mixtures. The soft sealing technique has been shown to degrade on thermal cycling, though solutions to this are described in both Chapter 3 and Chapter 6.

6 Membrane Test Results

6.1 Pure Hydrogen Flow Test

The property of the palladium membranes, which is of most interest, is their ability to pass hydrogen. The initial experimental procedure carried out on the membranes is that of the hydrogen flow test. After the preliminary air treatment and leak test, the hydrogen permeate through the membrane is recorded as a function of the hydrogen feed and the pressure drop over the membrane. The standard test procedure is carried out with an ambient downstream pressure (i.e. 1 bara) and the inlet pressure controlled by the back pressure regulator to between 3 and 9 barg depending on the available gas supply pressure. The feed flow rate is varied between 3 and 30 slm. It is not always necessary to continue to increase the feed right up to this higher value as it soon becomes evident that a plateau has been reached.

The plot shown in Figure 6.1 shows the results of a pure hydrogen flow test using a standard membrane. The term standard membrane denotes a 7.5 μm 23% Ag/Pd membrane. In all the experimental data, the flow rates are considered from a single tube and the data presented is that of the experimentally recorded values. For the purposes of this work it is sufficient to present the data in this way, though for comparison with other membranes a normalised value would be calculated to produce values for permeability independent of membrane area, thickness and pressure drop. From the plot it can be seen that the hydrogen permeate increases directly with inlet flow with a unity gradient until eventually a plateau is reached. The level of the plateau is dependent on the membrane pressure drop. With a 3 barg pressure drop the hydrogen permeate reaches around 6 slm, at 5 barg this is 9.5 slm, 7 barg 12.75 slm and at 8.4 barg this is 15 slm.

The permeate flow rates at the plateau are indicative of the performance of the membrane in terms of the maximum hydrogen that will pass through the membrane at a given pressure. Of course, if the membrane had a high leak, then these values of hydrogen permeation would not be reliable and so it is important to ensure that the leak through the membrane is kept to a minimal level. A 'good' membrane will have

an N_2 leak of less than 10 sccm when operating at 440 °C and with a 3 barg pressure drop. Due to some degree of variation in the quality of the substrate material and the lab-scale membrane fabrication methods, there will also be some variation in the membrane performance, which can be up to ±1 slm of hydrogen at 3 barg and 440 °C. The results presented in Figure 6.1, are typical though of a standard membrane.

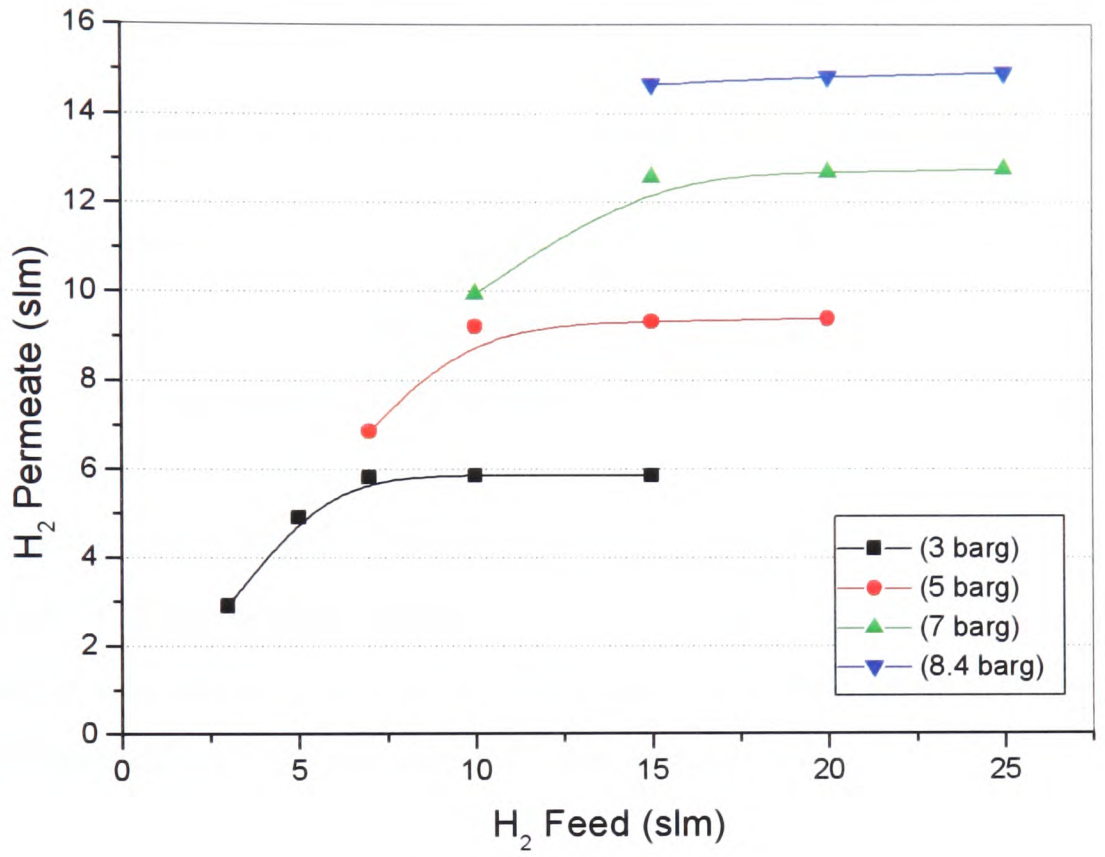

Figure 6.1: *Pure hydrogen flow test of a standard 7.5 μm Pd/Ag membrane at 440 °C with a downstream pressure of 1 bara.*

6.2 Reformate Flow Test

The envisaged application for palladium membranes is for use in purifying the products of reforming to provide a hydrogen rich feed for a fuel cell. Although different reforming processes and conditions will produce reformate mixtures of varying compositions, they will all comprise hydrogen, carbon dioxide and carbon monoxide. In order to test the palladium membranes with a view for use as a clean-up system for on-board gasoline autothermal reforming, the following reformate composition was used: H_2 = 40%, N_2 = 38%, CO_2 = 12%, CO = 10%. This reformate composition will in future be described as 10% CO reformate. The mixture is supplied in high pressure gas cylinders at 170 barg and regulated to 9 barg. The reformate supply is a dry mixture which simplifies the design of the test stand and experimental

procedure. Experiments with a wet reformate mixture have also been carried out and are detailed in Section 6.7. A flow test with the reformate mixture is carried out in a similar manner to that of the pure hydrogen, whereby hydrogen permeate is recorded as a function of the inlet feed flow rate and the pressure drop over the membrane. The membrane temperature is maintained at 440 °C as it has been found that below this level, the presence of CO begins to act as a poison and the hydrogen flux through the membrane is reduced. For comparison between tests, 440 °C was chosen as the optimum operating temperature.

The results of a reformate flow test with a typical standard 7.5 μm Pd/Ag membrane are shown in Figure 6.2. In contrast with the pure reformate flow test, the hydrogen permeate has a more gradual increase before it begins to plateau out. Due to the composition of the reformate mixture, the hydrogen partial pressure drop is reduced compared with pure hydrogen. Therefore, the maximum hydrogen permeate through the membrane is also reduced. With a 3 barg pressure drop, the hydrogen permeate plateaus out at just under 1 slm, with 5 barg this is increased to 2.05 slm and with 7 barg and 9 barg this is 3.05 slm and 3.85 slm respectively.

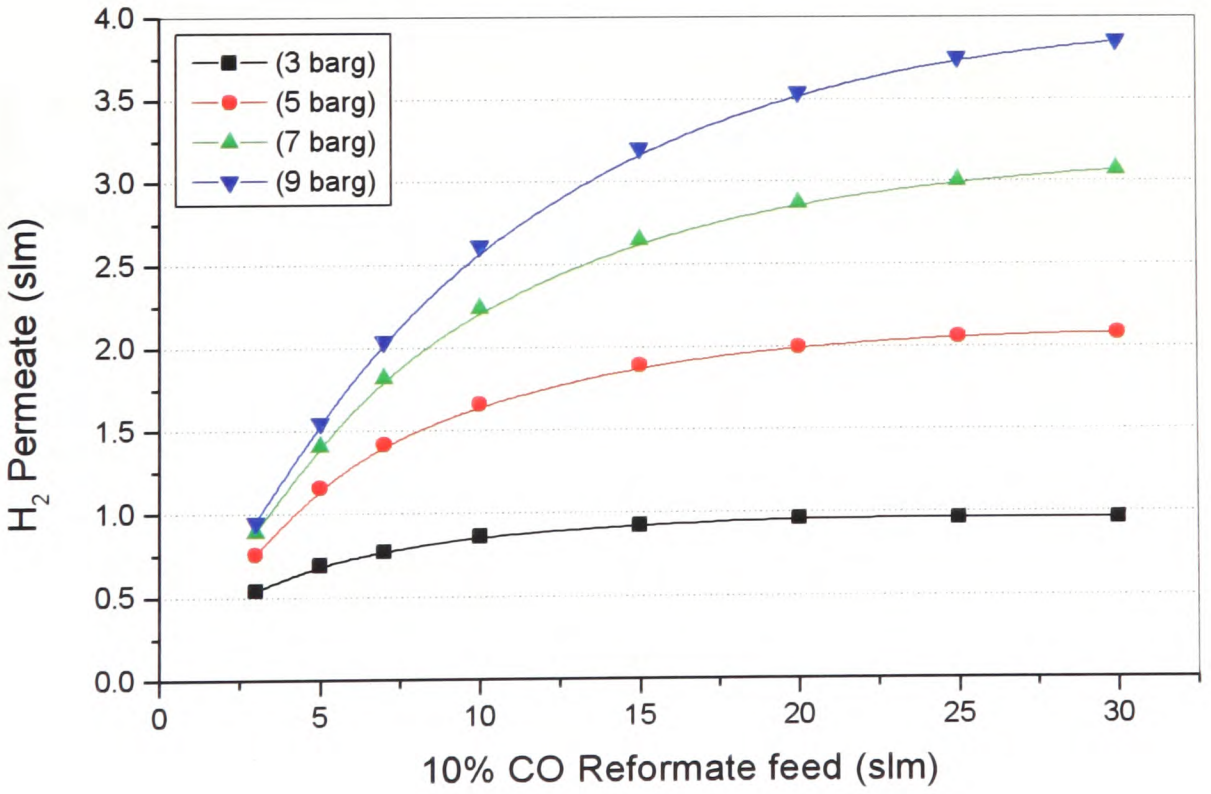

Figure 6.2: *Flow test of a standard 7.5 μm Pd/Ag membrane using 10% CO reformate with an operating temperature of 440 °C and downstream pressure of 1 bara.*

A standard 7.5 μm Pd/Ag membrane will typically produce a pure hydrogen stream containing less than 200 ppm carbon monoxide when using a 10% CO reformate feed with a 3 barg pressure drop operating at 440 °C. Extremely high quality tubes fabricated at Johnson Matthey have achieved CO levels less than 10 ppm using a 2% CO reformate feed (EC, 2003). Depending on the purity of hydrogen desired, the use of a catalyst layer on the permeate side of the membrane could be used to remove any permeating CO (Doyle, 1997).

6.3 Transient Response

Whilst undertaking reformate flow tests with a data logging device it was found that on initial switching from a nitrogen to a hydrogen containing feed stream, there was an initial rise in the level of hydrogen permeate above the steady state level, as shown in Figure 6.3. This is due to the initial hydrogen permeate stream pressure being lower than 1 bara. The downstream hydrogen partial pressure then stabilises as the permeate stream becomes saturated with hydrogen and finally attains 1 bara.

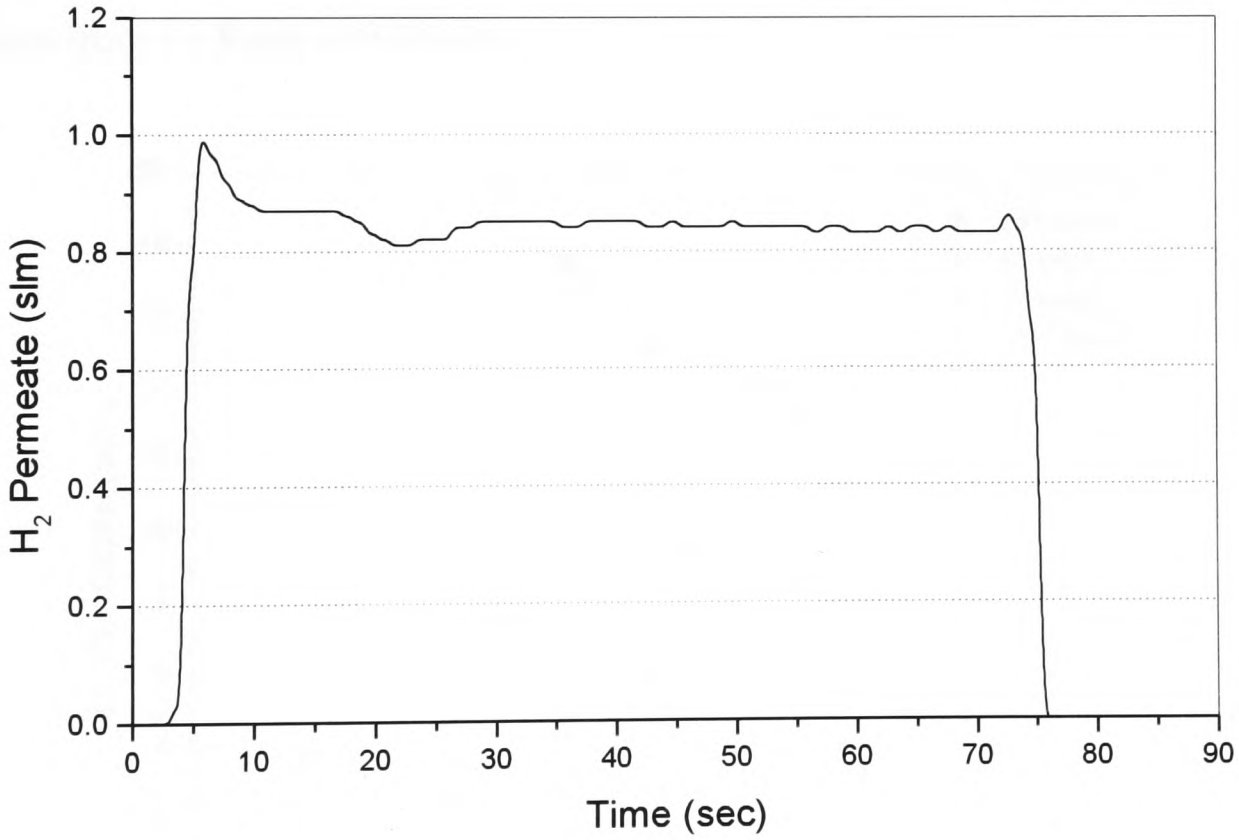

Figure 6.3: *Transient hydrogen permeation response with a 3 bara 10% CO reformate feed and 1 bara downstream pressure using a standard 7.5 μm Pd/Ag membrane. 15 slm feed flow and 440 °C membrane temperature.*

6.4 Membrane Thickness Variation

Although a 7.5 μm membrane is the standard membrane thickness in terms of producing a reliably consistent and coherent membrane, a number of membranes of varying thickness were fabricated. It was important to maintain a consistent alloy composition for all the membranes i.e. 23% Ag to avoid membrane embrittlement. In all the investigations into thickness variation, the hydrogen permeate value was taken from the plateau i.e. the maximum hydrogen permeate that could be obtained.

6.4.1 Hydrogen

The first series of experiments into membrane thickness were carried out with pure hydrogen. The results are to be seen in Figure 6.4. With increasing membrane thickness the hydrogen permeate decreases in all cases. As membrane thickness is increased from 4.75 μm to 13.25 μm with a pressure drop of 3 barg, the hydrogen permeate decreases from 7.4 slm to 4.1 slm respectively. As the pressure is increased there is a steeper decline in the hydrogen permeate with increasing thickness. Over the same thickness range, with a pressure drop of 9 barg, the hydrogen permeate decreases from 19.5 slm to 9.05 slm.

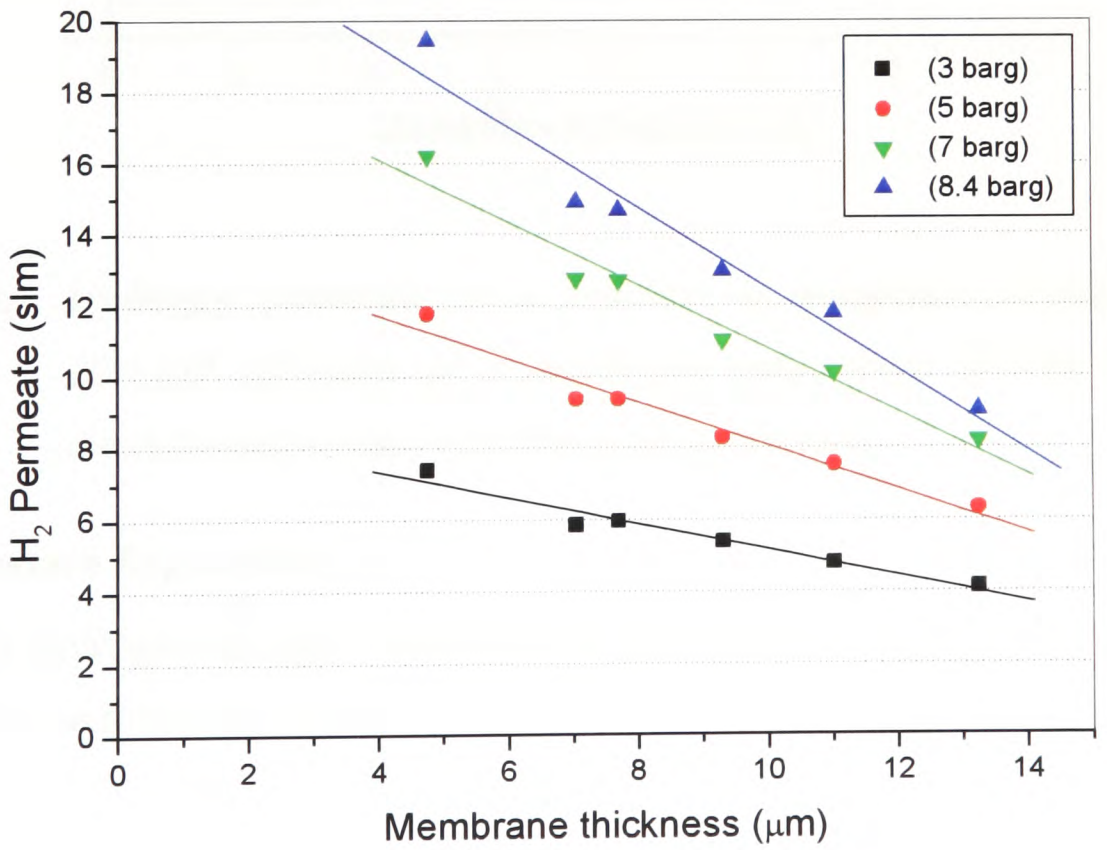

Figure 6.4: *Hydrogen permeate as a function of membrane thickness using pure hydrogen at a membrane temperature of 440 °C with a downstream pressure of 1 bara and 30 slm feed.*

6.4.2 Reformate

The membrane thickness experiments were repeated using 10% CO reformate. Again there is a decrease in the hydrogen permeate as the membrane thickness is increased. With a 3 barg pressure drop, the hydrogen permeate decreases from 1.1 slm to 0.8 slm as the membrane thickness increases from 4.75 μm to 13.25 μm respectively. Over the same thickness range, with a pressure drop of 9 barg, the hydrogen permeate decreases from 4.5 slm to 3.2 slm. In all cases the decrease in hydrogen permeate is less evident than with pure hydrogen.

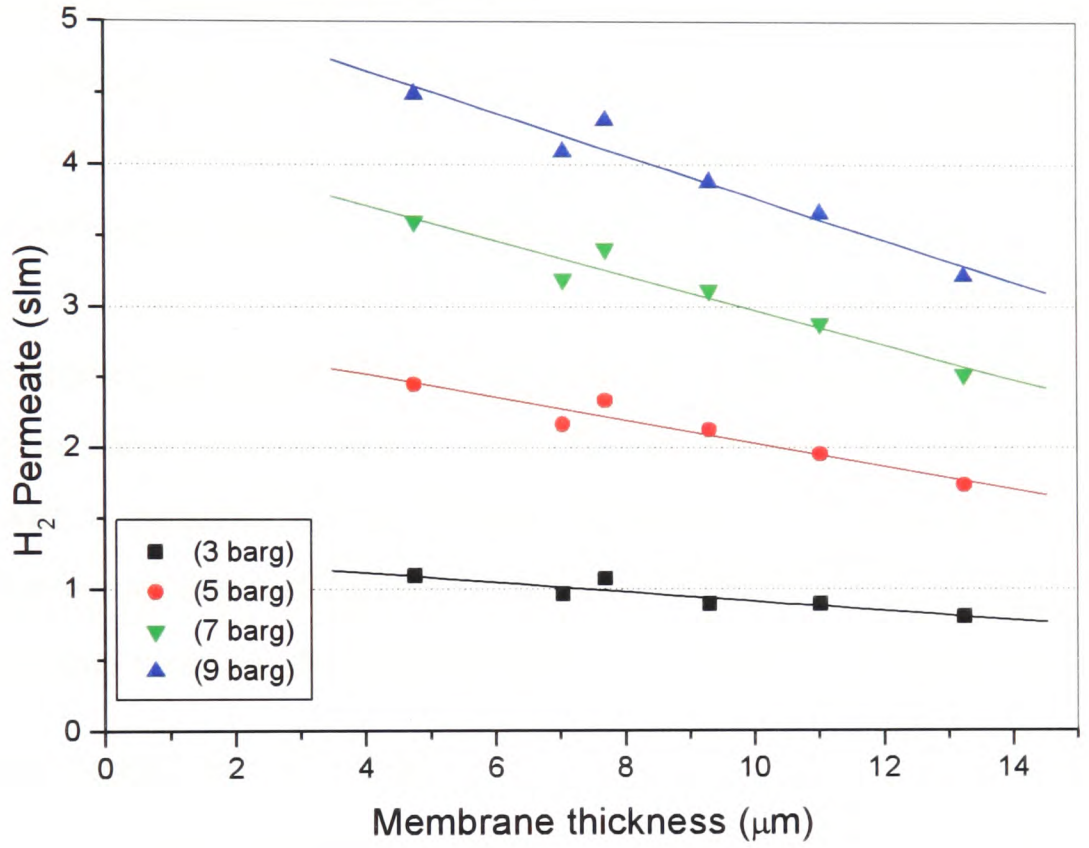

Figure 6.5: *Hydrogen permeate as a function of membrane thickness using 10% CO reformate at a membrane temperature of 440 °C with a downstream pressure of 1 bara and 30 slm feed.*

6.4.3 Pressure Exponential, *n*

The flux of hydrogen through a membrane is described by Sievert's law and can be expressed in the following form:

$$J_{H_2} = \frac{\rho_{H_2}}{X_{metal}} (P_{H_2\,feed}{}^{n} - P_{H_2\,perm}{}^{n})$$

where: J_{H_2} is the hydrogen flux

ρ_{H_2} is the hydrogen permeability

X_{metal} is the membrane thickness

$P_{H_2\,feed}$ is the hydrogen partial pressure in feed stream

$P_{H_2\,perm}$ is the hydrogen partial pressure in permeate stream

n is the pressure exponential.

The value of n, the pressure exponential, varies depending on which step in the hydrogen transport through the membrane is more dominant. With the bulk diffusion of hydrogen through the membrane predominating as the rate determining step, the value of n has been found to be $n = 0.5$ (Hurlbert and Konecny, 1961). With supported membranes, other flow processes such as Knudsen diffusion become more prevalent and the value of n tends towards $n = 1$. At high temperatures (>300 °C), the surface adsorption and dissociation is fast and the diffusion through the bulk is the rate controlling step (Athayde *et al.*, 1994). From consideration of the pure hydrogen flow data with a standard 7.5 μm Pd/Ag membrane, it is possible to determine the value of the pressure exponential using graphical methods. This is done by assuming a linear relationship between the hydrogen flux, J_{H_2}, and the hydrogen partial pressure and exponent component of Sievert's law, $(P_{H_2\,feed}{}^{n} - P_{H_2\,perm}{}^{n})$. Taking the maximum hydrogen flux at each membrane chamber pressure, and plotting this against the pressure component over a range of values of n (see Figure 6.6), the fit of the line can be assessed to determine which value of n is most descriptive of the data. In all experimental cases the permeate pressure is taken to be 1 bara. This simplifies the expression as $1^n = 1$ for all values of n, leaving simply $(P_{H_2\,feed}{}^{n} - 1)$. Linear best fit lines are then drawn for each value of n and the correlation factor R^2 which is nearest to 1 indicates the best linear fit and thus the pressure exponential.

From consideration of Figure 6.6, it can be seen that a pressure exponential value of $n = 0.85$ provides a good linear fit to the experimental data with a correlation coefficient of $R^2 = 0.99998$. This would suggest that the rate of hydrogen diffusion through the membrane is not controlled by the bulk diffusion of hydrogen through the membrane, but that the diffusion through the substrate has an effect on the flow and is indicative of Knudsen flow whereby the size of the pores in the substrate material is

of the same order of magnitude as the mean free path of the species flowing through the material. It may be argued that all values of *n* produce a reasonable fit.

The determination of the pressure exponential, *n*, was repeated for the selection of membranes of various thickness from 4.5 μm to 13.5 μm. In the majority of cases the value of *n* by this method, was found to be of the order 0.8 to 0.85. However in the case of the thickest membrane the value of *n* was 0.6, which would suggest that the dominant diffusion mechanism in this case is the bulk diffusion of hydrogen through the membrane. A blank substrate was also considered and a pressure exponential of $n = 1.4$ was determined. This would suggest the presence of viscous flow where the size of the pores is significantly greater than the mean free path of the species.

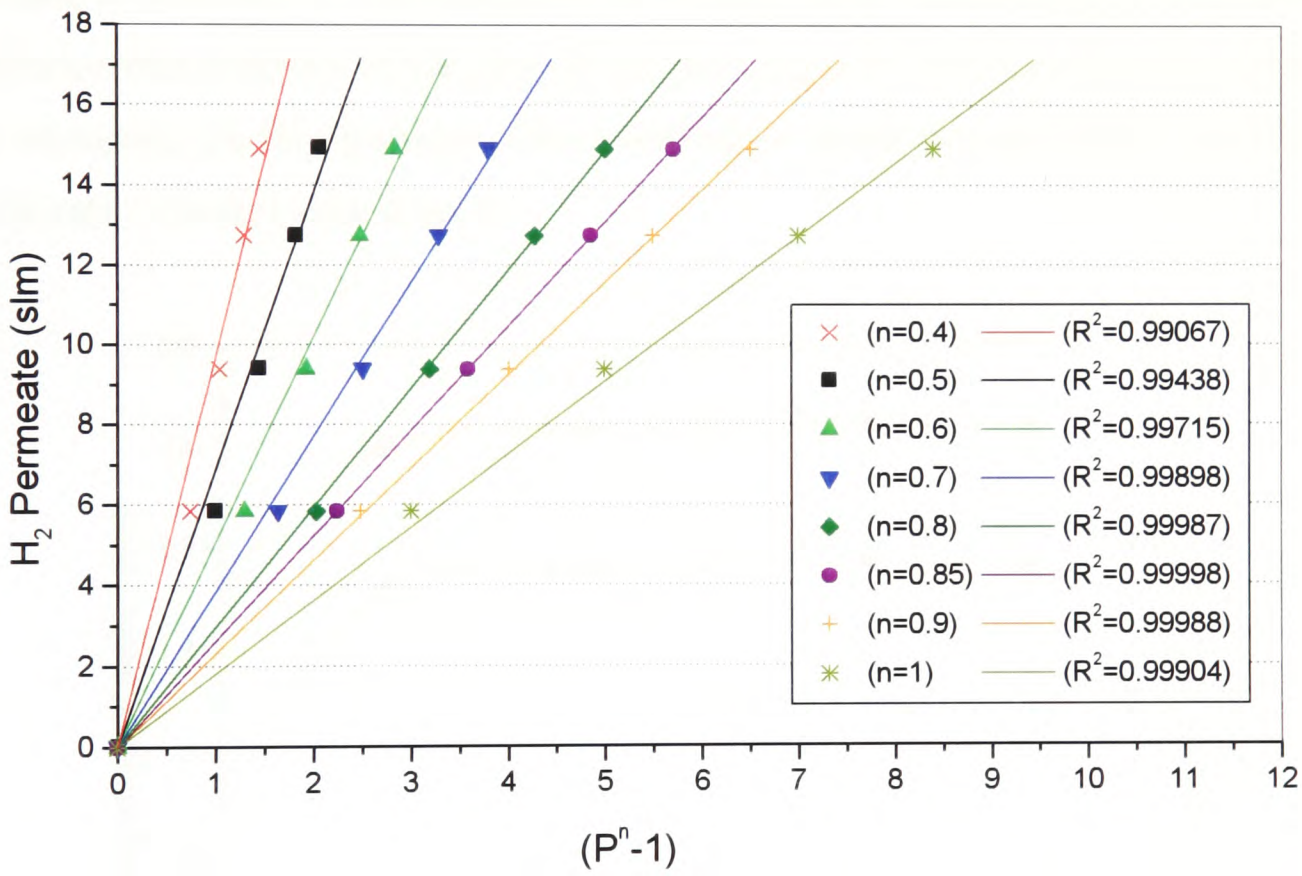

Figure 6.6: *Graphical determination of the power exponent in Sievert's law for a standard 7.5 μm Pd/Ag membrane operating at 440 °C and a downstream/permeate pressure of 1 bara.*

6.5 Sweep Tests

Investigations were carried out into the use of a sweep (or purge) gas to improve the hydrogen permeation through the membrane. A standard 7.5 μm Pd/Ag membrane was installed into the test chamber and then a purge line was attached which could

supply nitrogen to the centre of the membrane tube. The sweep gas flow rate could be controlled using a mass flow controller. The temperature of the membrane was maintained at 440 °C and 10% CO reformate was supplied as a feed gas. The results can be seen in Figure 6.7. The experiment was run with a reformate feed flow rate of 15 slm. With the sweep gas set at 3 slm or 20% of the reformate feed, there is a significant improvement in the hydrogen permeate. In the case of the 3 barg pressure drop, hydrogen permeate increases from 1.1 slm to 1.85 slm. In the 5 barg case this increase is from 1.85 slm to 2.4 slm. The increases are 68% and 30% for the 3 barg and 5 barg cases respectively. It is thought the presence of a sweep gas helps to reduce the partial pressure of hydrogen on the downstream side by purging the membrane. This effect has also been observed when hydrogen is first fed to the chamber as discussed in Section 6.3. The results of the sweep testing would suggest that reducing the downstream pressure would provide greater benefit in terms of hydrogen permeate than increasing the feed pressure. Other methods of producing this effect would be to incorporate a downstream vacuum.

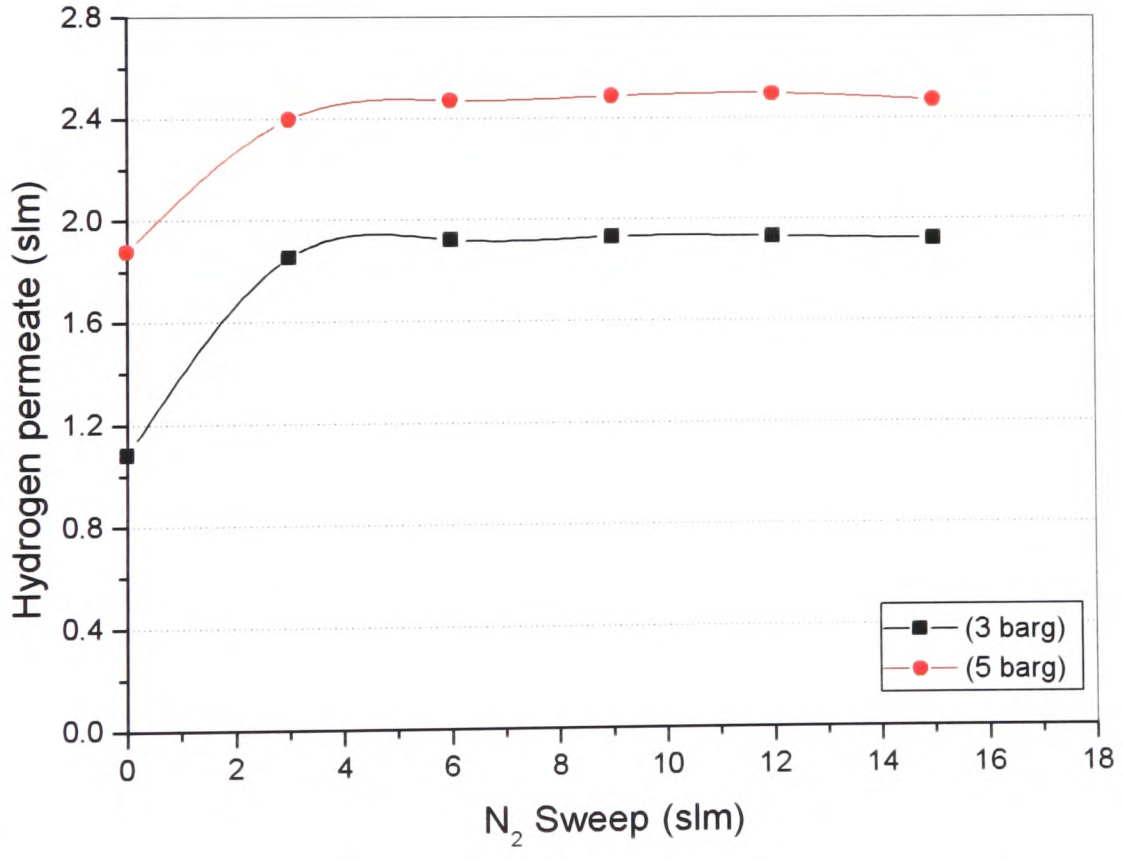

Figure 6.7: *Sweep tests with a standard* 7.5 µm *Pd/Ag membrane using 10% CO reformate as a feed and nitrogen as the sweep with a membrane temperature of 440 °C and downstream pressure of 1 bara.*

6.6 Temperature Effect

As discussed in Section 6.2, membranes are typically operated at a temperature of 440 °C to prevent CO poisoning. There is also a degradation in the hydrogen permeate with pure hydrogen as the temperature is reduced. These investigations into the effect of temperature on hydrogen permeate with both pure hydrogen and 10% CO reformate were performed with a standard 7.5 μm Pd/Ag membrane and with a feed flow sufficient that the maximum hydrogen permeate would be attained. The temperature was then varied and the hydrogen permeate recorded at the corresponding membrane temperature.

6.6.1 Hydrogen

The initial temperature variation experiment was performed with pure hydrogen and the results are shown in Figure 6.8. In the case of each pressure drop, an s-shape curve is produced. Peak hydrogen permeates are 5.9 slm, 9.5 slm and 12.9 slm for the 3 barg, 5 barg and 7 barg pressure drops respectively. From the standard operating temperature of 440 °C to 300 °C, the reduction in hydrogen permeate is quite gradual. The steepest part of the curve in each case begins around 275 °C and the hydrogen permeate decreases to less than 1 slm below 100 °C.

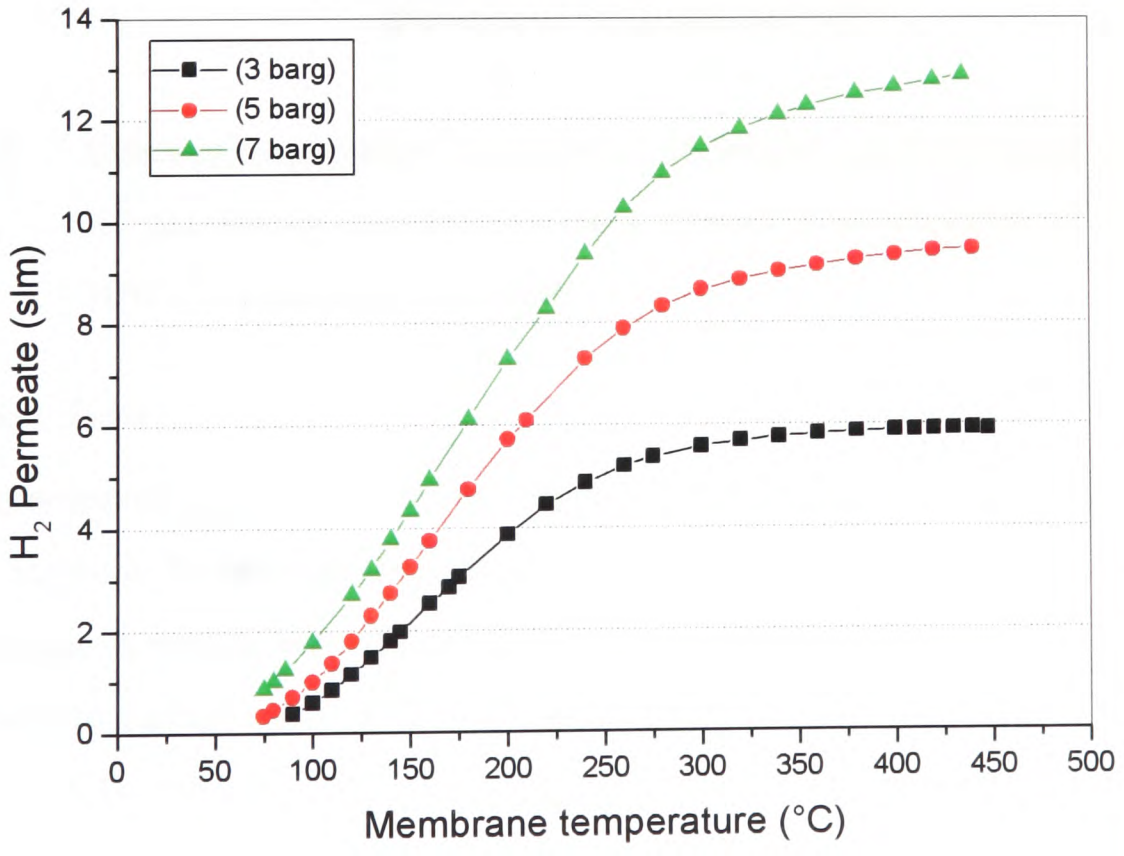

Figure 6.8: *Effect of temperature variation on hydrogen permeate using a standard 7.5 μm Pd/Ag membrane with a downstream pressure of 1 bara and pure hydrogen.*

6.6.2 Reformate

Results demonstrating the effect of temperature on hydrogen permeate using 10% CO reformate are shown in Figure 6.9. As with the pure hydrogen test, the hydrogen permeate begins to tail off around the 300 °C mark, though in contrast the hydrogen permeate decreases more rapidly and by 200 °C the value is less than 0.1 slm. These results would suggest that operating the membranes at 440 °C will prevent this fall off.

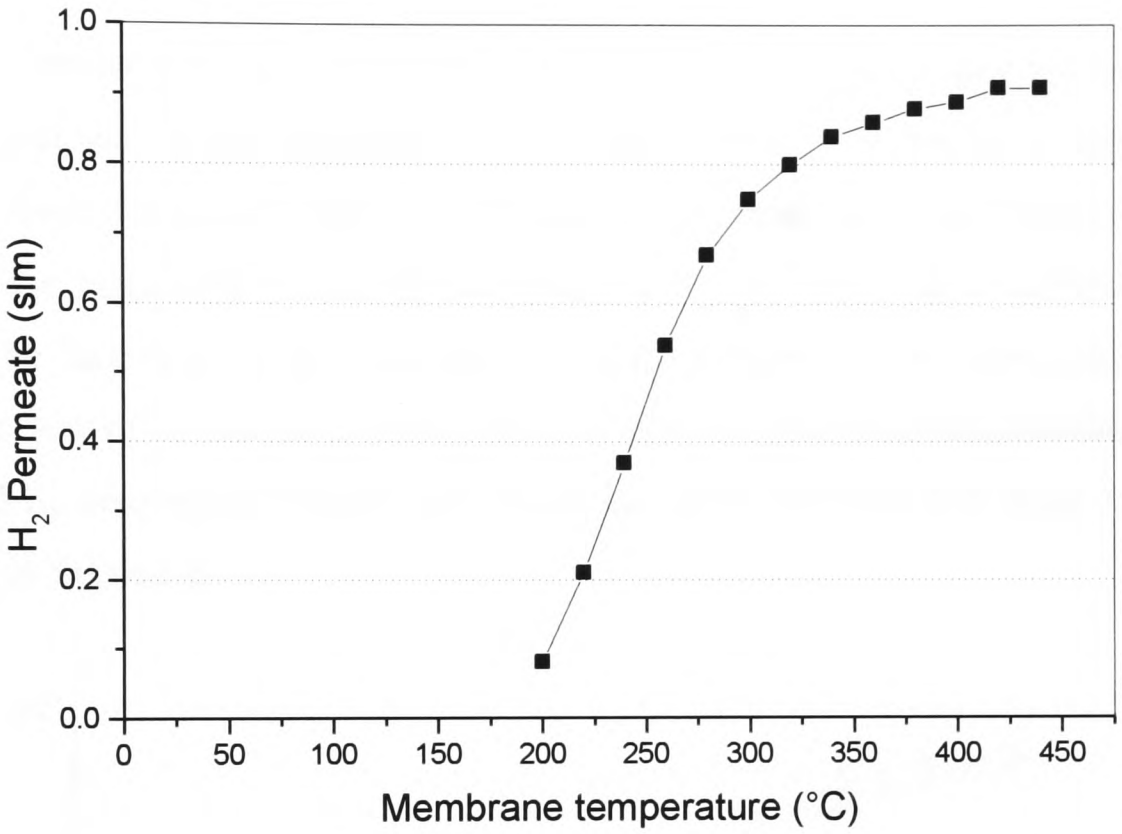

Figure 6.9: *Effect of temperature variation on hydrogen permeate using a standard 7.5 μm Pd/Ag membrane with a downstream pressure of 1 bara and 10% CO reformate at 4 bara.*

6.7 Steam Tests

All the experimental work carried out with reformate so far was with a dry 10% CO reformate mixture. In practise the output of a reformer would contain an amount of water as steam. A typical wet reformate from a gasoline autothermal reformer (ATR) with a steam to carbon ratio, SCR = 2, would comprise the following: H_2 = 28.8%, N_2 = 27.36%, CO_2 = 8.64%, CO = 7.2%, H_2O = 28%. This can be produced by mixing 10% CO reformate with water in a steam generator in the correct proportions.

In order to be able to compare with results using 10% CO reformate it was important to keep the partial pressures of H_2 and CO consistent. A dry gas feed of 15 slm was

used and mixed with 4.68 ml of water per minute in order to produce the desired composition. The feed stream pressure into the chamber with the wet reformate was 5.55 bara thereby maintaining the partial pressure of H_2 at 1.6 bara for comparison with the dry reformate at 4 bara. The results are shown in Figure 6.10. For reference, the hydrogen permeate using pure hydrogen is shown with a feed pressure of 1.6 bara. This is equivalent to the H_2 partial pressure of the feed streams in the experiments using wet and dry reformate mixtures.

All three plots have a peak at 440 °C with around 0.9 slm hydrogen permeate. This confirms that the partial pressures of H_2 in each stream are the same and that the steam has been dosed correctly. The wet and the dry reformate plots follow an almost identical line beginning to tail off around 350 °C and reaching a minimum under 200 °C. The fact that the dry and wet reformate streams are so close indicates that with these flow rates, the steam acts only as a diluent. Mass balance calculations were performed to determine whether any water gas shift occurred and these results are discussed in Section 6.7.1.

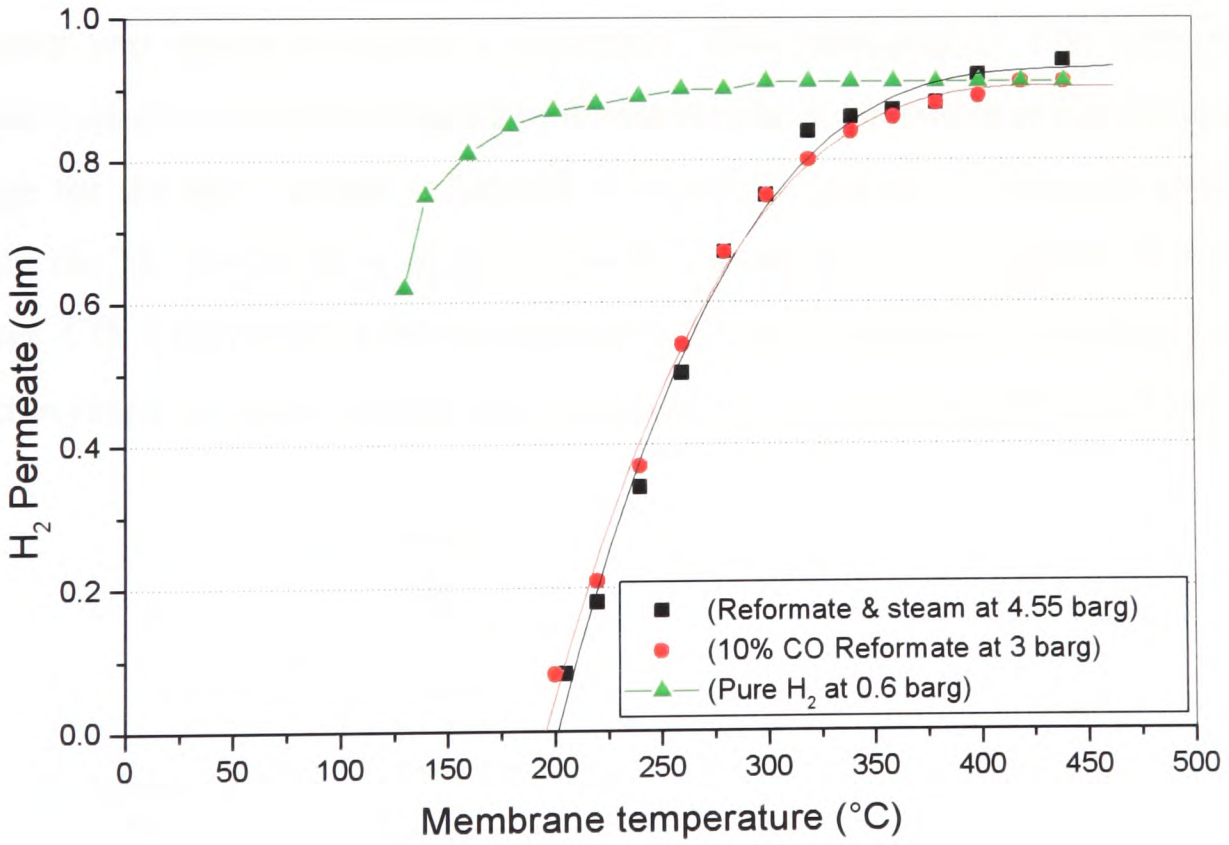

Figure 6.10: *Wet and dry reformate tests with varying temperature using a standard 7.5 μm Pd/Ag membrane with a downstream pressure of 1 bara.*

6.7.1 Investigations into Water Gas Shift Activity on Pd Membranes

With a wet reformate mixture in the presence of palladium, it was conjectured that carbon monoxide present in the feed gas may undergo the water gas shift (WGS) reaction to form carbon dioxide and additional hydrogen. The WGS reaction proceeds as follows:

$$CO + H_2O \rightarrow CO_2 + H_2$$

If such a reaction were present then there would be an decrease in the CO poisoning effect on the palladium as well as an increase in the hydrogen partial pressure in the feed stream and thus improved membrane performance. In order to investigate this reaction, a flow test was performed using a standard 7.5μm Pd/Ag membrane and a 10% CO reformate feed which was then mixed with steam to provide a wet reformate mixture containing 28% H_2O. In order to compare the wet reformate results with dry reformate results, the hydrogen partial pressure drop was maintained by using a 4.55 barg pressure drop. The membrane test temperature was maintained at 440 °C. Some initial results using a 15 slm reformate feed suggested that the space velocity may be too high and so the reformate feed was varied between 2.5 slm and 15 slm. The steam was dosed to ensure a consistent 28% composition. The retentate and permeate streams were then sampled to determine the composition of the streams. The H_2 range for the gas analyser is limited to 90 vol % and thus it was not possible to ascertain the H_2 composition in the permeate stream to a good degree of accuracy. However, CO, CO_2 levels in the permeate as well as H_2 levels in the retentate streams fell within range. The gas streams were sampled at the points indicated in Figure 6.11.

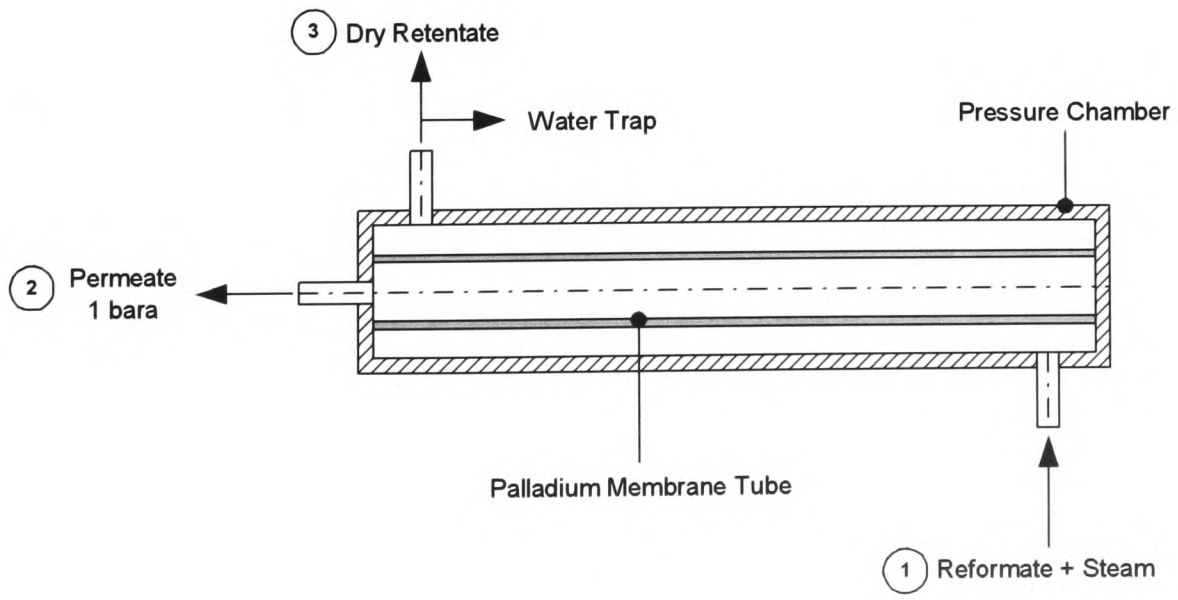

Figure 6.11: *A schematic of Pd membrane chamber and gas sampling points.*

Molar mass balances were then carried out on the three components, H_2, CO and CO_2 as follows:

H_2: $(\dot{M}_{H_2})_{(1)} + x = (\dot{M}_{H_2})_{(2)} + y[H_2]_{(3)}$

CO: $(\dot{M}_{CO})_{(1)} - x = (\dot{M}_{CO})_{(2)} + y[CO]_{(3)}$

CO_2: $(\dot{M}_{CO_2})_{(1)} + x = (\dot{M}_{CO_2})_{(2)} + y[CO_2]_{(3)}$

Where: x is the molar flow rate in mol/min of each species produced due to WGS (e.g. for H_2 this is $(\dot{M}_{H_2})_{WGS}$) and from consideration of the WGS equation, x is equal for each species

y is the dry molar flow rate in mol/min at sampling point (3)

subscripts (1), (2) and (3) denote the sampling points

square parentheses [] indicate mole fraction

The following values can be measured at the three sampling points:

(1) $\dot{M}_{CO}, \dot{M}_{CO_2}, \dot{M}_{H_2}, \dot{M}_{N_2}, \dot{M}_{H_2O}$

(2) $\dot{M}_{CO}, \dot{M}_{CO_2}, \dot{M}_{H_2}$

(3) $[CO], [CO_2], [H_2]$

The molar flow balances can then be solved simultaneously to determine the value of x, e.g. the quantity of H_2 produced due to WGS. The value of x was found to be 3.3×10^{-4} mol/min and showed that there was negligible evidence of WGS activity under these conditions. This was backed up by the composition plots of the permeate and retentate streams as shown in Figure 6.12 and Figure 6.13 respectively.

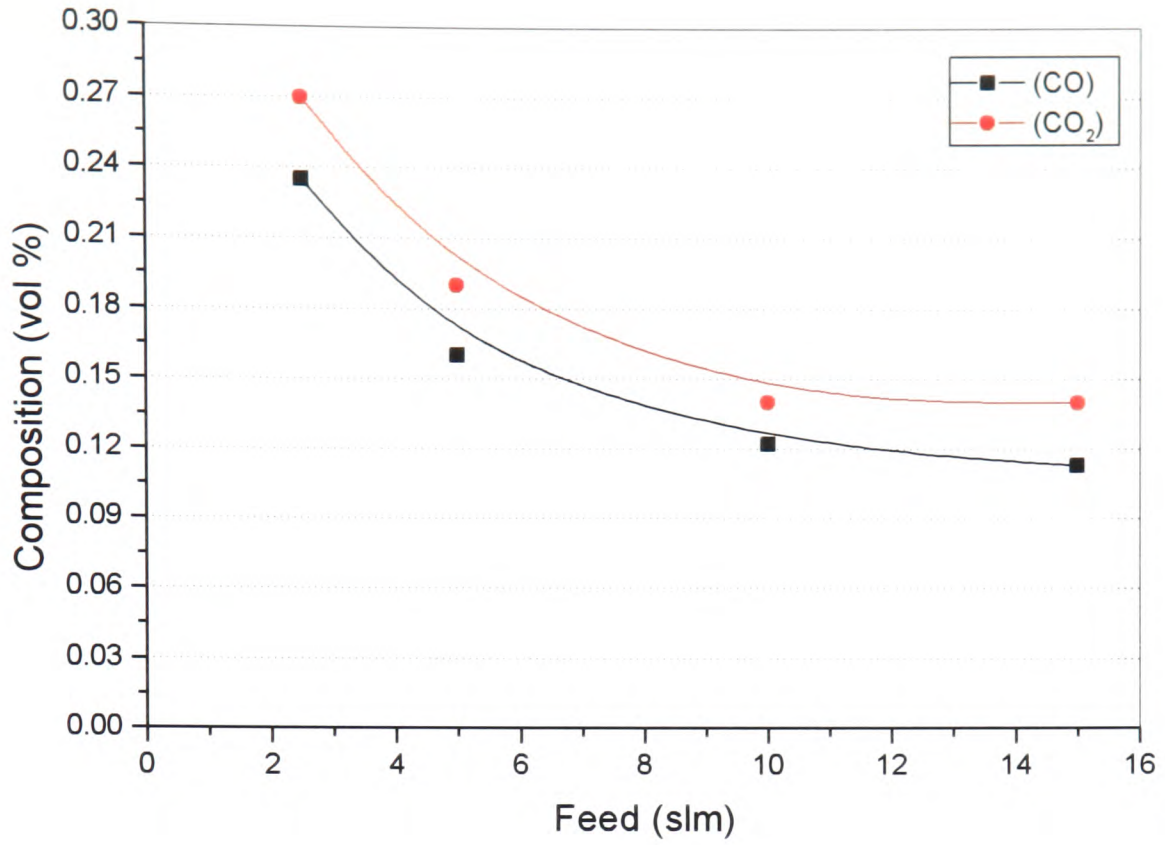

Figure 6.12: *Permeate stream gas composition analysis using a standard 7.5µm Pd/Ag membrane with a wet 10% CO reformate feed and a 4.55 barg pressure drop at 440 °C.*

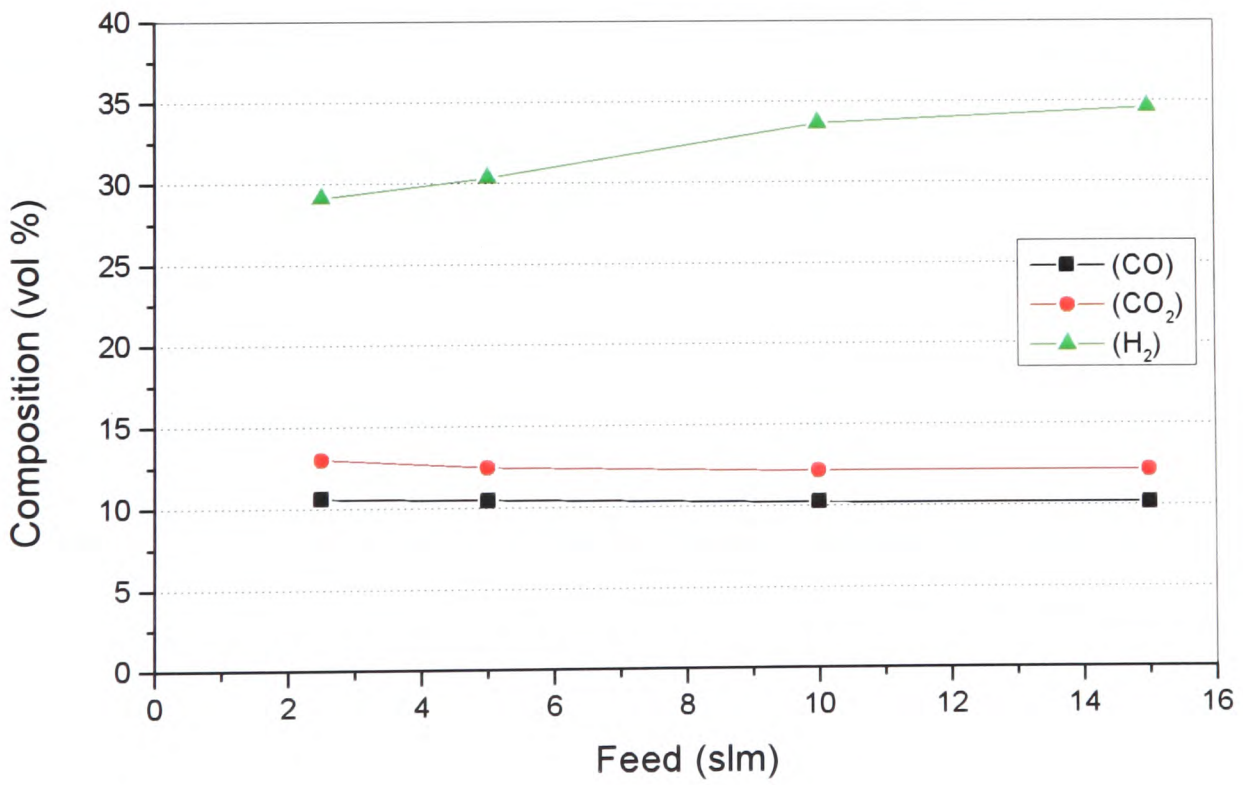

Figure 6.13: *Retentate stream gas composition analysis using a standard 7.5µm Pd/Ag membrane with a wet 10% CO reformate feed and a 4.55 barg pressure drop at 440 °C.*

From consideration of Figure 6.12, the composition of CO and CO_2 in the permeate stream both reduce by 0.12 vol % as the feed is increased form 2.5 to 15 slm. The decrease in the composition values of these species is due to the increase in H_2 that results from the increased feed flow rate. The fact that the difference between CO and CO_2 remains the same indicates that there is no observable reduction in the CO or corresponding increase in CO_2 as might be expected if there was water gas shift activity present.

From Figure 6.13, the retentate composition remains reasonably consistent though there is again a reduction in the vol % of both CO and CO_2 as the feed is increased. This is due to the increase in H_2 flowing into the retentate stream as the feed is increased as the membrane permeability limit is reached.

6.8 Hydrogen Partial Pressure Variation

This experiment was performed to determine the effect of the hydrogen partial pressure on the hydrogen permeation through a standard membrane. Hydrogen was mixed with nitrogen to produce a range of compositions and the hydrogen permeate recorded with a 3 barg total pressure drop over the membrane and a combined flow rate of 30 slm. The results are shown in Figure 6.14. Negative partial pressure drops were achieved with hydrogen constituting less than 30% of the inlet mixture corresponding to a partial pressure drop of 0.2 barg. A negative pressure drop results in no hydrogen permeate. However, increasing the concentration above 30% there is a linear relationship between the partial pressure drop and the hydrogen permeate. A partial pressure drop of 0.6 barg corresponds to that with 10% CO reformate resulting in a hydrogen permeate of around 0.9 slm. Increasing the partial pressure drop to 3 barg (corresponding to pure H_2) results in a hydrogen permeate of 6 slm. These individual results have been shown previously if only in a different form. These results also back up the determination of the pressure factor n as described in Section 6.4.3 being closer to $n = 1$ for supported membranes than $n = 0.5$ for unsupported thick membranes.

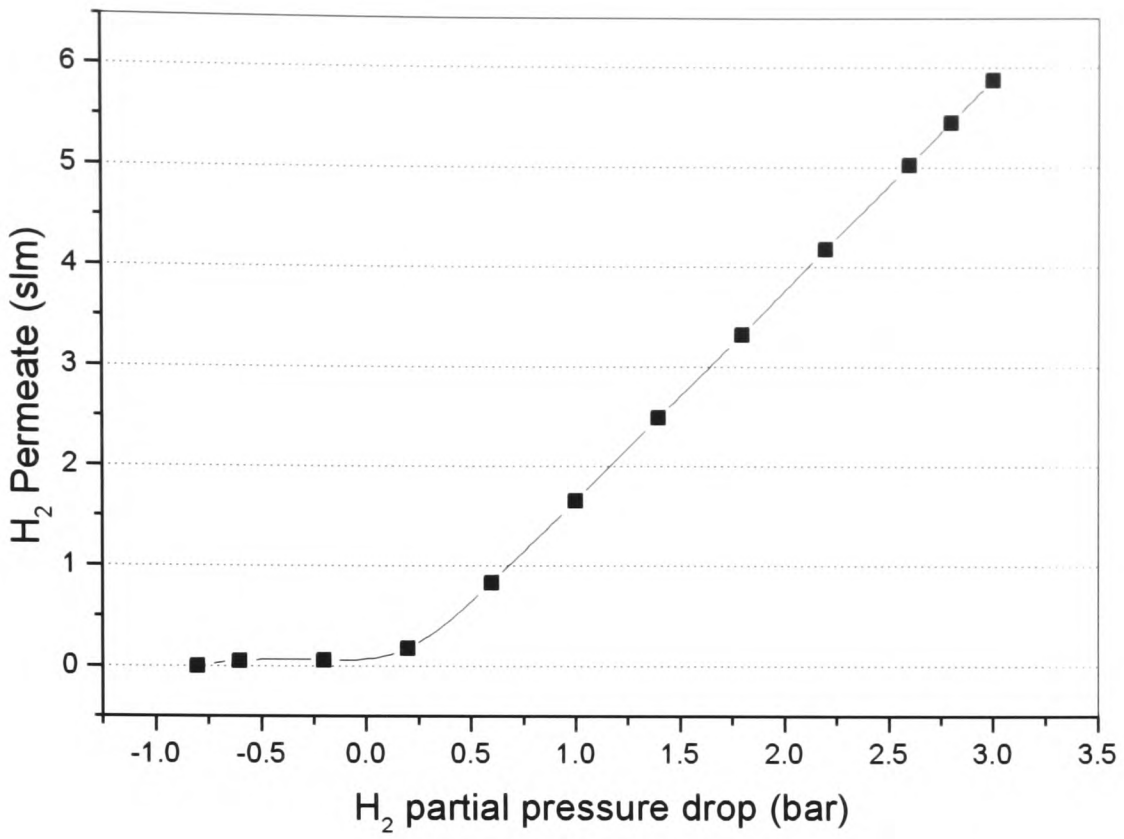

Figure 6.14: *Effect of variation in H_2 concentration on hydrogen permeate with a standard membrane with a 3 barg pressure drop.*

6.9 Carbon Monoxide Concentration

Experiments were carried out to determine the effect of the CO concentration on the hydrogen permeate with variation in membrane temperature. Cylinders were available with differing CO concentrations, but all with constant H_2 compositions. A standard 7.5 μm Pd/Ag membrane was used with a feed pressure of 3 barg and a downstream pressure of 1 bara. The results are shown in Figure 6.15. It can be seen that all three compositions produce an almost identical hydrogen permeate of 0.9 slm at 440 °C. However with decreasing temperature the effect of the CO concentration becomes more marked. The lower the CO concentration the greater the shift of the curve to the left indicating reduced poisoning. The shift is around 20 °C as the composition is reduced from 10% to 5% CO and a further 20 °C shift from 5% to 2% CO.

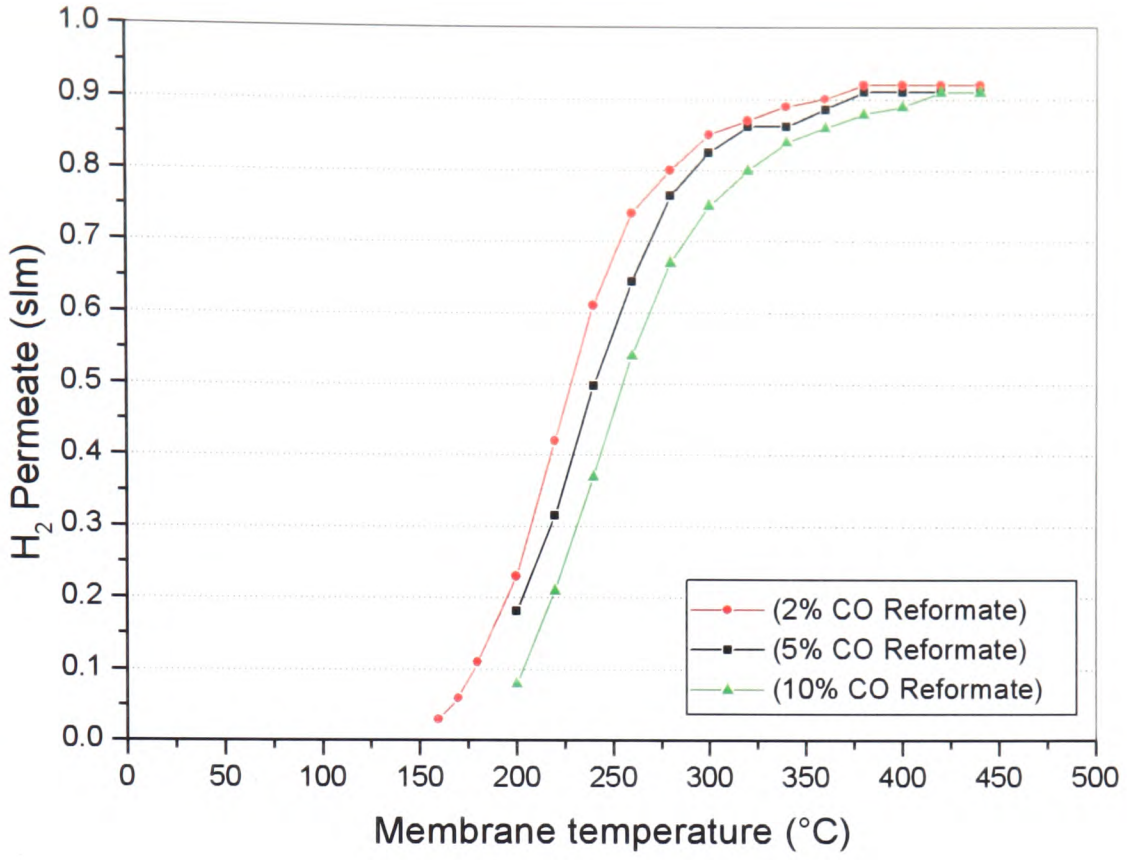

Figure 6.15: *Effect of CO concentration on hydrogen permeate with variation in membrane temperature using a standard 7.5 μm membrane with a 3 barg pressure drop.*

6.10 Other Impurities

The effect of carbon monoxide on the hydrogen flux through palladium membranes has been shown experimentally to cause reduced membrane performance. Carbon monoxide blocks the available hydrogen dissociation sites (Amandusson *et al.*, 2000; 2001; Sakamoto et al., 1996) though operating at temperatures greater than 673 K is sufficient to prevent this (Hou and Hughes, 2002). Little influence of the presence of CO_2 or CH_4 has been observed experimentally on the hydrogen flux and this finding is supported in the literature (Flanagan *et al.*, 2000). It is possible to regenerate any coking of the membrane such as with the air treatment performed prior to flow testing or after poisoning has occurred (Chabot *et al.*, 1988).

The presence of sulphur-containing compounds, H_2S, can cause poisoning of reforming catalysts, but these are a common contaminant from coal gasification or from refined petroleum. Sulphur compounds are also often added to natural gas as an

odouriser in the form of mercaptans (Edlund, 2002). Commercial methods for removal produce other pollutants such as sulphur oxides and metal sulphides. Sulphur also acts as a poison through surface blocking of dissociation sites (Castro *et al.*, 2002). European directives propose sulphur levels below 10 mg/kg by 2009 for gasoline and diesel fuels and these will be described as sulphur free (DFT, 2004).

Although no testing has been carried out with sulphur containing gas mixtures, it is assumed that for the benefit of both the steam reformer catalyst and the palladium membrane clean-up module in a proposed system, a low sulphur fuel would be used or a sulphur trap incorporated as discussed in Chapter 2.

6.11 Blank Substrate

The following experiments were carried out with the blank ceramic substrate to look at its flow characteristics without the presence of a membrane. The first experiment involved studying the effect of temperature on the nitrogen permeate, the results of which can be seen in Figure 6.16. As the temperature is increased there is actually a decrease in the nitrogen permeate from 10.4 slm at 35 °C to 4.8 slm at 440 °C. This is indicative of the transport processes involved which in this case is Poiseuille.

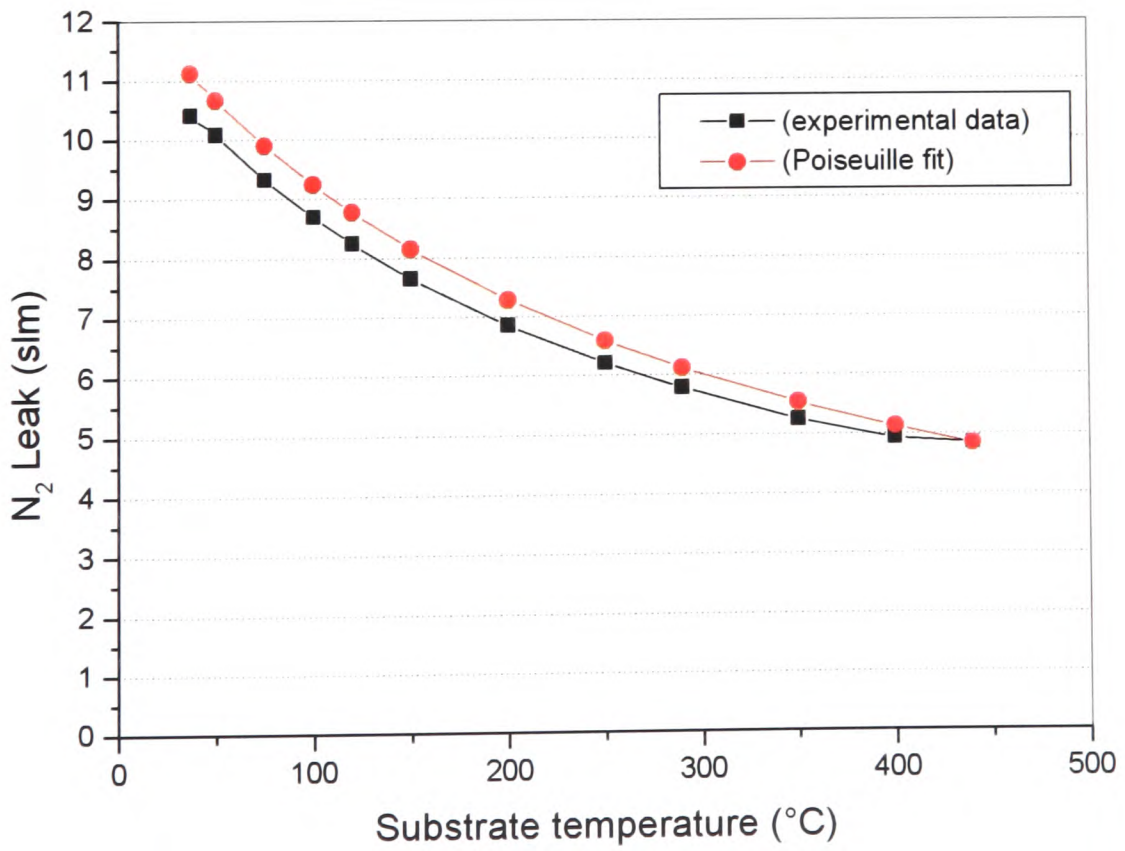

Figure 6.16: *Effect of temperature on nitrogen permeation through blank ceramic substrate with 30 slm feed flow rate and 3 barg pressure drop.*

The Poiseuille fit in Figure 6.16 is based on the nitrogen flow at 440 °C and shows that flow is inversely proportional to temperature (see Chapter 2).

If operating the substrate with a membrane, it is hydrogen that will be passing through the substrate material and so experiments were done to look at the effect of temperature on hydrogen permeate through the substrate. The maximum permeate is shown against pressure drop for both 440 °C and 50 °C. The flow of nitrogen at 440 °C is also shown for reference. The results are shown in Figure 6.17. From the plot it can be seen that the flow of nitrogen through the substrate is reduced at higher temperatures. At 440 °C the flow at 3 barg is 14 slm which compares with 28 slm at 50 °C. However, considering the flow through a standard Pd/Ag membrane at 440 °C with a 3 barg pressure drop is of the order 6 slm, this is 8 slm less that the bare substrate can pass. It therefore follows that the substrate plays a role in limiting the hydrogen permeate possible, though not enough to suggest the substrate is the limiting step in the diffusion process.

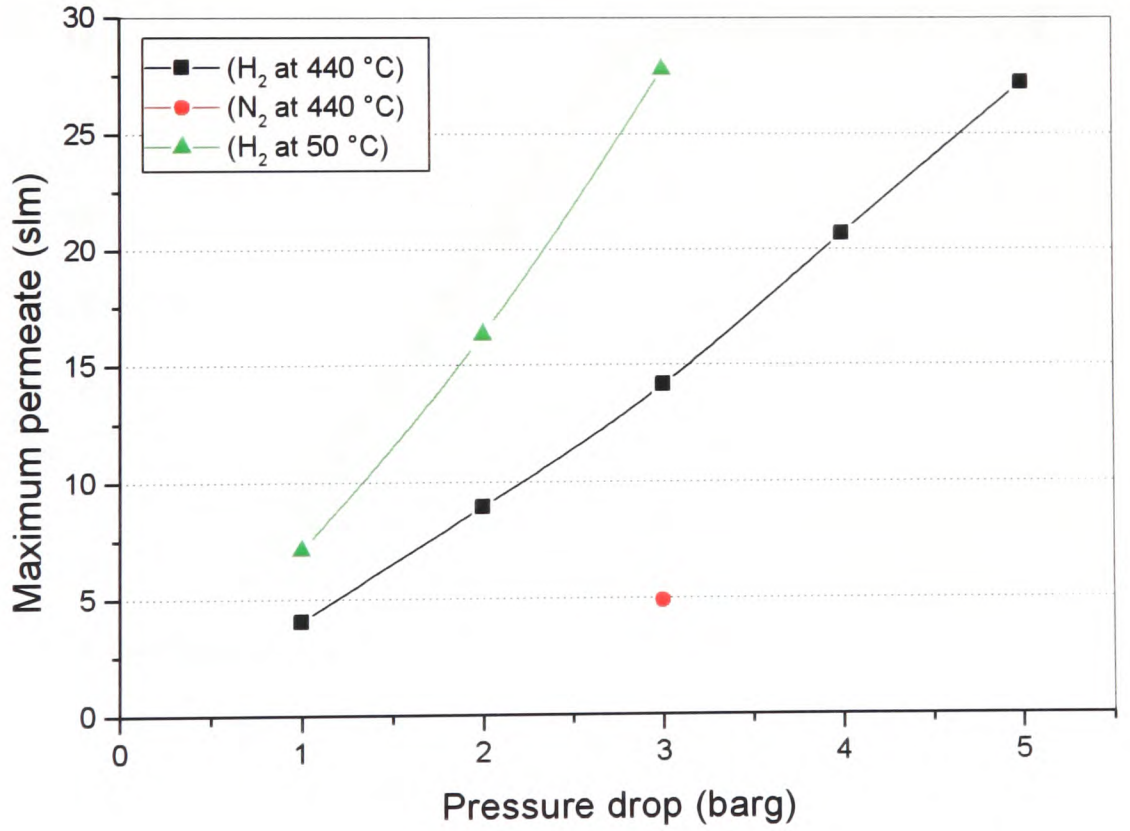

Figure 6.17: *Hydrogen permeate through blank ceramic substrate at 50 °C and 440 °C as a function of pressure drop.*

6.11.1 Membrane Processing

The results shown in Section 6.11 are for the as-received substrate material, but further testing has been carried out to investigate the effect of membrane processing such as sanding/firing and sol-gel application on the hydrogen flow. The results are shown in Figure 6.18. It can be seen from the plot that the various stages of processing have very limited effect on the hydrogen flow through the substrate. The hydrogen flow of the as received substrate is of the order 14.3 slm with a 3 barg inlet pressure and 1 bara downstream pressure. After the substrate has been fired there appears to be a slight reduction in the hydrogen flow through the membrane by 0.2 slm to 14.1 slm, but the application of a sol-gel layer and final firing cycle increases the flow to 14.6 slm. These are very minor differences of around 2% and can simply be put down to experimental error such as sealing in the chamber. The overall conclusion would be that the processing steps described above have negligible effect on the ability of the substrate material to pass hydrogen.

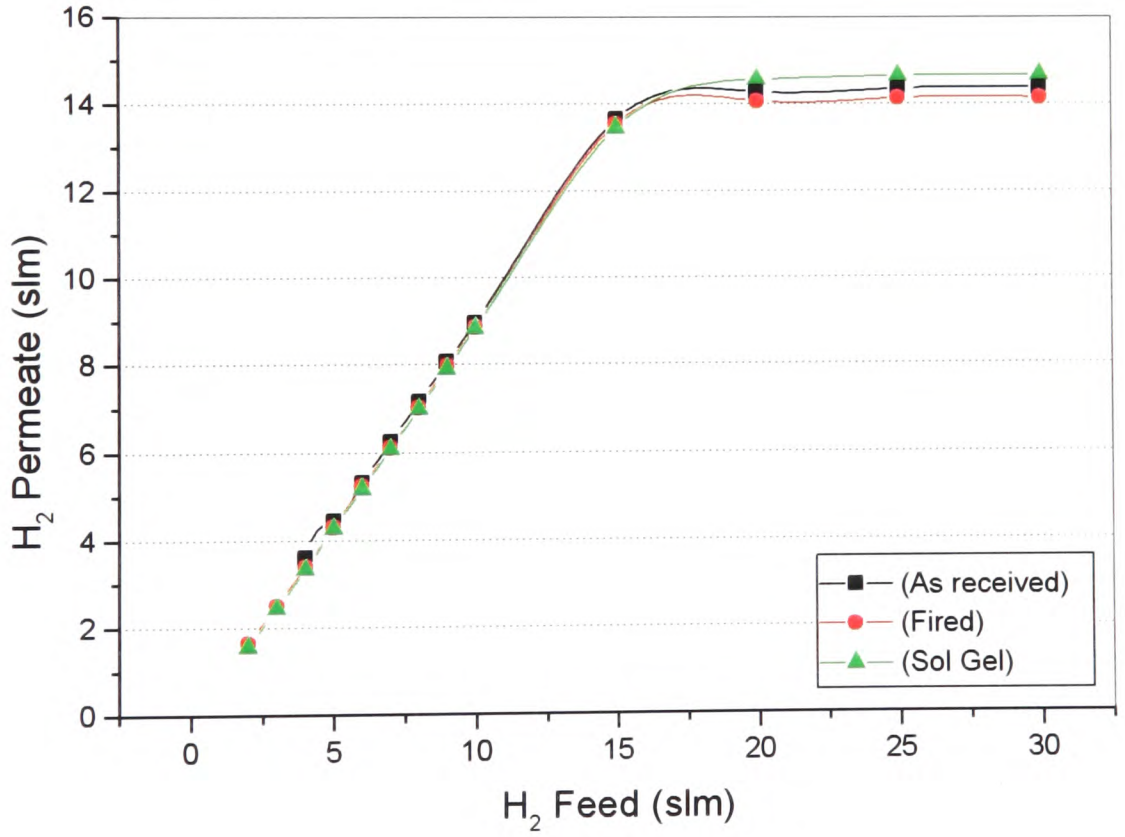

Figure 6.18: *Comparison of H_2 flow testing on ceramic substrate after various stages of processing with a 3 barg pressure drop at 440 °C* (Bennet, 2001)

6.12 Stainless Steel Substrates

The flow testing with stainless steel substrates was limited due to the membranes suffering delamination after only one temperature cycle, as a result of weak adhesion of the membrane to the substrate material as discussed in Chapter 4. Some flow data was produced however and this is summarised in Table 6-1.

Substrate	Membrane Thickness/ μm	H_2 flow / slm	Leak/ sccm	Permeance/ $m^3/m^2.hr.atm^{0.5}$	Selectivity (H_2/N_2)
Ceramic	7.5	6.0	5	25.7	1200
Thin-walled s.steel	5	13.7	82	122	167
Thick-walled s.steel	10	9	36	39	252

Table 6-1: *Flow test summary of stainless steel substrates and ceramic for comparison. Tests at 440 °C and 3 barg pressure drop.*

If the durability of the stainless steel substrates is neglected, it can be seen that these substrates have higher permeabilities, up to 5 times in the case of the thin-walled stainless steel substrate. However, when the leaks and consequently the selectivity of the membranes are examined, the membranes fabricated using a ceramic substrate have extremely high selectivities, around 5 times that of the thin-walled substrate. There was also evidence that in the case of the thin-walled substrate using the conventional plating procedure, which was found to result in a palladium membrane forming within the zirconia layer, the flux of hydrogen was significantly lower than in the case of the colloid prepared layer (up to 4 times lower than the value in Table 6-1).

Although stainless steel supported membranes were not tested above 440 °C, investigations by Mardilovic *et al.*, 1998, suggest that 550 °C is the limit of temperature before a drop in flux is observed. This was thought to be due to intermetallic diffusion.

Further investigation into the use of more porous support materials and the application of a more durable membrane could result in increased flux through the composite

membrane (Itoh *et al.*, 1994). The current performance of stainless steel supports, although not at a suitable level for hydrogen purification, is thought encouraging enough to recommend further work. The performance of the membranes on the ceramic substrate in terms of selectivity and flux is however suitable for application to hydrogen purification, and it is these membranes which will be considered in the subsequent simulations of a hydrogen purification system.

6.13 Sealing

Investigations were carried out into the graphite sealing method to determine the cause of its deterioration. It was conjectured that the expansion and subsequent contraction of the substrate on temperature cycling was responsible for easing the seals. By performing two tests, one using two solid alumina rods (see Figure 6.19) and another using a single alumina rod (see Figure 6.20), it could be determined whether the axial or radial expansion was at the heart of the problem. The alumina rods were made of Alsint, a non porous alumina, that had an external diameter equal to that of the conventional substrate material. Temperature cycling was carried out between 50 °C and 420 °C in nitrogen, and nitrogen leak tests were performed with a 3 barg pressure drop. The results of the two experiments are shown in Figure 6.21. Although the data is rather noisy, the experiment with the two rods produced no increase in leak over 45 cycles whereas the single rod seal degrades very rapidly with an increase in leak after only 2 cycles. The results indicate that the deterioration in the graphite seals is due to the repeated axial expansion and contraction of the substrate upon temperature cycling.

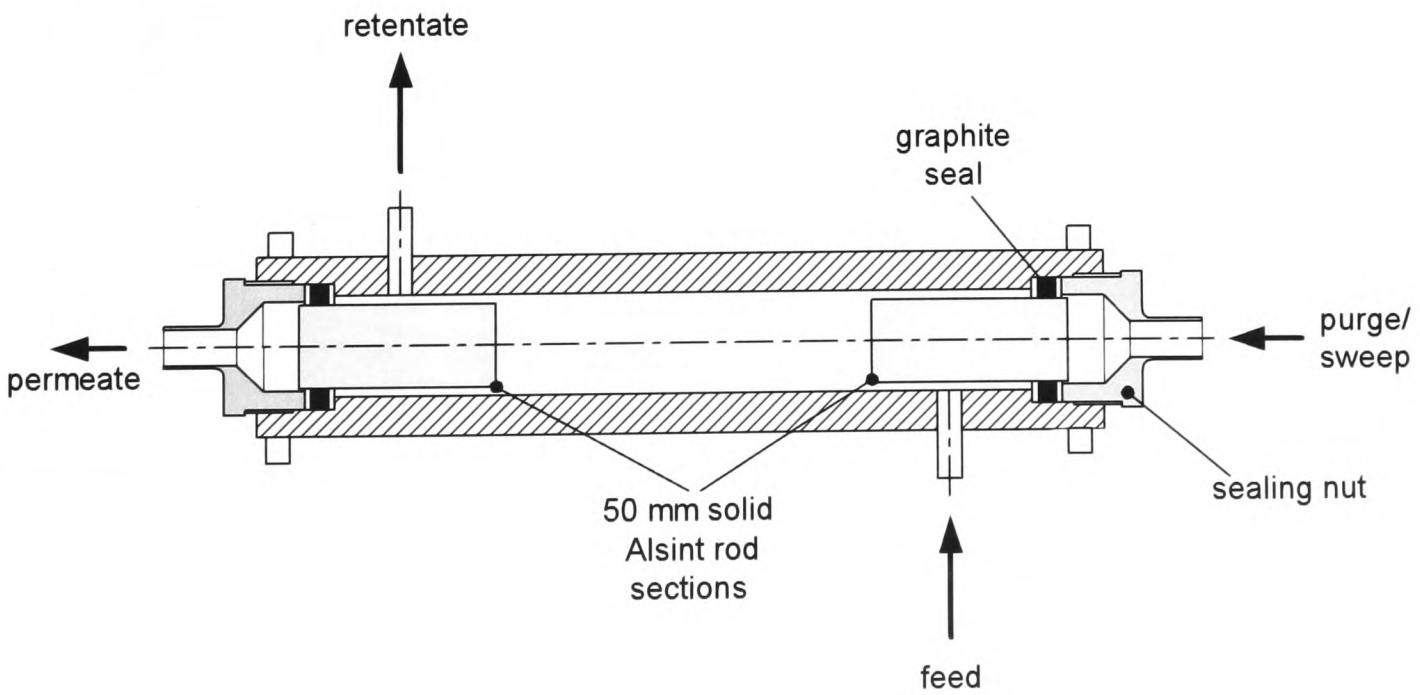

Figure 6.19: *Cross section of membrane test chamber with two solid alumina rods.*

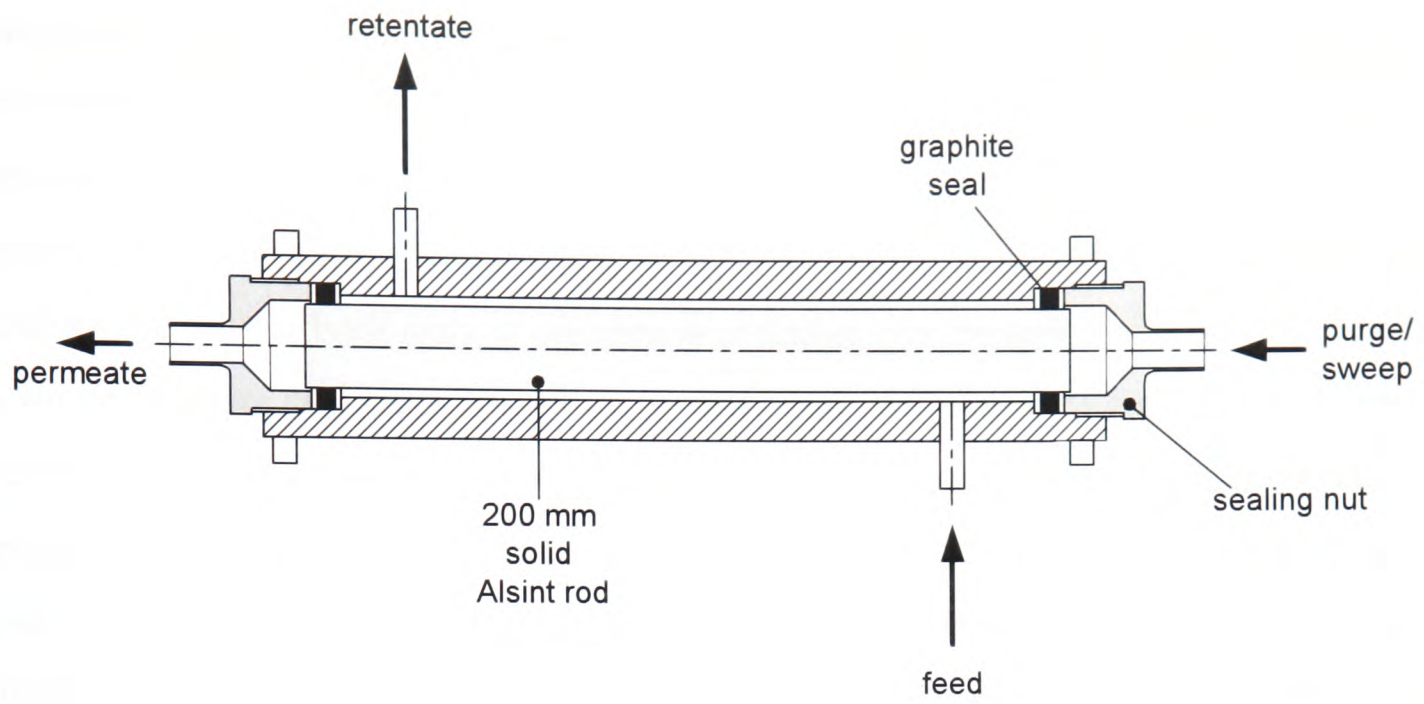

Figure 6.20: *Cross section of membrane test chamber with one solid 200 mm alumina rod.*

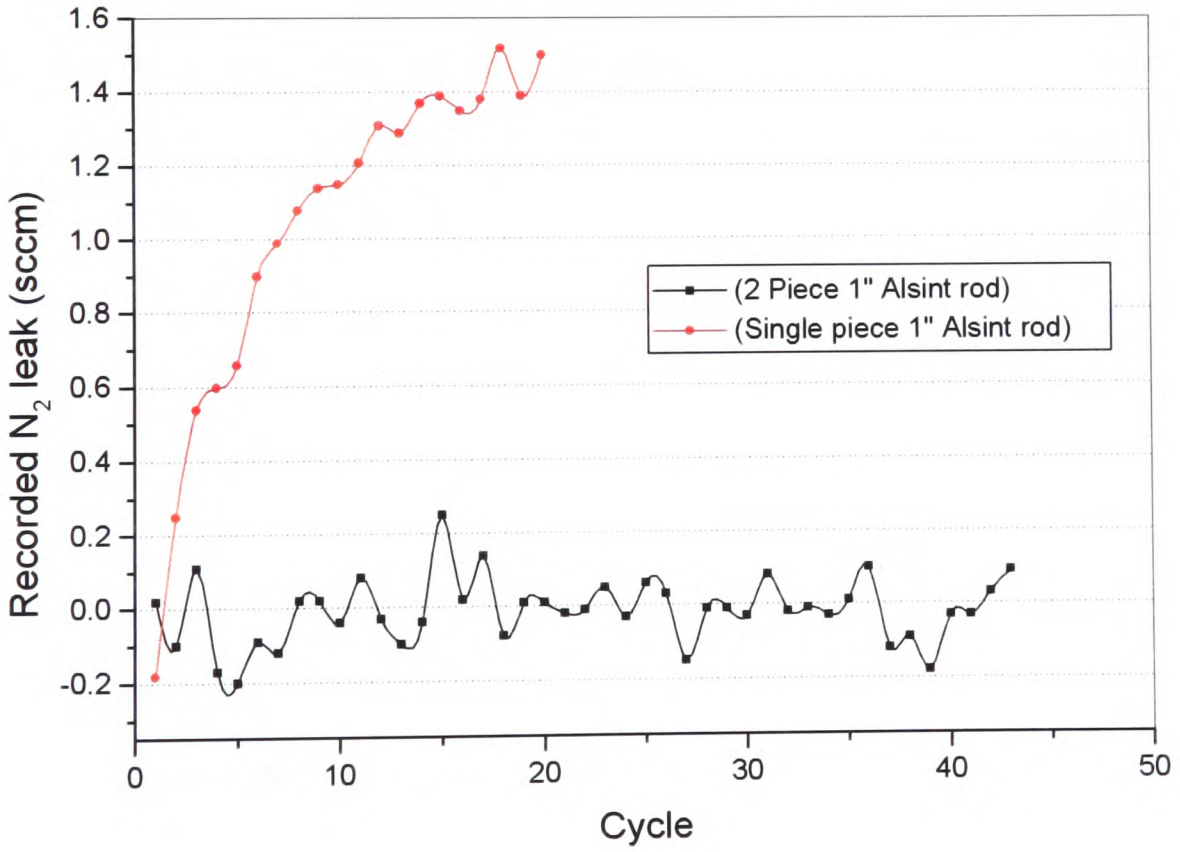

Figure 6.21: *Durability testing of graphite seals between 50 °C and 420 °C using solid alumina rods and a 3 barg pressure drop.*

6.13.1 Single Graphite Seal Arrangement

As described in Chapter 3 of this report, the use of a Kovar collar for sealing the membrane was investigated. However, the increased processing time made this solution impractical and it was also found that some residue was left after the brazing process. A simpler solution resulted as a consequence of the findings described in Section 6.13 and further work using the graphite seals was carried out. Rather than sealing the tube at both ends, a membrane chamber was designed and fabricated with a single graphite seal arrangement at the open end of the tube. With a single graphite seal it was necessary to ensure the Pd/Ag membrane was coherent around the closed end of the tube to ensure low leakage levels. A schematic of the single-ended graphite seal arrangement can be seen in Figure 6.22. A loose fitting graphite o-ring was also used to protect the membrane from damage on insertion into the tube, but this o-ring does not provide any sealing effect. The arrangements for the purge gas are different than in the standard membrane arrangement and in the modified design a purge tube is inserted into the open end of the tube with the permeate flowing out of the tube in an annular tube around this purge tube. Sealing the membrane at one end also has the advantage that there is less likelihood of damaging the membrane and substrate when tightening the end nut. There is also a tube at the closed end of the membrane which is used to aid the removal of the membrane from the chamber, but is sealed when in operation.

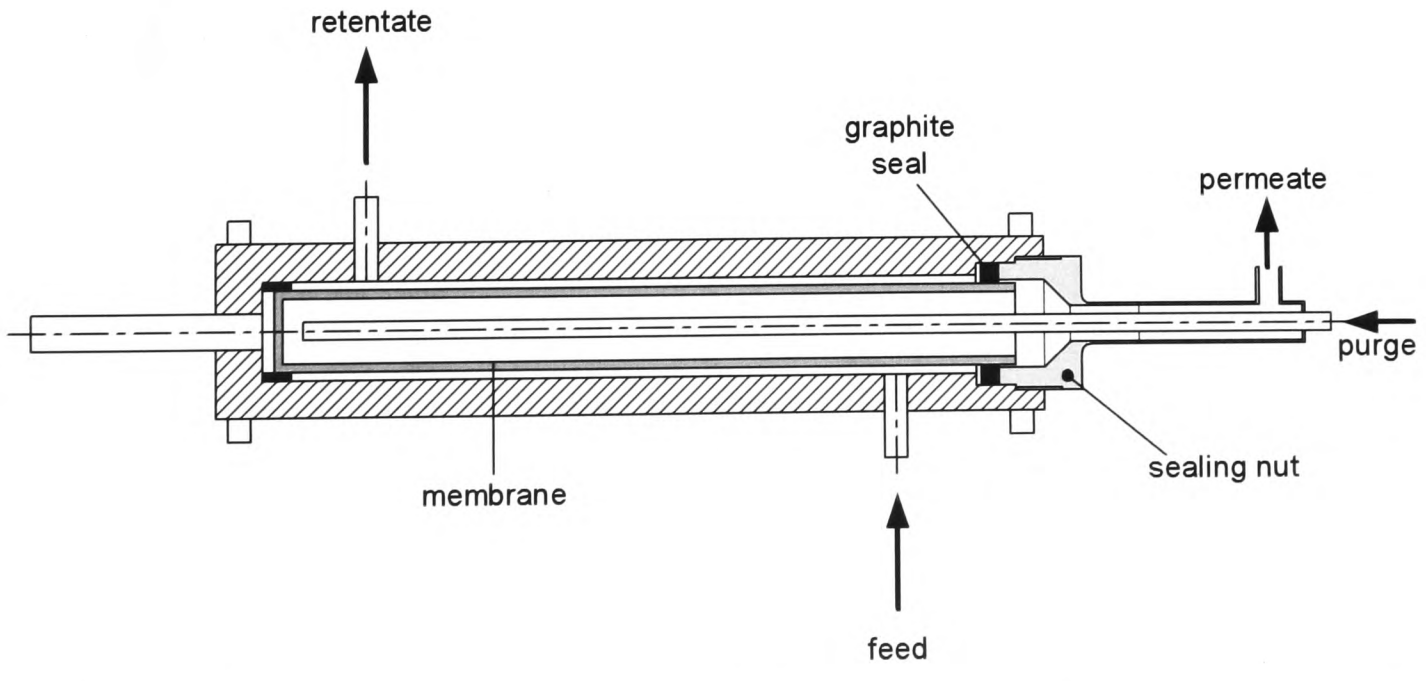

Figure 6.22: *Modified membrane pressure chamber incorporating a single graphite seal arrangement.*

The modified membrane chamber was connected to the standard flow test rig replacing a standard chamber. In order to test the integrity of the new sealing arrangement, a similar temperature cycling experiment was carried out, as with the solid alumina rod investigations, though in addition hydrogen flow tests were also performed. Temperature cycling was carried out between 50 °C and 420 °C in nitrogen, and nitrogen leak tests were performed with a 3 barg pressure drop followed by a hydrogen flow test also with a pressure drop of 3 barg. The results of the temperature cycling with the modified membrane chamber design are shown in Figure 6.23. Although the leak increases from around 1 sccm to 10 sccm over the 20 temperature cycles, attempting to tighten the seals (as indicated in the figure) had no effect in reducing the leak. It can therefore be said that the sealing of the membrane tubes at one end removes the leak associated with the axial expansion of the substrate against the graphite seals. Further work is suggested though in improving the membrane quality around the closed end of the substrate to both improve the durability of the membrane as well as to reduce any leakage.

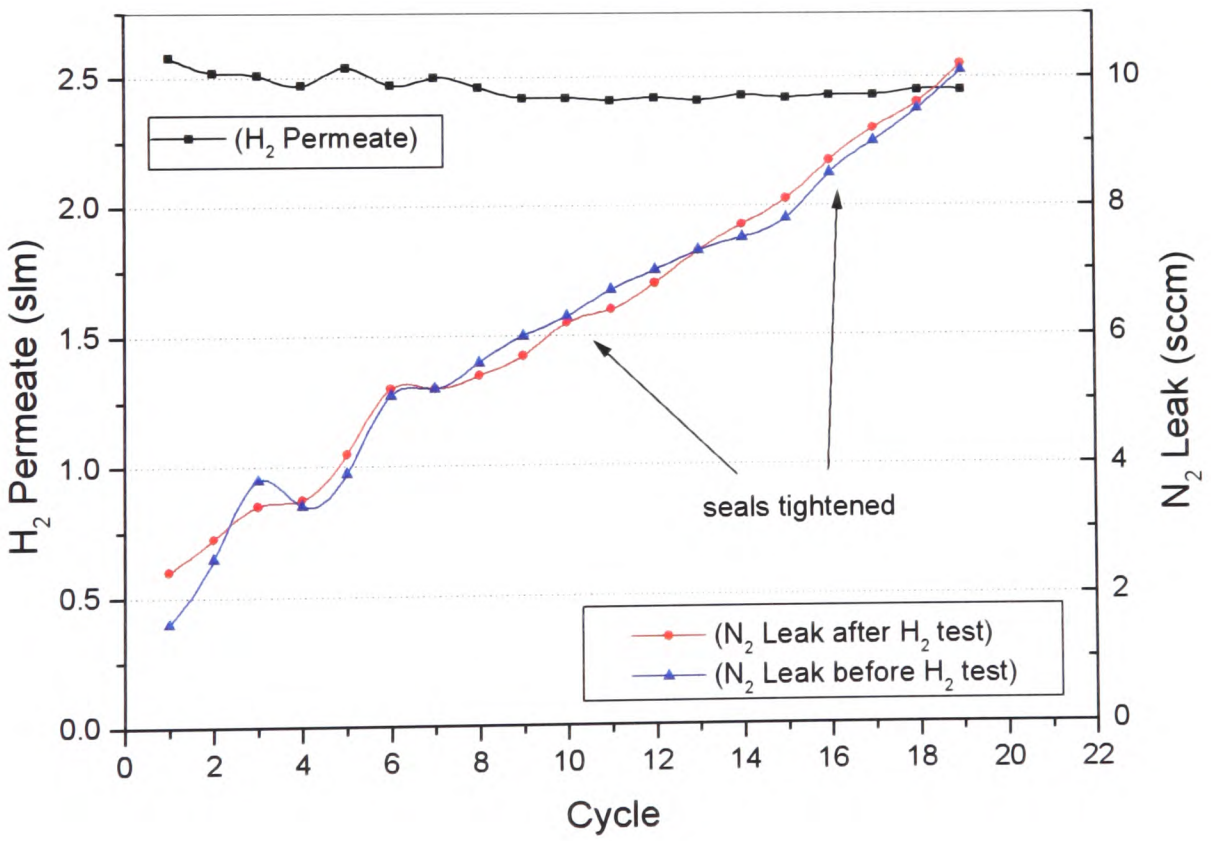

Figure 6.23: *Durability testing of a Pd/Ag membrane using a modified chamber design with a single graphite seal at the open end.*

6.14 Conclusions

Flow testing of the standard Pd/Ag membranes has been carried out using a comprehensive range of feed flow compositions. Experimental testing has demonstrated the impact of carbon monoxide concentration on the poisoning of the membranes. The effect of temperature has also been investigated and shown that operating the membranes over 400 °C ensures that the effect of carbon monoxide is minimised in terms of membrane surface poisoning. Wet reformate flow tests have been carried out which have demonstrated that the presence of steam in the feed stream acts purely as a diluent under the conditions described. Further analysis of the effect of steam has shown no water gas shift effect on the retentate stream. The incorporation of a sweep or purge gas has shown improvements in hydrogen permeate and this is due to a reduction in the hydrogen partial pressure on the permeate side.

The effect of membrane thickness variation has been investigated and this demonstrates the optimum thickness of the membrane, using the current fabrication procedure, to be 7.5 μm. This has led to analysis of the pressure exponential according to Sievert's Law and suggests the flow through the membranes is limited by the diffusion of hydrogen through the bulk of the membrane and substrate as opposed to surface adsorption.

Investigations into the soft sealing arrangement have shown the axial expansion of the membrane tube to be the cause of the gradual increase in leak on repeated thermal cycling. A single ended sealing arrangement has shown that the leaks caused by this sealing solution can be reduced. The membranes have been shown to deteriorate on continued thermal cycles and indicate that the most suitable application of the palladium membranes in their current form would be a stationary steady flow system.

7 Membrane Sub-Model and Its Validation

Part of the work already carried out at Johnson Matthey, in partnership with the Aerosol and Particle Technology Laboratory in Thessaloniki, Greece, has been to develop a model to describe the diffusion of hydrogen through the standard Johnson Matthey supported thin palladium membrane (Konstandopoulos *et al.*, 2001). The model was developed to be compatible with the chemical engineering modelling package Aspen Plus (version 11.1).

Modelling can be very useful to accelerate the progress of development work, by reducing the number of experiments that need to be performed. In addition to this, the fact that the manufacture of membranes takes approximately 2 weeks, and that their relatively fragile nature requires unnecessary handling to be kept to a minimum means that a model can be extremely beneficial. The model consists of a Fortran based user model block, which can be incorporated into an Aspen flow sheet. The model was designed to enable analysis of various feed flows, pressures, feed compositions, membrane thickness and substrate permeabilities in order to assess the potential for application as a hydrogen purification system. The model also allows the effect of a purge gas to be investigated.

The model was designed using experimental data recorded at Johnson Matthey using the flow test stands, and further validation was carried out on delivery of the Fortran code. As this initial data was limited in terms of membrane operating condition, additional developments were made to the Fortran code to provide a more accurate description of the membranes. The Fortran model code is proprietary and although the exact details of the code are not revealed in this thesis, the fundamentals of the delivered model, based on the descriptions of the mass flux as well as the revisions made on validation of the model are explained below.

7.1 Model of Thin Supported Hydrogen Diffusion Membrane

This model of hydrogen diffusion is based on a six-step mechanistic description of the processes involved through the membrane and substrate as shown in Figure 7.1.

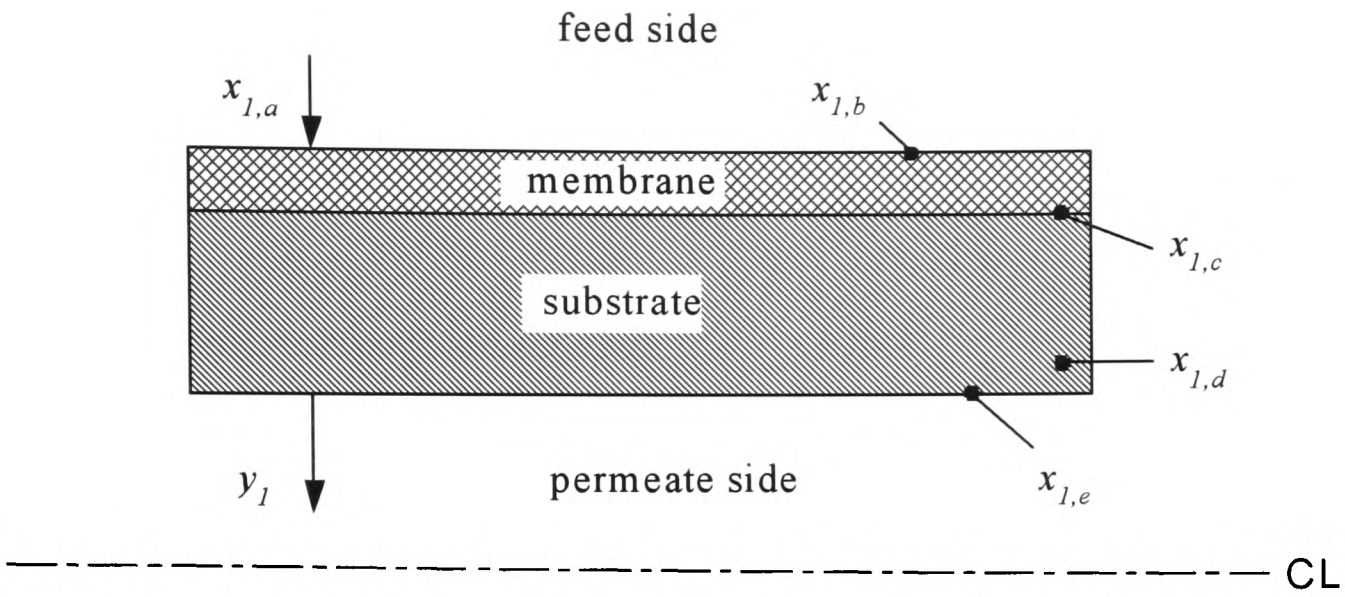

Figure 7.1: *Cross section of membrane and substrate showing the locations of each mass transfer stage as used by the mechanistic model description.*

Each step has an associated expression given below. The diffusion and mass transfer coefficients are expressed by k with subscripts corresponding to the transport step. The hydrogen mole fraction is given by x at each stage before permeation and by y on the permeate side of the membrane. P is the absolute pressure where the suffixes 1 and 2 represent the upstream and downstream sides of the membrane respectively.

1. mass transfer at the retentate stream:

$$J_1 = k_{m1} P_1 (x_1 - x_{1,a})$$

Equation 7-1

2. adsorption on the membrane surface (retentate side):

$$J_2 = k_a P_1 x_{1,a} - k_d x_{1,b}^2$$

Equation 7-2

3. solid state diffusion:

$$J_3 = k_{sd}(x_{1,b} - x_{1,c})$$

Equation 7-3

4. desorption on the membrane surface (permeate side):

$$J_4 = k_d x_{1,c}^2 - k_a P_2 x_{1,d}$$

Equation 7-4

5. diffusion through the substrate:

$$J_5 = k_c P_2 (x_{1,d} - x_{1,e})$$

Equation 7-5

6. mass transfer resistance at the retentate stream:

$$J_6 = k_{m2} P_2 (x_{1,e} - y_1)$$

Equation 7-6

In the model, the hydrogen transport through the palladium membrane denoted by steps 2-4 is described using Sievert's law and the flux, $J_{2\text{-}4}$, is expressed as follows:

$$J_{2-4} = K_1((x_{1s}P_1)^n - (y_1 P_2)^n)$$

Equation 7-7

where: K_1 is the specific permeability coefficient

x_{1s} is the hydrogen mole fraction above the feed side of the membrane

y_1 is the hydrogen mole fraction on the permeate side of the membrane,

P is the absolute pressure

n is the pressure exponential

If the rate determining step is the solid diffusion through the membrane then $n = 0.5$ for hydrogen. Initial data supplied for development of the model found n to have a

value of $n = 0.7$. Specific permeability coefficients are used to enable simulation of membranes of varying thickness.

The permeability coefficient K_1 is modified to account for the CO poisoning of the membrane surface by the following expression:

$$K_1 = \frac{K_1'}{1 + K_p x_N P_1}$$

Equation 7-8

where: K_1' is the temperature permeability coefficient

$x_N P_1$ is the CO partial pressure

K_p is the CO poisoning coefficient (see below)

The other species denoted by suffix i flow through cracks and the flux, J_i, can be described by a linear flux law (where the suffixes 1 and 2 represent the feed side and permeate side of the membrane respectively) and is given by the following equation:

$$J_i = K_i(x_i P_1 - y_i P_2)$$

Equation 7-9

7.1.1 CO Poisoning Coefficient, K_p

At temperatures below 400 °C, the palladium membrane is increasingly poisoned by the presence of carbon monoxide. The original model takes into account the CO poisoning effect, and the poisoning coefficient, K_p, is given by the following van 't Hoff equilibrium expression:

$$K_P = A_P \exp(-\Delta H_P / RT)$$

Equation 7-10

where: A_p is the pre-exponential factor

ΔH is the adsorption enthalpy

R is the molar gas constant

T is the absolute temperature

The CO poisoning coefficient as a function of temperature from experimental data can be seen in Figure 7.2. It can be seen that poisoning is significant below 300 °C.

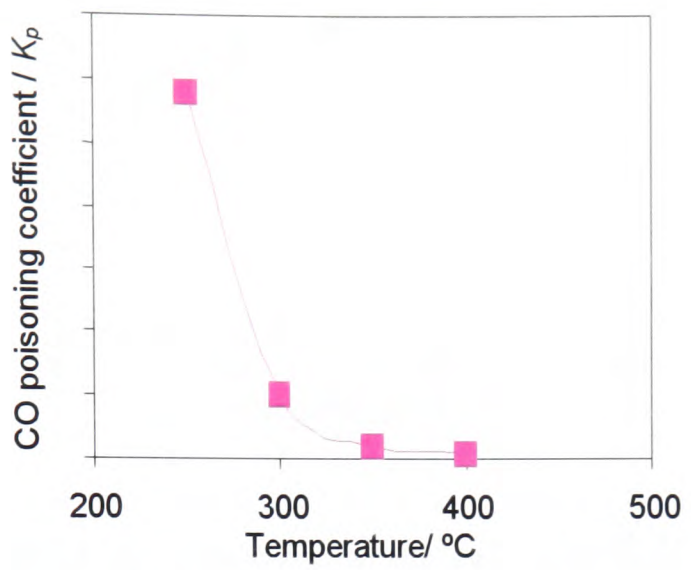

Figure 7.2: *The effect of temperature on the CO poisoning coefficient (values removed at request of JM)* (Evans, 2001).

Consequently it is necessary to operate the membrane at temperatures high enough to prevent CO poisoning. In general the membranes are operated at 440 °C.

7.1.2 Temperature Permeability Coefficient, K'_1

The permeability as a function of temperature, K'_1, is given by an Arrhenius kinetic equation as follows:

$$K_1^{'} = A_1^{'} \exp(-E_a / RT)$$

Equation 7-11

where: E_a is the activation energy

A'_1 is the pre-exponential factor

The effect of temperature on the hydrogen permeability as seen from experimental measurements can be seen in Figure 7.3 where permeability increases with temperature.

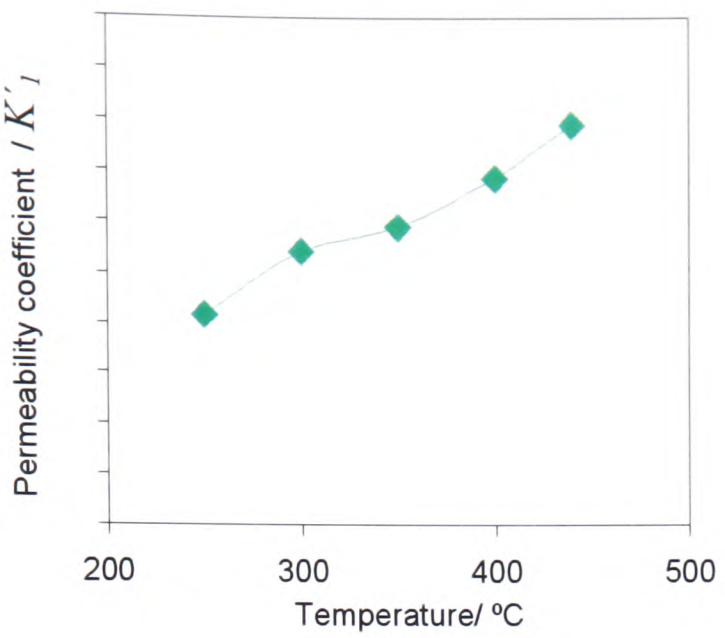

Figure 7.3: *The effect of temperature on the hydrogen permeability coefficient (values removed at request of JM),* (Evans, 2001).

7.1.3 Mass Diffusion

The mass transfer coefficients, k_{mi} are given in terms of the local Sherwood number which is analogous to Nusselt number as follows:.

$$k_{mi} = \frac{Sh_i D(P_1, T)}{(R_2 - R_1)} \frac{1}{RT}$$

Equation 7-12

where: Sh is the Sherwood number

D is the diffusion parameter

R_2 and R_1 are the inner and outer membrane tube radii respectively

R is the universal gas constant

T is the absolute temperature

The Sherwood number is a function of the axial distance along the membrane and mean velocity and for an explanation as to its derivation, the reader is referred to Transport Processes in Chemically Reacting Flow Systems (Rosner, 1986).

The diffusion parameter, D, is dependent on temperature and pressure according to the following:

$$D = \frac{a}{P}\left(\frac{T}{300}\right)^{n}$$

Equation 7-13

where: T is temperature

P is pressure

a and n are constants which are fitted to the experimental data

Species mass balances equations are produced which are integrated across the membrane wall to produce a system of ordinary differential equations. The total hydrogen permeate through the supported palladium membrane using the expressions described is then solved using modified solution algorithms as found in Numerical Recipes in FORTRAN (Press, 1996). The variables which have been provided for fine tuning the membrane model are as follows:

- Membrane thickness
- Pre-exponential factor for H_2 permeability, $A_1^{'}$
- Activation energy for H_2 permeability, E_a
- Permeability of N_2, H_2O, CO_2 and CO, K_i
- Reactor inside radius, outer radius and length
- Pre-exponential factor for CO poisoning, A_p
- Activation energy for CO poisoning, H_p
- Substrate permeability
- Permeability to adsorption rate ratio termed PARAT

7.1.4 Flow in an Annulus

Analysis of the flow in the annular membrane set-up was carried out to determine the degree of turbulent flow. The feed flow of gas over the membrane may be considered similar to the flow through an annular tube. In terms of adsorption of hydrogen the degree of turbulent flow is of interest and was calculated for a 10% CO reformate feed. A schematic of the flow in an annular tube is shown in Figure 7.4.

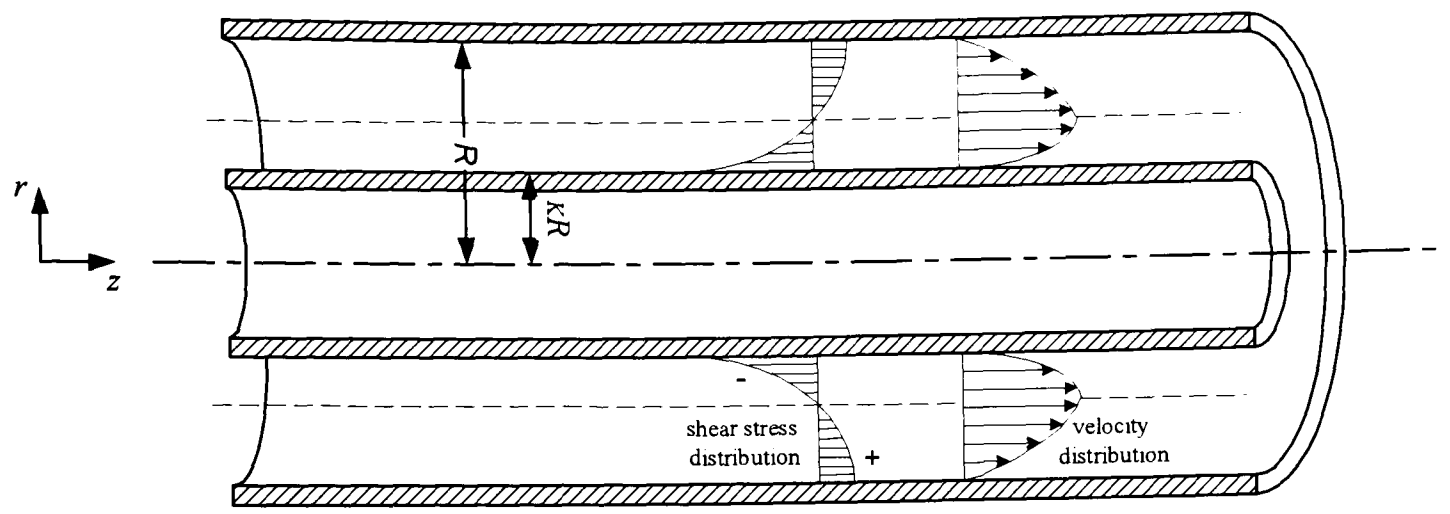

Figure 7.4: *Flow through a cylindrical annulus* (Bird *et al.*, 1960)

The Reynolds number for flow in an annulus is given by the following expression (Bird *et al.*, 1960):

$$\mathrm{Re} = 2R(1-\kappa) < v_z > \frac{\rho}{\mu}$$

Equation 7-14

where: μ is the viscosity of the fluid

κ is the ratio of inner and outer annular radii

ρ is the density of the fluid

$< v_z >$ is the average velocity

For a gas mixture at low density the following semi-empirical Wilke formula can be used to evaluate the viscosity:

$$\mu_{mixture} = \sum_{i=1}^{n} \frac{x_i \mu_i}{\sum_{j=1}^{n} x_j \Phi_{ij}}$$

in which:

$$\Phi_{ij} = \frac{1}{\sqrt{8}} \left(1 + \frac{M_i}{M_j}\right)^{-1/2} \left[1 + \left(\frac{\mu_i}{\mu_j}\right)^{1/2} \left(\frac{M_j}{M_i}\right)^{1/4}\right]^2$$

Equation 7-15

where: n is the number of chemical species in the mixture

x_i and x_j the mole fractions of species i and j

μ_i and μ_j the viscosities of species i and j at the system temperature and pressure

M_i and M_j the corresponding molar masses

The coefficient of viscosity at absolute temperate T of a gas of molar mass M may be written in terms of the parameters σ, the characteristic diameter of the molecule in Å, and ε, the characteristic energy of interaction between molecules. The values of which can be obtained in tables (Bird *et al.*, 1960).

$$\mu = 2.6693 \times 10^{-5} \frac{\sqrt{MT}}{\sigma^2 \Omega_\mu}$$

Equation 7-16

where: Ω_μ is a slowly varying function of the dimensionless temperature $\kappa T/\varepsilon$ and is available in tables (Bird *et al.*, 1960).

The viscosities for the individual components of a reformate mixture can be calculated at the membrane operating temperature of 440 °C using Equation 7-16 and the following values were obtained:

μ_{CO} = 3.3075×10^{-4} g cm^{-1} s^{-1}

μ_{CO2} = 3.0097×10^{-4} g cm^{-1} s^{-1}

μ_{H2} = 1.5812×10^{-4} g cm^{-1} s^{-1}

μ_{N2} = 3.2464×10^{-4} g cm^{-1} s^{-1}

The mixture viscosity of a 10% CO, 12% CO_2, 38% N_2 and 40% H_2 reformate mixture was then determined using Equation 7-15 and found to be:

$\mu_{mixture}$ = 3.1355×10^{-4} g cm^{-1} s^{-1}

The value of the Reynolds number was calculated using Equation 7-14 using a weighted average for the mixture density at a system pressure of 4 bara and found to vary between 11 to 330 as the feed flow was increased from 1 to 30 slm. As the laminar turbulent transition occurs in the region of Re = 2000, this suggests that laminar flow occurs through the annulus of the membrane chamber.

7.2 Sub-Model Validation

The as-received membrane model was validated against the preliminary experimental data. The model can be used as a stand alone user block in the Aspen Plus simulation engine. A block diagram of the model is shown in Figure 7.5, where the membrane is represented by the block labelled MEMBRANE. The user model uses a number of variables which can be altered to describe the geometry of the membranes as well as coefficients for some of hydrogen diffusion expressions. The reformate feed, sweep, retentate and permeate streams are entitled REF, SWP, RET and PERM respectively. The heaters, H1, H2, H3 and H4 serve to alter the temperature and pressure of the streams to produce flow values in standard litres per minute (slm) to enable direct comparison with experimental data as recorded from the mass flow meters.

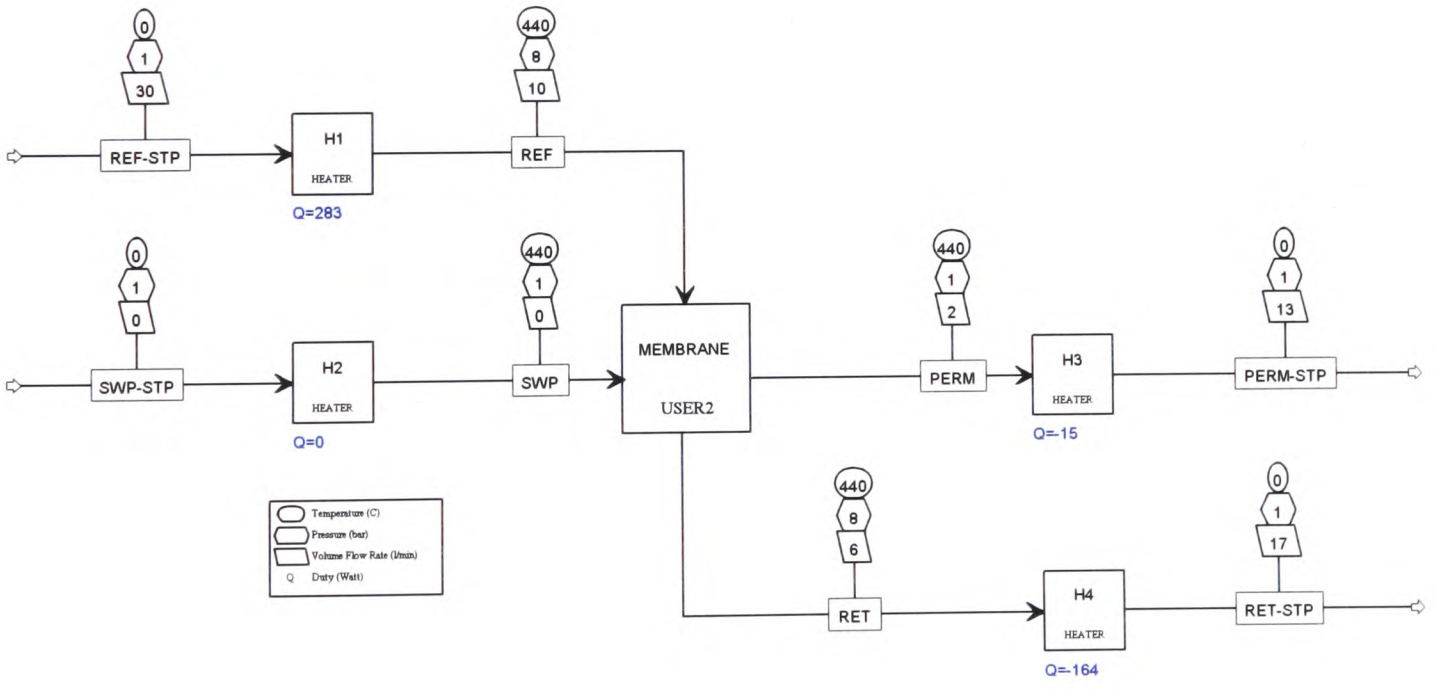

Figure 7.5: *Schematic of Aspen membrane model.*

The results of the as-received membrane model are described in the sections below and show that the model required some fine tuning to match the experimental data by alteration of the user variables. Further experimental work over a wider range of conditions showed that some areas of the model required more advanced alterations to

the expressions describing hydrogen flux in order to match the later experimental data. These alterations are also described in the following sections.

7.2.1 Pure Hydrogen Flow Simulation

Initial simulations using the palladium membrane sub-model showed a good correlation with the experimental data. However it was soon realised that the value of one of the user variables for the membrane length had been incorrectly set to the full length of the fabricated supported membrane (i.e. 200 mm) rather than the active length as bounded by the graphite seals (i.e. 172 mm). On correcting the active length there was a disparity between the experimental and simulated data and it was necessary to fine tune the variable describing the permeability to adsorption rate ratio (PARAT). Before this fine tuning, the initial simulation produced the results which can be seen in Figure 7.6.

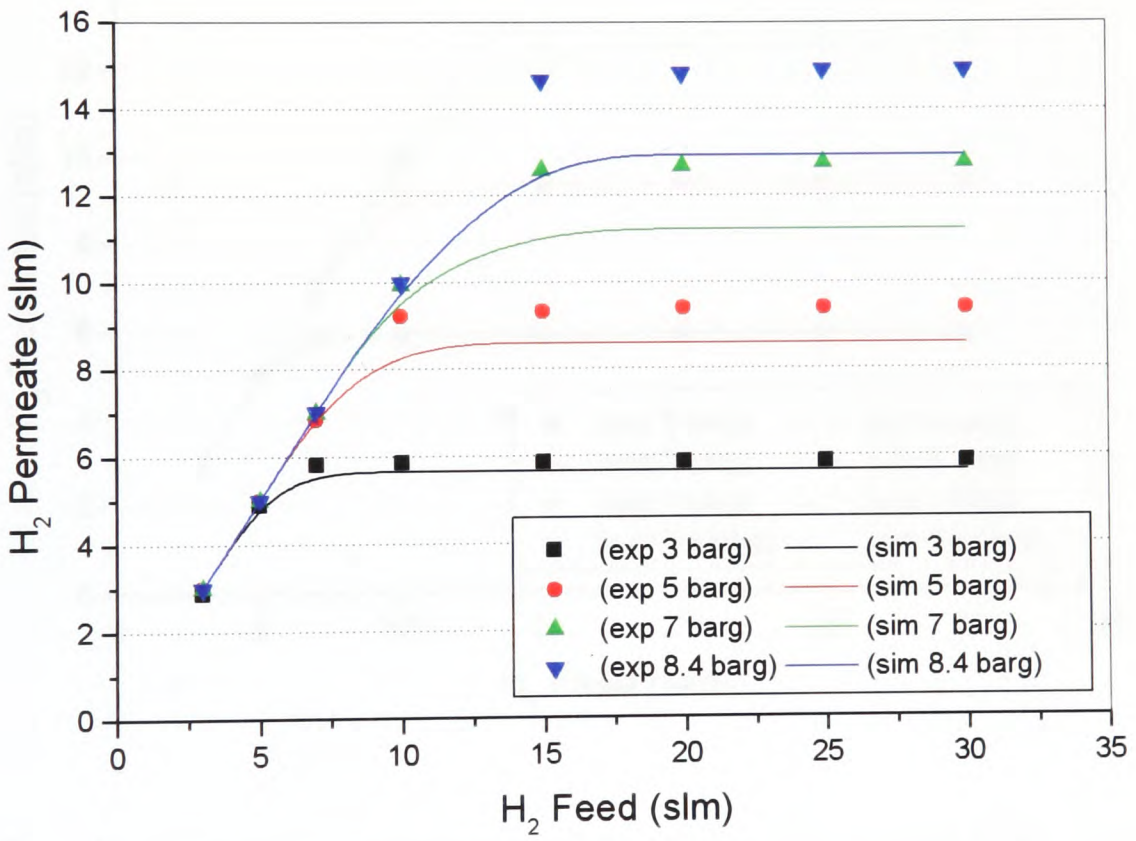

Figure 7.6: *Initial Aspen simulation flow results for a standard 7.5 μm Pd/Ag membrane operating at 440 °C and 1 bara downstream pressure using pure hydrogen plotted with experimental results.*

At 3 barg, there appears to be good correlation between the experimental and simulated data, though as the membrane pressure drop is increased, the simulation

increasingly underestimates the hydrogen permeate through the membrane. This difference is up to 1.5 slm with a 8.4 barg inlet pressure. As the simulation initially had an overestimate in the membrane active length, this underestimate is to be expected as the active length is corrected to its lower value. The general trend of the simulation and experimental results is a unity gradient for each pressure condition until a level plateau is reached; this being the flow limit for the membrane under those conditions.

Fine tuning of the permeability to adsorption rate ratio improved the simulation to take account of the reduced membrane active length. The results of this fine tuning can be seen in Figure 7.7.

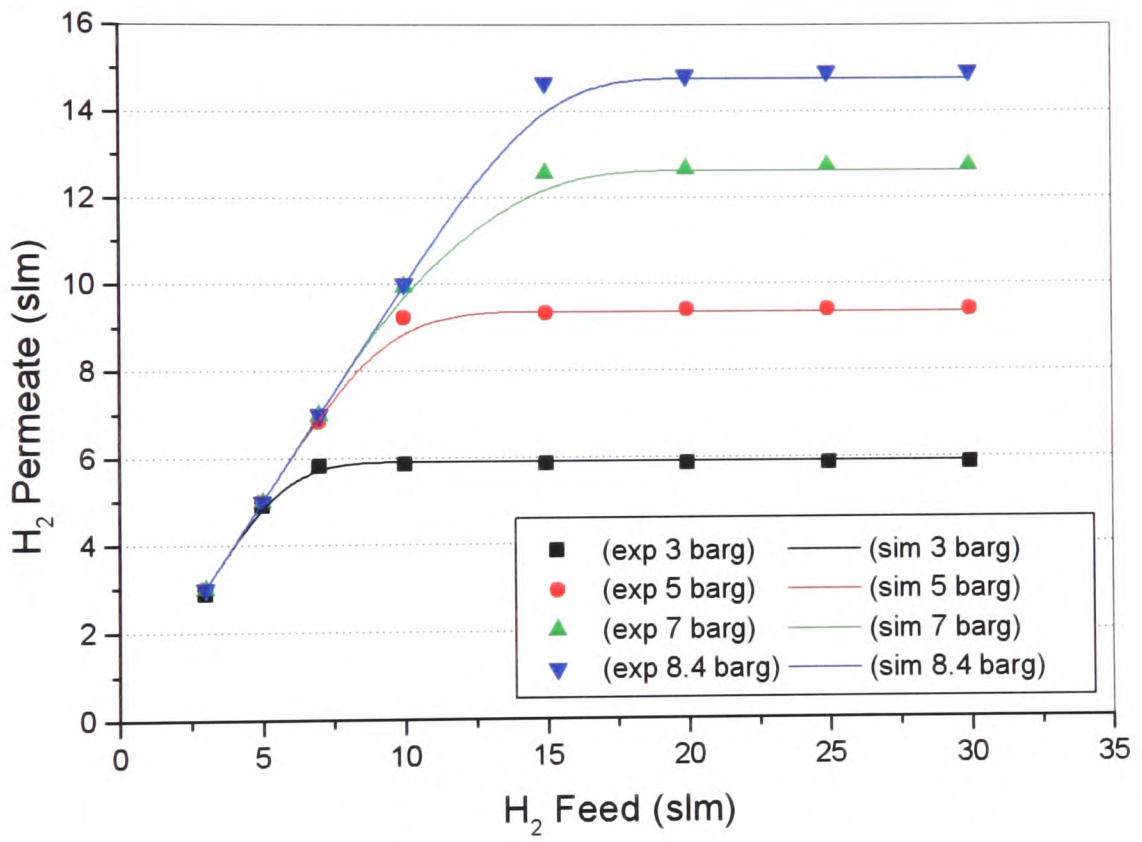

Figure 7.7: *Revised Aspen simulation flow results for a standard 7.5 μm Pd/Ag membrane operating at 440 °C and 1 bara downstream pressure using pure hydrogen plotted with corresponding experimental data.*

The simulations using the revised Aspen model give an extremely good match to the experimental data over the pressure range 3 barg to 8.4 barg. The initial version of the model required the value of the permeability to adsorption rate ratio to be manually altered depending on whether pure hydrogen or a CO containing gas mixture was

being fed over the membrane. Although this was practical when using the sub-model as a stand-alone unit, it would make it difficult to use in a system model where outputs from the membrane clean-up modules may well be fed back into the system prior to the membrane module itself. Code was added into the sub-model to enable this variation in the permeability to adsorption rate ratio to occur automatically.

7.2.2 Simulation of Temperature Effect with Pure Hydrogen

The experimental data that was initially supplied for the development of the palladium membrane model as regards temperature variation was limited to a temperature range between 300 °C and 440 °C. The more significant reduction in hydrogen permeability below this temperature range was therefore not realised until additional membrane testing was done. This reduction in permeability due to temperature, and also the disparity in the membrane active length gives rise to the readily visible differences between simulated and experimental data as shown in Figure 7.8.

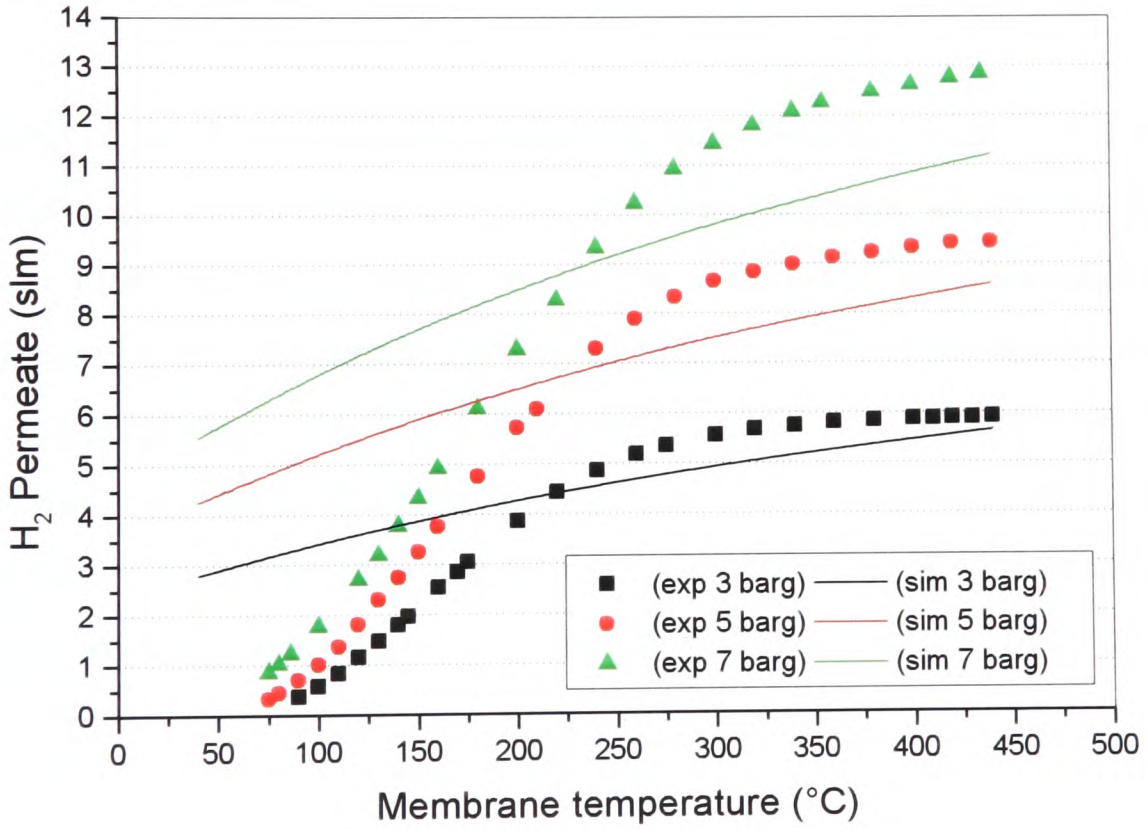

Figure 7.8: *Initial Aspen simulation showing the effect of temperature variation on the hydrogen permeate using a standard 7.5 μm Pd/Ag membrane with a downstream pressure of 1 bara and using pure hydrogen plotted with corresponding experimental data.*

If the adjustment in the permeability to adsorption rate ratio is taken into account, the simulation would provide a reasonable fit to the experimental data above around 275 °C. However, below this temperature, the rapid fall off in hydrogen permeate is not simulated by the model. Although in practise the palladium membranes may well not be operated at such reduced temperatures, a system model may well require start-up or shut-down conditions to be investigated.

To more accurately simulate the temperature effect for pure hydrogen a Wiebe function was used as this produces the characteristic s-shape required. The Wiebe function is a mathematical function providing an output between 0 and 1 and is expressed as follows:

$$y = 1 - \exp(-a(x^*)^{m+1})$$

where: a and m are constants and x^* is the fraction along the x-axis.

As the output of the Wiebe function produces a value between 0 and 1, it is necessary to use a coefficient to then obtain the peak hydrogen permeate value when the Wiebe function produces an output equal to 1. The x-axis as described above is the temperature axis and x^* the membrane temperature expressed as a fraction of the peak operating temperature of 440 °C. The constants a and m were fitted by choosing points at the top and bottom of the steepest part of the curve and solved simultaneously. The values of a and m were also found to have a dependence of system pressure and expressions were also incorporated in the modified code to account for this.

The simulation results using the model incorporating the Wiebe function for pure hydrogen are shown in Figure 7.9. The simulated data now provides a much better fit to the experimental data particularly above 150 °C. Below this temperature there is minimal disparity.

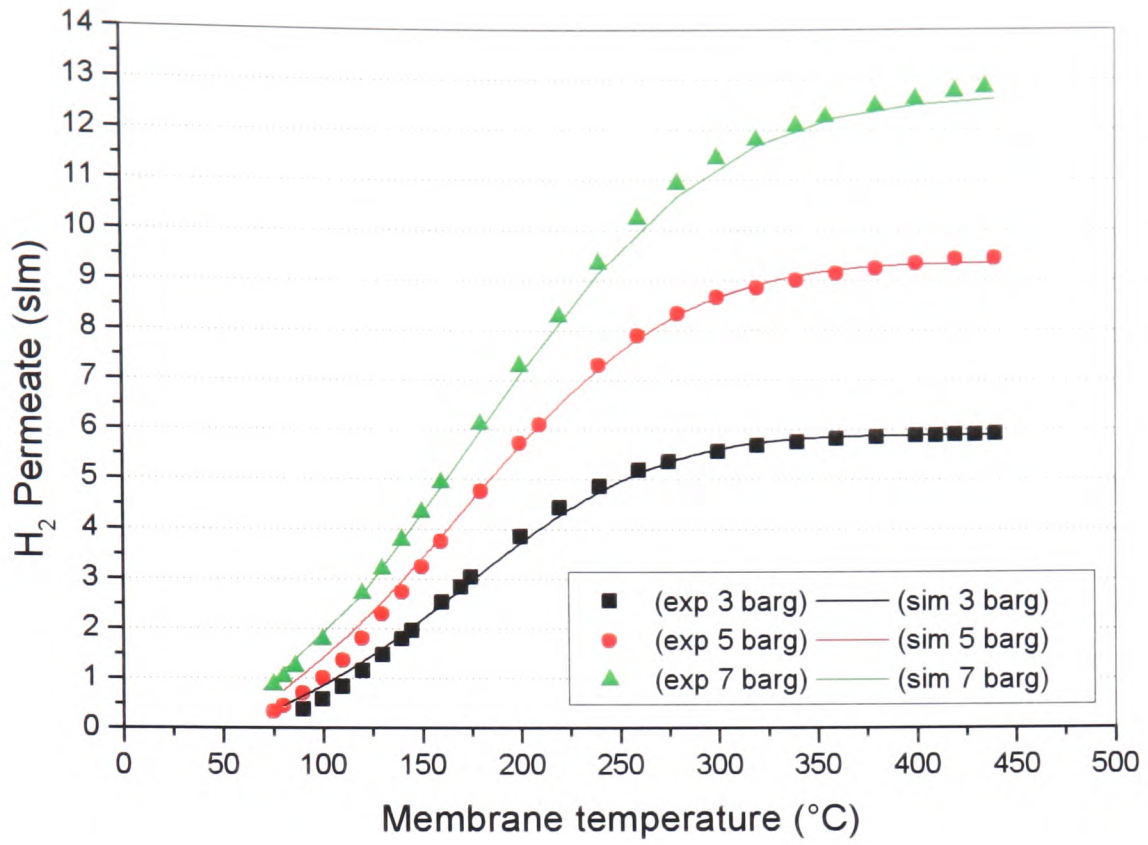

Figure 7.9: *Revised Aspen simulation showing the effect of temperature variation on the hydrogen permeate using a standard 7.5 μm Pd/Ag membrane with a downstream pressure of 1 bara and using pure hydrogen plotted with the corresponding experimental data.*

7.2.3 Reformate Flow Simulation

The differences in simulated hydrogen permeation due to the active length underestimation in the initial model also meant that simulations with reformate mixtures also produced underestimates. The standard reformate flow test is with a 10% CO reformate mixture, and the results with the initial model are shown in Figure 7.10. Although there is an increasing difference in the peak values of the hydrogen permeate as the pressure drop over the membrane increases, the general shape of the simulation results appear correct, suggesting that the model provides a good description of the mass transfer properties due to changes in the feed flow.

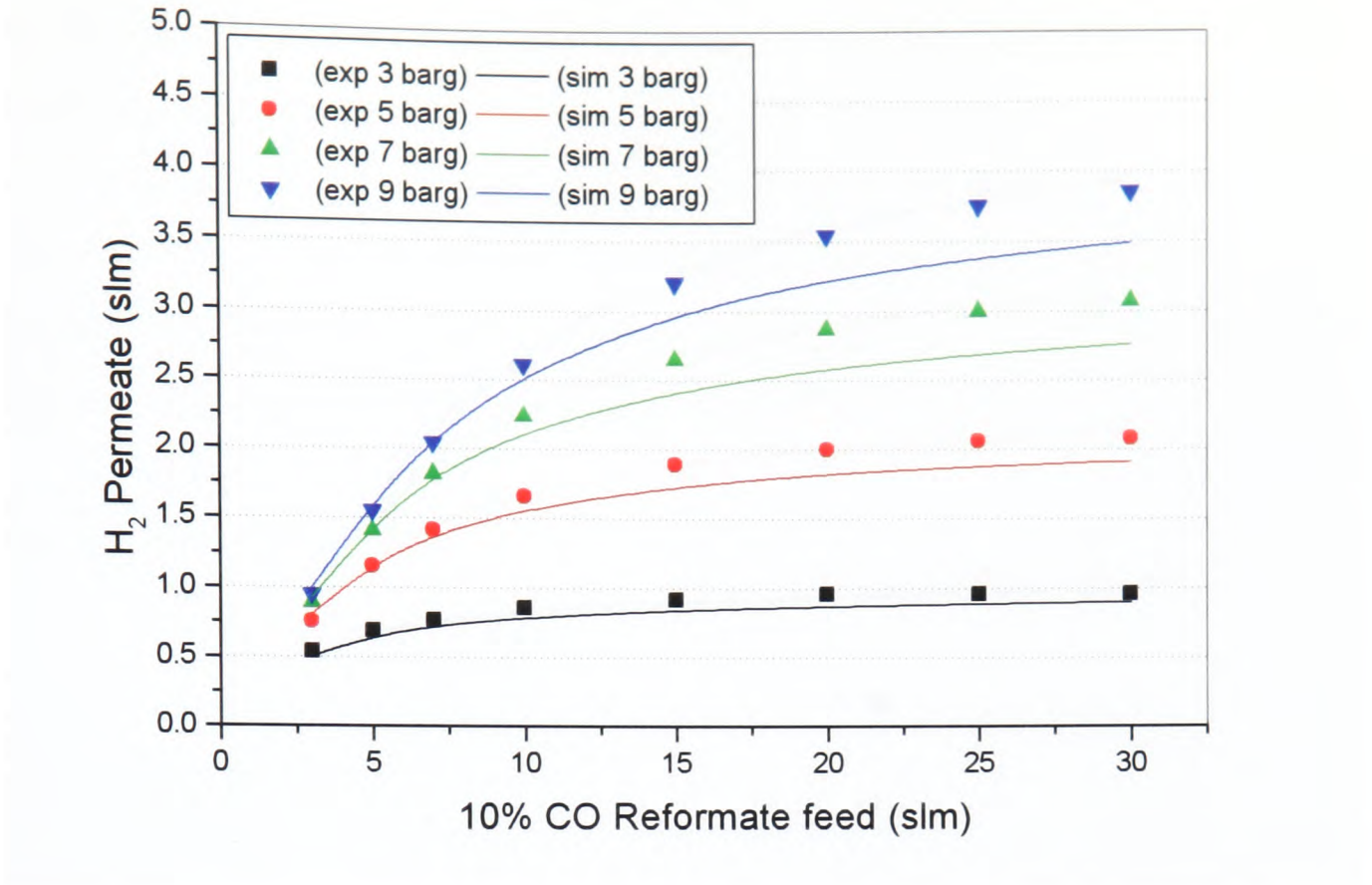

Figure 7.10: *Initial Aspen simulation of a 10% CO reformate flow test of a standard 7.5 μm Pd/Ag membrane with a downstream pressure of 1 bara plotted with corresponding experimental data.*

As found previously with the pure hydrogen testing, fine tuning of the permeability to adsorption rate ratio brings the simulated results more in line with the experimental results. This can be seen in Figure 7.11. There is a good correlation over the full feed flow range and good agreement as regards the limiting values for each pressure drop simulated. The membrane model has been validated over the full range of standard flow tests as well as a comprehensive investigation into the effect of temperature on the membrane performance. Prior to this work only limited assessment as regards membrane temperature had been carried out. The improvements made to the membrane model code have ensured that the model accurately describes the performance of the membrane under these conditions. The following validations are based on flow testing procedures which have previously not been performed with the membranes and will determine the robustness of the membrane model over a wider range of conditions.

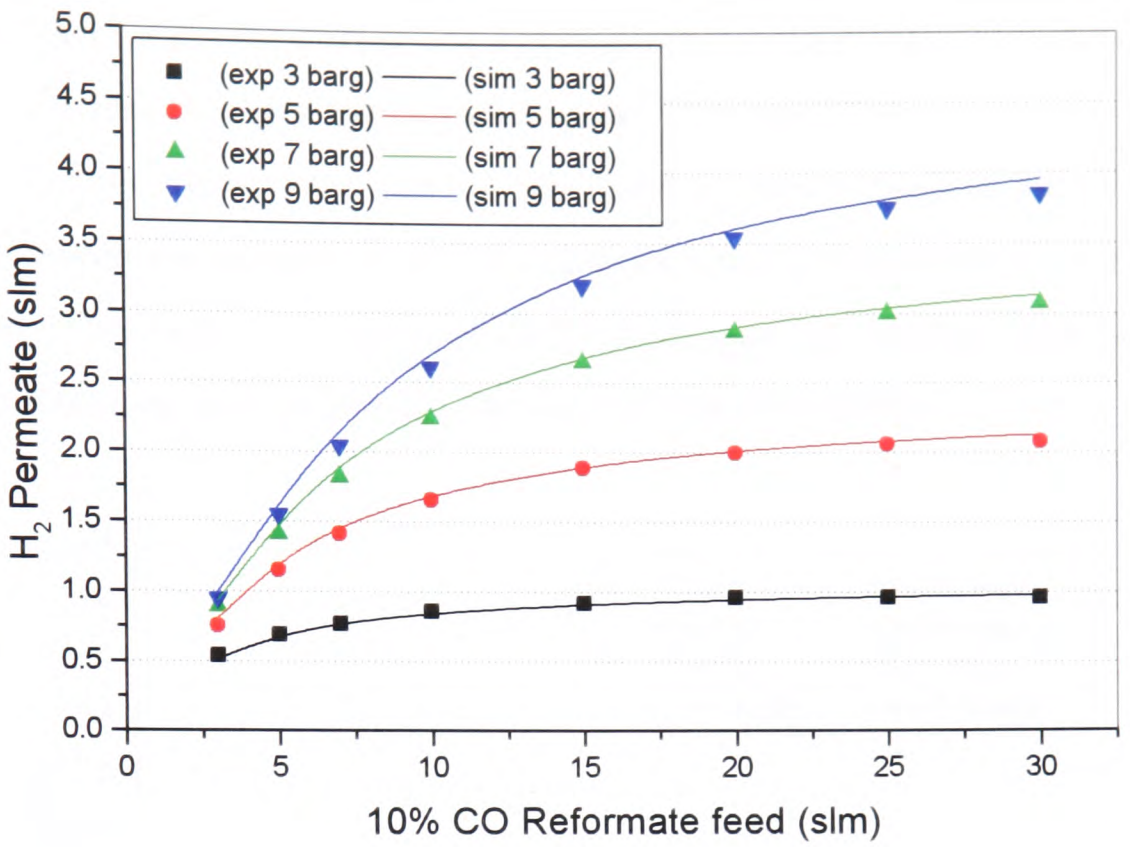

Figure 7.11: *Revised Aspen simulation of a 10% CO reformate flow test of a standard 7.5 μm Pd/Ag membrane with a downstream pressure of 1 bara plotted with corresponding experimental data.*

7.2.4 Membrane Thickness Variation

The sub-model was compared with experimental data with regard to variation in the membrane thickness. The initial case is with a pure hydrogen feed to the membrane. The results of the simulation and the experimental data are shown in Figure 7.12.

At lower feed pressures the simulation matches the experimental data more closely and passes through the 7.5 μm point as this is the point which has been used in the work described previously to improve the model correlation. With a membrane thickness lower than 7.5 μm, the simulated data appears to overestimate the hydrogen permeate for each membrane pressure drop. With the thinnest membrane of 4.7 μm, the difference is up to 3 slm with a pressure drop of 8.4 barg. This equates to a difference of 15% over the experimental value. With increased membrane thickness, the simulated flow data underestimates the hydrogen permeate when compared with the experimental data. The difference between the experimental and the simulated

data is less pronounced than with the thinner membrane thickness and is around 0.5 slm with a 13.3 μm membrane and a pressure drop of 8.4 barg. This is a difference of around 5% less than the experimental data. The overestimation of the simulated data with thinner membranes can be attributed to the increasing effects that the interface between the membrane and the substrate or sol gel layer has on the hydrogen permeation. The expected improvement in hydrogen permeation with decreasing membrane thickness is therefore not realised fully experimentally.

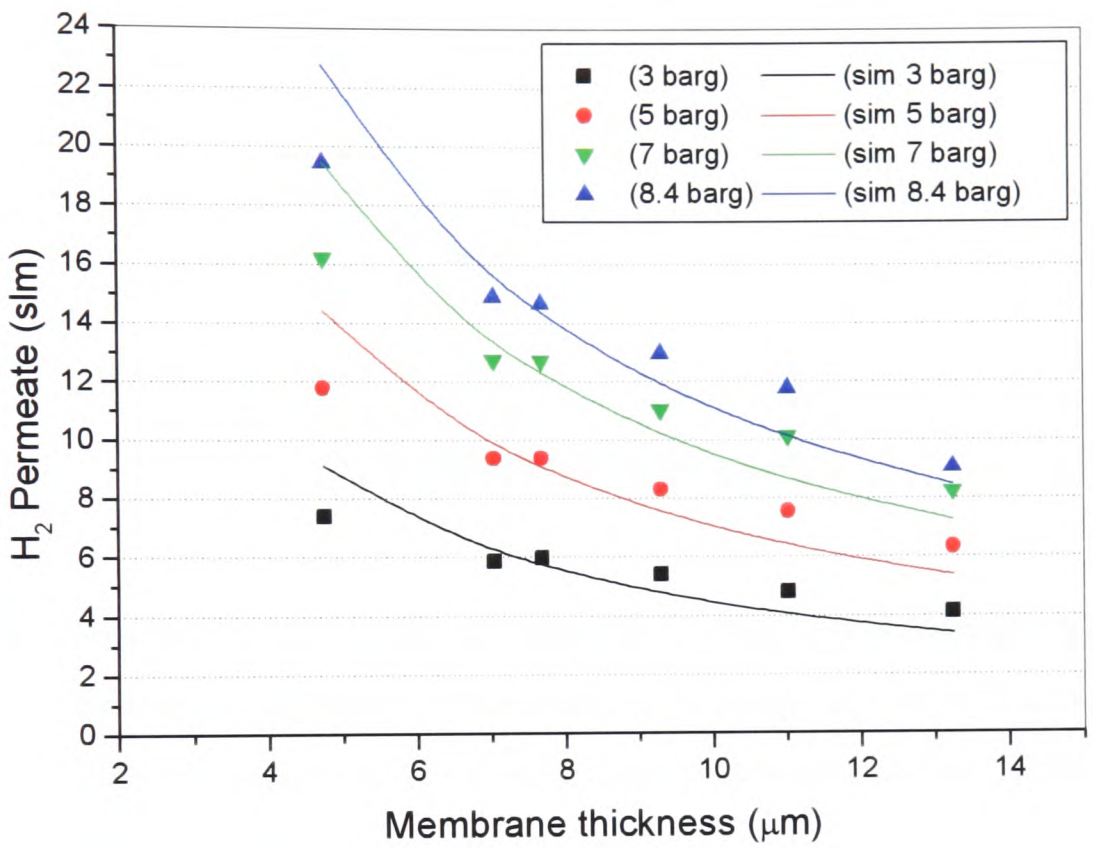

Figure 7.12: *Aspen simulation showing the effect of varying membrane thickness on hydrogen permeate. Membrane operating at 440 °C with a 30 slm pure hydrogen feed and 1 bara permeate pressure. Corresponding experimental data is also shown.*

Comparison of the simulated data with experimental data for the case with a 10% CO reformate feed is shown in Figure 7.13. There are greater relative disparities between the simulated and the experimental data at the two extremes of membrane thickness, though again the simulated data matches the experimental data for the 7.5 μm membrane case. In the case of a 4.7 μm membrane, the simulated level of hydrogen permeate is 1 slm higher than the experimental results with a 9 barg pressure drop. This is approximately a 20% difference. With a membrane of 13.3 μm, the difference

between the simulated and experimental hydrogen permeate is 0.75 slm with a pressure drop of 9 barg.

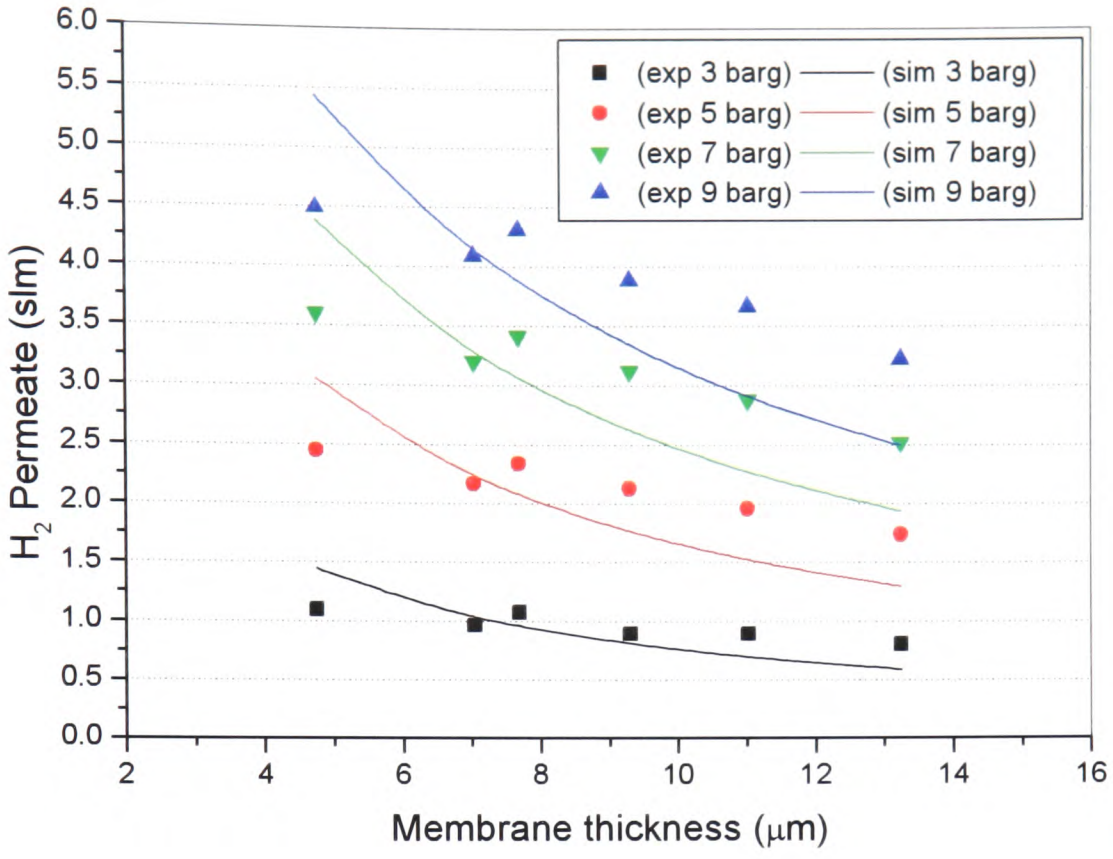

Figure 7.13: *Aspen simulation showing the effect of varying membrane thickness on hydrogen permeate. Membrane operating at 440 °C with a 30 slm 10% CO reformate feed and 1 bara permeate pressure. Corresponding experimental data is also shown.*

The reasons for the disparities between the experimental and simulated data can be attributed to the assumption of an ideal finite membrane layer which does not interface with the sol gel or substrate layer. It is difficult to account for the effect of this interface in the model. The correlation of the model to the experimental data for the standard 7.5 μm membrane however is good and in practise this thickness of membrane is the optimum, combining a coherent, crack free membrane with good hydrogen permeability and selectivity. For the purposes of this work, a 7.5 μm membrane will be assumed.

7.2.5 Simulation of Reformate Composition Variation

The standard reformate flow test uses a 10% CO reformate mixture as this is accepted as the reformate gas from a typical gasoline ATR. It will not always be the case that

this reformate mixture is fed directly into the palladium membrane module and so simulation/testing of cases with varying compositions are required. The proportion of carbon monoxide has been shown in experimental work to cause different levels of poisoning of the palladium membrane, whereas other species have a dilutory effect on the mixture and thereby reduce the hydrogen partial pressure and consequentially the hydrogen permeate.

The initial simulations shown in Figure 7.14, include the fine tuning made to account for the active length of the membrane and thus it is purely the effect of CO on the hydrogen permeate which is being considered.

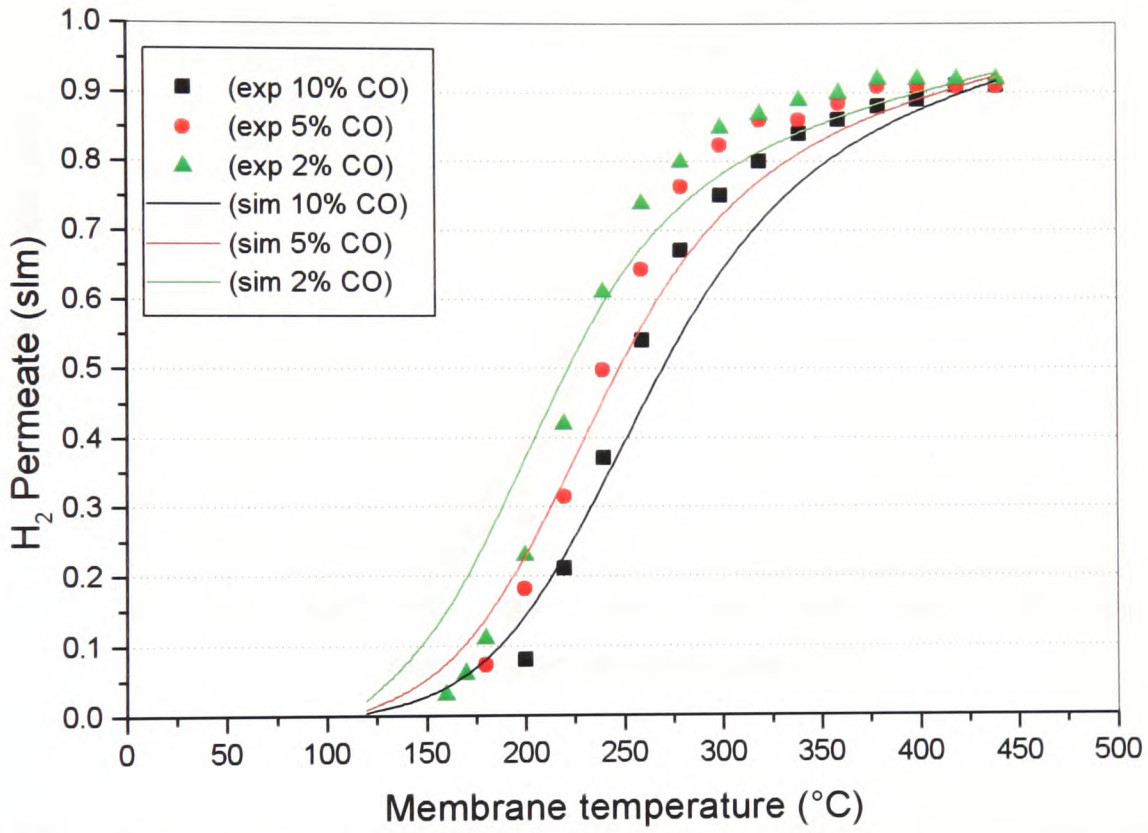

Figure 7.14: *Initial Aspen simulation showing the effect of CO concentration in the reformate mixture on the hydrogen permeate with varying temperature using a standard 7.5 μm Pd/Ag membrane with a 3 barg feed and a 1 barg down stream pressure. Corresponding experimental data is also shown.*

The chart shows a significant difference between the simulated and experimental results. All three compositions show a premature reduction in the hydrogen permeate as the temperature falls from 440 °C. The simulated hydrogen permeate does however

more closely follow the experimental data below 250 °C, but it would be expected that any realistic use of the palladium membranes would be above 300 °C to reduce the CO poisoning effect.

To resolve the mismatch, the coefficients for the pre-exponential factor of CO influence and the activation energy for CO influence were fine tuned to reduce the premature fall off in hydrogen permeance and simulate the experimental results more closely. The results of this fine tuning can be seen in Figure 7.15.

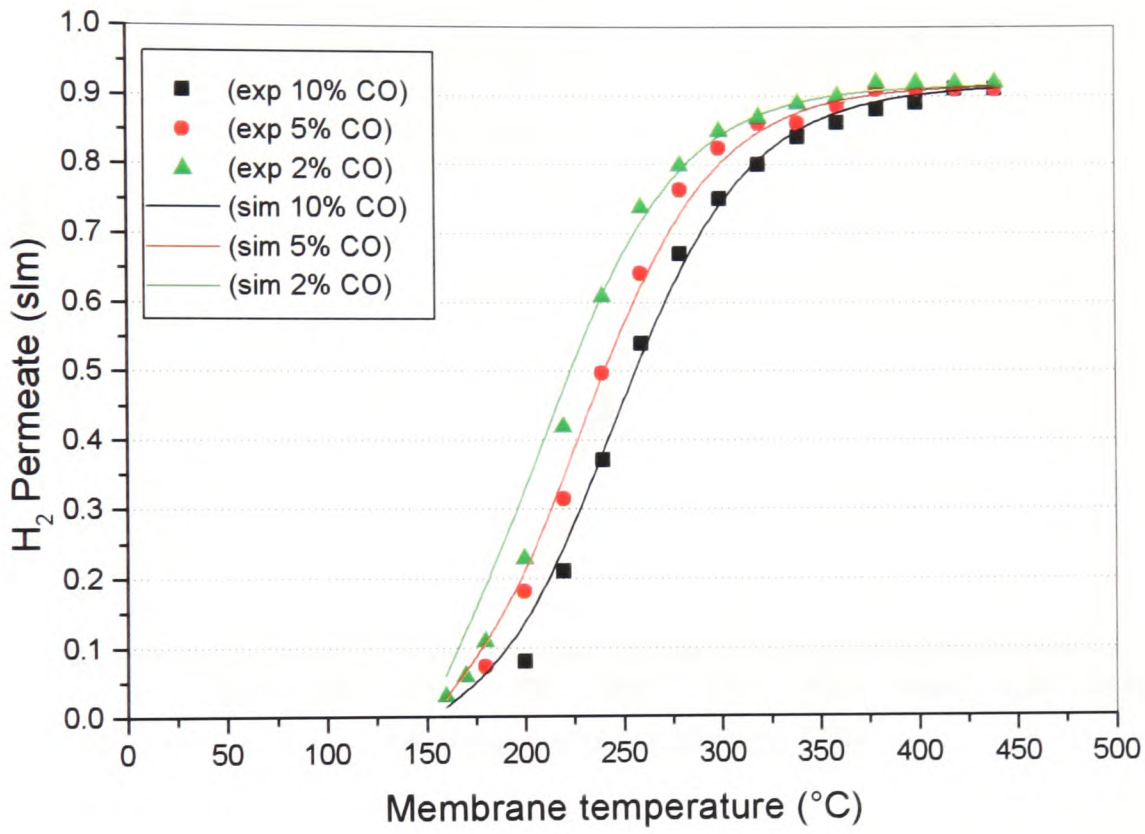

Figure 7.15: *Revised Aspen simulation showing the effect of CO concentration in reformate mixture on hydrogen permeate with varying temperature using a standard 7.5 μm Pd/Ag membrane with a 3 barg feed and a 1 barg down stream pressure. Corresponding experimental data is also shown.*

In the revised simulation, the experimental data is well matched above 225 °C and up to 440 °C, which is the likely range of any practical use of the palladium silver membranes. Below 225 °C, the hydrogen permeate in the simulation is 0.025 slm higher than that seen in the experimental data, though this difference is only around 2.5%.

7.2.6 Simulation of Wet and Dry Reformate

The introduction of steam into the feed stream to the membrane was found experimentally to have a dilutory effect on the mixture. In order to ensure the hydrogen partial pressure was maintained at a level to be comparable with a dry reformate mixture containing 10% CO at 3 barg, it was necessary to operate the membrane at 4.55 barg with the wet reformate mixture. These simulations used the revised palladium model as described in the preceding sections.

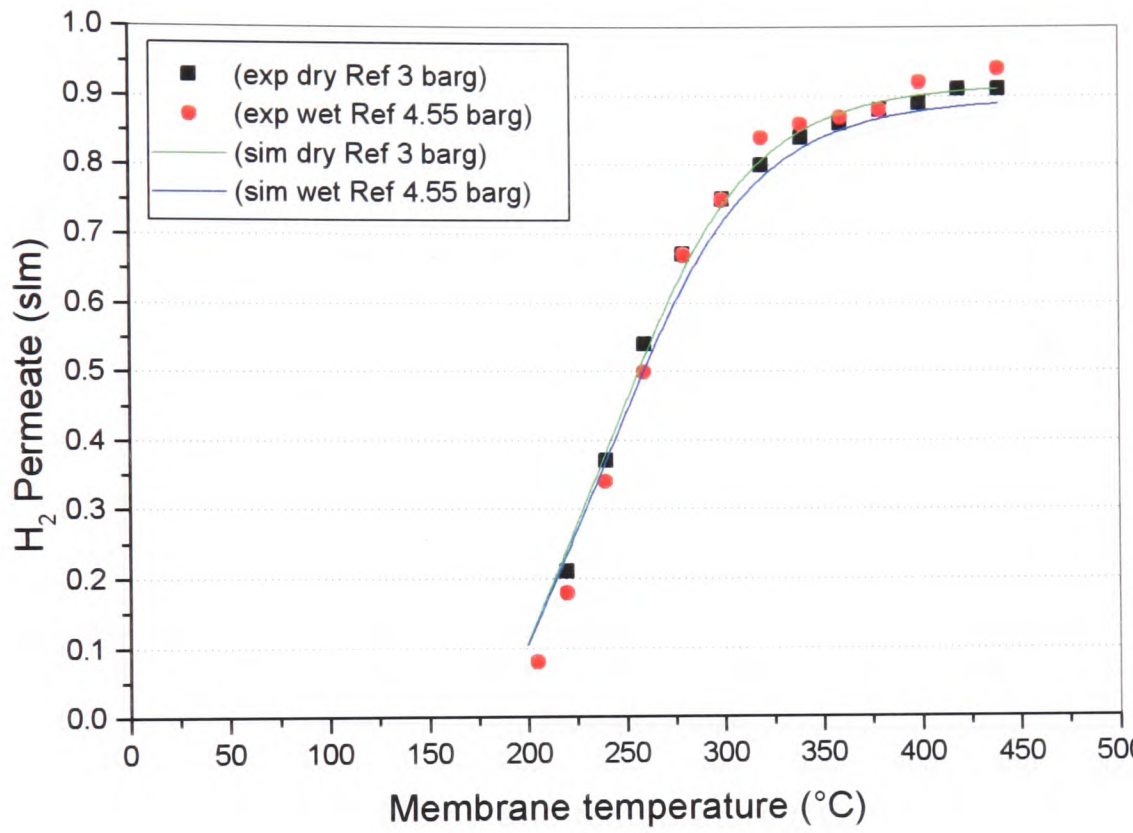

Figure 7.16: *Aspen simulation showing the effect of temperature on hydrogen permeate using dry and wet reformate mixtures with a standard 7.5 μm Pd/Ag membrane. Corresponding experimental data is also shown.*

The simulation shows good agreement to the experimental data over the full range of temperature and both with and without the addition of steam.

7.2.7 Sweep Testing

The use of a sweep or purge gas through the centre of the membrane tube has also been incorporated into the sub-model. The results of the Aspen simulation are to be seen in Figure 7.17. As has been shown in the previous validations without sweep, the simulated data using the revised membrane model matches the experimental data

well. With a membrane pressure drop of 3 barg, the correlation between the experimental and the simulated data is good with a difference of 0.1 slm or around 5%. With a membrane pressure drop of 5 barg, the difference between the experimental and simulated data is around 0.15 slm or 5%. There is also a good correlation between the experimental data and the simulated data with regard the point in the rise of hydrogen permeate with the introduction of a sweep flow.

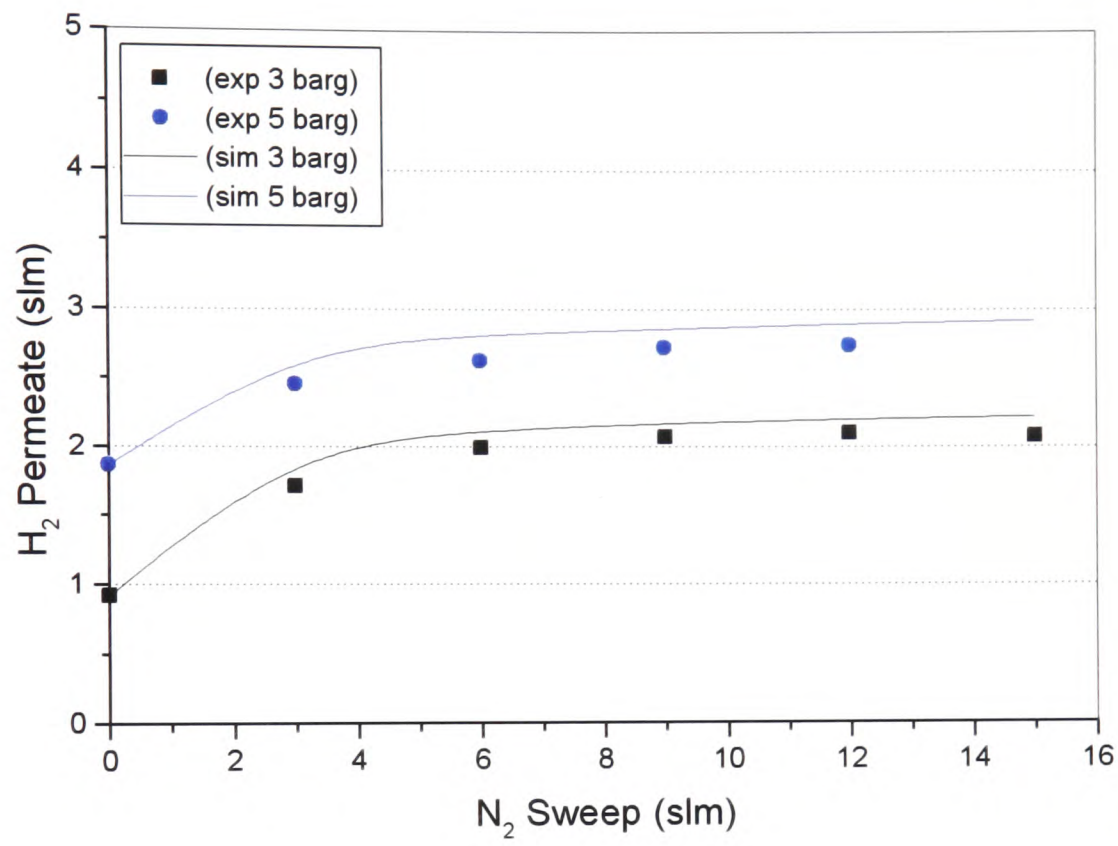

Figure 7.17: *Aspen simulation showing the effect of nitrogen sweep on the hydrogen permeate using a standard 7.5 μm Pd/Ag membrane with 15slm 10% CO reformate feed operating at 440 °C. Corresponding experimental data also shown.*

7.3 Conclusions

The sub-model has been refined and comprehensively validated with the experimental data as regards membrane temperature, thickness, pressure, feed composition and flow. The model was improved to ensure correlation to the experimental data which had been limited during its initial development. This provides enough evidence to ensure the model produces realistic results for all envisaged cases where the sub-model may be used in a larger system model. Although the simulations of varying

membrane thickness show some disparity with the experimental results, it is the standard 7.5 μm Pd/Ag membrane that is of most interest for implementation in a system. Model validations for this standard membrane have shown excellent correlation to experimental data. The membrane is assumed to be ideal in that no cracks are present and has a near infinite selectivity for hydrogen. Any palladium membrane clean-up module in a system based on this model is an arrangement of these individual membranes.

8 Sub-Model Simulations

8.1 Membrane Module Requirements

In a fuel processing and purification system requiring more than a few litres of hydrogen, a single standard 7.5 μm Pd/Ag membrane will not be sufficient to purify the necessary quantity of hydrogen. If the membrane module is not sized correctly, then a significant proportion of the hydrogen in the reformate feed to the unit will simply pass by the membrane in the retentate stream and be burnt in the afterburner. The following simulations were carried out to investigate the potential membrane requirements for a 10 kW_e system. With a move away from on-board ATR reforming, steam reforming will be the most widely used method of hydrogen generation and achieves a higher wet concentration (typically 57%) of hydrogen compared with autothermal reforming (typically 29%) and no nitrogen. The simulations presented below have been performed assuming the product of a gasoline steam reformer with the following composition:

Steam Reformer

Iso-octane fuel with a steam to carbon ratio, SCR = 2

H_2	57%
CO	15.5%
CO_2	8%
CH_4	1.27% (for purposes of model considered inert)
H_2O	18%

In the initial case, the membrane was assumed to be running at a temperature of 440 °C with a possible feed pressure of at least 3 barg and no more than 10 barg.. Two different downstream or permeate pressure conditions were considered: 1 bara (e.g. atmospheric) and 0.3 bara (using a 0.7 bara vacuum). These simulations use solely the palladium membrane model and assume that the temperature of the membrane can be maintained at 440 °C.

A series of simulations, whereby the reformate flow rate was varied, were carried out. The resulting hydrogen permeate for each feed flow was then plotted. The data was also used to determine the hydrogen recovery efficiency i.e. the purified hydrogen as a percentage of the hydrogen in the reformate fed into the membrane. It has been proposed that a 10 kW_e fuel cell stack would require a feed in the order of 4.5 mol/min hydrogen (EC, 2003). The simulated data was then used to determine the number of standard palladium membranes which would be required to fulfil this hydrogen requirement. In the following simulations, the molar flow rates are used which, when water vapour is present in the reformate stream, provides a less ambiguous quantity than using standard litres per minute (slm).

8.1.1 3 barg Inlet Pressure

Initial simulations were performed with a 3 barg inlet pressure, this being the lowest pressure that the membrane might be expected to work with. In Figure 8.1, the results of varying the feed flow on the hydrogen permeate are shown. It can be seen that after an initial steep rise in hydrogen permeate, the hydrogen permeate begins to plateau out. In the standard operating mode with a 1 bara permeate or downstream pressure this plateau is in the region of 0.09 mol/min.

One method of increasing the hydrogen permeate considered was by reducing the downstream permeate pressure, thereby reducing the hydrogen partial pressure in the permeate stream and hence increasing the hydrogen partial pressure drop over the membrane. The effect of reducing the permeate pressure by 0.7 bara, produces a marked increase in the hydrogen permeate. The plateau reached in this case was 0.15 mol/min. In practice a vacuum would be used to produce this reduction in permeate pressure. However, if the palladium membrane was included in an integrated reformer and fuel cell system, the down stream system components such as the fuel cell stack would require a hydrogen feed at atmospheric pressure or higher. This would mean that the improvement in membrane performance would have to be balanced with the work required for further adjustments to the hydrogen permeate stream pressure. It should also be noted that a slight reduction in permeate pressure has a greater improvement on the membrane efficiency than increasing the reformate feed pressure by a similar amount. This is due to the fact that the reformate contains

57% hydrogen in this case and an identical increase in the reformate feed pressure will increase the hydrogen partial pressure by only 57% of the pressure rise.

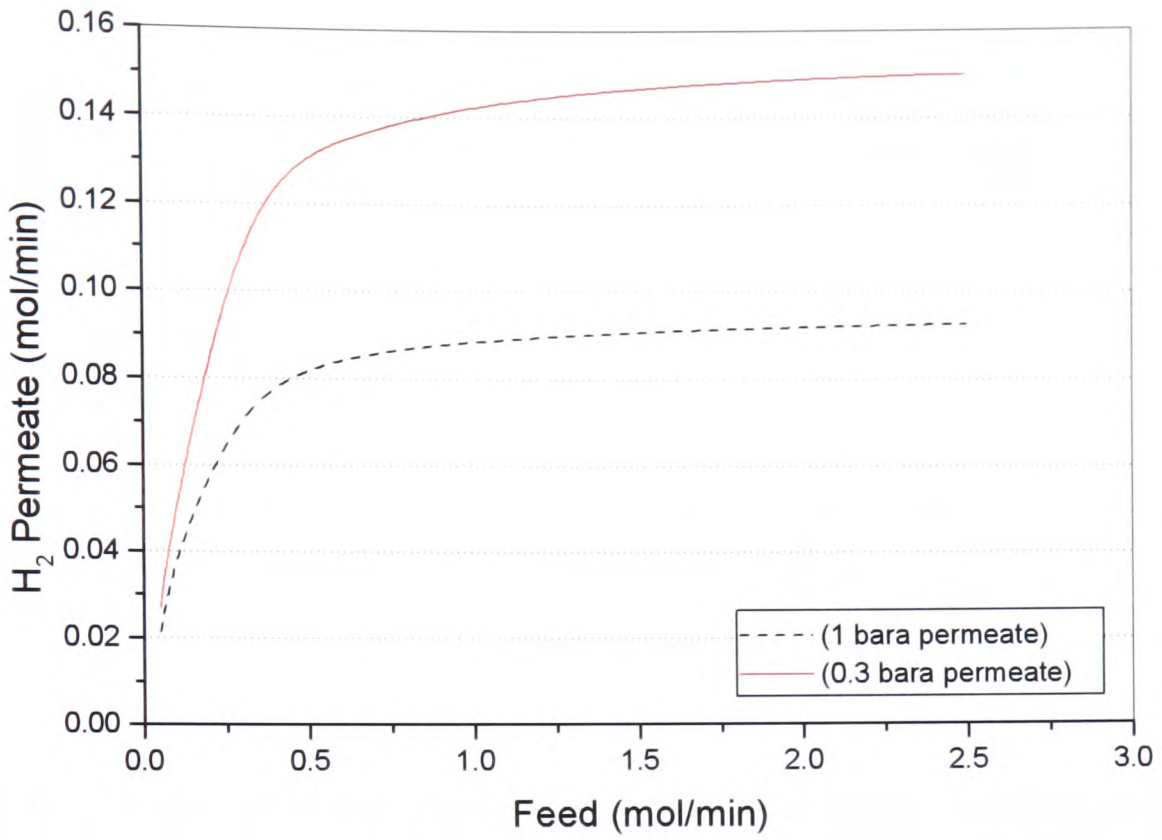

Figure 8.1: *Aspen simulation showing the effect of permeate vacuum on hydrogen permeate with a standard 7.5 μm Pd/Ag membrane with a 3 barg inlet pressure using a steam reformer feed operating at 440 °C.*

Once the hydrogen permeate begins to reach its plateau, an increasing proportion of the hydrogen in the reformate feed is remaining in the retentate. Although the energy available in this hydrogen may be used by combusting it, in terms of producing a hydrogen rich mixture for the fuel cell, it is lost. The plot shown in Figure 8.2 gives an indication of the proportion of hydrogen in the feed which passes through the membrane as opposed to flowing out in the retentate stream. This is termed the hydrogen recovery efficiency and gives an indication as to what flow rate the membranes should be run with to ensure as efficient an operation as possible. With a feed flow of just 0.1 mol/min, the hydrogen recovery efficiency with a 1 bara permeate pressure is 75%. The effect of the 0.7 bara downstream vacuum, increases this recovery efficiency to 95%. After this, the fall off in efficiency for both cases is quite steep and below a 0.75 mol/min feed there is a further slope change and a more gradual decline in the hydrogen recovery efficiency.

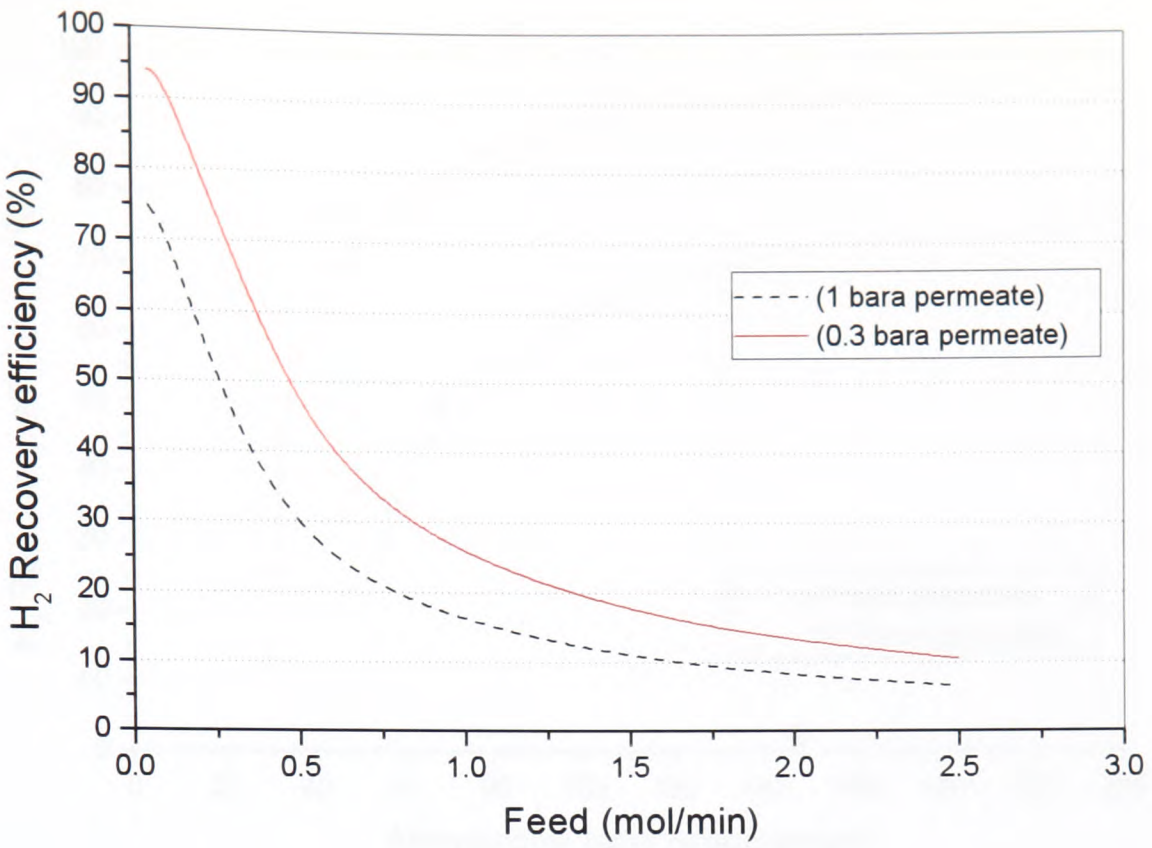

Figure 8.2: *Aspen simulation showing the effect of permeate vacuum on hydrogen recovery efficiency with a standard 7.5 μm Pd/Ag membrane with a 3 barg inlet pressure using a steam reformer feed operating at 440 °C.*

To estimate the number of membranes which may be required to provide the hydrogen requirements of a 10 kW_e system, it was assumed that there was no limit to the available reformate feed. The number of tubes was based on the hydrogen permeate from a single tube and the results presented in Figure 8.3 show how the number of tubes increases the recovery efficiency assuming a parallel arrangement of tubes. In the case with a permeate pressure of 1 bara, then with 50 tubes a hydrogen recovery of just 10% can be achieved. This means that although the 4.46 mol/min hydrogen requirements can be met, 40.14 mol/min of hydrogen are lost in the retentate stream. As the number of tubes in the module is increased, the recovery efficiency increases to reach a plateau of 75% with over 200 tubes. In the case of the 0.7 bara downstream pressure the recovery efficiency increases from 10% with 30 tubes to 95% with some 160 tubes. The more tubes there are, the less the return in increased efficiency and so an optimum level of tubes may be determined by considering the portion of the chart where the line begins to plateau. By visual inspection this is 80% with 60 tubes for the 0.3 bara permeate case and 55% with 90 tubes for the 1 bara permeate case.

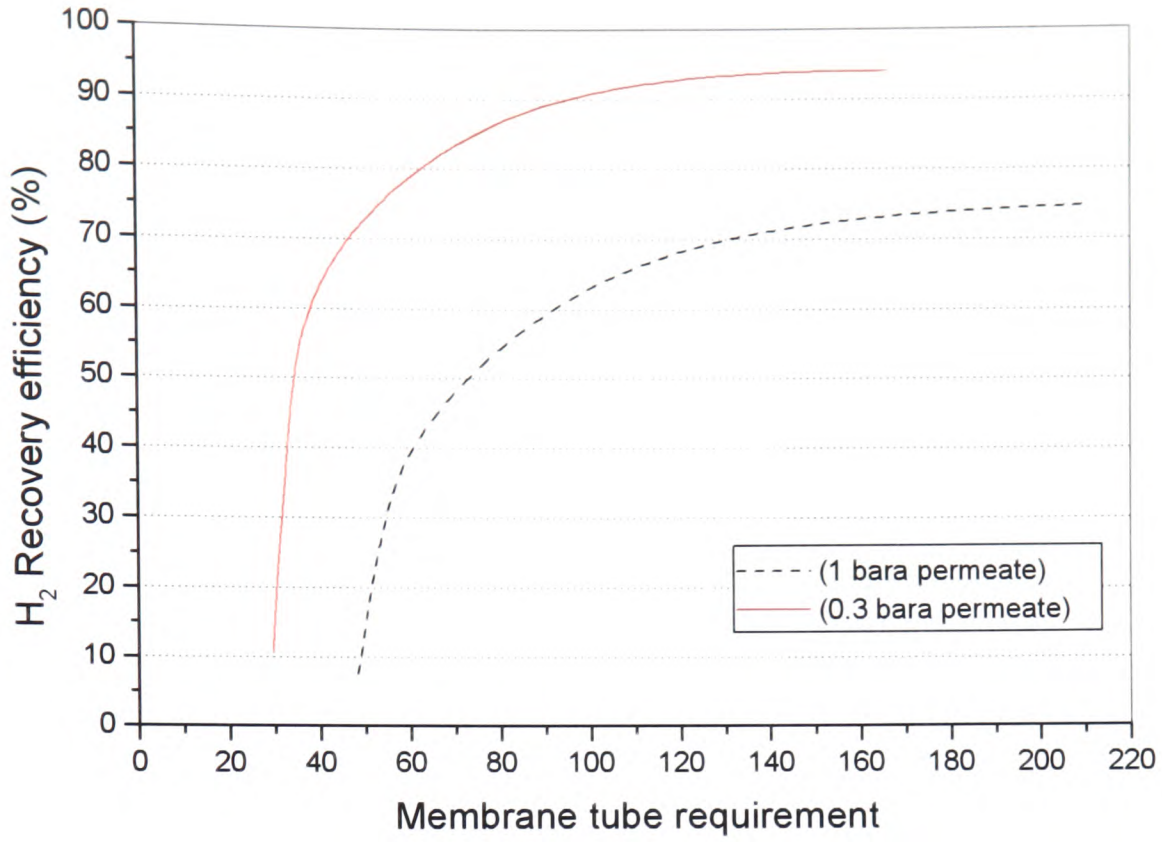

Figure 8.3: *Aspen simulation showing the effect of a permeate vacuum on the membrane requirements using standard 7.5 μm Pd/Ag membranes with a 3 barg inlet pressure and using a steam reformer feed operating at 440 °C.*

The above simulations have indicated the need for a number of standard membranes to be employed to provide the required hydrogen. The membrane area could also have been used, but quoting a number of tubes is more tangible. Increasing the number of tubes does increase the hydrogen recovery efficiency, though the cost of a membrane module would increase. The economic aspect of producing palladium membranes is considered later in Chapter 9, but qualitatively it might be suggested that the value of the hydrogen produced will have to be balanced with both the material and fabrication costs of the membranes. Lifetime estimates for current membranes undergoing thermal cycling are poor, though in a stationary, constant load application such as a refuelling station, the economics of the membranes would become increasingly acceptable. This work will concern itself with energy and determining the optimum usage of membranes in a system. Further work in this area would be to investigate the membrane and in particular the substrate design in order to improve the performance and reduce the pressure drop required over the membrane.

8.1.2 10 barg Inlet Pressure

The simulations carried out with a 3 barg reformate feed were then repeated using a 10 barg reformate feed; this being the higher end of the pressure range so far tested for a standard Pd/Ag membrane. The hydrogen recovery efficiency is shown against the reformate feed in Figure 8.4. With a feed of 0.1 mol/min the recovery efficiency is 98% and 93% with the 0.3 bara and 1 bara permeate pressure respectively. At the elevated reformate pressure of 10 barg, the effect of the 0.3 bara permeate pressure is less marked than at the lower reformate pressure of 3 barg and the recovery efficiency falls off less rapidly than in the case with the lower feed pressure.

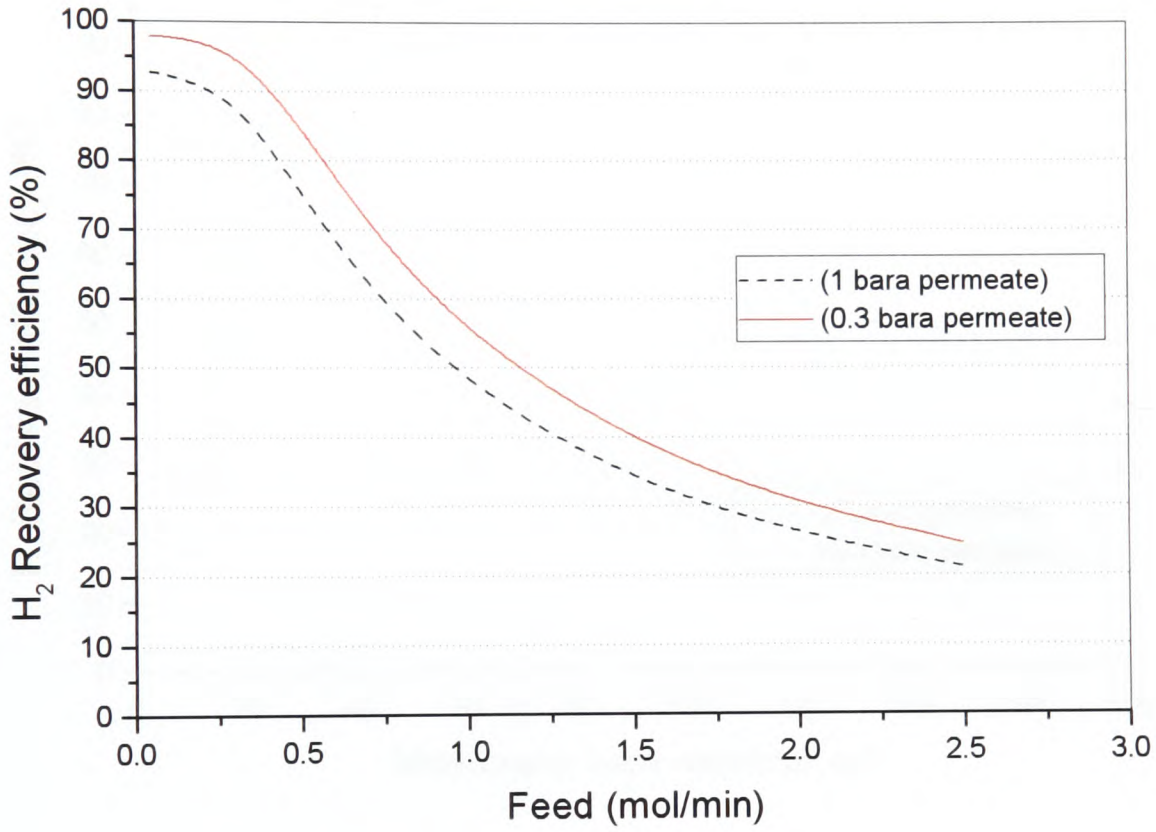

Figure 8.4: *Aspen simulation showing the effect of a permeate vacuum on hydrogen recovery efficiency with a standard 7.5 μm Pd/Ag membrane with a 10 barg inlet pressure and using a steam reformer feed operating at 440 °C.*

From consideration of Figure 8.5, the membrane requirements are reduced with a 10 barg feed pressure than in the case with a 3 barg feed pressure. From a visual inspection of the curve the most effective number of membranes as regards efficiency is 30 tubes for 85% recovery efficiency in the case with a 1 bara permeate pressure for the 10 barg reformate feed compared with a 75% recovery efficiency with 200 tubes for the 3 barg case.

The use of the 0.7 bara vacuum results in a reduction in the number of tubes to 160 with a 90% efficiency in the 3 barg feed case compared with 27 tubes and 96% efficiency in the case with a 10 barg feed pressure.

It can be seen from these results that the increased feed pressure significantly reduces the number of tubes required to process the necessary amount of hydrogen in this example. The lower the number of tubes, the less palladium usage and the more compact and simple the design of the membrane module.

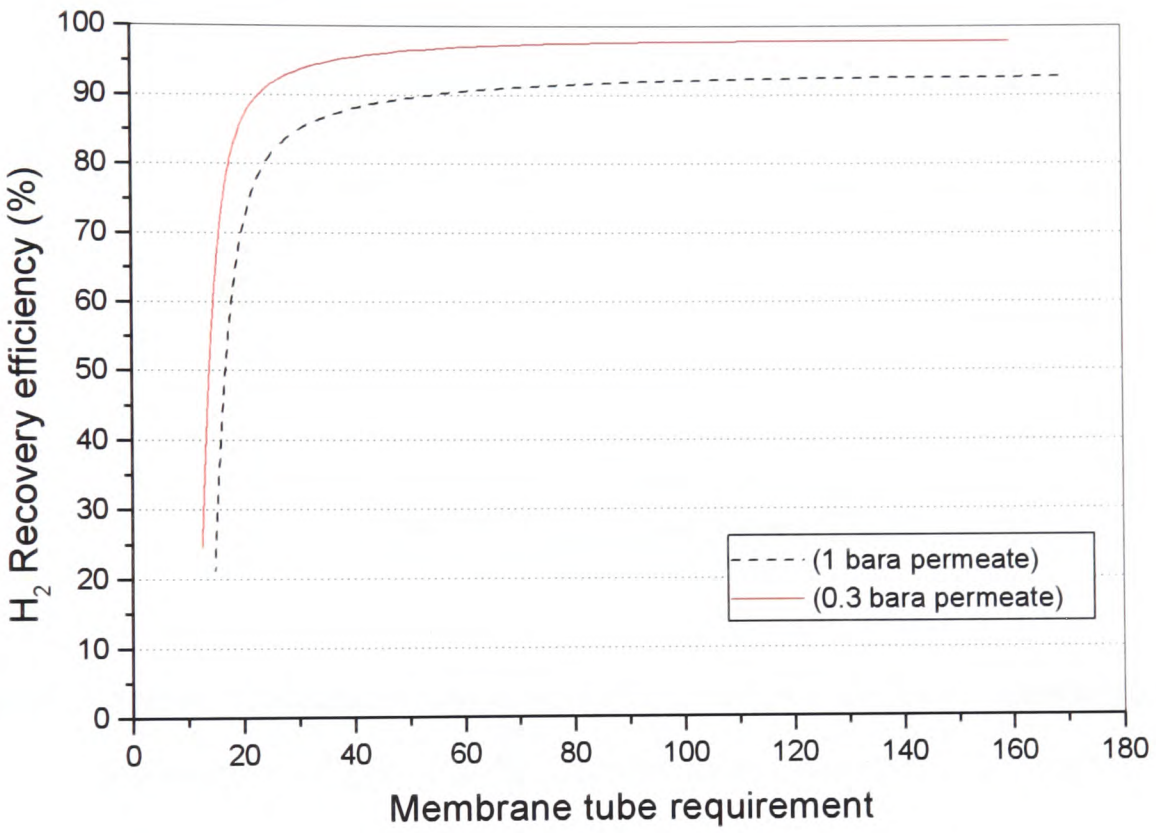

Figure 8.5: *Aspen simulation showing the effect of a permeate vacuum on the membrane requirements using standard 7.5 μm Pd/Ag membranes with a 10 barg inlet pressure and using a steam reformer feed operating at 440 °C.*

Efforts to increase the feed pressure as well as the number of standard membrane tubes does not always provide a similar increase in hydrogen recovery; the law of diminishing returns. Therefore it is necessary to find an optimum point where the number of membranes as well as the increased pressure are balanced with the gains in performance to be expected.

8.2 Membrane Configuration

The above simulations assume a parallel configuration of membrane tubes. Simulations were also run to investigate series and parallel tube arrangements. The results are to be seen in Figure 8.6.

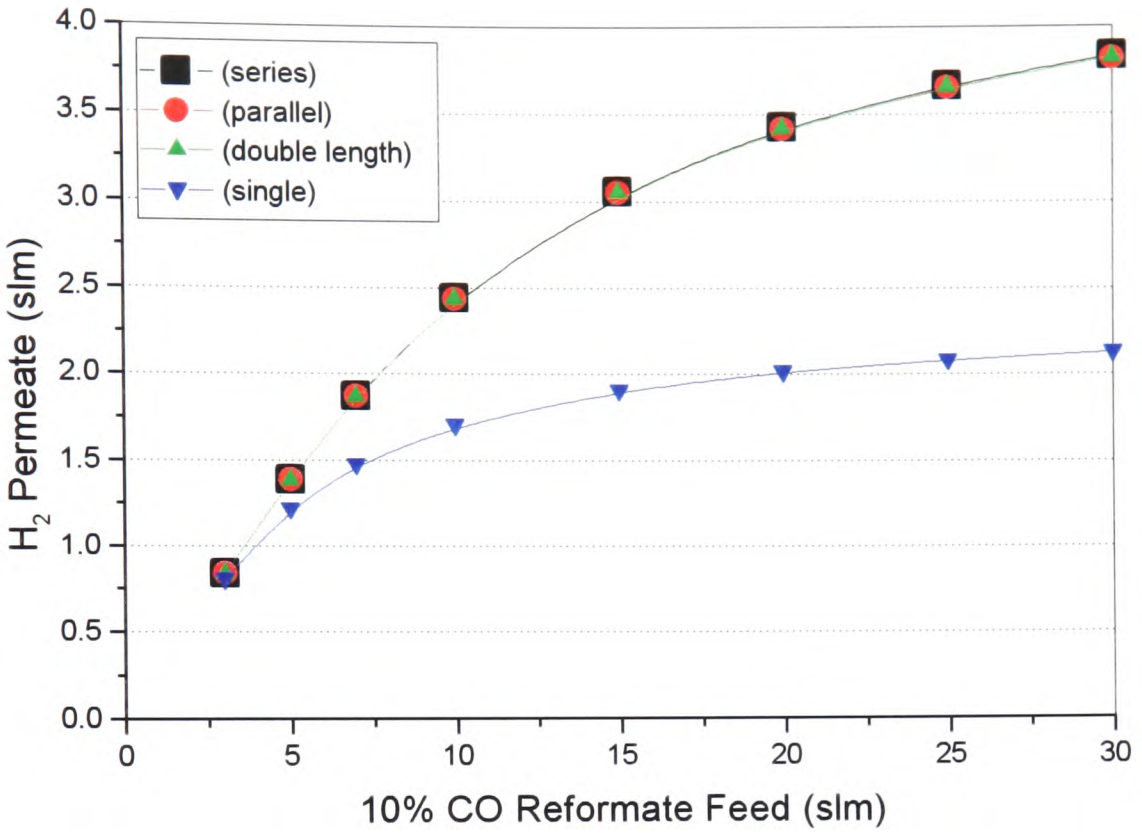

Figure 8.6: *Aspen simulation showing effects of membrane configuration using standard 7.5 μm Pd/Ag membranes operating at 440 °C with a 10% CO reformate feed at 5 bara.*

The results of the simulation show that for parallel and serial membrane configurations consisting of only two membranes, there is not an observable difference in the H_2 permeate achieved between the two configurations. This similarity is explained by the fact that the retentate pressure drop is quite low over a membrane and so in the serial case the feed from the first to the subsequent membrane is at virtually the same inlet pressure and consequently the pressure drop is the same. The parallel and series tubes produce twice as much hydrogen permeate as a single tube, around 3.8 slm compared with just over 2 slm with a 30 slm reformate feed, which is due to twice the available membrane surface area. The double length tube confirms the accuracy of the series arrangement of tubes. It is proposed though that a palladium membrane module would follow a parallel configuration of tubes. This

would ensure the same high pressure drop over each tube to maximise the purified hydrogen permeate. A parallel configuration would also have the advantage that faulty membranes could be removed from the system without interrupting the entire system. It would also be possible to isolate tubes depending on the purification requirements.

8.3 Conclusions

The simulations presented in this chapter have shown how the hydrogen recovery efficiency may be improved using an arrangement of parallel standard membrane tubes. The hydrogen recovery efficiency may also be improved through the use of a vacuum on the downstream side of the membrane by improving the hydrogen partial pressure drop over the membrane. If this is combined with high membrane feed pressures, hydrogen recovery efficiencies of up to 95% may be achieved. The effect of a vacuum is however less evident with higher feed pressures. The membrane requirement needs to be balanced with the desired hydrogen recovery efficiency and it should be noted that hydrogen recovery increases at a decreasing rate as the number of tubes is increased. A full system model, incorporating a gasoline steam reformer is presented in Chapter 9.

9 System Modelling

The progress in on-board gasoline reforming for fuel cell vehicles has been disappointing and automotive manufacturers, notably Daimler-Chrysler and Ford have abandoned such programmes in favour of high pressure hydrogen storage solutions (Smith, 2003). The reasons cited in opposition to on-board reforming have been the complexity and cost as well as toxicity concerns with fuels such as methanol (Emonts *et al.*, 1999). On-board reforming also has the disadvantage that pollutants are produced locally. This move towards on-board high pressure hydrogen storage has led to increasing efforts in researching and developing a hydrogen refuelling infrastructure.

The world's first public hydrogen filling station was developed for BMW's hydrogen vehicle programme with automated refuelling robots (Pehr *et al.*, 2000). There are now reported to be 87 hydrogen refuelling stations around the world (Geiger, 2004). All of these facilities though are demonstration projects such as those for the European Union supported Clean Urban Transport for Europe (CUTE) fuel cell bus programme across 9 countries. The capacity for these stations is limited to a small number of vehicles and public fears of cryogenic hydrogen storage in London has resulted in a planned refuelling site run by BP being delayed.

The current hydrogen refuelling stations either store hydrogen produced elsewhere or reform natural gas on site in preference to premium processes such as electrolysis (Fairlie and Scott, 2001; JMTC, 2000). There is a chicken and egg problem as regards the development of a hydrogen infrastructure (Malaina, 2003) in that:

1. Customers will not purchase fuel cell vehicles unless adequate fuelling is available.
2. Manufacturers will not produce vehicles that people will not buy.
3. Fuel providers will not install hydrogen stations for vehicles that do not exist.

It is estimated that between 4500 and 17000 hydrogen refuelling stations in an area such as California would be required to initiate an infrastructure. Lessons learnt during the development of other fuel infrastructures such as compressed natural gas, CNG, in terms supply network provision should be heeded to ensure adequate take up (Flynn, 2002). Economic analyses of developing a hydrogen infrastructure have suggested reduced health costs as a result of lower emission. This could outweigh some of the state investment in infrastructure development costs (Mercuri *et al.*, 2002).

Analyses of hydrogen refuelling have concentrated on natural gas reforming (Mathiak *et al.*, 2004), diesel reforming (Amphlett *et al.*, 1998) or have made use of very simplistic gas separation models (Lee *at al.*, 2003). This chapter looks at exploiting the existing gasoline supply infrastructure for on-site reforming and the use of a palladium membrane based hydrogen clean-up module based on extensive validation. An on-board reformer system was considered, though for the reasons already presented as regards automotive manufacturers' preference for compressed H_2 as well as the current durability limitations and space requirements of the thin palladium membranes, it was decided that such a system would be unviable. A stationary application without temperature cycling would however be a realistic opportunity. The subsequent system simulations aim to demonstrate the feasibility of such a system.

9.1 Hydrogen Refuelling Station

The main application where a palladium membrane module will be considered is that of a hydrogen refuelling station where the fuel to be supplied to the station is gasoline. In this way, the existing energy supply network is utilised, therefore providing an immediate medium term solution to hydrogen supply before sufficient renewable energy is available. The gasoline is then converted using a steam reforming reaction to produce a hydrogen rich gas. In the practical case of a refuelling station the hydrogen is stored as a compressed gas. Other studies of hydrogen refuelling stations are based on natural gas and use very simple clean-up models. The system model presented in this work will give a quantitative analysis of the effectiveness of palladium membranes for such an application through the use of the validated palladium membrane sub-model.

An overall simplified schematic of the hydrogen refuelling station system can be seen in Figure 9.1. The Aspen flow sheet for each stage of the modelling will be presented with the results, but apart from a few minor alterations, is identical in nature to the schematic. The individual components that make up the refuelling station are described below.

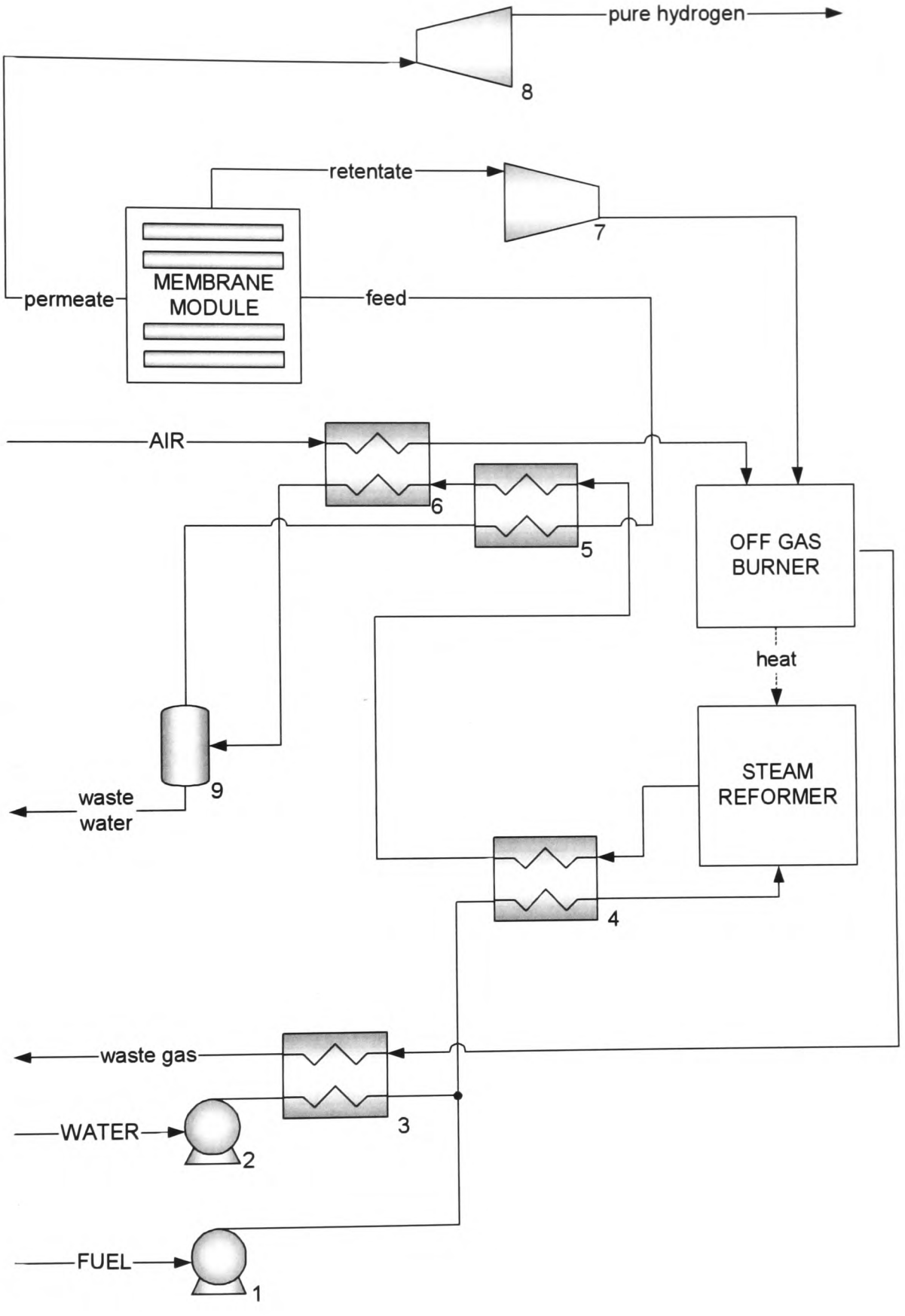

Figure 9.1: *Schematic of hydrogen refuelling station.*

9.1.1 Steam Reformer

The steam reformer model is a Willard Gibbs reactor and uses equilibrium to calculate the products based on the inlet temperature pressure and composition. The steam reformer is assumed to operate at a temperature of 750 °C and this temperature is maintained by heat supplied from the afterburner. Apart from the temperature being fixed, the other parameters such as pressure, steam to carbon ratio and feed composition will be altered in order to find the optimum operating conditions for the system.

9.1.2 Combustion Chamber – Afterburner

The combustion chamber makes use of the membrane module retentate stream which contains a mixture of CO, CO_2, CH_4 and H_2, and combines this with additional air in order to produce heat to sustain the endothermic steam reformer reaction.

9.1.3 Membrane Module

The term membrane module is used to describe a collection of standard, 7.5 μm Pd/Ag membrane tubes combined to form a module. Combining several individual membrane sub-model blocks in the Aspen flow sheet may be suitable when the module size is small, but in some instances the module size may be over 1000 individual tubes. It would be unwieldy and inefficient use of the Aspen processing power to attempt to combine 1000 tubes within the flow sheet. In order to simulate a palladium membrane module a number of assumptions are made. Firstly, the tubes are arranged in a parallel configuration, where each tube in the module takes an equal share of the total flow through the membrane module. Secondly, the pressure drop over each individual membrane tube is the same as the pressure drop over the whole module. It is also assumed that the module is maintained at the desired temperature by the heated gas feed streams. All the Aspen simulations assume a steady state. Using these assumptions the feed stream to the module is scaled down to a fraction, which is equal to the reciprocal of the number of tubes in the module. Only one membrane sub-model is then required. The permeate and retentate streams are then scaled back up by the number of tubes in the module in order to maintain the mass balances through the membrane module. It is also necessary to perform a flash calculation on the output streams from the membrane sub-model to maintain the material properties of the gas streams. This flash calculation might seem unnecessary, but errors were found that

were due to Aspen not correctly re-calculating the thermodynamic data. With the membrane tubes in their current form, this is one possible way to model the module. The Aspen flow sheet connectivity of the membrane module is shown in Figure 9.2.

In the applications considered, the sweep stream is not utilised as the aim is to produce as pure a hydrogen permeate stream as possible. The palladium membrane sub-model requires the sweep stream to be connected, but the flow rate is set to a negligible value.

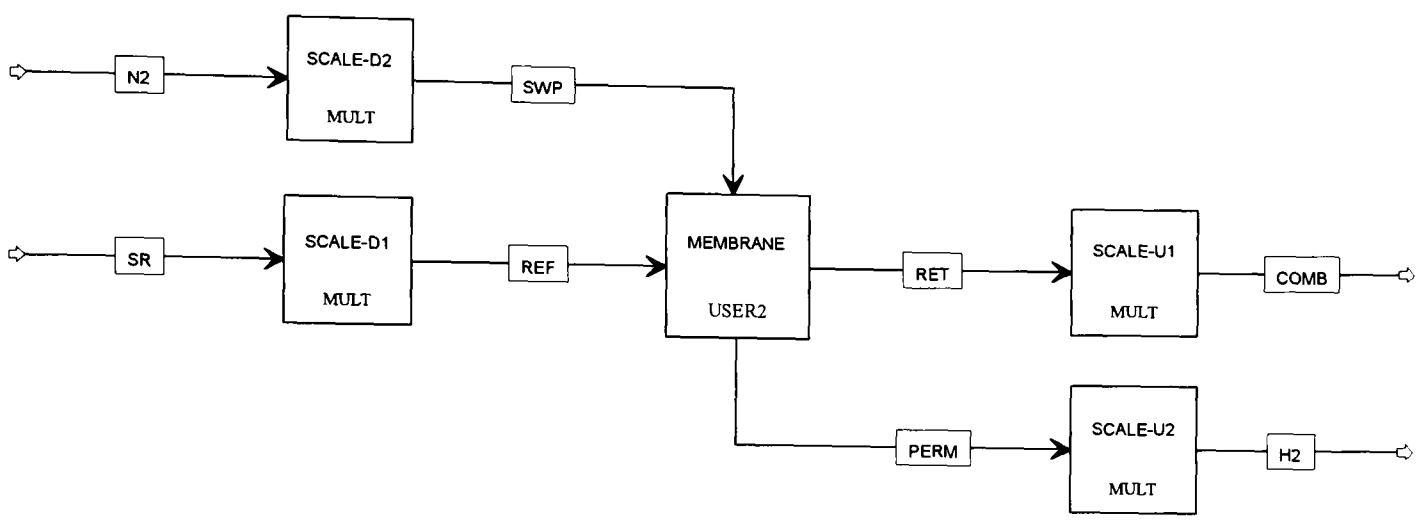

Figure 9.2: *Aspen flow sheet membrane module connectivity.*

9.1.4 Pumps/Expanders

The fuel and water streams are supplied to the steam reformer at pressure and an Aspen pump model is used for this purpose. The pump model (labelled 1 and 2 in Figure 9.1) is suitable for simulating liquid pumps and provides details of the power requirements for a given flow rate and outlet pressure.

9.1.5 Multi-Stage Compressor

The multistage compressor (component 8 in Figure 9.1) is used to pressurise the pure hydrogen produced for storage at the refuelling station. The compressor suitable for such an operation is a positive displacement compressor with a number of intercooled stages. Demands for comparable vehicle ranges and improvements in composite high pressure storage tanks have led to proposals that a refuelling station storage pressure of 1000 bara will be required (FCB, 2004) with a storage pressure of 700 bara in the vehicle. It is assumed a reciprocating compressor with 3 or 4 stages of compression would be used with a 72% polytropic efficiency.

9.1.6 Heat Exchangers

To ensure good system efficiency, heat exchangers are used to reduce the amount of external heat supplied to the system. The Aspen heat exchanger models (components 3 to 6 in Figure 9.1) enable zonal examination to be carried out to ensure that pinch point constraints are avoided. The heat exchangers' flow streams are run in a countercurrent arrangement.

9.1.7 Heaters/Coolers

Although not present in Figure 9.1, heater blocks were used both for heating and cooling requirements in simulations. These perform flash calculations on the streams.

9.1.8 Water Trap

Water vapour is present in the steam reformer product gas and this decreases the effective partial pressure of the hydrogen in the feed to the palladium membrane module. The proportion of water vapour in the feed stream can be such that the hydrogen recovery efficiency of the membrane module is significantly reduced (~15% reduction). The water vapour may be removed from the stream by firstly cooling the gas stream below the dew point and then removing the liquid water in a water trap.

9.1.9 Fuel

The first fuel used for the simulations is iso-octane, C_8H_{18}, which is a primary reference fuel for gasoline. The octane rating of iso-octane is arbitrarily set at 100 and is a measure of resistance to knocking and all other fuels are compared to this value. Simulations with alternative fuel mixtures are discussed later in this chapter.

9.2 Simulations

Initial simulations were carried out using a fuel feed flow of 1 mol/min as a base case to assess the design and arrangement of the components. Heaters were also used in place of heat exchangers before the heating/cooling requirements were assessed.

9.2.1 Steam Reformer Conditions

Simulation and experimental testing of the palladium membrane module has demonstrated that the greater the hydrogen partial pressure drop, the greater the hydrogen recovery efficiency of the membrane module. If the steam reformer were to be operated at atmospheric pressure then the product gases would have to be

subsequently compressed to the desired pressure to achieve the required feed pressure for the membrane module. The work required to pressurise gases is significantly greater than that required to pressurise liquids to the same degree. The steam reformer can be operated at elevated pressure but the thermodynamic equilibrium composition of the product stream changes. In Figure 9.3, the effect of varying the steam reformer operating pressure on the composition of the product stream is shown. The results are for a fixed steam to carbon ratio of SCR = 2 and a temperature of 750 °C which are typical operating conditions for steam reforming. One of the most important results of increasing the system pressure is the increase in the proportion of methane in the steam reformer product stream. As four hydrogen atoms are used for every one carbon atom, this increase in methane is in effect wasting the hydrogen produced in the steam reformer reaction.

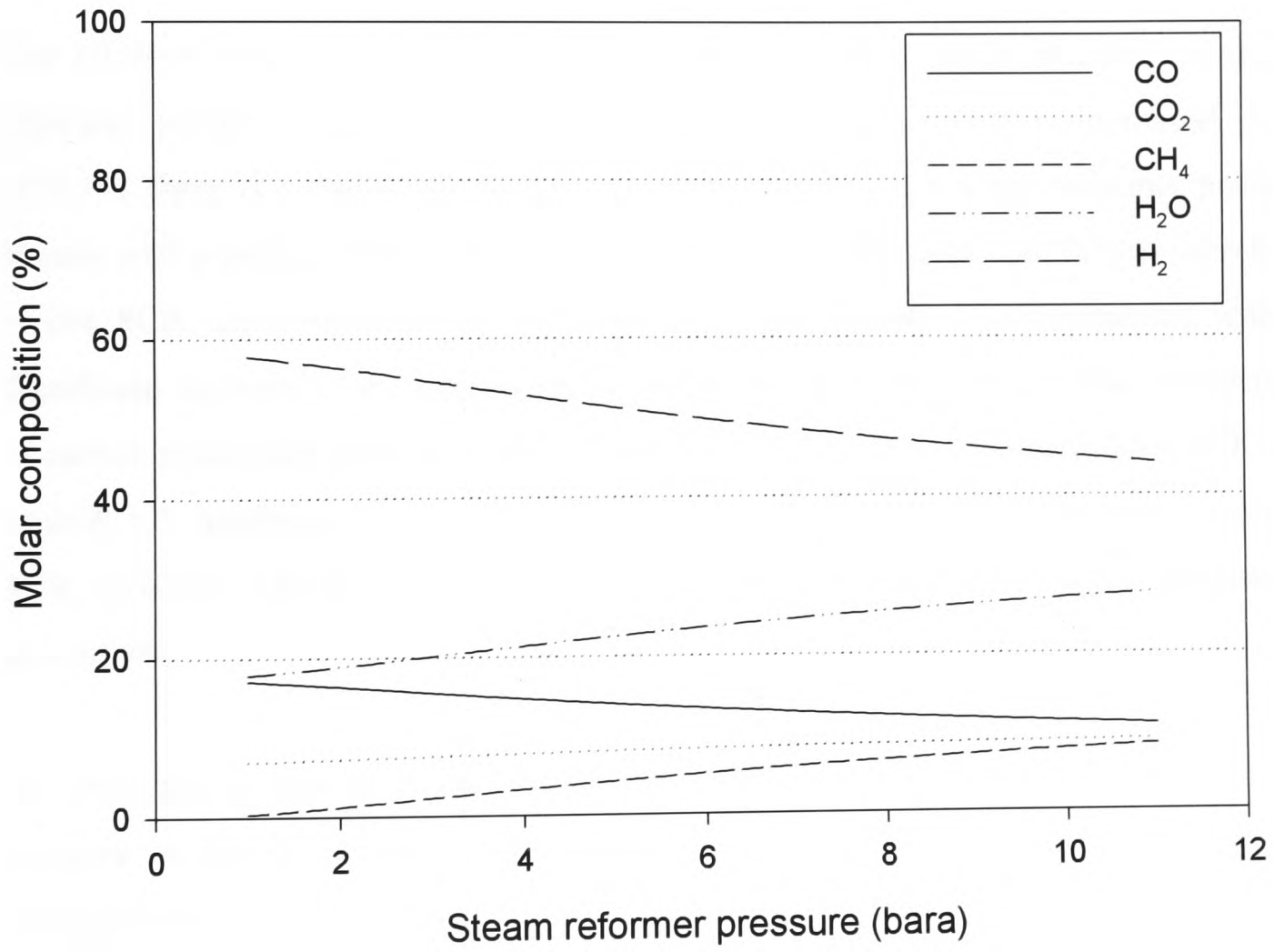

Figure 9.3: *Effect of pressure on product composition of steam reformer with an SCR = 2, an operating temperature of 750 °C and an iso-octane fuel feed.*

Increasing the reforming pressure has a detrimental effect on the composition of hydrogen in the product stream. The molar composition of hydrogen falls from around 55% with a pressure of 2 bara to around 45% with a pressure of 10 bara. However, although the proportion of hydrogen decreases, the proportion of water vapour in the steam reformer product stream increases. If this water vapour were to be removed from the product stream the proportion of hydrogen in the product stream would increase and improve the hydrogen partial pressure for the membrane module. The effect of a water trap on the hydrogen recovery efficiency is looked at later in this chapter. The proportion of carbon dioxide in the steam reformer remains at a reasonably constant level of 8% over the pressure range. There is also a decrease in the proportion of carbon monoxide from around 18% to 12% as the system pressure is increased over the range 2 bara to 10 bara. This reduction in carbon monoxide has the most beneficial influence on the performance of the membrane module.

The effect of varying the steam to carbon ratio, SCR, on the composition of the steam reformer product stream is shown in Figure 9.4. As the SCR is increased from SCR = 1 there is a rise in the proportion of hydrogen in the steam reformer product stream with a peak of around 46% with an SCR = 1.8. However with further increases in the SCR, the proportion of hydrogen decreases though is accompanied with a significant increase in the proportion of water vapour in the stream. The proportions of carbon monoxide decrease from 17% to 5% as the SCR is increased from SCR = 1 to SCR = 5. Methane also decreases from 20% to less than 1% over the same range of SCR variation. The proportion of carbon dioxide remains approximately constant at around 9%.

As with the previous results for varying system pressure, the hydrogen partial pressure in the membrane module feed stream is important for achieving a high hydrogen recovery efficiency. The proportion of water vapour in the steam reformer product stream increases from around 13% to 50% over the range SCR = 1 to SCR = 5. This would significantly reduce the hydrogen partial pressure in any subsequent membrane module stage and highlights the need for a water trap.

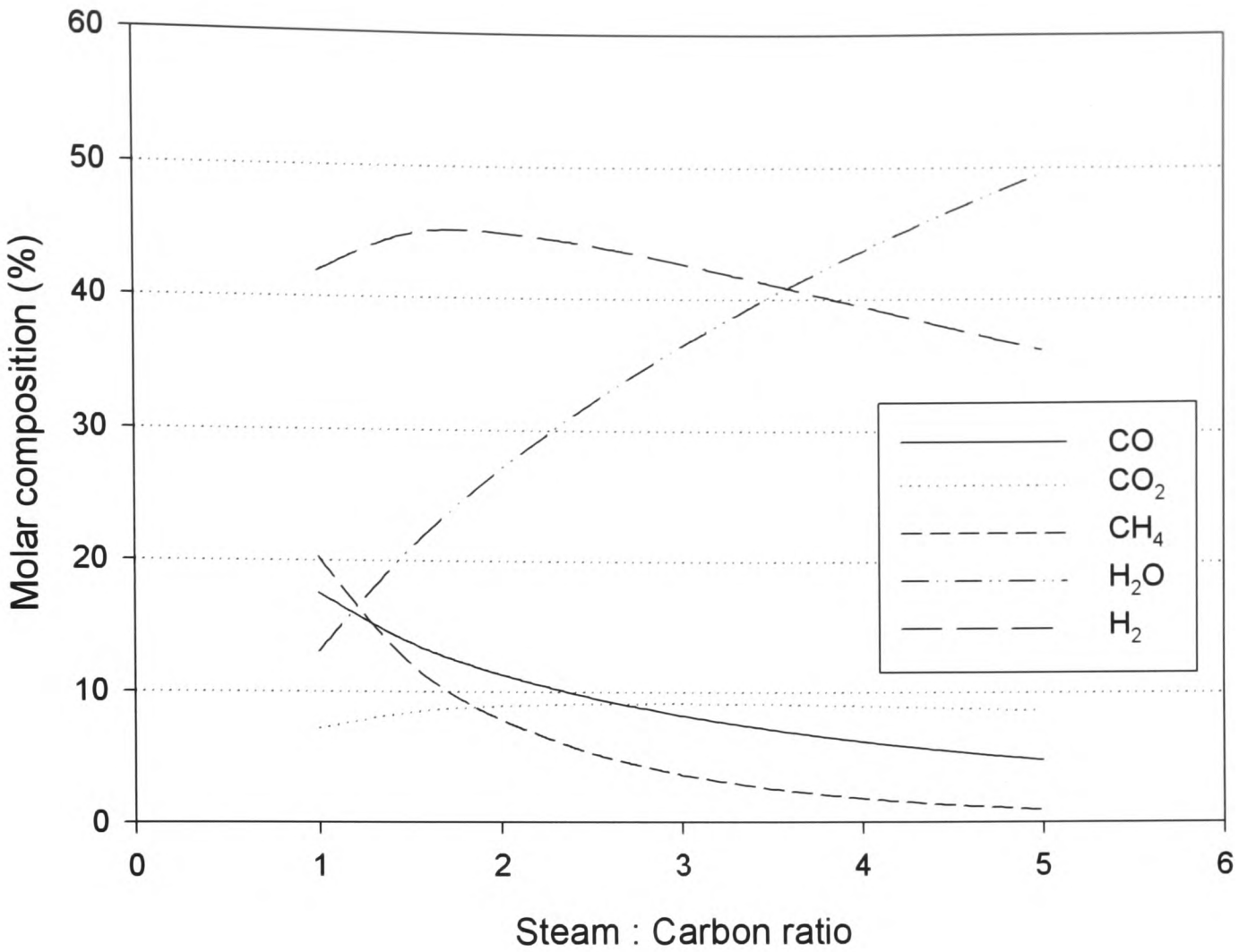

Figure 9.4: *Effect of Steam : Carbon ratio (SCR) on product composition of steam reformer with an operating pressure of 10 bara, an iso-octane fuel feed and a temperature of 750 °C.*

For comparison, the dry product composition is shown in Figure 9.5. Now that the proportion of water in the steam reformer product has been discounted, the hydrogen molar composition reaches a plateau at around 70%. The CO molar composition is now slightly higher, though the proportion of hydrogen to carbon monoxide is high and this will have the greatest benefit on the hydrogen recovery efficiency of the palladium membrane module. These results only go to reiterate the benefit that may be obtained from the removal of the water in the membrane module stream. The conditions of a water trap to do just this are discussed later in this chapter.

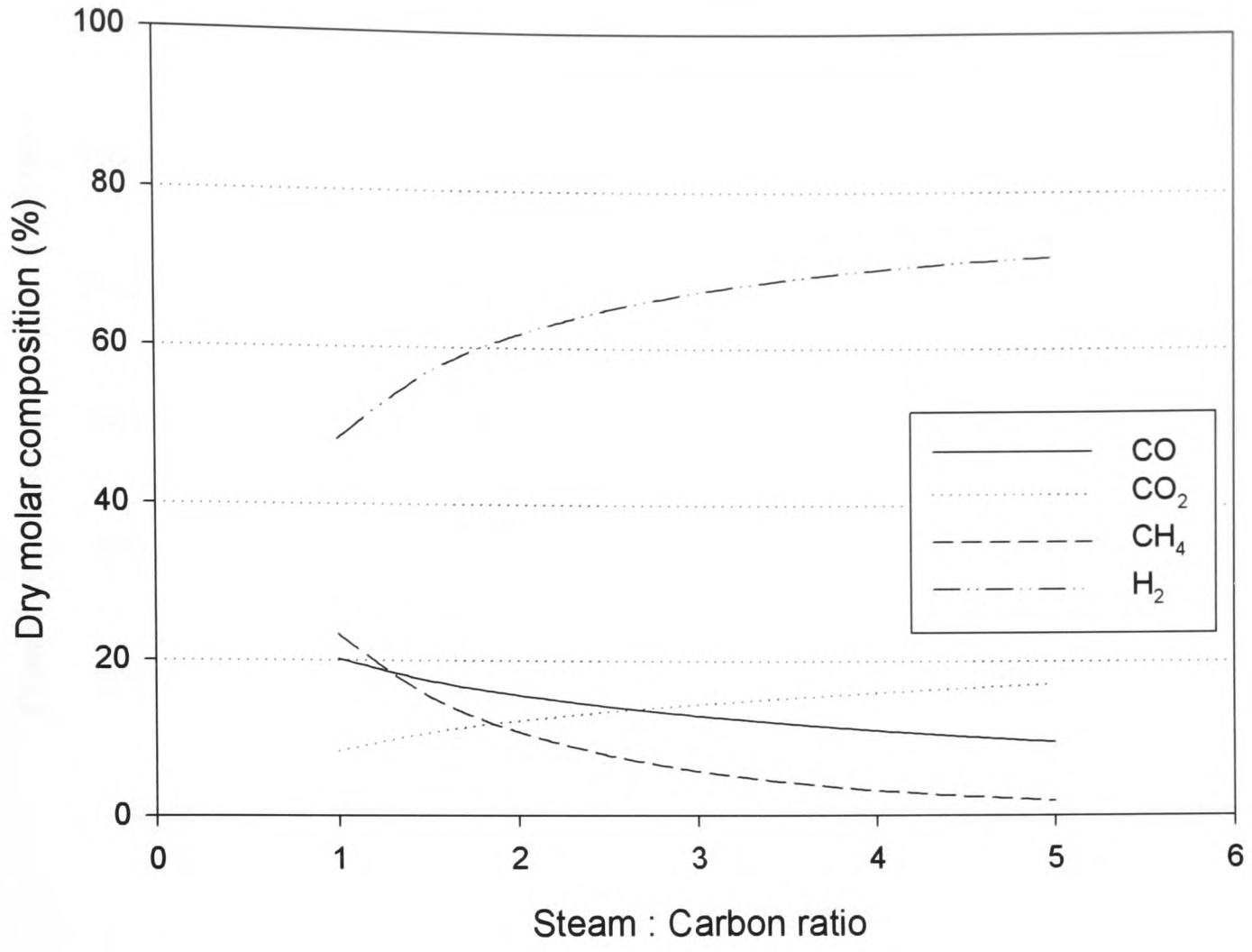

Figure 9.5: *Effect of Steam : Carbon ratio (SCR) on dry product composition of steam reformer with an operating pressure of 10 bara, an iso-octane fuel feed and a temperature of 750 °C.*

Figure 9.3, Figure 9.4 and Figure 9.5 show the composition of the steam reformer product stream. The plot presented in Figure 9.6 shows how the product stream flow rates vary. The simulation was run with a fuel feed of 100 mol/min though the results may be scaled according to the fuel feed. Increasing the steam to carbon ratio produces a steady increase in the hydrogen flow rate. The flow rate increases by just over a factor of 10 from 250 mol/min to 2750 mol/min as the steam to carbon ratio varies from SCR = 1 to SCR = 5. The flow rate of water vapour in the product stream also increases though at a decreasing rate from 750 mol/min with an SCR = 1 to 2000 mol/min with an SCR = 5. There is a very slight decrease in the flow rate of carbon monoxide from around 350 mol/min to around 300 mol/min over the SCR range. The flow rate of methane decreases from around 400 mol/min to around 50 mol/min as the steam to carbon ratio is increased to SCR = 5.

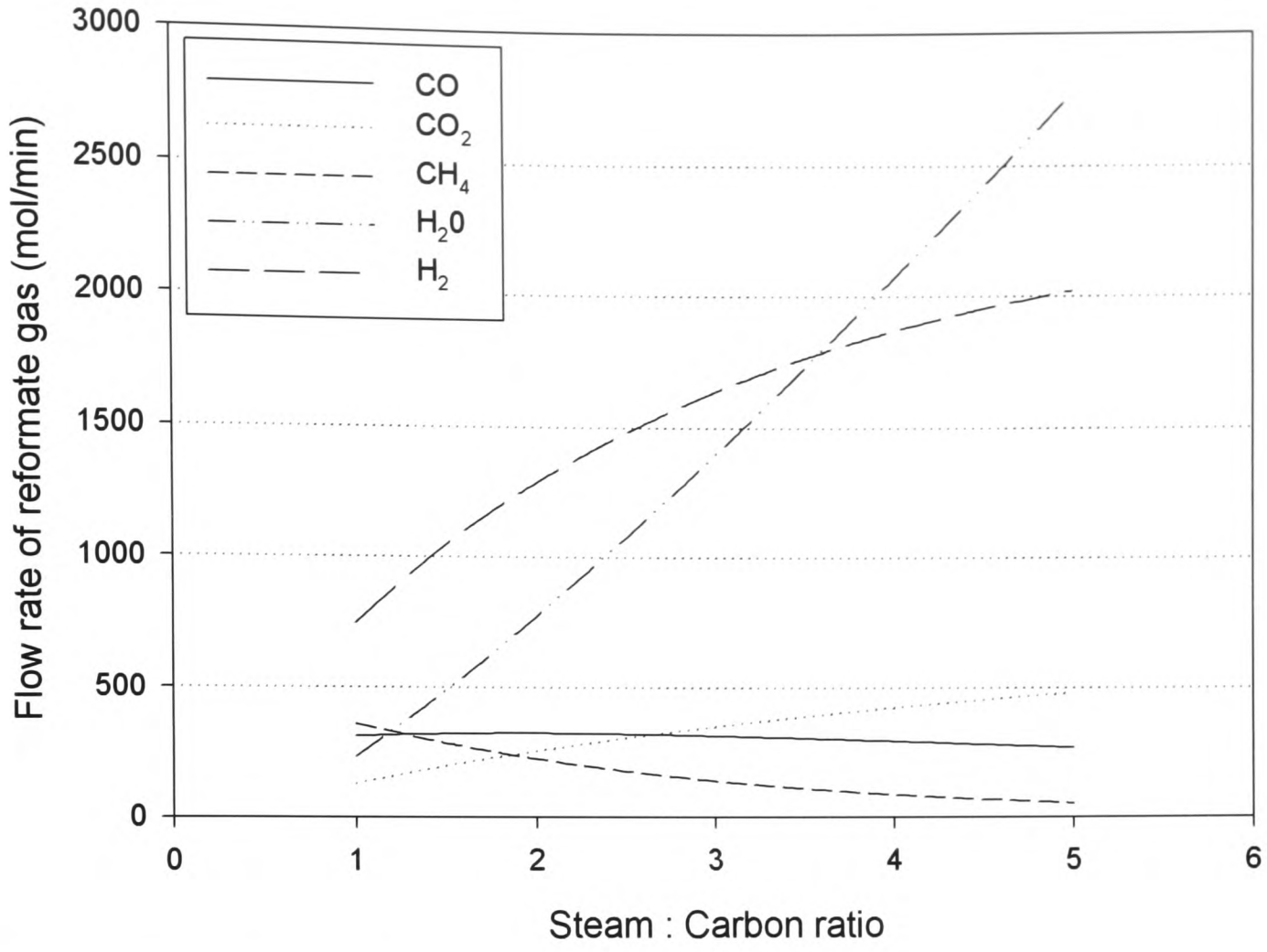

Figure 9.6: *Effect of Steam : Carbon ratio (SCR) on product flow rate of steam reformer with an operating pressure of 10 bara, an iso-octane fuel feed of 100 mol/min and a temperature of 750 °C.*

A contour plot which shows both the effect of the variation in the steam to carbon ratio and steam reformer pressure on the concentration of hydrogen in the steam reformer product stream as well as the flow rate of hydrogen is shown in Figure 9.7. It would suggest that the optimum conditions for hydrogen product would be with a pressure as near atmospheric as possible and a steam to carbon ratio around SCR = 2.5. A balance must be reached however between the benefits of a low pressure reformer to reduce methane formation and hydrogen concentration, and the additional work then required to pressurise the reformer product prior to the membrane clean-up module.

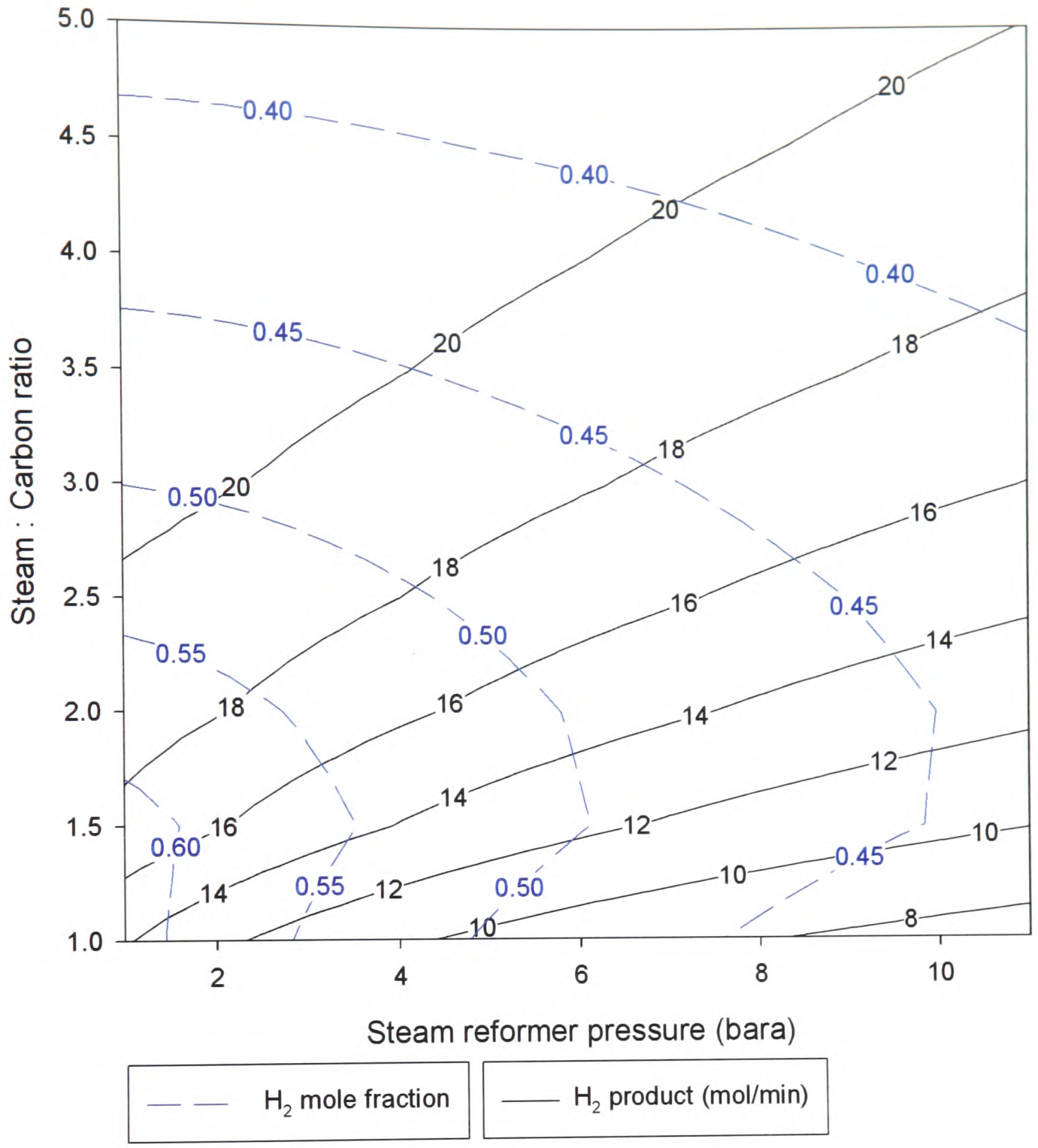

Figure 9.7: *Effect of Steam : Carbon ratio (SCR) and pressure on hydrogen flow rate and mole fraction of the steam reformer product with operating temperature of 750 °C and 1 mol/min iso-octane fuel feed.*

9.2.2 Membrane Module Performance

The composition of the steam reformer product stream has been shown to be dependent on the steam to carbon ratio and the system pressure. The efficiency of the membrane module is now assessed, where the performance is defined as the hydrogen

recovery efficiency, i.e. the hydrogen permeate through the membrane as a percentage of the hydrogen in the feed stream to the membrane.

9.2.3 Feed, Permeate Pressure and Tube Number

The plot shown in Figure 9.8 gives an indication of the hydrogen recovery efficiency with varying feed and permeate pressure for the membrane module. Previous experimental results and Aspen simulations of the palladium membranes have shown that an operating temperature above 400 °C is required in order to minimise the effect of carbon monoxide poisoning the membrane surface. Experimentally a temperature of 440 °C is used.

The feed pressure to the membrane module was varied over the range 3 bara to 11 bara. The permeate pressure was also varied from 1 bara to 0.5 bara so as to induce a vacuum on the downstream side of the module. The steam reformer is operating with an SCR = 2 and at a temperature of 750 °C. The fuel feed flow rate to the steam reformer is 1 mol/min of iso-octane.

Two module sizes are shown for comparison in Figure 9.8, one consisting of 40 standard tubes and another consisting of 160 identical standard tubes. It is the hydrogen recovery efficiency that is considered in these simulations. In the case of the 40 tube module, the hydrogen recovery efficiency increases from less than 20% with a feed pressure of 3 bara and a permeate pressure of 1 bara up to 60% recovery with a feed pressure of 10 bara and permeate pressure at 1 bara. These recovery efficiencies can be increased by reducing the permeate pressure and thereby increasing the hydrogen partial pressure drop over the membrane module. In the case of the 40-tube module the efficiencies increase to over 20% and 65% at 3 bara and 10 bara respectively.

The clean-up module with 160 tubes shows considerable improvement in hydrogen recovery efficiency over the range of feed pressures when compared with the 40-tube module. With a feed pressure of 3 bara, the recovery is around 35%, though this increases to just under 90% when the feed pressure is 10 bara. Both of these results are with a permeate pressure of 1 bara. Reducing the permeate pressure also increases

the hydrogen recovery with values of over 60% and 95% with feed pressures of 3 bara and 10 bara respectively.

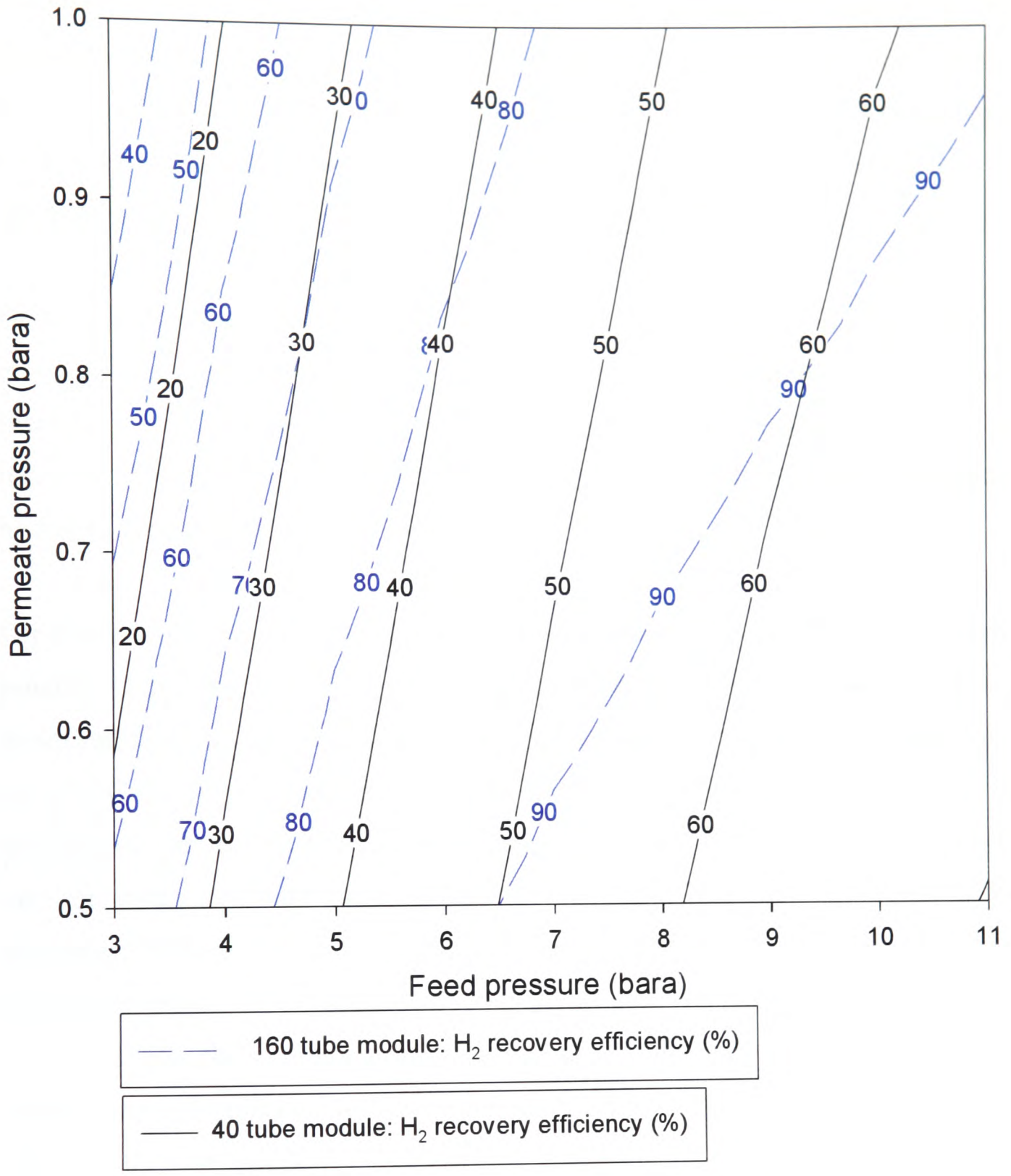

Figure 9.8: *Comparison of a 160 and 40 tube membrane module showing effect of feed and permeate pressure on hydrogen recovery efficiency. Membrane operating temperature 440 °C. Feed gas from steam reformer operating at 750 °C, SCR = 2 with 1 mol/min iso-octane fuel feed.*

9.2.4 Water Trap Conditions

As has been previously discussed, removing the water vapour in the reformer product stream would increase the hydrogen partial pressure in the feed stream to the membrane module. This can be achieved through the use of a water trap. It is necessary to cool the stream containing water vapour to below the dew point. In Figure 9.9, the water trap conditions and their effect on both the water recovery of the water trap and the hydrogen recovery efficiency of the membrane are shown. The steam reformer is being operated with an SCR = 2 and at a temperature of 750 °C.

Decreasing the temperature of the steam reformer product stream for the water trap increases the water recovery, as is expected from consideration of steam tables. Increasing the pressure of the system also has the effect of increasing the water recovery. The improvement in water recovery in the water trap leads to improved hydrogen recovery in the membrane module.

For the system it would be preferable to maintain the pressure of the system as high as possible to improve the hydrogen recovery efficiency. The water trap requires the steam reformer product to be cooled, but then subsequently reheated to a temperature of 440 °C for the palladium membrane module. A suitable arrangement of heat exchangers can be used to make effective use of all available heat streams including the hot steam reformer product with a view to improving the overall system efficiency. With a pressure of 10 bara, a water recovery of just under 90% can be achieved if the stream is cooled to 80 °C. The hydrogen recovery from the membrane module is over 90% under these conditions. The hydrogen recovery efficiency and membrane requirements must be balanced with the need to provide heat for the steam reformer by combustion of the membrane module retentate stream. Therefore, a hydrogen recovery efficiency of 90% is deemed sufficient in terms of a respectable utilisation of the fuel delivered to the system and ensure the sustainability of the combustion process to sustain the steam reforming reaction. These conditions for the water trap will be assumed in subsequent simulations. The other advantage of removing the water from the stream is that the water may be recirculated to provide part of the water requirement for the steam reforming reaction. The recirculation of the water from the steam reformer product stream is discussed later in Section 9.3.7.

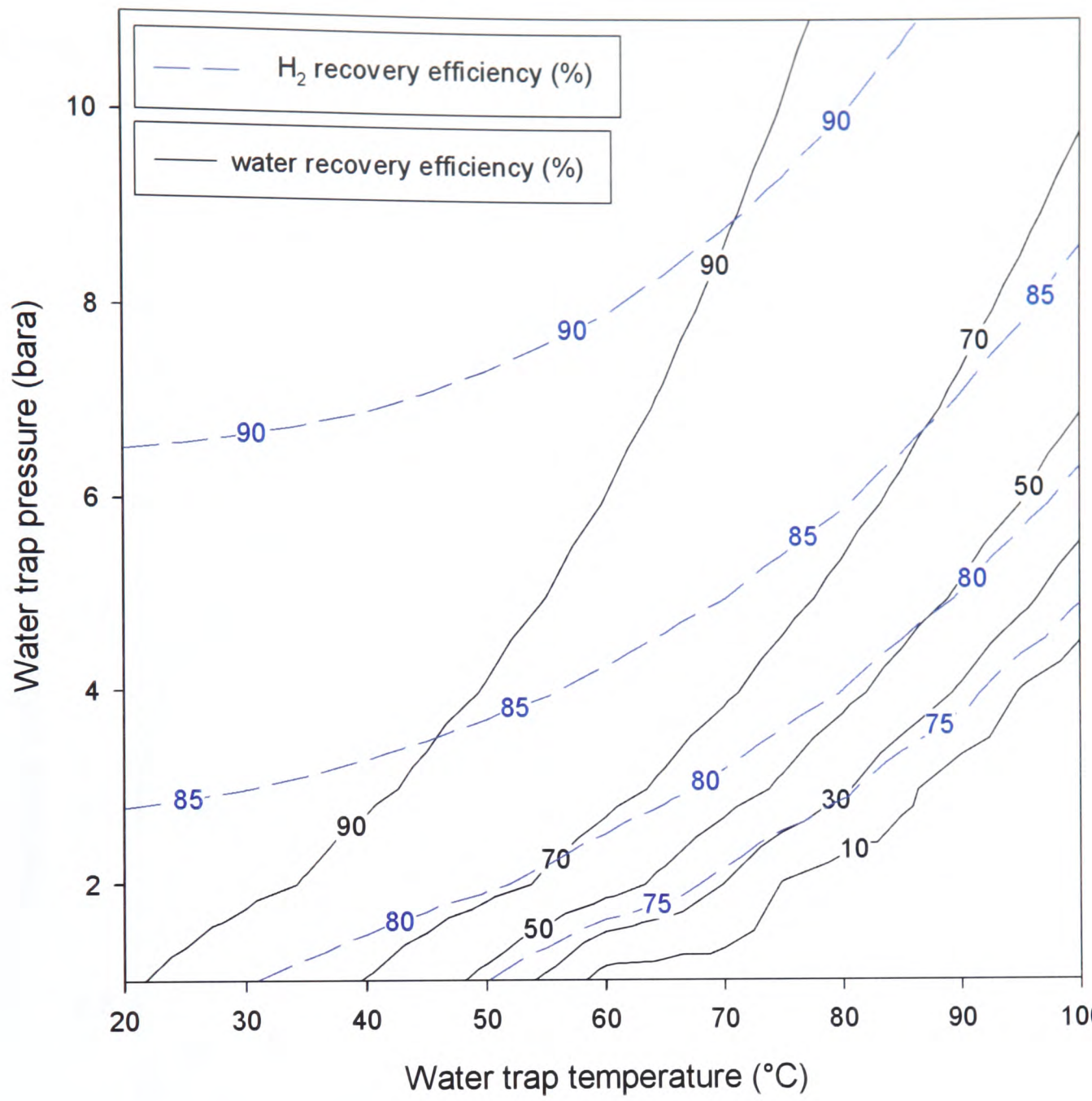

Figure 9.9: *Effect of temperature and pressure on removal of water in water trap and subsequent hydrogen recovery efficiency of palladium membrane module with a feed pressure of 10 bara. Feed to water trap from steam reformer with SCR = 2, temperature=750 °C and pressure as shown in the contour plot. (Module size equivalent to 60 tubes with 1 mol/min fuel feed)*

9.2.5 Effect of Water Trap on Hydrogen Recovery

A comparison of a system with and without a water trap and the effect on the hydrogen recovery efficiency can be seen in Figure 9.10. The effect of feed pressure and permeate pressure is shown. A water trap increases the hydrogen recovery

efficiency with a low feed pressure (3 barg) by up to 25%. At higher feed pressures the water trap shows a less significant improvement and with a feed pressure of 9 barg, the improvement is between 5 and 10%. A hydrogen recovery efficiency of over 90% requires a 10 bara feed pressure if a permeate pressure of 1 bara is assumed.

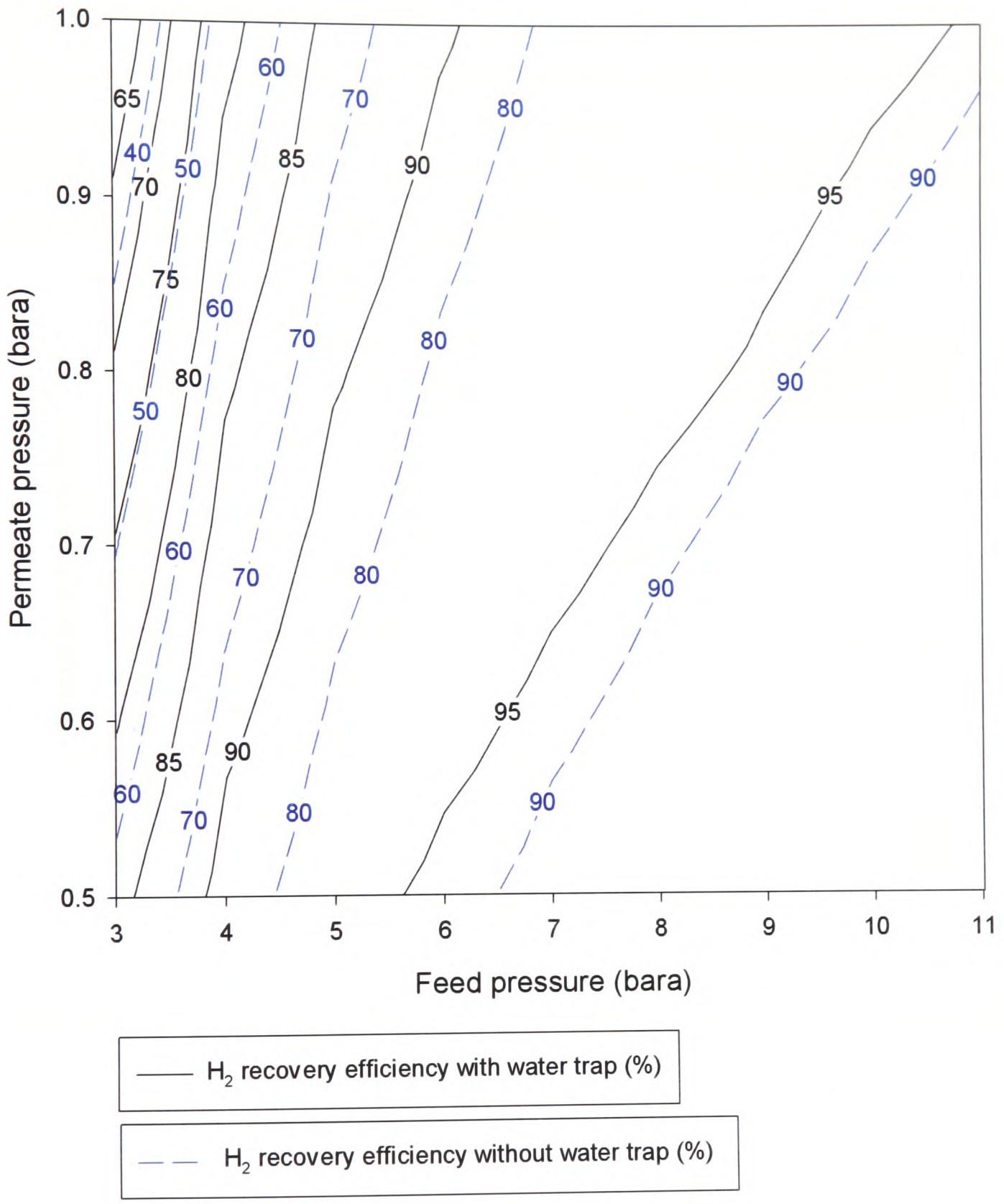

Figure 9.10: *160 tube membrane module showing effect of water trap on hydrogen recovery efficiency with varying feed and permeate pressure. Membrane operating temperature 440 °C. Feed gas from steam reformer operating at 750 °C, SCR = 2 with 1 mol/min iso-octane fuel feed.*

Decreasing the permeate pressure improves the H_2 recovery. Pressurising the liquid feed streams for the steam reformer is significantly more efficient in terms of pump work than compressing gas streams for the membrane module and this solution will be assumed in the subsequent full scale system simulations.

9.2.6 Fuel Feed and Module Size

The previous simulations have enabled some of the system conditions to be assessed, though the size of the membrane module needs to be determined to provide an adequate hydrogen recovery efficiency. The effect of feed flow per tube on the hydrogen recovery efficiency is shown in Figure 9.11.

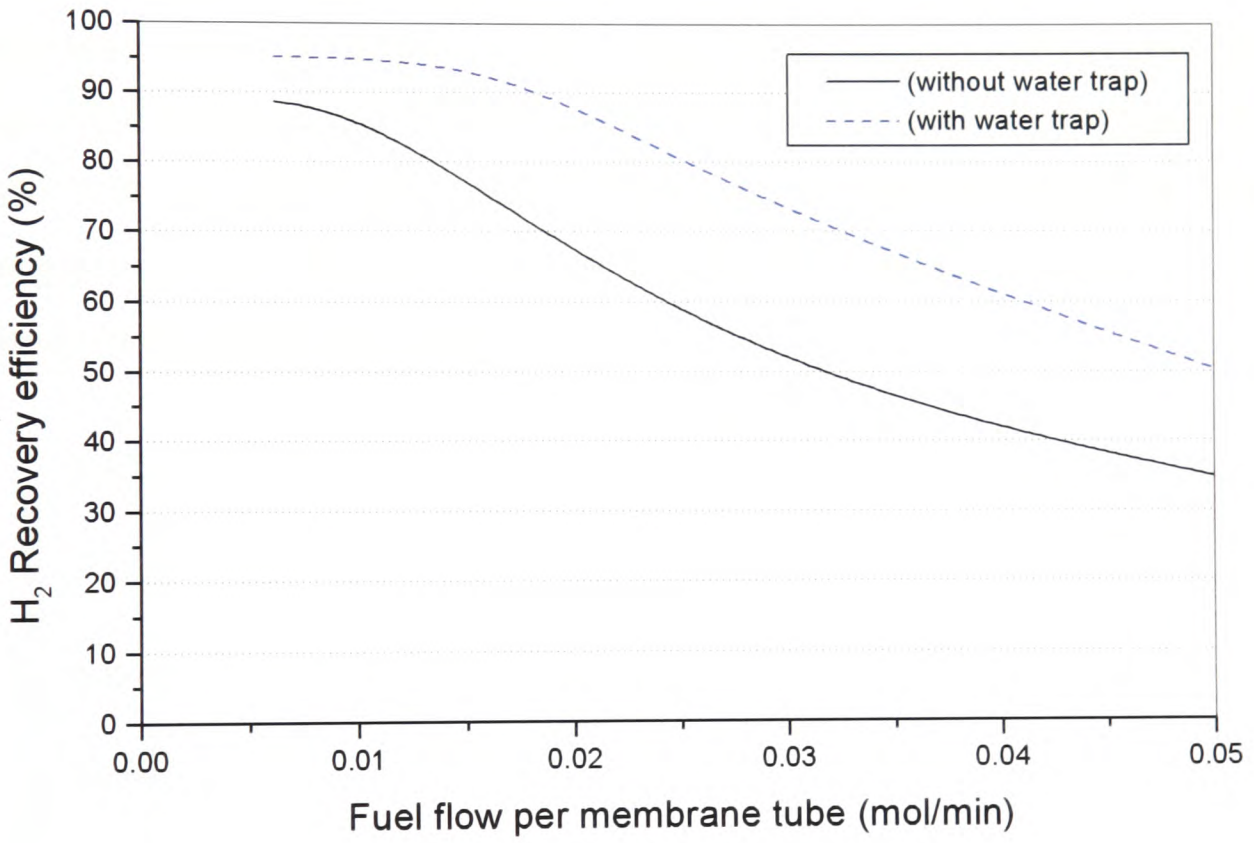

Figure 9.11: *Effect of fuel feed rate per tube on hydrogen recovery efficiency with a membrane module feed pressure of 10 bara. Feed gas from steam reformer operating at 750 °C and SCR = 2.*

The steam reformer is assumed to be running with an SCR = 2 and at a temperature of 750 °C. The feed pressure to the membrane module is 10 bara. A system with and without a water trap are shown for comparison. The flow rate of fuel is given per tube in the membrane module. If a particular hydrogen recovery is chosen then the results may be scaled up to calculate the membrane module size for any desired fuel flow

rate. With a fuel feed of 1 mol/min the hydrogen recovery efficiency is 90% with a module containing 50 tubes (0.02 mol/min per tube) and a water trap. Without the water trap the highest recovery efficiency envisaged is 80% with around 70 tubes for a 1 mol/min feed.

In order to scale the system to provide sufficient hydrogen for the application of a hydrogen refuelling station, the effect of fuel feed per tube on the hydrogen permeate flow per tube was investigated. The results of this are shown in Figure 9.12. The steam reformer is run with an SCR = 2 and at a temperature of 440 °C. For a given fuel feed rate per tube there is a point where increasing the number of tubes in the membrane module shows reduced returns in hydrogen permeate. This result has already been shown in Chapter 6. This is signified as the slope of the curve levels out above a fuel feed per tube of 0.025 mol/min. From analysis of both Figure 9.11 and Figure 9.12, a module size must be determined which provides an acceptable hydrogen recovery efficiency and also a sufficient hydrogen product to satisfy the demands of the refuelling station.

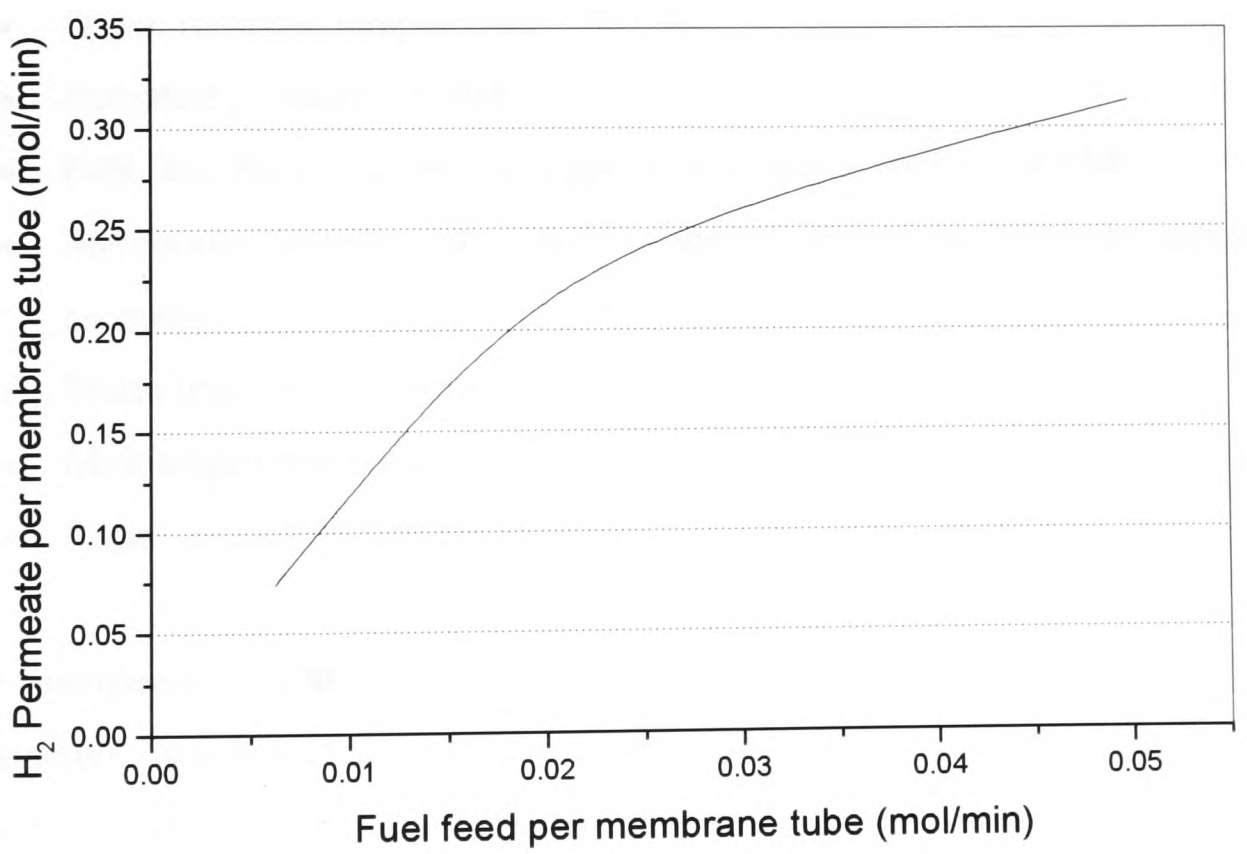

Figure 9.12: *Effect of fuel feed rate per tube on hydrogen permeate flow per tube with a membrane module feed pressure of 10 bara and water trap. Feed gas from steam reformer operating at 750 °C and SCR = 2.*

9.2.7 Hydrogen Refuelling Station Demands

Research carried out into the development of a hydrogen infrastructure in California estimates that a refuelling station will serve around 650 FCV cars per day or about 77 FC buses a day (Ogden, 1999). Assuming an annual average vehicle mileage of 11000 miles and gasoline equivalent fuel economy of 106 mpg leads to a FCV requiring 108.4 scf/day. A refuelling station producing 1 million scf/day would be able to fuel around 9223 vehicles. With a range of 425 miles, a refuelling station would serve 654 vehicles on a daily basis. 1 million standard cubic feet of hydrogen per day is equivalent to 28.32 million standard litres of hydrogen per day. This is equivalent to 1.26 million moles of hydrogen per day or 875 mol/min. The system simulations use this figure as a guide to sizing the refuelling station.

9.3 Full Scale System Model Simulations

Having performed the preliminary system simulations, the following conditions were decided upon:

- Steam reformer and membrane feed pressure - 10 bara
- Steam reformer temperature – 750 °C
- Permeate pressure - 1 bara
- Fuel feed flow - 100 mol/min iso-octane equivalent to 8.44 MW
- Membrane module size - 6000 standard membrane tubes to achieve 90% recovery
- Water trap temperature – 80 °C
- Multistage compressor – 5 stages with intercooling to produce 1000 bara
- Steam to Carbon Ratio – SCR = 2

The membrane module size, steam to carbon ratio and system pressure are parameters, which will be varied to assess the optimum operating conditions of the system. Scaling up from the 1 mol/min iso-octane feed to 100 mol/min is simply done by increasing the feed flow and adjusting the size of the membrane module multiplier blocks. The aim is to now increase the system efficiency to make effective use of all available heat streams.

9.3.1 Heat Exchangers

Heat exchangers play an important role heating the steam reformer, cooling the retentate combustion and minimising wasted heat from the system. Cooling is required in the steam reformer product stream in order to reach the dew point and remove water from the membrane feed stream. Heating is required to return this stream to the membrane operating temperature of 440 °C. Heating is also required to vaporise the water stream which is fed to the steam reformer. The arrangement of the heat exchangers is shown in Figure 9.1 and the Aspen flow sheet in Figure 9.13.

9.3.2 Design Optimisation and Constraints

The design optimisation was set to reduce the temperature of the combustion chamber product gas after it had provided the sufficient heat to sustain the steam reformer reaction. The constraints are summarised as follows and all have a tolerance of ± 1 °C:

- Heat exchanger minimum internal temperature approach ≥ 10 °C
- System exhaust temperature ≥ 50 °C
- Combustion temperature ≥ 760 °C to ensure heat transfer to steam reformer
- Combustion temperature ≤ 850 °C for material constraints
- Combustion temperature downstream of steam reformer ≥ 610 °C

The main tool used to ensure these constraints are met is the additional air which is supplied to the combustion chamber over the stoichiometric amount.

9.3.3 System Efficiency

The overall system was considered to determine the net system efficiency. This takes into account all of the work required to pressurise the fuel and water feed streams using the pumps as well as the work required to pressurise the hydrogen permeate to a storage pressure of 1000 bara. The net system efficiency is given by the following expression:

$$\eta = \frac{H_{2,permeate} \times LHV_{H_2} - W_{pump+compressor}}{Iso-Octane_{feed} \times LHV_{iso-octane}}$$

where: $LHV_{H_2} = 241.8$ kJ/mol

$LHV_{iso\text{-}ocatne} = 5065.4$ kJ/mol

The efficiency analyses are based on the lower heating values, LHV, of the fuel, which assumes any water produced in the combustion remains in vapour form. Use of LHV as opposed to higher heating values (HHV) is the conventional method for calculating efficiency.

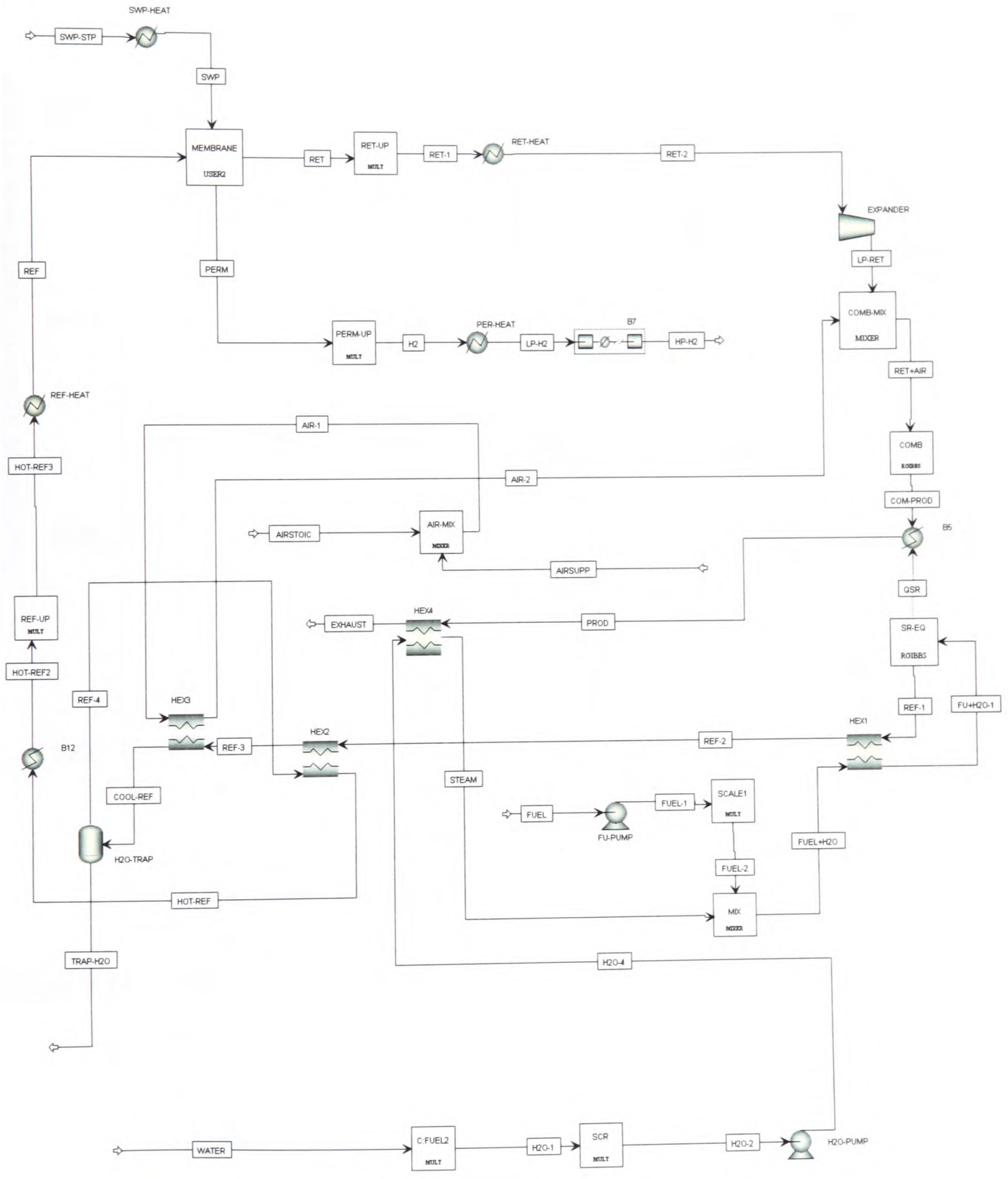

Figure 9.13: *Aspen flow sheet of hydrogen refuelling station.*

The sensitivity function within Aspen was used to vary the steam to carbon ratio and the membrane module size whilst upholding the constraints imposed on the system components. The effect of steam to carbon ratio and membrane module size is shown in Figure 9.14.

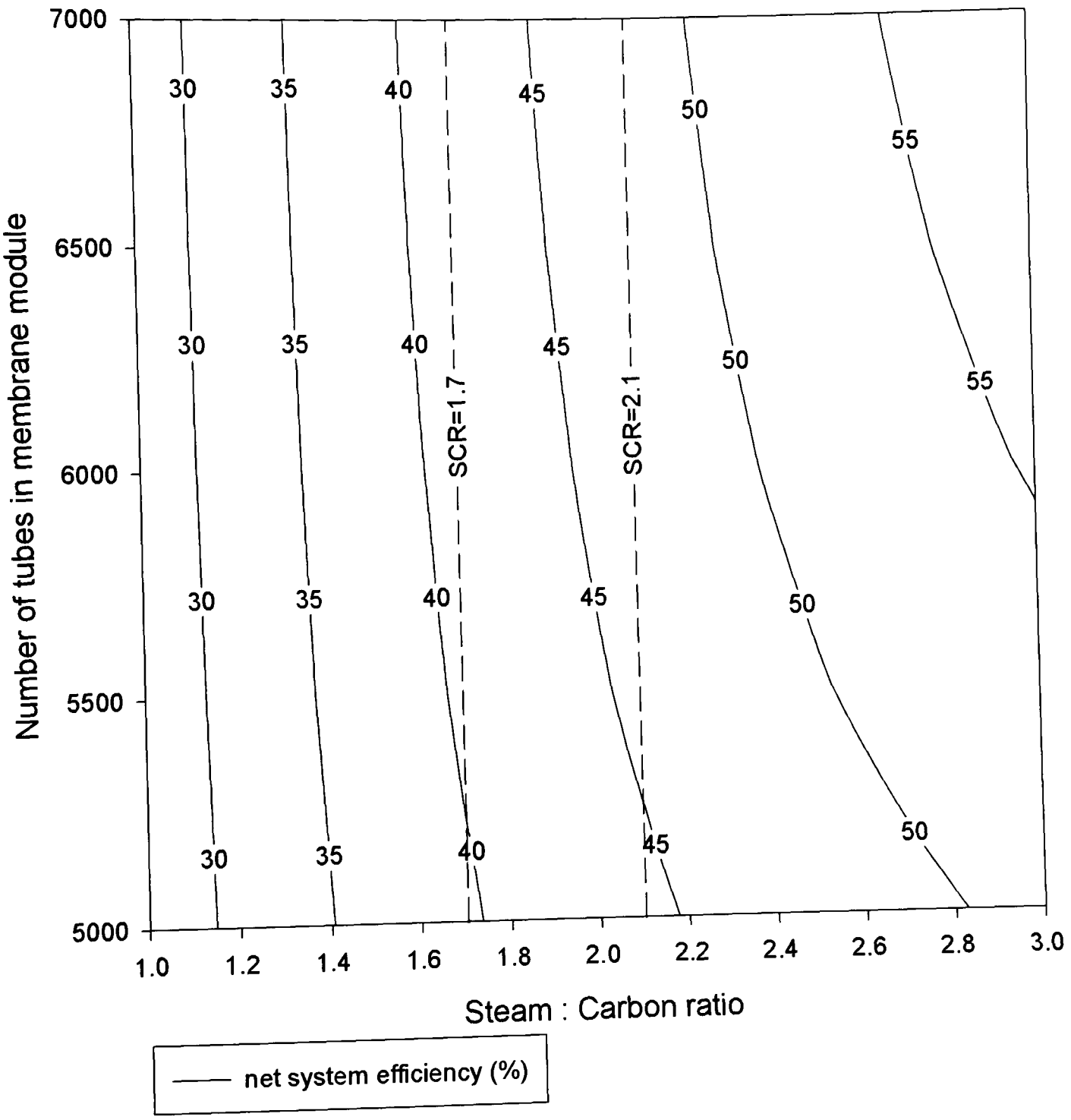

Figure 9.14: *Effect of SCR and membrane module size on overall system efficiency with an iso-octane fuel feed of 100 mol/min. Steam reformer operating at 10 bara and at a temperature of 750 °C. Membrane module operating at a temperature of 440 °C and with a feed pressure of 10 bara and permeate pressure of 1 bara.*

It can be seen that for a given steam to carbon ratio, increasing the number of tubes in the membrane module has a decreasing improvement on the system efficiency. With a steam to carbon ratio below around SCR = 1.6, there is little improvement in the system efficiency over the module size 5000 to 7000 tubes. This is shown by the near vertical orientation of the system efficiency contours. Above an SCR = 2, the increase in the number of tubes in the membrane module has a greater improvement as there is an increasing molar flow of hydrogen in the steam reformer product to purify and the larger the membrane module the more of this hydrogen is purified.

All of the constraints were met over the full range of steam to carbon ratio apart from constraints set on the heat exchangers. The dashed vertical lines, at SCR = 1.7 and SCR = 2.1, show the limits of steam to carbon ratio. At the limit of SCR = 2.1, the maximum system efficiency is around 46% with 7000 tubes. Outside of these limits, the temperature approach constraints in the heat exchangers are violated. With a steam to carbon ratio greater than SCR = 2.1, it is heat exchanger HEX3 in Figure 9.13 (component 6 in Figure 9.1) which limits any further increase in steam to carbon ratio. With a steam to carbon ratio less than SCR = 1.7, the limiting heat exchanger is HEX2 in Figure 9.13 (component 6 in Figure 9.1). Where the constraints are violated, temperature crossover occurs in these heat exchangers. The heat exchanger blocks used in the Aspen flow sheet enable zonal analysis to be carried out to determine the pinch points. These results are summarised in Section 9.3.4. With this arrangement of heat exchangers, which was used to optimise the usage of available heat within the system, there is therefore a limit to the steam to carbon ratio and consequently the system efficiency too. An alternative to this arrangement of heat exchangers is discussed in Section 9.3.5.

The other contour plot based on the results from this arrangement of heat exchangers can be seen in Figure 9.15. In this case the effect of steam to carbon ratio and the number of tubes in the membrane module on the hydrogen permeate flow rate is shown. Again, the steam to carbon ratio limits at SCR = 1.7 and SCR = 2.1 are shown as vertical dashed lines. The contours follow a very similar pattern to those for the overall system efficiency which would suggest that the increase in hydrogen permeate outweighs the extra compression work required to increase the purified hydrogen to a pressure of 1000 bara. Within the limits imposed by the heat exchangers on the steam

to carbon ratio, the hydrogen produced by the refuelling station would be sufficient to satisfy the requirements for the case of a 650 car/day refuelling station, which was estimated to be 875 mol/min, or 3.526 MW of hydrogen, over the 24 hour period. At the lowest point, 1000 mol/min would be produced and around 1225 mol/min at the highest.

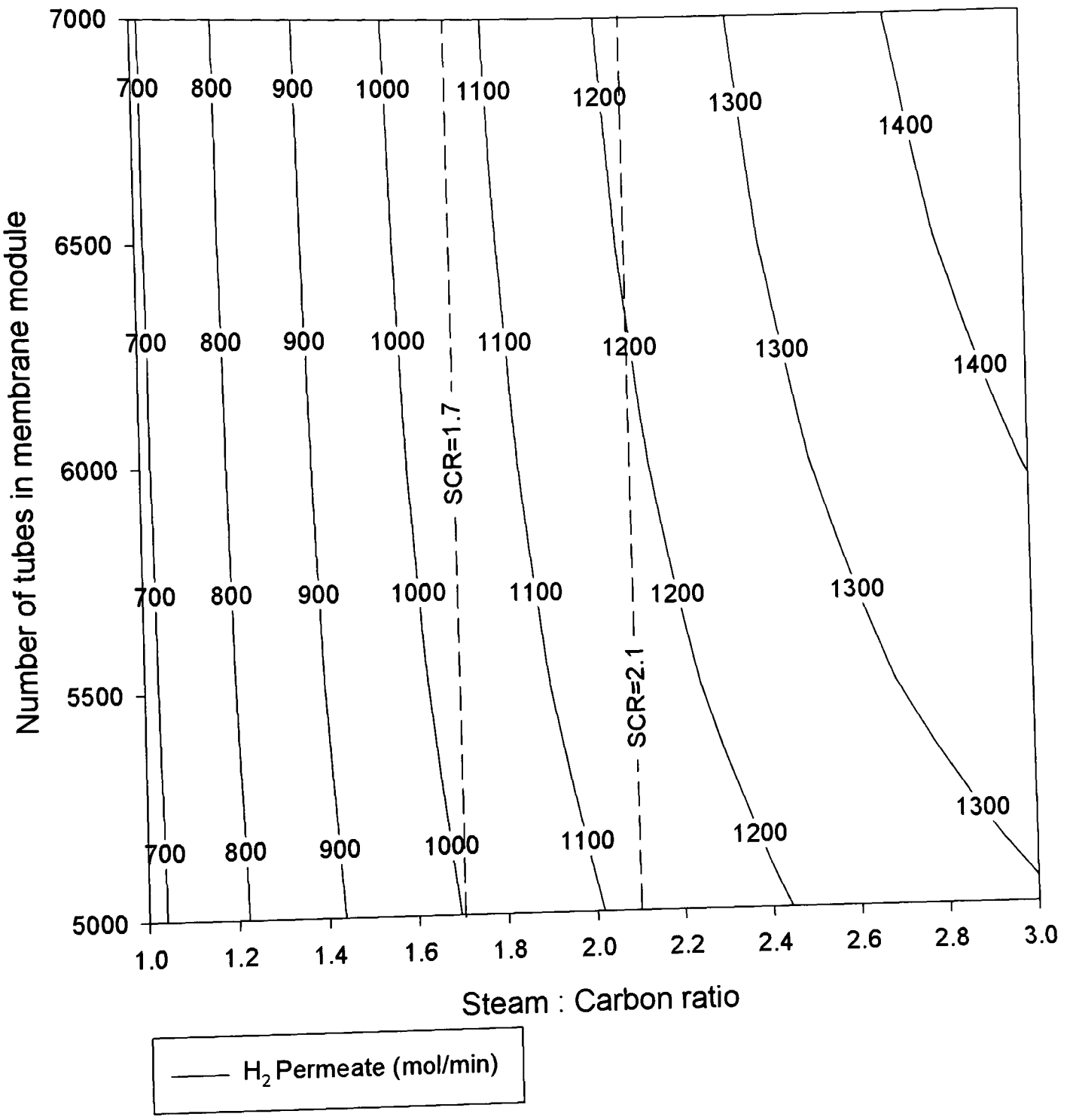

Figure 9.15: *Effect of SCR and membrane module size on hydrogen permeate flow rate with an iso-octane fuel feed of 100 mol/min. Steam reformer operating at 10 bara and at a temperature of 750 °C. Membrane module operating at a temperature of 440 °C and with a feed pressure of 10 bara and permeate pressure of 1 bara.*

The molar mass of iso-octane is 114.2 g/mol and by multiplying this figure by the 100 mol/min flow rate over a 24 hour period, a daily requirement of 16445 kg/day is obtained. Taking the density of iso-octane as 0.6919 g/ml, the daily volumetric requirement is 23770 litres/day. With a gasoline transporter having a capacity of 9200 gallons (34825 litres), a delivery every other day would be envisaged. The volumetric requirement per vehicle is found to be around 35 litres, which is the typical tank capacity of a small car. These results show that supplying a hydrogen refuelling station based on gasoline would be similarly practicable to supplying a conventional gasoline station.

A further simulation using a 50:50 mixture of iso-octane and toluene is discussed in Section 9.3.6. In order to compare the gasoline requirements assuming this new mixture, the same mass flow rate will be used i.e. 16445 kg/day or 11.42 kg/minute. The molar mass of toluene, C_7H_8, is 92.14 g/mol which results in a molar mass of 103.17 g/mol for the mixture. For comparison in the simulation, a molar flow rate of 110.7 mol/min will be implemented in the simulation.

A higher production rate would provide either excess hydrogen that may be used in ancillary equipment or, if required, time for system regeneration with an inert purge. The estimate for 875 mol/min assumes a certain fuel tank capacity (1530 scf hydrogen) and vehicle size, so this increased output from the refuelling station would be able to contend with some larger capacity vehicles running with larger powered fuel cell stacks. In all of these cases it is a question of balancing the number of palladium membrane tubes in the module with the system efficiency, hydrogen recovery efficiency, hydrogen production and system flexibility.

9.3.4 Pinch Point Analysis

In order to ensure heat transfer in the heat exchangers a minimum temperature difference must be maintained. Difficulties arise especially when there are phase changes occurring within the heat exchangers. Manually attempting to ensure these temperature differences are maintained and that there is no occurrence of temperature crossover is difficult. Aspen provides a feature which allows design specifications to be optimised whilst adhering to fixed constraints. The following figures provide a

summary of the zonal analysis of the heat exchangers at the limits of steam to carbon ratio highlighted in Section 9.3.2.

The first heat exchanger considered is HEX1 in Figure 9.13 (component 4 in Figure 9.1). The temperature-enthalpy plots are shown in Figure 9.16. The purpose of this heat exchanger is to utilise the hot outlet stream of the steam reformer (hot stream) to preheat the fuel and steam feed to the steam reformer (cold stream). In both the case with an SCR = 1.7 and an SCR = 2.1, there is no temperature crossover and a temperature difference of around 150 °C is maintained throughout the heat exchanger.

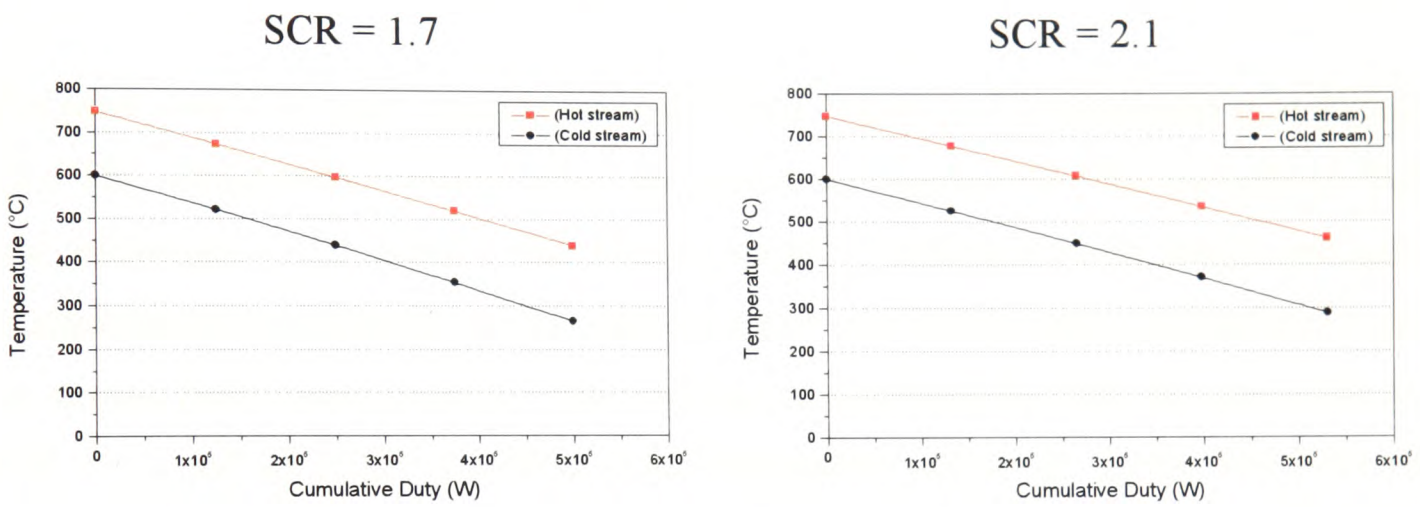

Figure 9.16: *Zonal analysis of heat exchanger 1 (HEX1 in Figure 9.13 and component 4 in Figure 9.1).*

The second heat exchanger considered is HEX2 in Figure 9.13 (component 5 in Figure 9.1). The temperature-enthalpy plots are shown in Figure 9.17. The purpose of this heat exchanger is to provide the first stage of cooling for the steam reformer product stream (hot stream) prior to the water trap, which requires a temperature of 80 °C. The cooling is provided from the water trap gas outlet stream (cold stream), which is required to be raised to the membrane module operating temperature of 440 °C. In the case with an SCR = 2.1, the temperature difference is maintained over the 10 °C limit. However in the case with an SCR = 1.7, the temperature profiles of the hot and cold streams come very close. In fact this actually violated the 10 °C temperature difference but there was no temperature crossover. It is this heat exchanger which prevents any operating condition with a lower steam to carbon ratio with the current system set-up.

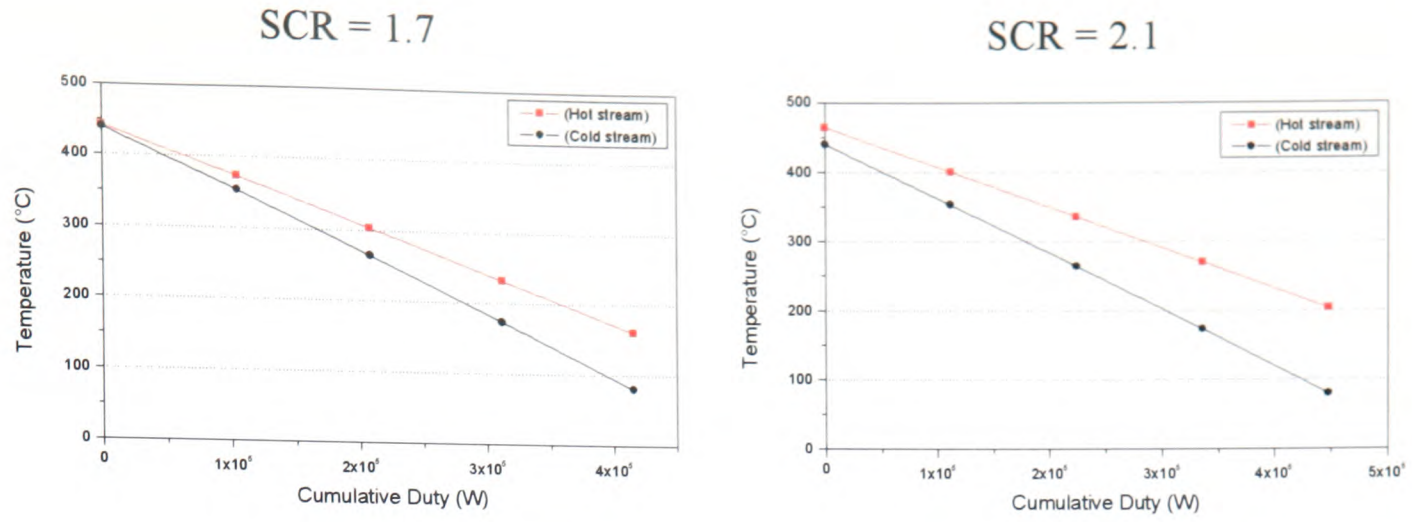

Figure 9.17: *Zonal analysis of heat exchanger 2 (HEX2 in Figure 9.13 and component 5 in Figure 9.1).*

The third heat exchanger considered is HEX3 in Figure 9.13 (component 6 in Figure 9.1). The temperature-enthalpy plots are shown in Figure 9.18. The purpose of this heat exchanger is to provide the second stage of cooling for the steam reformer product stream (hot stream) prior to the water trap and also provide pre-heating for the air stream (cold stream) before the combustion chamber. In both the case with an SCR = 1.7 and an SCR = 2.1 there is no temperature crossover. In the case with an SCR = 2.1, there is a temperature approach between the two streams, though this does not violate the 10 °C minimum temperature difference constraints. It is this heat exchanger which limits any further increase in steam to carbon ratio with this arrangement of heat exchangers as beyond SCR = 2.1, temperature crossover is observed. An alternative solution to overcome this limit is discussed in Section 9.3.5.

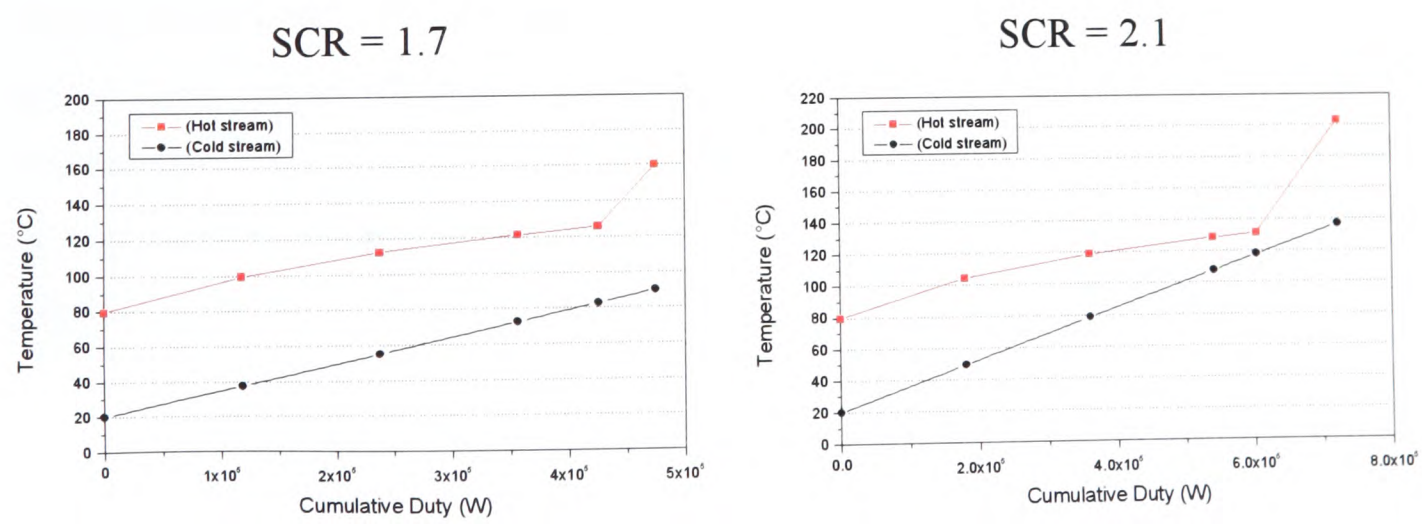

Figure 9.18: *Zonal analysis of heat exchanger 3 (HEX3 in Figure 9.13 and component 6 in Figure 9.1).*

The fourth and final heat exchanger considered is HEX4 in Figure 9.13 (component 3 in Figure 9.1). The temperature-enthalpy plots are shown in Figure 9.19. The purpose of this heat exchanger is to provide the heat for vaporising the water (cold stream) for the steam reformer by utilising any remaining heat in the combustion chamber outlet stream (hot stream). In both the case with an SCR = 1.7 and an SCR = 2.1 there is no temperature crossover. Notable is the phase change observed within the heat exchanger as the horizontal line in the cold stream profile.

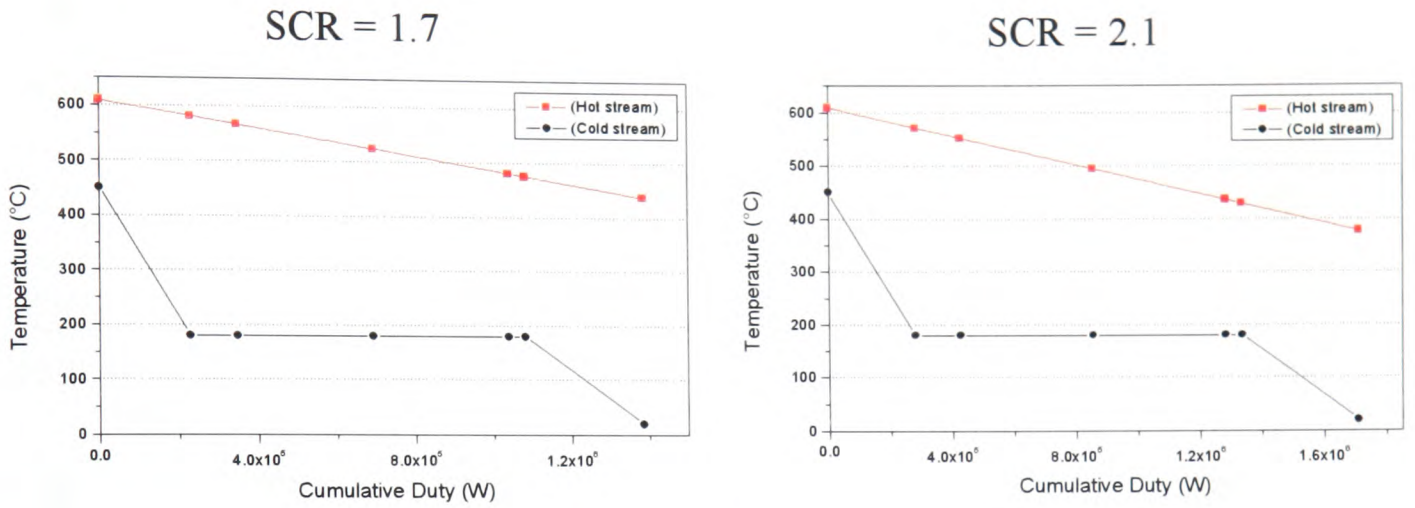

Figure 9.19: *Zonal analysis of heat exchanger 4 (HEX4 in Figure 9.13 and component 3 in Figure 9.1).*

9.3.5 Alternative System Arrangement with Cooler

In order to overcome the steam to carbon ratio limitations discussed previously, a heater block was implemented in place of the HEX3 to provide the second stage of cooling of the steam reformer product stream prior to the water trap. This removes the risk of temperature crossover occurring in the heat exchangers. Apart from the removal of a heat exchanger, the Aspen flow sheet is identical in all other respects to the previous flow sheet shown in Figure 9.13. The revised Aspen flow sheet is shown in Figure 9.20.

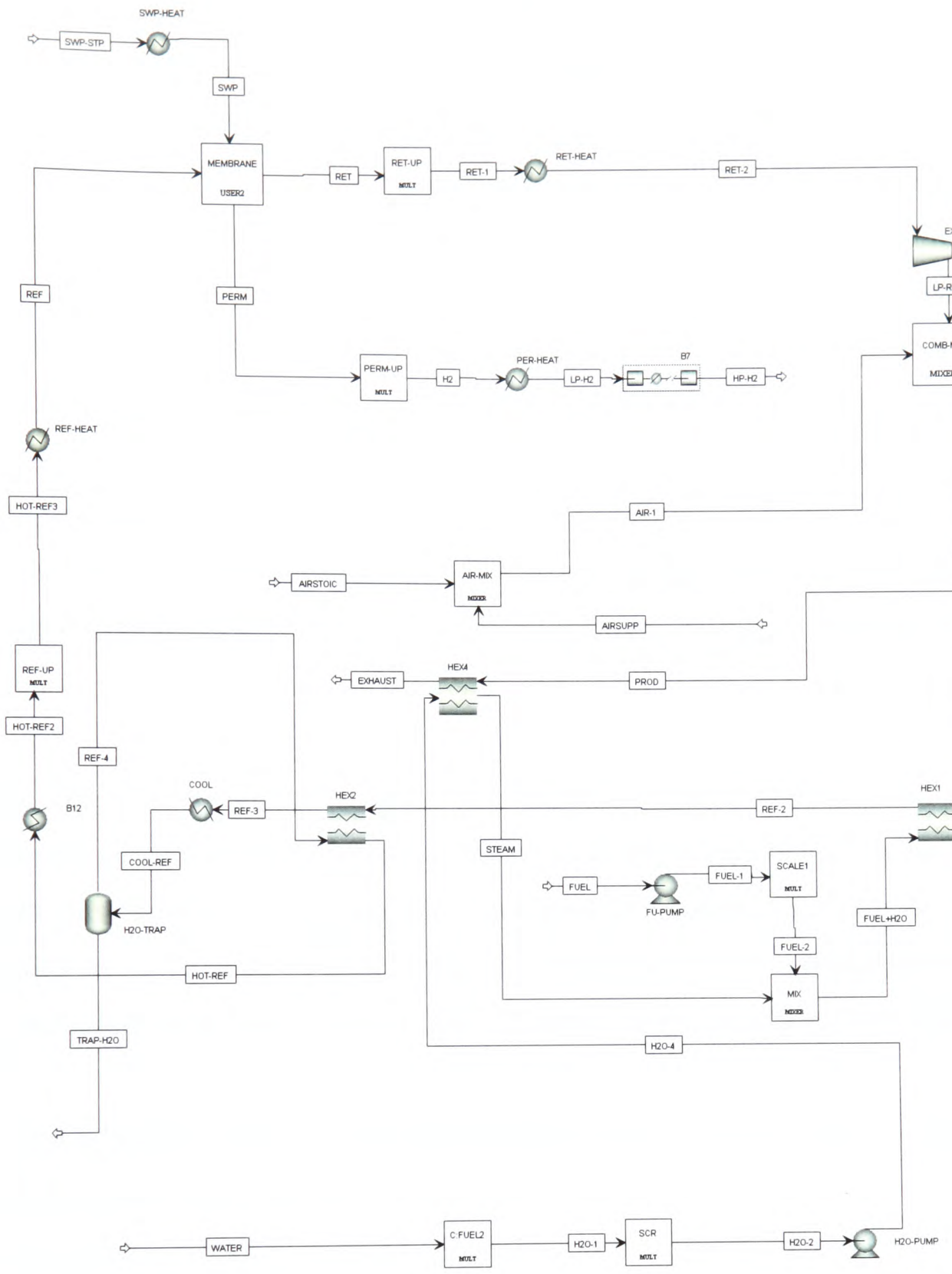

Figure 9.20: *Aspen flow sheet of hydrogen refuelling station incorporating a cooler.*

The heater block is actually used to cool the stream, though it is defined as a heater block in Aspen. Using this cooling block, the system does not suffer the same limitations in steam to carbon ratio as in the previous arrangement of heat exchangers. The calculations for system efficiency are still valid as excess heat is simply being dumped from the system. This is however a waste of the available heat and it would be useful to try and recapture this for use in other parallel processes which require lower grade heat at the refuelling station.

The other constraint, which has been lifted in this case, is that of the combustion stream temperature. It is assumed in this case that the material limits can be lifted where the combustion chamber is in effect a single unit in conjunction with the steam reformer so that there is direct heat transfer between the two. The effect of steam to carbon ratio and the membrane module size on system efficiency can be seen in Figure 9.21. The higher the steam to carbon ratio, the higher the system efficiency. As the number of tubes in the membrane module is increased, the effect of more tubes becomes less advantageous as the lines of system efficiency become more vertical.

The amount of hydrogen produced from the system is exactly the same as in the case of the system incorporating the heat exchangers as the steam reformer and membrane module conditions are identical in both simulations. As these values are identical, the results have not been redrawn here, but can be seen in Figure 9.15.

The effect of membrane module size and the steam to carbon ratio on the now theoretical combustion temperature stream is shown in Figure 9.22. It can be seen that with this removal of temperature constraint, increasing the steam to carbon ratio results in an increase in the theoretical temperature of the combustion stream. The combustion temperature is up to 1000 °C with a steam to carbon ratio, SCR = 2.8.

Again a balance must be achieved between steam to carbon ratio and the number of membranes in the clean-up module and the system efficiency that can be achieved. The optimum proposed system has operating conditions as follows:

- 6000 tube membrane module for 90% hydrogen recovery efficiency
- Steam to carbon ratio, SCR = 2.5 to ensure high fuel conversion
- Fuel feed flow 100 mol/min iso-octane to satisfy hydrogen demand
- Combined combustion chamber and steam reformer
- Water trap to increase hydrogen recovery efficiency
- Make effective use of heat exchangers for fuel and steam preheating though use of cooler before water trap

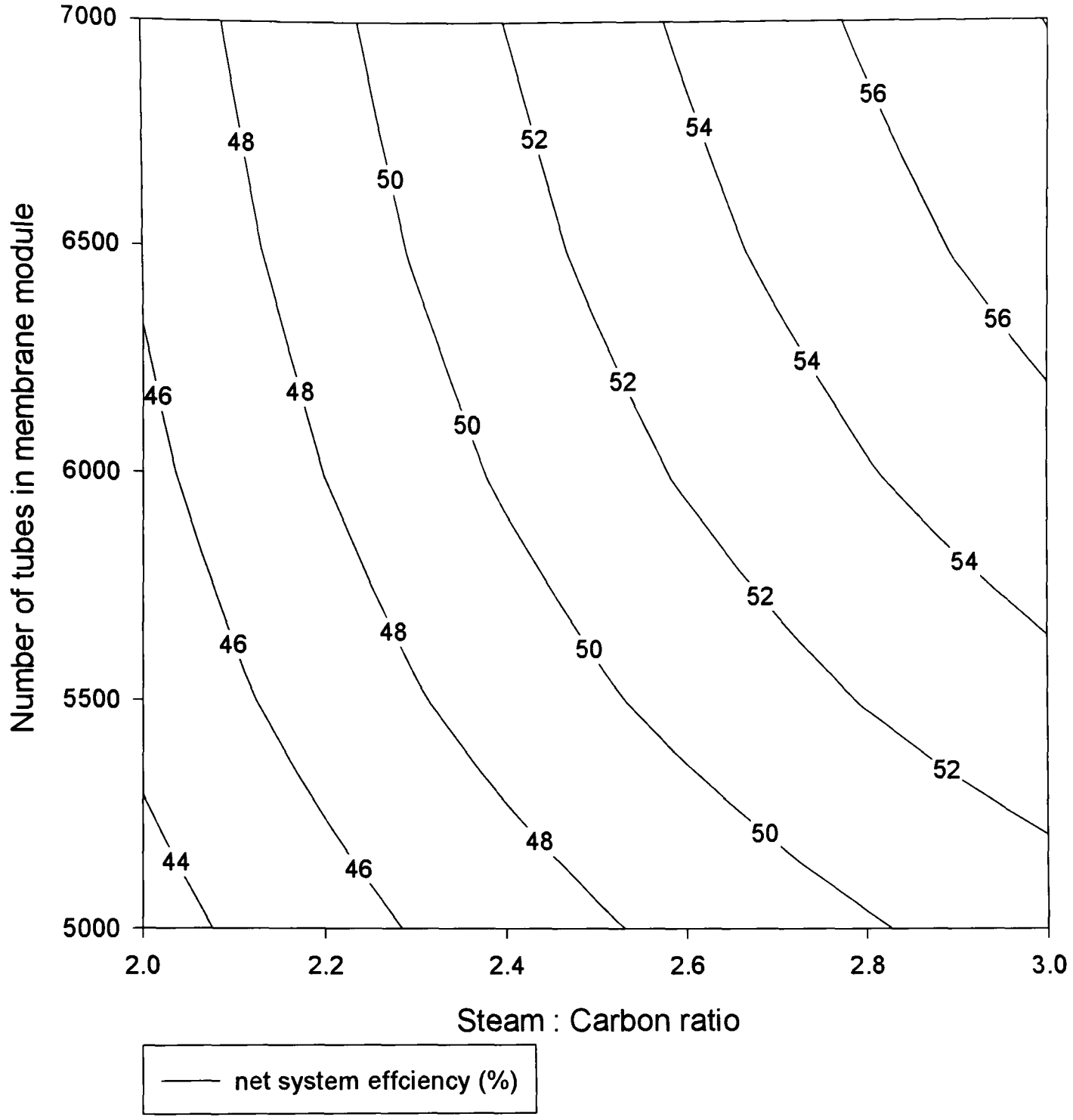

Figure 9.21: *Effect of SCR and membrane module size on overall system efficiency incorporating a cooler with an iso-octane fuel feed of 100 mol/min. Steam reformer operating at 10 bara and at a temperature of 750 °C. Membrane module operating at a temperature of 440 °C and with a feed pressure of 10 bara and permeate pressure of 1 bara.*

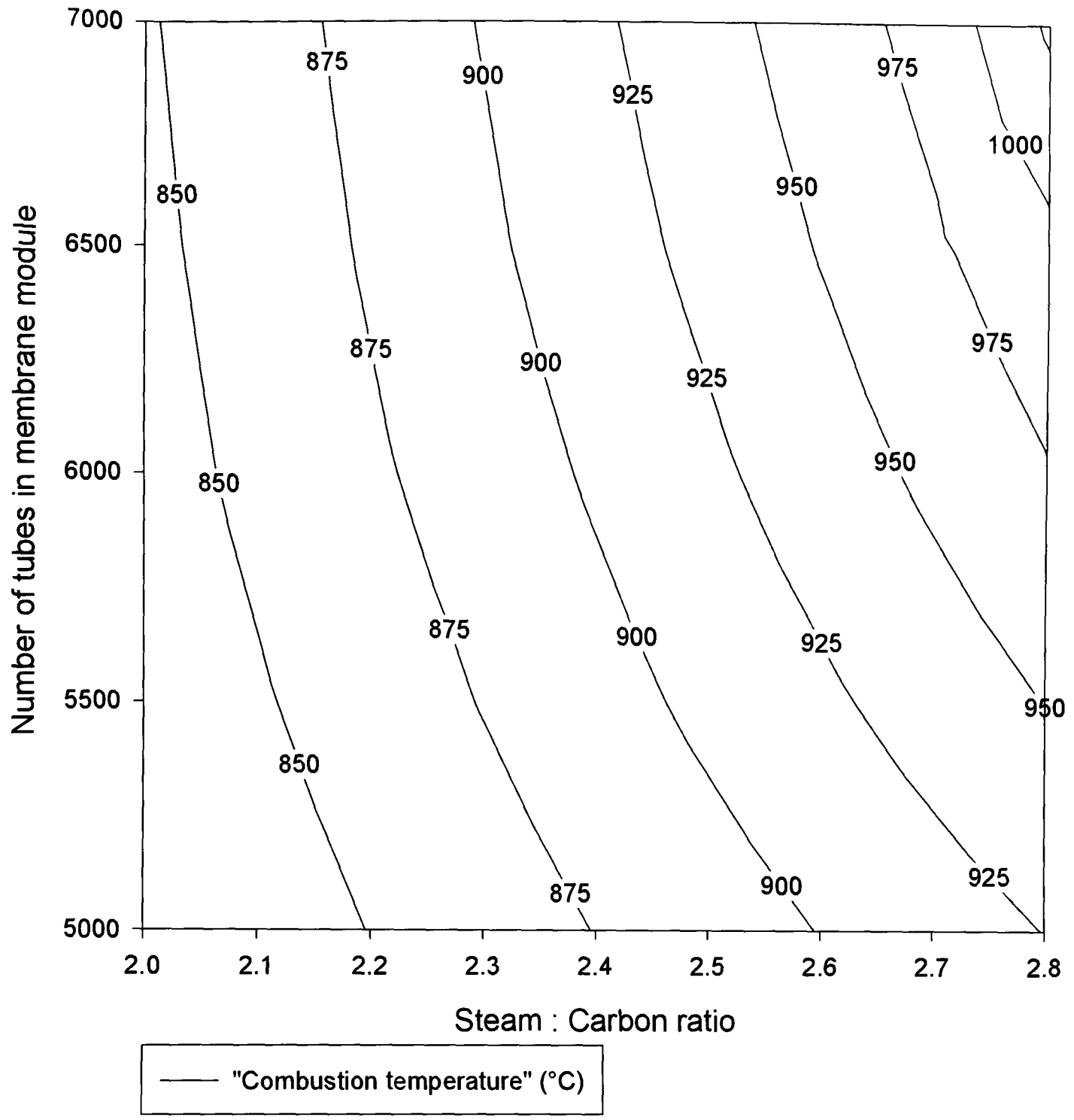

Figure 9.22: *Effect of SCR and membrane module size on the notional combustion temperature with an iso-octane fuel feed of 100 mol/min. Steam reformer operating at 10 bara and at a temperature of 750 °C. Membrane module operating at a temperature of 440 °C and with a feed pressure of 10 bara and permeate pressure of 1 bara.*

9.3.6 Alternative Fuel Composition

As gasoline has a hydrogen to carbon ratio of around H/C = 1.8 and iso-octane has a ratio of H/C = 2.25, an alternative fuel composition was considered to simulate a more gasoline like mixture. A simple 50:50 mixture of iso-octane and toluene, C_7H_8, having

a hydrogen to carbon ratio H/C ≈ 1.73 was proposed. The composition of the steam reformer product with varying steam to carbon ratio using this fuel mixture is shown in Figure 9.23. The proportion of hydrogen increases with increasing steam to carbon ratio reaching a plateau of just over 70% above an SCR = 3. The level of CO_2 increases with steam to carbon ratio whereas CO decreases, but is below around 10% above an SCR = 2. Methane falls quite rapidly as the steam to carbon ratio is increased and at an SCR = 2 it falls below 5%. Compared with the results for iso-octane in Figure 9.5, the composition of CO and CO_2 are very similar. The level of H_2 is initially around 10% higher with the iso-octane/toluene mix with an SCR = 1, but with increasing steam to carbon ratio, attains the same peak value of around 70%. The level of methane, CH_4, is though less for all steam to carbon ratios in the iso-octane/toluene mix case, being around 4% lower at around 1% with an SCR = 3. This suggests less hydrogen is wasted in the formation of methane.

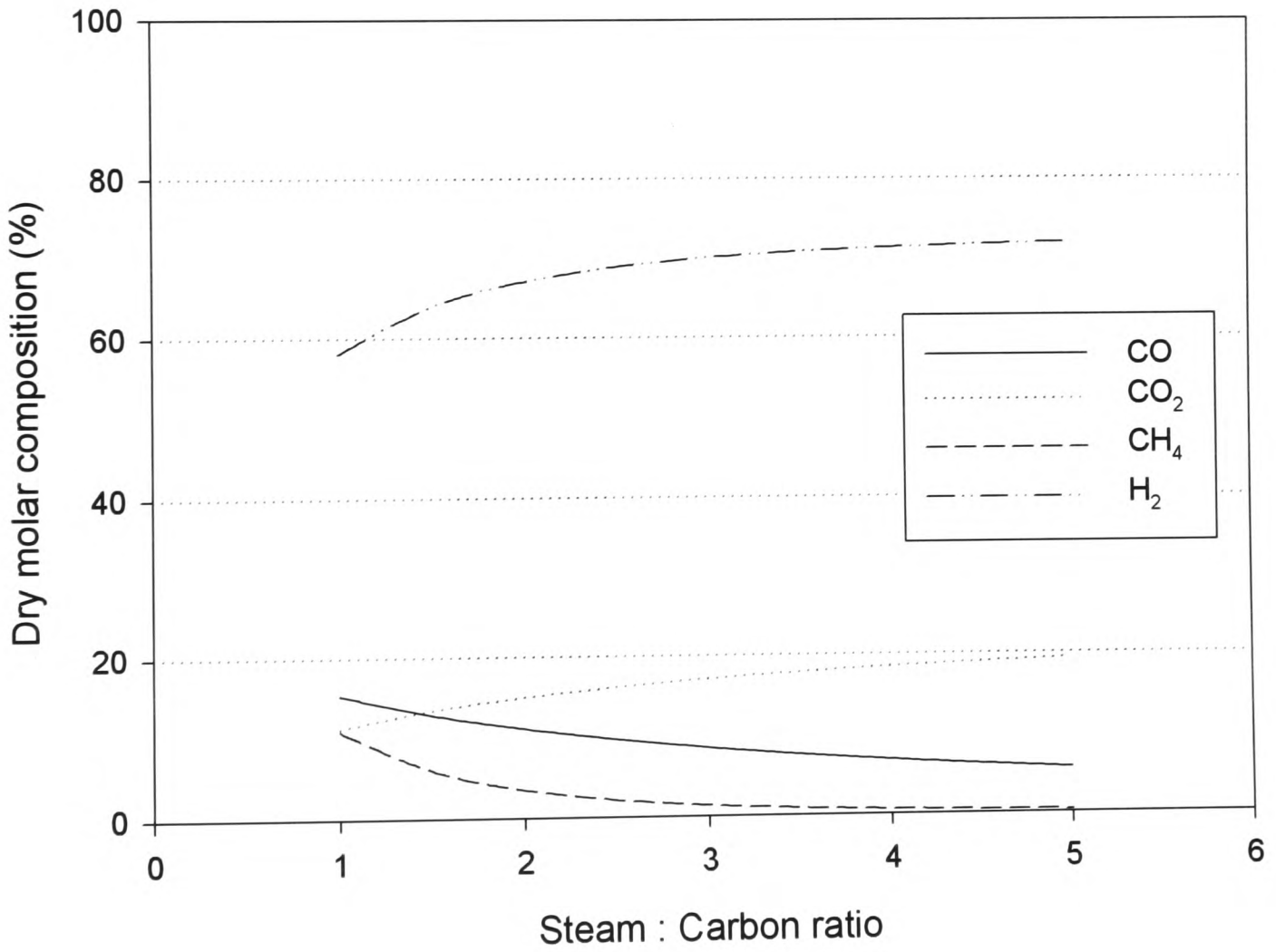

Figure 9.23: *Effect of Steam : Carbon ratio (SCR) on dry product composition of steam reformer with operating pressure of 10 bara and temperature of 750 °C with a 50:50 iso-octane: toluene fuel mixture.*

As discussed in Section 9.3.3, a practical comparison of the system models requires the use of identical mass flow rates rather than molar flow rates and so a feed of 110.7 mol/min was used in this case. Identical system analyses were performed as with the pure iso-octane case with the new fuel mixture and the system efficiency in relation to steam to carbon ratio and module size can be seen in Figure 9.24. A lower heating value for toluene of $LHV_{toluene}$=3734.3 kJ/mol was used.

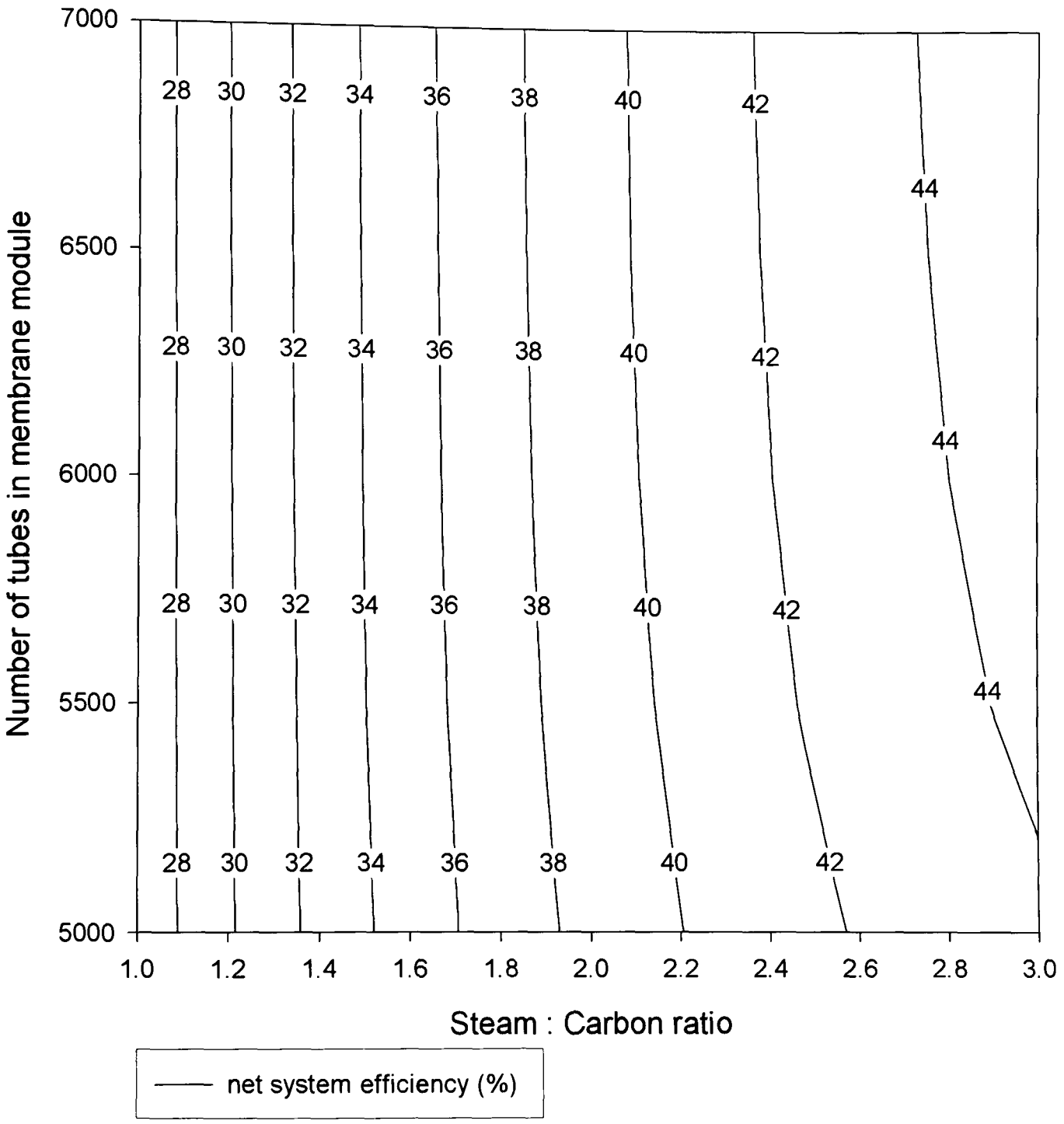

Figure 9.24: *Effect of SCR and membrane module size on overall system efficiency incorporating a cooler with a 50:50 iso-octane : toluene fuel feed of 110.7 mol/min. Steam reformer operating at 10 bara and at a temperature of 750 °C. Membrane module operating at a temperature of 440 °C and with a feed pressure of 10 bara and permeate pressure of 1 bara.*

A similar trend in system efficiency can be seen compared with the results for the pure iso-octane fuel case shown in Figure 9.14. With a membrane module size of around 6000 tubes, there is a 6% reduction in the overall system efficiency with the iso-octane/toluene mix when compared with the pure iso-octane case. Increasing the number of tubes in the membrane module has a similar effect in both cases, with no significant increase being observed below a steam to carbon ratio less than SCR = 2.6. The maximum system efficiency with a steam to carbon ratio, SCR = 3, and a membrane module containing 6500 palladium membrane tubes is of the order 45%. This is around 10% less than the pure iso-octane case and demonstrates the greater hydrogen available in the fuel.

Figure 9.25 shows the effect of steam to carbon ratio and membrane module size on the hydrogen permeate from a system with an iso-octane/toluene feed. The maximum hydrogen permeate within the range studied is around 1100 mol/min with a steam to carbon ratio of SCR = 3 and a membrane module containing 6500 tubes. When the results are compared with those for the pure iso-octane feed in Figure 9.15, it can be seen that the hydrogen production from the iso-octane/toluene system is considerably lower than in pure iso-octane case. With a steam to carbon ratio of SCR = 2, the level of hydrogen permeate is around 200 mol/min less than in the pure iso-octane simulation. Despite this reduction in hydrogen, the system is able to satisfy the requirements assumed for a hydrogen refuelling station supplying 650 vehicles when the steam to carbon ration is greater than SCR = 1.8.

These simulations have demonstrated the effect of the fuel composition used for the hydrogen refuelling station. It is possible to slightly oversize the system with a membrane module containing a larger number of tubes, though the additional hydrogen and system efficiency should be balanced with the increased cost of the system. Increasing the steam to carbon ratio may increase the hydrogen yield from the steam reformer, but this increase must also be balanced with the water requirements of the system and ensuring that there is sufficient retentate passing to the combustion chamber to provide the heat for the steam reforming reaction.

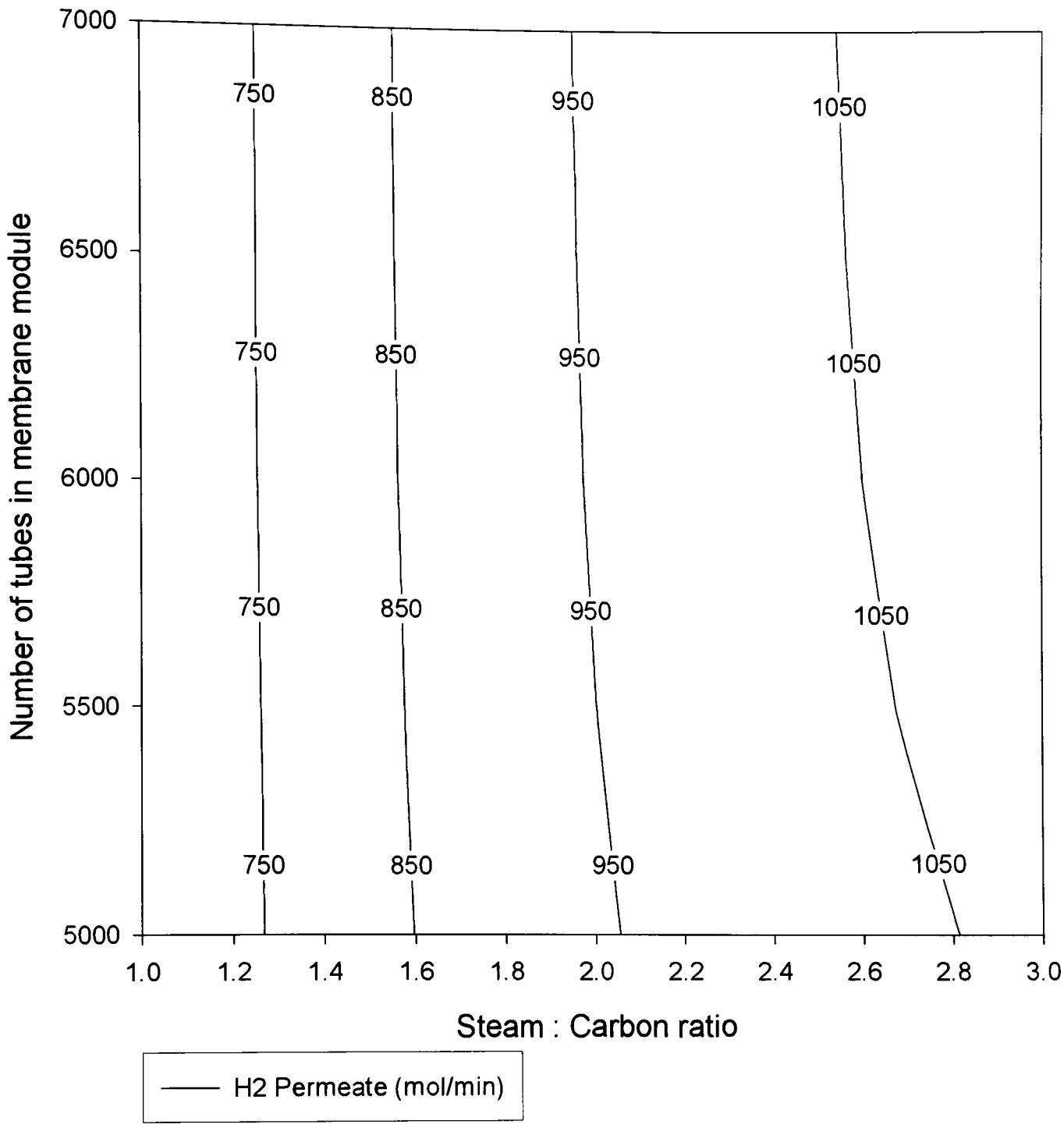

Figure 9.25: *Effect of SCR and membrane module size on hydrogen permeate flow rate with a 50:50 iso-octane: toluene fuel feed of 110.7 mol/min. Steam reformer operating at 10 bara and at a temperature of 750 °C. Membrane module operating at a temperature of 440 °C and with a feed pressure of 10 bara and permeate pressure of 1 bara.*

9.3.7 Water Management

The supply of pure water to the system can be an expensive exercise and so reducing the water requirement is beneficial. The hydrogen refuelling station was modified to

recirculate the water from the water trap and mix this with new water to produce the steam for the steam reformer. The Aspen flow sheet can be seen in Figure 9.26.

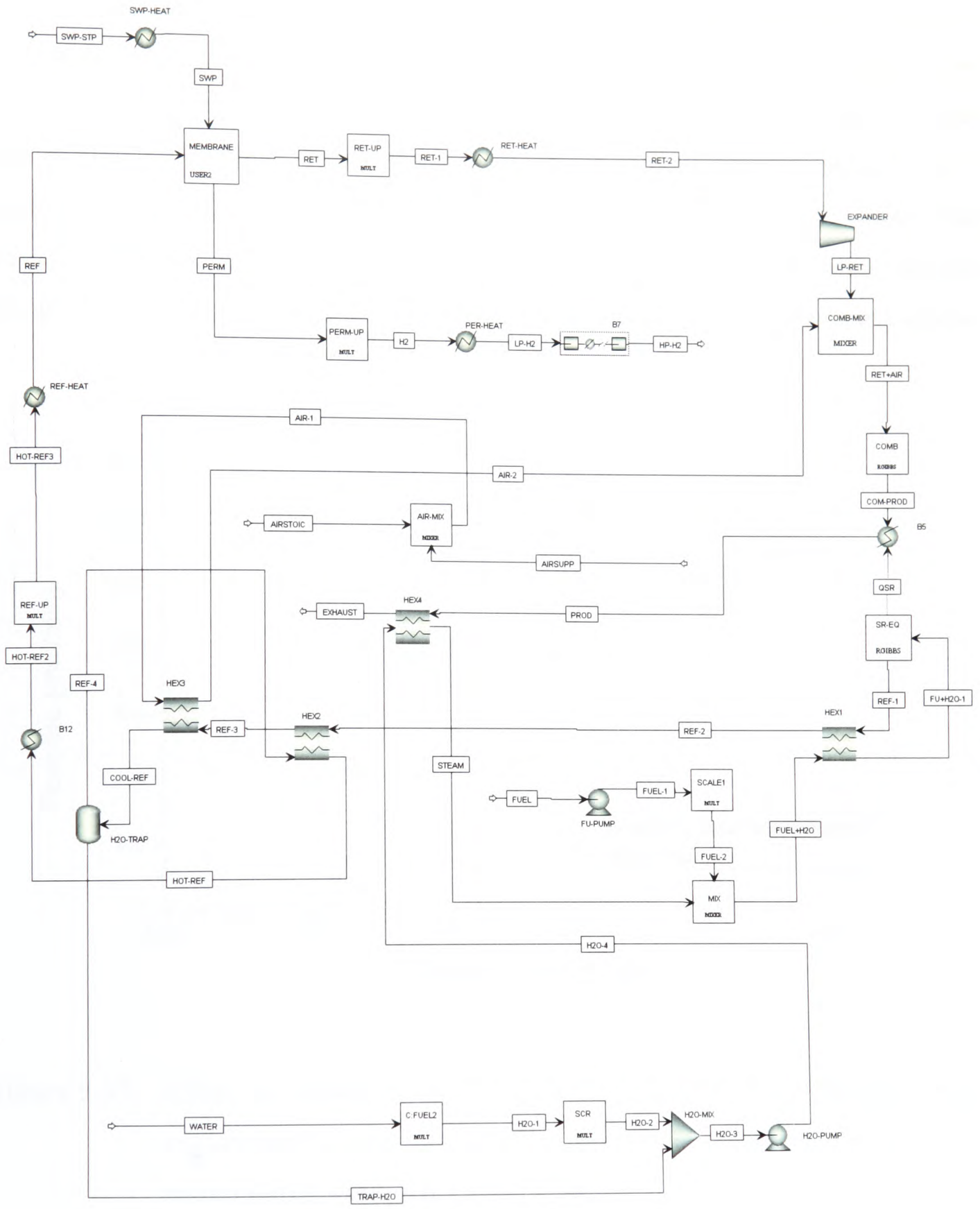

Figure 9.26: *Aspen flow sheet of hydrogen refuelling station incorporating water recirculation from water trap.*

A sensitivity analysis was performed to determine the flow rate of additional water that is required to fulfil the requirements as the steam to carbon ratio is increased from SCR = 1 to SCR = 3. The results of this can be seen in Figure 9.27. As the steam to carbon ratio is increased, the additional water requirement increases, but at a decreasing rate. With a steam to carbon ratio, SCR = 1, the additional water requirement is 640 mol/min which is over 3 times the flow of water from the water trap at just 160 mol/min. This difference decreases as the steam to carbon ratio is increased and finally crosses around a steam to carbon ratio, SCR = 2.7. In all cases though, additional water will be required to sustain the steam reforming reaction, though recirculation reduces this demand by up to half that without any recirculation.

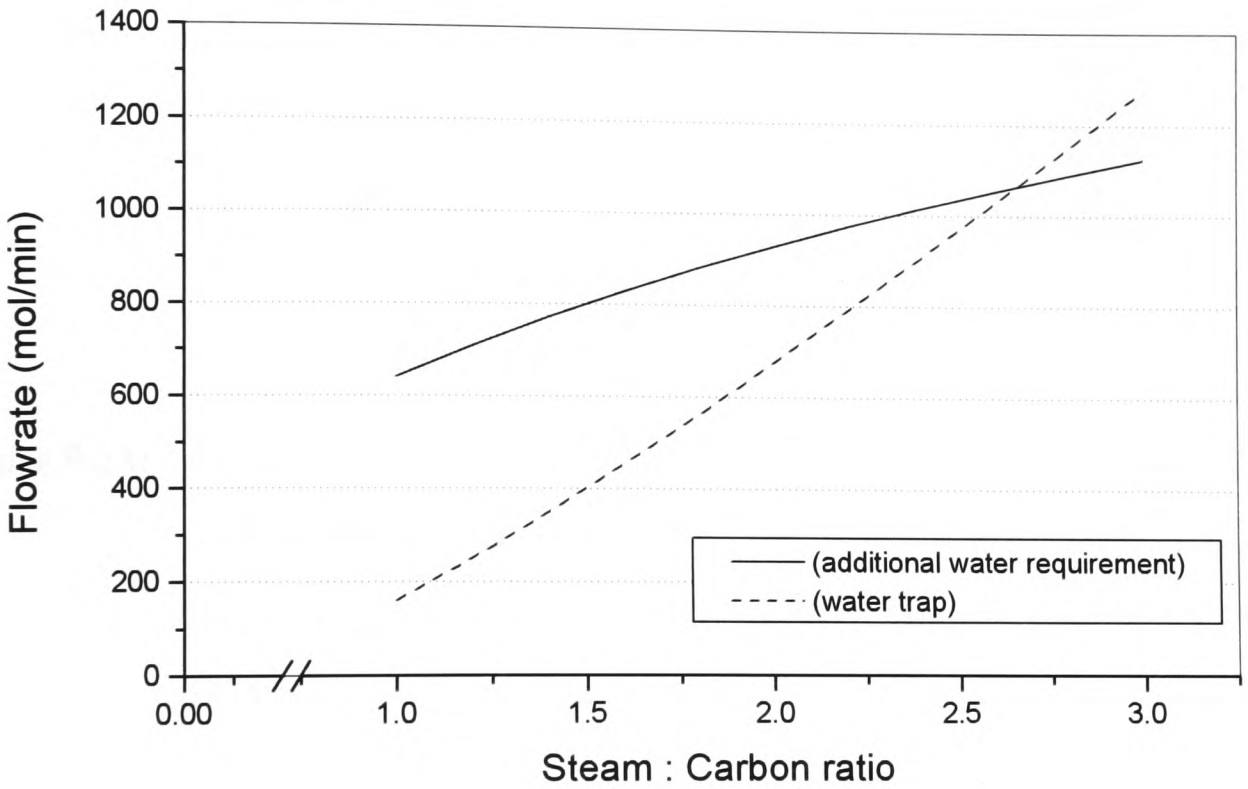

Figure 9.27: *Effect of steam to carbon ratio (SCR) on the additional water requirements for hydrogen refuelling system incorporating recirculating water from water trap.*

9.3.8 Energy Balance

In Figure 9.28, the power of system components such as the pumps and compressors is shown. Also shown is the fuel consumption and hydrogen production based on the lower heating values. The chart shows how much work is required to compress the

feed and product streams which have an impact on the system efficiency. Increasing the steam to carbon ratio requires additional pumping of water into the system, but the increased hydrogen production both outweighs this increased pump work and the additional hydrogen product compression and results in improved overall system efficiency (see Figure 9.21).

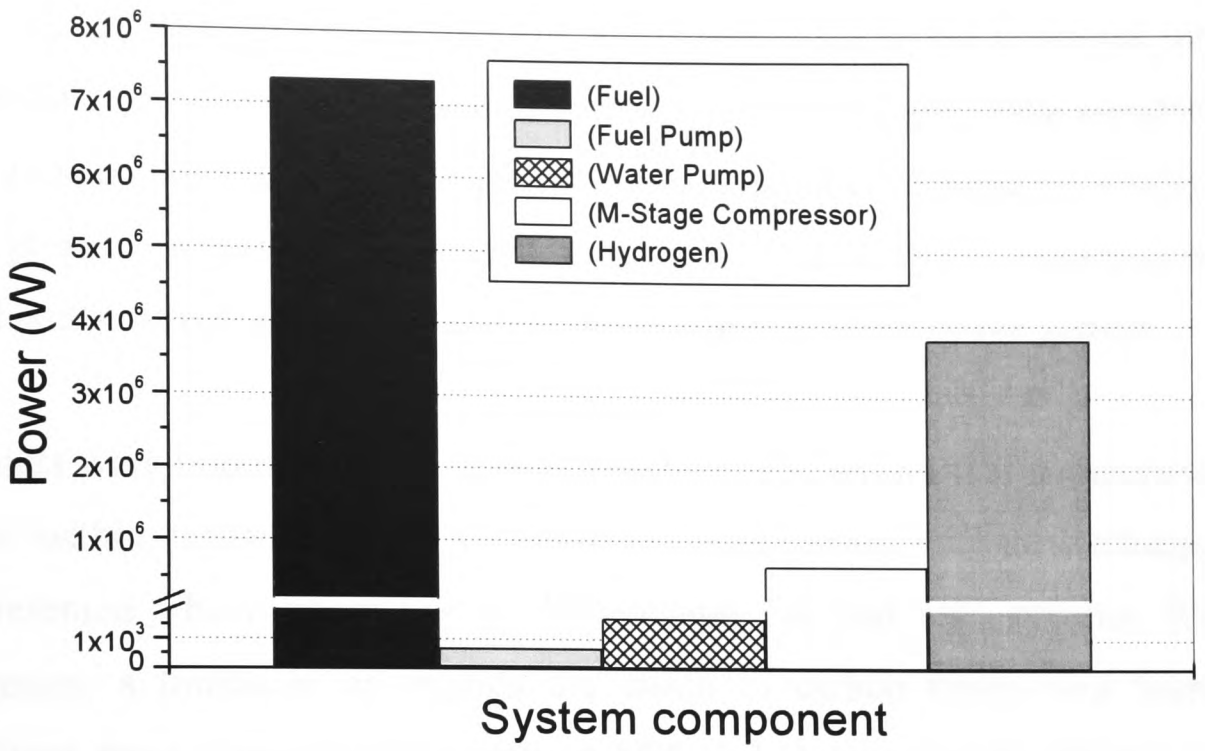

Figure 9.28: Comparison of power usage from system components with fuel feed and hydrogen product. System run with an SCR = 2.5, 100 mol/min iso-octane feed, 6500 tube membrane module and a 10 bara feed pressure.

9.4 Conclusions

The simulations within this chapter have shown that a palladium membrane module would provide a viable clean-up stage in a hydrogen refuelling station in terms of producing a high purity hydrogen product for delivery to fuel cell vehicles. It has been shown that a membrane module consisting of 6000 standard membrane tubes would provide a hydrogen recovery of at least 90% when operated at 440 °C, with a 10 bara feed pressure and running with iso-octane in the steam reformer. The incorporation of a water trap has increased the hydrogen partial pressure in the membrane feed stream and resulted in an improved hydrogen recovery. The retentate stream was used to provide the heating requirements for the steam reformer reaction and thus the

hydrogen in this retentate stream is not wasted. The simulation also feeds this retentate, which is at high pressure, through an expander. Although this work is not utilised in these simulations, some of the other ancillary equipment such as the fuel and water pumps could be powered from this source.

The hydrogen refuelling system was scaled to provide the hydrogen requirements of upwards of 650 fuel cell vehicles per day. For such a demand, the hydrogen refuelling station would be run continually and this would prolong the life of the membranes by avoiding undue thermal cycling. A parallel configuration of membranes would ensure a high pressure drop over the membranes as well as enabling membranes to be isolated and removed for maintenance without total shut down of the system.

Constraints were imposed on the system simulations to ensure that components were operated within realistic limits. An optimised arrangement of heat exchangers has been presented which makes use of the available hot and cold streams. With this arrangement, a limitation as regards the steam to carbon ration was found with temperature cross over occurring with an SCR>2.1. Increasing the steam to carbon ratio was found to increase the hydrogen production in the steam reforming reaction and reduce the level of methane. To overcome the heat exchanger limitations and improve hydrogen production, a cooler was incorporated to dump heat from the system. The overall system efficiency was found to be in the region of 52% with a steam to carbon ration of SCR = 2.5, an iso-octane fuel feed and a module consisting of 6000 individual membrane tubes. Further increases in membrane module size showed little additional improvement in system efficiency and 6000 tubes was therefore seen as an optimum module size.

Simulations were also carried out into the use of a 50:50 iso-octane/toluene gasoline mixture. This showed a reduction in the overall system efficiency of around 10%, due to the lower carbon to hydrogen ratio of the fuel mixture. It followed that the mixture would produce a less pure hydrogen product, though this still met molar requirements of the hydrogen refuelling station.

The water requirements of the system were also considered and a simulation into recirculating pure water from the water trap was performed. It was found that with a

steam to carbon ratio of SCR = 2.5, the recirculated water would have to be matched to suffice the steam reforming reaction. In all cases considered, additional water was required.

Estimating the full capital cost of a palladium membrane based hydrogen refuelling station is not within the scope of this work but some estimations can be made as to the material fabrication costs of the palladium membranes. The two key elements of the membrane module may be estimated as follows:

- Substrate material - $50/tube
- Palladium cost per tube - $8 (assuming 1g/tube)

The palladium cost is based on the current market price and this may fluctuate depending on the demand. The substrate material will reduce in cost if the volumes increase. The current $50/tube price is based on a batch of 1000 tubes. According to research by the Boston Consulting Group (Davies, 1976), every doubling of cumulative output reduces costs by about 20%. For one hydrogen refuelling station a tube price of $30/tube may be envisaged and if say 100 stations were build, this could be reduced further to less than $10. If one station is initially proposed, assuming a module consisting of 6000 membranes, this would make the cost of these two elements in the module around $228,000. On top of these costs would be the membrane processing and the high pressure module chamber costs. A batch process is currently envisaged for the membrane manufacture. Again, if the production scale were increased, then the price could be reduced.

In the longer term, an alternative membrane design might be employed, possibly consisting of flat membranes arranged like the plates in a heat exchanger. This might go some way to reducing the overall membrane module size though the key issue would be sealing the membranes. The advantages of a palladium membrane based purification system are the high purity of the hydrogen, due to the near infinite selectivity of the membranes, and the steady flow when compared with pressure swing adsorption methods. The valve control systems of pressure swing adsorption also make it complicated and expensive. A palladium membrane system is simpler in comparison and is also able to handle a variety of feed streams without significant

redesign. The disadvantages of a palladium membrane system are the elevated operating temperatures and the durability. However, a steady state application, such as the hydrogen refuelling station, would overcome this limitation.

10 Conclusions and Recommendations for Further Work

This work has revolved around the fabrication, testing and modelling of palladium membranes. A thin Pd/Ag membrane has been successfully applied to a porous ceramic support material using a proprietary Johnson Matthey process. The fabrication process on ceramic substrates was improved to consistently produce high quality membranes with low leaks (less than 2 sccm). The membranes were examined using optical and electron microscopy techniques and showed a consistent membrane thickness and alloy composition along the length of the tubes. The use of alternative ceramic substrate materials, including alternative topologies, should be investigated to further progress the quality and permeability of the membranes.

Work on plating stainless steel substrates has shown some extremely encouraging results and the development of improved barrier layers and surface finishing techniques would be recommended in any future work.

The membrane sealing solution was assessed and analysis of the mode of failure ascertained to suggest alternatives such as a hard sealing solution using Kovar collars and that of a soft single-ended sealing arrangement. The changing priorities of the project meant that the hard sealing solution was not fully investigated and for a commercially viable membrane, based on stainless steel, continued efforts in this area are suggested.

The palladium membranes were tested over a wide range of conditions to demonstrate for the first time the full effect of temperature and feed composition on the membrane performance. Flow testing with wet reformate mixtures showed a dilutory effect and that there was no presence of water gas shift under the conditions considered. Membranes of varying thickness were fabricated and tested to demonstrate the limitations of the current plating procedure.

The experimental testing was used in the development of a Fortran based model for implementation in Aspen Plus to simulate the hydrogen purification properties of the membranes. An extensive validation of the model with experimental data was performed under all envisaged operating conditions. Improvements to the model with regard to the effect of temperature and carbon monoxide were implemented. These showed excellent correlation to the experimental data and proved the robustness of the model.

Simulations were performed to demonstrate the improvement in hydrogen recovery efficiency achieved through the use of a combination of individual membrane tubes. The membrane configuration was examined and the results suggested that a parallel configuration would be preferable for optimum hydrogen recovery and for practical issues.

A hydrogen refuelling station was modelled using Aspen Plus incorporating a membrane module made up of a parallel configuration of standard membrane tubes. The refuelling station was sized to provide the requirements for around 650 vehicles a day based on work in the literature. The use of a water trap and a high pressure membrane feed was found to improve the hydrogen recovery efficiency of the module. Pressurising the liquid fuel and water feeds to the system was found to be less energy intensive than pressurising the steam reformer product prior to any membrane module. The purified hydrogen storage pressure was taken as 1000 bara, as a future pressure value has been envisaged for high pressure on-board storage systems of 750 bara.

The system was optimised through configuration of heat exchangers to exploit all the available hot and cold streams. Pinch point analysis was performed on the heat exchangers to ensure that no temperature cross over occurred. The limits of the system were ascertained and a solution was found to overcome these limits and increase the overall system efficiency. An overall system efficiency of around 52% was found with a membrane module size of 6000 tubes and a system pressure of 10 bara when running off an iso-octane fuel feed with a steam to carbon ratio of SCR = 2.5.

An alternative fuel mixture of 50:50 iso-octane/toluene for the steam reformer was considered and found to affect the overall system efficiency. Therefore the clean-up module would need to be sized for the fuel in question. The fuel requirements of the system were also estimated and found to be near identical to supplying a conventional gasoline station. The water requirements of the system were assessed and it was found that recirculation of the water trapped prior to the membrane module could reduce the water requirements for the system by half.

Palladium membranes offer the advantage of infinite selectivity and improved hydrogen flux in comparison with alternative membrane clean-up processes such as silica membranes. In their current form, the durability of palladium membranes when undergoing thermal cycling has been shown to be relatively poor. This is however due to the different expansion coefficients of the substrate and the membrane rather than the palladium silver alloy composition which has been chosen to hinder the phase change in the palladium on adsorption of hydrogen. Stainless steel substrates would more closely match the expansion of the membrane as well as providing a hard sealing option. Stainless steel supported membranes are seen as a likely successor to the conventional ceramic supported membranes and further efforts in this area are recommended. The long-term durability of the membranes is a characteristic which should be investigated as the hydrogen refuelling station model assumes that the system runs continuously.

Given the relatively high material costs of palladium and the requirement for a large number of tubes to fulfil the hydrogen requirements of a refuelling station, improvements in the membrane packaging may go some way to reducing the overall system cost. If the durability issues can also be overcome, a membrane-based system becomes increasingly attractive, offering greater selectivity over other hydrogen purification systems and an ability to cope with a wide range of feeds. Palladium membranes will continue to be used at the premium end of the hydrogen purification market in their unsupported form for applications in the semiconductor industry where extremely high purities are demanded and afforded. The application of supported palladium membranes for on-board reforming has however been abandoned as automotive manufacturers move away from the complexities associated with the reforming technology. It is unlikely that there will be sufficient renewable energy to

produce hydrogen by electrolysis in the near term. Supported membrane technology therefore provides a means of exploiting the existing gasoline infrastructure in order to aid the development and commercial success of fuel cell vehicles and lay the foundations of a hydrogen economy.

11 References

Aera (2004). Product Guide, http://www.advanced-energy.com/Upload/prod_guide.pdf

Amandusson, H., Ekedahl, L.-G., Dannetun, H. (2000). 'The effect of CO and O_2 on hydrogen permeation through a palladium membrane', *Applied Surface Science*, 153, pp 259-267

Amandusson, H., Ekedahl, L.-G., Dannetun, H. (2001). 'Hydrogen permeation through surface modified Pd and PdAg membranes', *Journal of Membrane Science*, 193, pp 35-47

Amphlett, J.C., Mann, R.F., Peppley, B.A., Roberge, P.R., Rodriges, A., Salvador, J.P. (1998). 'Simulation of a 250kW diesel fuel processor/PEM fuel cell system', *Journal of Power Sources*, 71, pp 179-184

Athayde, A.L., Baker, R.W., Nguyen, P. (1994). 'Metal composite membranes for hydrogen separation', *Journal of Membrane Science*, 94, pp 299-311

Bacon, F.T. (1969). 'Fuel Cells, Past, Present, and Future', *Electrochemica Acta*, 14, pp 569-585

Bassler, B.T., Malanga, D., Villani, M., Steinberg, J. (2002). 'A solution to kirkendall voiding in MLCC's through end termination composition and processing', http://www.4hcd.com/techpprs/absolut

Bennet, S. (2001). *Membrane flow testing*. Technical Report, Johnson Matthey Technology Centre, UK

Bird, R.B., Stewart, W.E., Lightfoot, E.N. (1960). *Transport Phenomena*. John Wiley & Sons, US

Bosco, R., Kamath, B.V., Rao, K.V., Rao, G.S., Krishnamurthy, K.R. (1998). 'Alumina through sol-gel route : influence of preparation parameters', *Studies in Surface Science and Catalysis*, 113, pp 591-598

Burch, R. (1969). 'On the role of silver atoms in the adsorption of hydrogen by palladium-silver alloys', *Solid State Communications*, 7, pp 1313-1317

Castro, F.J., Meyer, G., Zampieri, G. (2002). 'Effects of sulphur poisoning on hydrogen desorption from palladium', *Journal of Alloys and Compounds*, 330-332, pp 612-616

Chabot, J., Lecomte, J., Grumet, C., Sannier, J. (1988). 'Fuel clean-up system: poisoning of palladium-silver membranes by gaseous impurities', *Fusion Technology*, 14, pp 614-618

Chen, E. (1999). *The Way Fuel Cells Work*. Department of Engineering Science, University of Oxford, UK

CNN website, (2004). http://www.cnn.com

Collins, J.P., Way, J.D. (1993). 'Preparation and characterisation of a composite palladium ceramic membrane', *Ind. Eng. Chem. Res.*, 32, pp 3006-3013

Coulson, J.M., Richardson, J.F., (1998). *Chemical Engineering Volume 1 – Fluid Flow, Heat Transfer and Mass Transfer.* 5th edition. Butterworth-Heinemann, Bath

Coulson, J.M., Richardson, J.F., (1998). *Chemical Engineering Volume 2 – Particle Technology and Separation Processes.* 5th edition. Butterworth-Heinemann, Bath

Das, D., Veziroglu, T.N. (2001). 'Hydrogen production by biological processes : a survey of literature', *International Journal of Hydrogen Energy*, 26, pp 13-28

Davies, D., Banfield, T., Sheahan, R. (1976). *The Humane Technologist*, Oxford University Press

De Lange, R.S.A., Keizer, K., Burggraaf, A.J. (1995). 'Analysis and theory of gas transport in microporous sol-gel derived ceramic membranes', *Journal of Membrane Science*, 104, pp 81-100

Dempsey, R.P. (2001). 'Retail Supply of Hydrogen for Fuel Cell Vehicles', *Delegate Manual*, Seventh Grove Fuel Cell Symposium: Commercialising Fuel Cells: The Outstanding Issues, London, O8.2

Department for Transport - UK website, (2004), http://www.dft.gov.uk

Doyle, M.L. (1997). *Gas Separation Devices.* Johnson Matthey Patent, WO9746482

Duke, M.C., Diniz da Costa, J.C., Gray, P.G. (2003). *Molecular sieve silica membranes for H_2/CO separation,* Department of Chemical Engineering, University of Queendsland, Australia

Duke, M.C., Diniz da Costa, J.C., Lu, G.Q., Petch, M.,Gray, P.G. (2002). *Ultramicroporous membranes for hydrogen separation,* Department of Chemical Engineering, University of Queensland, Australia

Edland, D. (2003). *A membrane reactor for H_2S decomposition*, Bend Research Inc, Oregon, US

Edwards, N., Ellis, S.R., Frost, J.C., Golunski, S.E., van Keulen, A.N.J., Lindewald, N.G., Reinkingh, J.G. (1998). 'On-board hydrogen generation for transport applications: the HotSpot methanol processor', *Journal of Power Sources*, 71, pp 123-128

Emonts, B., Bøgild Hansen, J., Schmidt, H., Grube, T., Höhlein, B., Peters, R., Tschauder, A. (2000). 'Fuel cell drive system with hydrogen generation in test', *Journal of Power Sources*, 86, pp 228-236

European Community, (2003). Plasma and membrane supported catalytic gasoline fuel processor using hydrogen selective membranes - final technical report, Energy, Environment and Sustainable Development Project

Evans, J. (2001). *Temperature effect on Pd membranes*, Technical Report, Johnson Matthey Technology Centre, UK

Evans, J. (2001). *CO poisoning on Pd membranes*, Technical Report, Johnson Matthey Technology Centre, UK

Fairlie, M.J., Scott, P.B. (2001). *Filling up with hydrogen 2000*, Stuart Energy, California, USA

Financial Times Website, (2004), http://specials.ft.com/commodities/COM210504.pdf

Flanagan, T.B., Wang, D., Shanahan, K.L. (2000). 'Inhibition by gaseous impurities of hydrogen adsorption by Pd and by internally oxidized Pd-Al alloys', *Phys. Chem. Chem. Phys.*, 2, pp 4976-4982

Flynn, P.C. (2002). 'Commercialising an alternate vehicle fuel: lessons learnt from natural gas for vehicles', *Energy Policy*, 30, pp 613-619

Fuel Cells Bulletin, (2004), Kobe Steel develops 1000 bar compressor for FCV hydrogen stations.

Fuel Cell Today website, (2002), http://www.fuelcelltoday.com/FuelCellToday/EducationCentre

Geiger, S. (2004). Fuel cell market survey: automotive hydrogen infrastructure, Fuel Cell Today, UK

Glasstone, S. (1950). *Textbook of physical chemistry*, Van Nostrand, New York

Grashoff, G.J., Pilkington, C.E., Corti, C.W. (1983). 'The purification of hydrogen – a review of the technology emphasising the current status of palladium membrane diffusion', *Platinum Metals Review*, 27, pp 157-168

Grove, W.R. (1839). 'On voltaic series and the combination of gases by platinum', *Philosophical Magazine and Journal of Science*, 14, 86, pp 127-130.

Grove, W.R. (1842). 'On a gaseous voltaic battery', *Philosophical Magazine and Journal of Science*, 121, 140, pp 417-420.

Hollis, J., (2003). 'BMW AG - Hydrogen as a car fuel', IChemE Energy Conversion Technology Subject Group, Sourcing the Hydrogen Economy Seminar, London

Holleck, G.L. (1970). 'Diffusion and solubility of hydrogen in palladium and palladium-silver alloys', *Journal of Physical Chemistry*, 74, 3, pp 503-511

Hou, K., Hughes, R. (2002). 'The effect of external mass transfer, competitive adsorption and coking on hydrogen permeation through thin Pd/Ag membranes', *Journal of Membrane Science*, 206, pp 119-130

Hou, K., Hughes, R. (2003). 'Preparation of thin and highly stable Pd/Ag composite membranes and simulative analysis of transfer resistance for hydrogen separation', *Journal of Membrane Science*, 214, 43-55

Hunter, J.B. (1963). Symposium on the Production of Hydrogen, American Chemical Society, New York, 1963

Hurlbert, R.C., Konecny, J.O. (1961). 'Diffusion of hydrogen through palladium', *The Journal of Chemical Physics*, 14, 2, pp 655-658

Itoh, N., Wu, T-H., Haraya, K. (1995). 'Two- and three-dimensional analysis of diffusion through a dense membrane supported on a porous material', *Journal of Membrane Science*, 99, pp 175-183

Jayaraman, V., Lin, Y.S. (1995). 'Synthesis and hydrogen permeation properties of ultrathin palladium-silver alloy membranes', *Journal of Membrane Science*, 104, pp 251-262

Jemaa, N., Shu, J., Kaliguine, S., Grandjean, B.P.A. (1996). 'Thin palladium film formation on shot peening modified porous stainless steel substrates', *Ind. Eng. Chem. Res.*, 35, pp 973-977

Jobson, H. (2002). X-Ray diffraction analysis of sol-gel, Johnson Matthey Technology Centre, Reading, UK

Johnson Matthey Fuel Cells website, (2002), http://www.matthey.com/environment/fuelcell/products.html

Johnson Matthey Fuel Cells, (2002), http://www.matthey.com/environment/fuelcell/products.html

Johnson Matthey Gas Purification Technology Website, (2004), http://www.jmgpt.com/html/getter _purification.html

Johnson Matthey Technology Centre (2000). *JM Positioning in a future hydrogen economy – management brief,* Johnson Matthey, Reading, UK

Johnson Matthey Technology Centre (2001). *Hydrogen diffusion membranes*, Internal Report, Reading UK

Jun, C.-S., Lee, K.-H. (2000). 'Palladium and palladium alloy composite membranes prepared by metal-organic vapour deposition method (cold-wall)', *Journal of Membrane Science*, 176, pp 121-130

Kloed, C. (2001). 'Challenges and Opportunities of Building-Up a Hydrogen Infrastructure', *Delegate Manual*, Seventh Grove Fuel Cell Symposium: Commercialising Fuel Cells: The Outstanding Issues, London, O8.3

Knapton, A.G., (1973). *Foil membranes for hydrogen diffusion cells,* Metallurgy Group, Johnson Matthey Research Laboratories, UK

Konstandopoulos, A.G., Kostoglou, M., Housiada, P. (2001). *Simulation of thin Pd alloy membranes*, Aerosol and Particle Technology Laboratory, CERTH/CPERI, Greece

Koros, W.J., Mahajan, R. (2000). 'Pushing the limits on possibilities for large scale gas separation: which strategies?', *Journal of Membrane Science*, 175, pp 181-196

Larminie, J., Dicks, A. (2000). *Fuel Cell Systems Explained.* John Wiley & Sons, Chichester, UK

Ledjeff-Hey, K., Roes, J., Wolters, R. (2000). 'CO_2-scrubbing and methanation as purification system for PEFC', *Journal of Power Sources*, 86, pp 556-561

Lee, S., Li, S.W.S., Wong, P., Fowler, M. (2003). *Design and development of a hydrogen refuelling station,* Chemical Engineering Department, University of Waterloo, Canada

Lewis, F.A. (1967). *The Palladium Hydrogen System*, Academic Press, New York

Li, Y.Z., Maeda, H., Kusakabe, K., Morooka, S., Anzai, H., Akiyama, S. (1993). 'Preparation of palladium-silver alloy membranes for hydrogen separation by the spray pyrolysis method', *Journal of Membrane Science*, 78, pp 247-245

Lloyd, L., Riler, D.E., Twigg, M.V. (1996). *The water-gas shift reaction,* Catalyst Handbook, Manson Publishing Ltd, London, pp 283-339

Lucka, K., Köhne, H. (1999). 'Usage of cold flames for the evaporation of liquid fuels', Paper for the 5th international conference, combustion for a cleaner environment, Lisbon

Ma, Y.H., Engwall, E.E., Mardilovich, I.P. (2003). *Composite palladium and palladium-alloy membranes for hydrogen separation and reactor applications*, Center for Inorganic Membrane Studies, Worcester Polytechnic Institution, US

Mardilovich, P.P., She, Y., Ma, Y.H. (1998). 'Defect-free palladium membranes on porous stainless-steel support', *AIChE Journal*, 44, 2, pp 310-322

Mathiak, J., Heinzel, A., Roes, J., Kalk, Th., Kraus, H., Brandt, H. (2004). 'Coupling of a 2.5kW steam reformer with a 1kW_{el} PEM fuel cell', *Journal of Power Sources*, 131, pp 112-119

Melaina, M.W. (2003). 'Initiating hydrogen infrastructures: preliminary analysis of a sufficient number of initial hydrogen stations in the US', *International Journal of Hydrogen Energy*, 28, pp 743-755

Mercuri, R., Bauen, A., Hart, D. (2002). 'Options for refuelling hydrogen fuel cell vehicles in Italy', *Journal of Power Sources*, 106, pp 353-363

MesoFuel website, (2004), http://www.mesofuel.com

Mott Corporation website, (2004), http://www.mottcorp.com

Müller-Hellmann, A. (2000). *Ringvorlesung: Elektrische Energie aus regenerativen Quellen-Entwicklungsstand und Ausblick*, Lehrstuhl und Institut für Stromrichtertechnik und elektrische Antriebe, Aachen, Germany

Murray, H.S., Huff, J.R., Roach, J.F., Thayer, G.R. (1986). *DOT Fuel-Cell-Powered Bus Feasibility Study: Final Report*, Los Alamos National Technical Report LA-10933-MS, US

Ogden, J.M. (1999). 'Developing an infrastructure for hydrogen vehicles: a southern Californian case study', *International Journal of Hydrogen Energy*, 24, pp 709-730

Pall Corporation, (2004), http://www.pall.com

Pandey, P., Chauhan, R.S.(2001). 'Membranes for gas separation', *Progress in Polymer Science*, 26, pp 853-893

Pehr, K., Sauermann, P., Traeger, O., Bracha, M. (2001). 'Liquid hydrogen for motor vehicles – the world's first public LH_2 filling station', *International Journal of Hydrogen Energy*, 26, pp 777-782

Press, H.E. (1996). Numerical Recipes in FORTRAN 90 – the art of parallel scientific computing. 2nd Edition, Cambridge University Press, Cambridge

Qiao, G.J., Zhang, C.G., Jin, Z.H. (2003). 'Thermal cyclic test of alumina/Kovar joint brazed by Ni-Ti active filler', *Ceramics International*, 29, pp 7-11

Ricardo web site, (2000), http://www.ricardo.com

Roa, F., Block, M.J., Way, J.D. (2002). 'The influence of alloy composition on the H_2 flux of composite Pd-Cu membranes', *Desalination*, 147, pp 411-416

Roa, F., Way, J.D. (2003). 'Influence of alloy composition and membrane fabrication on the pressure dependence of the hydrogen flux of palladium-copper membranes', *Ind. Eng. Chem. Res.*, 42, pp 5827-5835

Roa, F., Way, J.D., McCormick, R.L. (2004). *Palladium-Copper Alloy Composite Membranes for H_2 Separation*, Department of Chemical Engineering, Colorado School of Mines, USA

Rogers, G.F.C., Mayhew, Y.R. (1996). *Thermodynamic and Transport Properties of Fluids*, 5th edition, Blackwell, UK

Rosner, D.E.(1986). Transport Processes in Chemically Reacting Flow Systems, Butterworths, Boston

Sakamoto, Y., Chen, F.L., Kinari, Y., Sakamoto, F. (1996). 'Effect of carbon monoxide on hydrogen permeation in some palladium-based alloy membranes', *International Journal of Hydrogen Energy*, 210, 11/12, pp 1017-1024

Smith, G.P. (2003). *Hydrogen and fuel cell activities at ford*, IChemE Energy Conversion Technology Subject Group, Sourcing the Hydrogen Economy Seminar, London

Stone, R and Ball, J.K. (2004). *Motor Vehicle Fundamentals*, Society of Automotive Engineers, to be published

Strathmann, H. (1981). 'Membrane separation processes – review', *Journal of Membrane Science*, 9, pp 121-189

Tosti, S., Bettinali, L., Castelli, S., Sarto, F. Scaglione, S., Violante, V. (2002). 'Sputtered, electroless, and rolled palladium-ceramic membranes', *Journal of Membrane Science*, 196, pp 241-249

Tovbin, Y.K., Votyakov, E.V. (2000). 'Evaluation of the influence of dissolved hydrogen on mechanical properties of palladium', *Physics of the Solid State*, 42, 7, pp 1192-1195

Uhlhorn, R.J.R., Keizer, K., Burggraaf, A.J. (1989). 'Gas and surface diffusion in modified γ-alumina systems', *Journal of Membrane Science*, 46, pp 225-241

Uemiya, S., Sato, N., Ando, H., Kikuchi, E. (1990). 'The water gas shift reaction assisted by a palladium membrane reactor', *Ind. Eng. Chem. Res.*, 30, pp 589-591

Uribe, F., Zawodzinski, T., Valerio, J., Bender, G., Garzon, F., Saab, A., Rochward, T., Adcock, P., Xie, J., Smith, W. (2002). 'Fuel cell electrode optimization for operation on reformate and air', *DOE 2002 Review*, Fuel Cell for Transportation Program, Materials Science Division, Los Alamos National Laboratory, US

Walker, P.A. (2001). Internal Johnson Matthey membrane durability test results of a typical 7 μm membrane

Warshay, M., Prokopius, P.R. (1990). 'The fuel cell in space: yesterday, today and tomorrow', *Journal of Power sources*, 29, pp 193-200

Weast, R.C. (1989). *CRC Handbook of Chemistry and Physics*, 69th edition, CRC Press Inc. Florida, US

Whysall, M., Picioccio, K.W. (1999). *Selection and revamp of hydrogen purification processes*, UOP LLC, Illinois, US

Wiessner, F.G. (1988). 'Basic and industrial applications of pressure swing adsorption (PSA), the modern way to separate gas', *Gas Separation & Purification*, 2, pp 115-119

Wilinson, D.P., Steck, A.E. (1997). 'General progress in the research of solid polymer fuel cell technology at Ballard'. In: O. Savadogo and P.R. Roberge, eds. Proceedings of the Second International Symposium on New Materials for Fuel Cell and Modern Battery Systems: New Materials for Fuel Cell and Modern Battery Systems II, Montréal École Polytechnique, Canada, , 27-41

Wilkinson, M., (2003). *BP-Hydrogen from natural gas with CO_2 storage*, IChemE Energy Conversion Technology Subject Group, Sourcing the Hydrogen Economy Seminar, London

Zhang, C., Qiao, G., Jin, Z. (2002). 'Active brazing of pure alumina to Kovar alloy based on the partial transient liquid phase (PTLP) technique with Ni-Ti interlayer', *Journal of the European Ceramic Society*, 22, pp 2181-2186